EFFECT OF COATING MATERIALS ON THE OXYGEN PERMEABILITY AND STABILITY OF THE ASYMMETRIC ION TRANSPORT MEMBRANE $Ba_{0.5}Sr_{0.5}Co_{0.8}Fe_{0.2}O_{3-\delta}$ (BSCF)

BY

AMIR HAMZA

A Dissertation Presented to the

DEANSHIP OF GRADUATE STUDIES

KING FAHD UNIVERSITY OF PETROLEUM & MINERALS

DHAHRAN, SAUDI ARABIA

In Partial Fulfillment of the
Requirements for the Degree of

DOCTOR OF PHILOSOPHY

In

MECHANICAL ENGINEERING

MAY, 2016

KING FAHD UNIVERSITY OF PETROLEUM & MINERALS

DHAHRAN- 31261, SAUDI ARABIA

DEANSHIP OF GRADUATE STUDIES

This thesis, written by **AMIR HAMZA** under the direction of his thesis advisor and approved by his thesis committee, has been presented and accepted by the Dean of Graduate Studies, in partial fulfillment of the requirements for the degree of **DOCTOR OF PHILOSOPHY IN MECHANICAL ENGINEERING.**

Dr. Khaled Mezghani
(Advisor)

Dr. Zuhair Gasem
Department Chairman

Dr. Jurgen Caro
(Member)

Dr. Salam A. Zummo
Dean of Graduate Studies

Dr. Mohamed A. Habib
(Member)

10/8/16
Date

Dr. Saheb Nouari
(Member)

Dr. Mohamed M. Faiz
(Member)

© Amir Hamza

2016

Dedicated to my father Umar Hayat, my mother Ismat Umar

And my wife Abeera Sikandar

ACKNOWLEDGEMENTS

In the name of Allah, most Gracious and most Merciful.

May Allah bestow peace on our beloved Prophet Mohammed (peace and blessings of Allah be upon him), and his family. I wish to acknowledge my indebtedness to the Allah Almighty for endowing upon me the potentials to carry out this project successfully.

I owe a special debt of thanks to my supervisor Dr. Khaled Mezghani for his invaluable help, advice and guidance in producing this research. His guidance and inspiration deserves my special gratitude.

I offer my sincerest thanks and appreciation to the committee members for my thesis, Dr. Jurgen Caro, Dr. Mohamed A. Habib, Dr. Saheb Nouari and Dr. Mohamed M. Faiz who have provided me with invaluable inputs and comments which have served to improve the quality of this work.

Acknowledgements are due to King Fahd University of Petroleum and Minerals which gave me the opportunity to pursue a PhD degree and also for all the support I received in carrying out this research. I am also grateful to the Technology Innovation Center for Carbon Capture and Sequestration at KFUPM (Project # CCS-5) for providing the necessary resources and support during this research.

I would also like to express my deep sense of gratitude to my family. Their continuous support and love made it possible for me to finish this study. Thanks also to

all my colleagues in the Mechanical Engineering department for making my time here memorable. My special thanks are due to all those who have contributed to this research directly or indirectly.

TABLE OF CONTENTS

LIST OF TABLES

LIST OF FIGURES

LIST OF ABBREVIATIONS

Ar	Argon
BSCF	$Ba_{0.5}Sr_{0.5}Co_{0.8}Fe_{0.2}O_{3-\delta}$
BSCFY	$Ba_{0.5}Sr_{0.5}Co_{0.8}Fe_{0.175}Y_{0.025}O_{3-\delta}$
CCS	Carbon Capture and Sequestration
CGO	$Ce_{0.9}Gd_{0.1}O_{1.95-\delta}$
CO	Carbon Monoxide
CO_2	Carbon Dioxide
EDS/EDX	Energy Dispersive X-ray Spectroscopy
GC	Gas Chromatograph
H_2	Hydrogen gas
H_2O	Water
He	Helium
ITM	Ion Transport Membranes
LCCF	$La_{0.6}Ca_{0.4}Co_{0.8}Fe_{0.2}O_{3-\delta}$
LCF	$La_{0.9}Ca_{0.1}FeO_{3-\delta}$
LCFO	$La(Co,Fe)O_{3-\delta}$
LNO	$La_2NiO_{4+\delta}$
LSCF	$La_{1-x}Sr_xCo_{1-y}Fe_yO_{3-\delta}$
LSTF	$La_{0.6}Sr_{0.4}Ti_{0.3}Fe_{0.7}O_{3-\delta}$

MIEC	Mixed Ionic Electronic Conducting
NOx	Mono-nitrogen oxides - nitric oxide (NO) and nitrogen dioxide(NO2)
O_2	Oxygen
OTM	Oxygen Transport Membranes
Pd	Palladium
Pt	Platinum
SCMF	$Sr_{0.5}Ca_{0.5}Mn_{0.8}Fe_{0.2}O_{3-\delta}$
SEM	Scanning Electron Microscope
SO_2	Sulfur dioxide
SOFC	Solid Oxide Fuel Cells
STP	Standard Temperature Pressure
WDS	Wavelength Dispersive X-ray spectroscopy
XPS	X-ray Photoelectron Spectroscopy
XRD	X-ray Diffraction
XRF	X-ray Fluorescence Spectrometer
YSZ	Yttrium Stabilized Zirconia

ABSTRACT

Full Name : Amir Hamza

Thesis Title : EFFECT OF COATING MATERIALS ON THE OXYGEN PERMEABILITY AND STABILITY OF THE ASYMMETRIC ION TRANSPORT MEMBRANE Ba0.5Sr0.5Co0.8Fe0.2O3−δ (BSCF)

Major Field : Mechanical Engineering

Date of Degree : May, 2016

Carbon dioxide emission is believed to be one of the major causes of global warming for our planet. The main source of CO_2 emission is the power industry using fossil-fuel. One of the solutions to reduce the CO_2 emission is to utilize oxy-fuel combustion. Oxy-fuel process is a technology in which the fuel is burnt in oxygen rich environment producing high concentration of CO_2 which can be captured and stored, thus stopping emissions from power plants. The oxygen rich environment can be created by using ion transport membranes (ITM) that are able to separate oxygen from air. The oxygen permeability, chemical stability under the CO_2 containing environment, and sealing of these membranes to the reactor setup at high temperatures are very important issues for this technology to mature. In this study, the ion transport membrane $Ba_{0.5}Sr_{0.5}Co_{0.8}Fe_{0.2}O_{3-\delta}$ (BSCF) has been selected to address these issues. The BSCF has been reported to have the highest oxygen permeation flux among all ITM; however, it has relatively low chemical stability in CO_2 rich environment.

In this work, the permeability behavior of BSCF membranes has been investigated with respect to microstructure, thickness and oxygen partial pressure. The membrane has shown to have excellent stability in inert environment. For example, at 920 ºC a 1.4 mm thick BSCF memebrane has continuously produced a constant oxygen flux of 0.83 μmol.cm^{-2}.s^{-1} for more than 1000 hours.

One of the challenges in this study is to find the proper sealing material for the ITM reactor. After studying different materials and mixtures, the best sealing material has been determined to be a mixture of 20 wt% Pyrex-glass and 80 wt% BSCF powders. This sealant mixture has provided excellent long-term solution of air leakage containment, desirable bond strength between the membrane and the ceramic tube and prevention of chemical reaction at the surface of the membrane.

The BSCF membrane has also been utilized inside a laboratory scale oxy-fuel combustion reactor. Methane has been used as fuel in this study. It is shown that the degradation of the BSCF membrane depends on the fuel flow rate. In addition, the study shows that the BSCF degradation can be prevented if the oxy-fuel reactor is operating at 15% excess oxygen. The study has also shown that an increase in the fuel rate significantly increases the permeability of the membrane. In order to achieve high oxygen permeability without degrading the BSCF, the permeate side of the membrane is coated with a mixture of $La_2NiO_{4+\delta}$ (LNO) and BSCF. The performance of the coated membrane is significantly enhanced. The results show that the coated membrane is stable during 140 hours continuous methane reaction with an oxygen flux of 1.35 μmol.cm^{-2}.s^{-1} at 920ºC. Also for improving stability, Platinum and

Palladium have been separately coated on the permeate and feed sides of the BSCF membranes. The results indicate that both metals have increased the stability of the BSCF. Furthermore, only Palladium has shown a catalytic activity on the feed side resulting in a higher permeability of the BSCF membranes.

Another approach for enhancing the oxygen permeability of BSCF is to use an asymmetric membrane, where a very thin dense layer of BSCF is coated on the top of a porous BSCF support. These membranes produced higher oxygen flux values (1.42 $\mu mol.cm^{-2}.s^{-1}$ at 920 ºC without fuel), allowing a further increase in the allowable fuel flow rate in the oxy-fuel reactor.

ABSTRACT (ARABIC)

الخلاصة

الاسم: أميرحمزه

عنوان الرسالة: أثر طلاء الأغشية النافذة للأيونات $Ba_{0.5}Sr_{0.5}Co_{0.8}Fe_{0.2}O_{3-\delta}$ (BSCF) **في استقرارها و نفاذية أيونات الأكسجين.**

التخصص: الهندسة الميكانيكية

تاريخ التخرج: 1437 هـ - (مايو 2016 م)

ثاني أكسيد الكربون هو أحد أكبر مسببات الاحتباس الحراري، و من أكبر منتجي هذه المادة هي صناعات الطاقة الحارقة للنفط و منتجاته. أحد الحلول للحد من انبعاثات ثاني أكسيد الكربون هو استخدام الاحتراق المسمى (oxy-fuel)؛ وهو احتراق الوقود في بيئة غنية بالأكسجين منتجا نسبة عالية من ثاني أكسيد الكربون الذي من الممكن جمعه و تخزينه، و بذلك يتم إيقاف الانبعاثات الغير مرغوب فيها من صناعات الطاقة. من الممكن استخدام الأغشية النافذة للأيونات (التي تمكننا من فصل الأكسجين عن المواد الأخرى في الهواء) لإنتاج البيئة الغنية بالأكسجين. أهم القضايا التي تحدد مدى نجاح هذه التكنولوجيا هي الاستقرار الكيميائي في وجود ثاني أكسيد الكربون، ونفاذية الأكسجين، والإغلاق المحكم لهذه الأغشية في جهاز الاحتراق في درجات حرارة عالية. في هذه الدراسة، الغشاء الناقل للأيونات المستخدم هو $Ba_{0.5}Sr_{0.5}Co_{0.8}Fe_{0.2}O_{3-\delta}$ (BSCF) بما أنه الأكثر نفاذية للأكسجين.

تمت دراسة علاقة نفاذية BSCF مع المتغيرات الآتية: الشكل المجهري، السماكة، والضغط الجزئي للأكسجين. أظهرت هذه الدراسة أن الغشاء BSCF مستقر بشكل جيد تحت ظروف غير نشطة كيميائيا، على

سبيل المثال: عند درجة حرارة 920 مئوية، غشاء BSCF بسماكة 1.4 ملليمتر أنتج تدفق مستمر للأكسجين بمقدار 0.83 ميكرو مول/سنتيمتر مربع · ثانية ($\mu mol.cm^{-2}.s^{-1}$) لأكثر من 1000 ساعة.

كانت من التحديات في هذه الدراسة إيجاد مادة مناسبة لعزل بيئة الإحتراق عن محيطها و إغلاقها بإحكام. بعد إجراء بعض الدراسات على مواد وأخلاط مختلفة، تم التوصل إلى أفضل خليط لاستخدامه في عملية العزل، وهو خليط من زجاج البوروسليكات (Pyrex-glass) بنسبة 20% وزنا و 80% مسحوق BSCF. هذا الخليط يعتبر الحل الأفضل للمدى الطويل لمنع تسرب الأكسجين للخارج أو الهواء الخارجي للداخل، كما أنه يوفر التصاق قوي بين الغشاء BSCF والأنبوب السيراميكي في جهاز الاحتراق، وأيضا يمنع حدوث أي تفاعل كيميائي على سطح الغشاء.

تم استخدام الغشاء BSCF في جهاز احتراق في المختبر مع اختيار غاز الميثان كوقود. أظهرت الدراسة أن تحلل الغشاء يعتمد على معدل تدفق الوقود، ومن الممكن منع التحلل من الحدوث اذا تمت عملية الاحتراق بمقدار فائض من الأكسجين يعدل 15%، كما أظهرت أن الزيادة في تدفق الوقود تؤدي الى زيادة عالية في نفاذية الغشاء. لتحقيق تدفق أكسجيني عالي مع إبقاء الغشاء من التحلل، تم طلاء الجهة النافذة للغشاء بخليط من $La_2NiO_{4+\delta}$ (LNO) و BSCF. بهذا، تم التوصل الى غشاء مستقر لمدى 140 ساعة من احتراق متواصل للميثان مع أكسجين بتدفق 1.35 ميكرو مول/سنتيمتر مربع · ثانية ($\mu mol.cm^{-2}.s^{-1}$) عند درجة حرارة 920 مئوية.

توجد طريقة أخرى لتحسين نفاذية الأكسجين للغشاء BSCF وهي باستخدام غشاء غير متماثل، بحيث يتم طلاء طبقة رقيقة جدا من الغشاء BSCF الكثيف فوق طبقة داعمة من الغشاء BSCF المسامي. هذا الغشاء المركب الغير المتماثل أظهر نفاذية أعلى، فأنتج تدفق أكسجيني بمقدار 1.42 ميكرو مول/سنتيمتر مربع · ثانية ($\mu mol.cm^{-2}.s^{-1}$) عند درجة حرارة 920 مئوية بعدم وجود وقود، مانحا زيادة في المقدار المسموح به لتدفق الوقود في جهاز الاحتراق.

.

CHAPTER 1

INTRODUCTION

1.1 THE PROBLEM OF CARBON EMISSION

The wellbeing of human population and economic growth of nations requires an access to abundant energy. The sustainable energy requirement of the world is ever increasing. It increased by a factor of 12 in the 20^{th} century, and according to the opinion of the experts, will grow by a factor of 3 to 4 during the 21^{st} century [1]. This presents an enormous challenge of provision of necessary energy in the future. This challenge is made much more difficult by climate change concerns. Today most of the energy production relies on the cosumption of fossil fuels. In 2011, energy from fossil fuels was accounting for 81% of all commmercial energy [2]. This has, inturn, caused the quantity of carbon dioxide in the atmosphere to increase dramatically. Since the advent of the industrial age the CO_2 concentration in the atmosphere has increased from 280 ppm to 400 ppm today. This increase is not sustainable as CO_2, a green house gas, causes severe harmful effect on the global environment when its concentration level is disturbed. The acceptable upper level of CO_2 in the environment could well be below the current level. Hansen et al. [3] have shown that going past 350 ppm level will destabilize the Greenland ice sheet that will have very serious consequences. So it is essential to understand that the

governments around the world have to act fast to make effective policies and the scientific community has to come through for effective and practical solutions to limit the climate change problem.

In order to avoid climate change, it is imperative to stabilize the carbon emission in the atmosphere. Stabilizing the CO_2 level in the atmosphere can only be achieved by either abandoning the use of fossil fuels in favor of alternatives in the energy sector, or by finding methods to keep the CO_2 resulting from the use of fossil fuels away from the atmosphere. Both these approaches have attracted considerable effort in the form of ongoing research around the world. It is important to understand that we cannot just focus on replacing the fossil fuels and ignore the vast resources of energy available to mankind. A sustainable way of using the untapped fossil fuel reservoirs for the growing energy demands has to be found. Carbon Capture and Sequestration (CCS) technologies are directed towards achieving this very goal. We are in need of mature technologies which can ensure, at the minimum, a smooth transition from fossil fuel use to alternatives, and at maximum, a capability to fully utilize the fossil carbon in a carbon constrained world.

1.2 CONCEPTS FOR CARBON CAPTURE

According to the 4th Assessment Report of the International Panel on Climate Change (IPCC) [4] about 26 Gt of CO_2 was emitted in the year 2005. Additionally, deforestation caused an additional annual CO_2 emission of 3-7Gt. In 2007 the global CO_2 emissions from coal, oil and natural gas were 12 Gt, 12Gt and 6 Gt respectively [5]. Fossil fuels are

primarily used for production of electricity. Hence, carbon capture has great potential for future reduction of CO_2 emission.

1.2.1 Techniques for CO_2 Capture

There are three techniques to capture CO_2 from power plants.

- Post-combustion capture
- Oxyfuel combustion
- Pre-combustion

In the post-combustion capture, the flue gas produced as exhaust during the combustion is de-carbonized. The most promising method to do so involves chemical absorption of CO_2. This process can be used with existing designs of the power plants. Another method to separate CO_2 post-combustion is by using polymer membranes. However, this process has higher energy cost as the flue gas from the exhaust of the power plant has to be compressed to compensate for the low CO_2 pressure.

In the pre-combustion process fuel gas is de-carbonized before the combustion takes place. It is possible to use this technique with the Integrated Gasification Combined Cycle (IGCC) and involves three steps [6]:

• Partial combustion of hydrocarbon (fuel) in either air or oxygen rich air to produce syngas which contains H_2 and CO.

• Conversion of this mixture to H_2 and CO_2. The reaction which is responsible for this is:

$CO + H_2O(g) \rightarrow CO_2 + H_2$

• Finally the CO_2 has to be separated from H_2. This may be done by chemical absorption process as described previously, pressure swing adsorption using adsorbents such as zeolite molecular sieves or cryogenic separation of CO_2 by condensation. Membrane separation is also used commercially for H_2 separation but their selectivity is low.

The oxy-fuel process is an oxygen/nitrogen separation of the air before it is supplied for combustion. Then the fuel is burnt in an oxygen-rich environment to produce a flue gas which has high concentration of CO_2 [7]. Carbon capture becomes much easier at higher CO_2 concentrations. The oxy-fuel flue gas comprises of relatively clean exhaust gases, H_2O and CO_2. Water vapor can be condensed and separated from CO_2 which can then be stored. Cryogenic distillation of air in an air separation unit (ASU) is the most widely used method for the separating oxygen from air. Pressure swing adsorption and gas separation membranes are other options which provide more flexibility.

From the three carbon capture technologies, four different gas separation tasks can be identified:

- CO_2 separation from flue gas
- CO_2 separation from shifted coal gas
- O_2 separation from air
- H_2 separation from shifted coal gas

In principal, many different methods exist for these gas separation tasks but not all are suitable for large scale applications. The promising methods are listed in Table 1.1. and shown in Figure 1.1. The details of these methods will not be discussed here as our focus will be on oxygen separation methods through membranes for oxy-fuel combustion. A summary of these methods for application in carbon capture is presented by Riensche et al [8]

Table 1.1 Separation routs, tasks and methods for carbon capture

Route	Separation Tasks	Methods
Post combustion	CO_2 vs N_2	Absorption with liquids Carbonate looping Absorption with solids Membranes
Oxyfuel	O_2 vs N_2	Cryogenic air separation Chemical looping combustion Membranes
Pre combustion	CO_2 vs H_2 H_2 vs CO_2	Absorption with liquids Carbonate looping Membranes Adsorption with solids Membranes

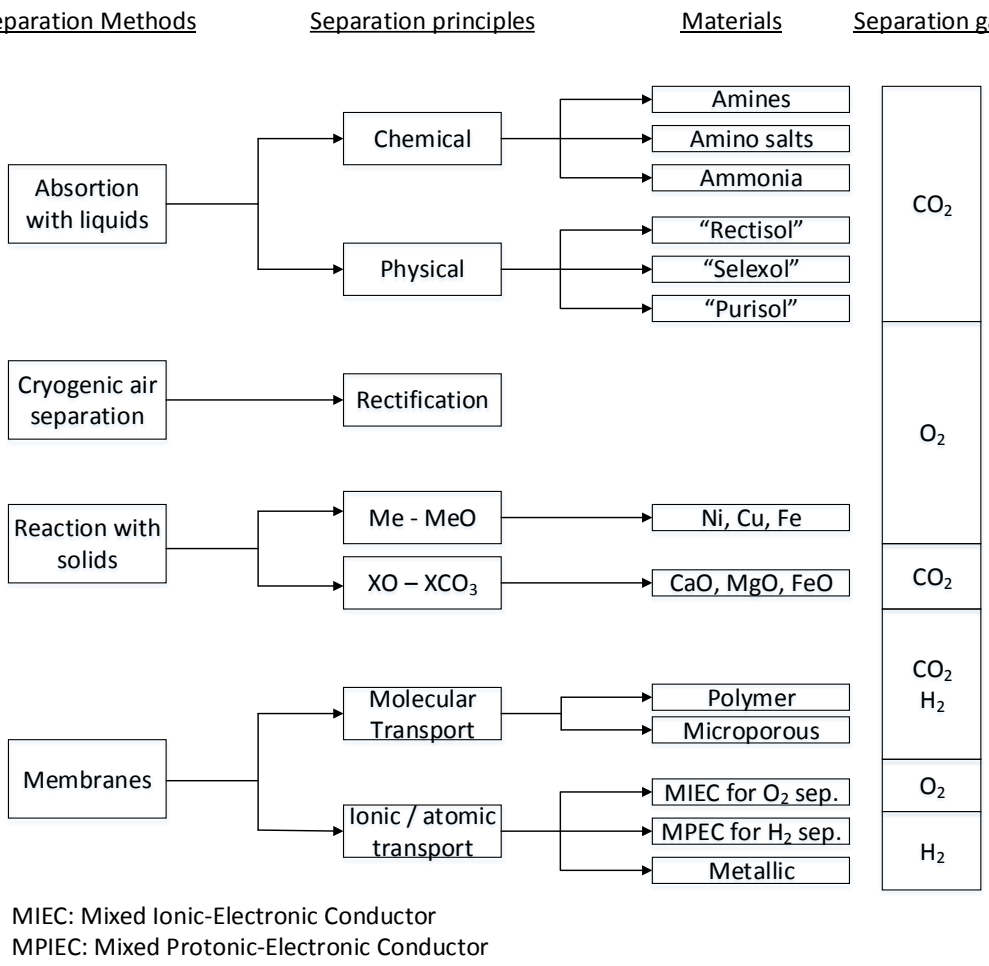

Figure 1.1. Gas separation methods, principles, and the materials utilized in carbon capture. X: Ca, Mg, Fe

1.3 GAS SEPARATION WITH MEMBRANES

Membrane technologies for CO_2 capture in power plants have been widely investigated, since they offer the potential for low energy demand for gas separation process. In addition to CCS application, they are also used for natural gas cleaning.

Generally speaking, the gas separation membranes can be divided into two categories, polymeric membranes and inorganic membranes.

1.3.1 Polymeric Membranes

With regard to polymeric membranes, Powell and Qiao [9] published a comprehensive review of different CO_2 selective structures developed for flue gas separation. Two types of polymeric membranes are widely in use commercially. Glassy membranes are rigid and glass like and operate below their glass transition temperatures. On the other hand, rubbery membranes are flexible and soft, and operate above their glass transition temperatures. Polymeric membranes can be used for CO_2 separation in post-combustion and pre-combustion. Some types of polymeric membranes separate H_2 and potentially applicable to pre-combustion. So far polymeric membranes have not been used for oxy-fuel combustion application.

1.3.2 Inorganic Membranes

In a fossil fueled power plant, inorganic separation membranes can find application in, for example, the separation of oxygen from air (oxy-fuel process) and the separation of hydrogen from syngas (pre-combustion process). Inorganic membranes can be divided into ceramic and metallic membranes. Figure 1.2 shows the main classes of ceramic and metallic membranes. Two types can be identified with respect to their transport mechanism through the membrane:

- Microporous membranes with either crystalline structure such as zeolites or amorphous structures such as sol-gel membranes. Both types work for CO_2-N_2 and H_2-CO_2 separation.
- Dense membranes are either mixed ionic-electronic conductors or metals. Mixed ionic conductors transport oxygen ions for O_2 separation and protons for H_2 separation, as the gas species. Metals transport H atoms for H_2 separation.

The structure of a microporous ceramic membrane is a graded porous multilayer with macroporous, mesoporous and microporous layers. Separation of different gas molecules is achieved through diffusion. Smaller gas molecules permeate through the porous structure whereas the larger molecules are sieved out. Therefore, the size of the relates gas molecule is important for the development of well-defined nanostructures. The kinetic molecule diameters lie in a very narrow range (H_2 0.289nm, CO_2 0.330nm, O_2 0.346nm and N_2 0.364nm) [10]. The transport equation for a gas component A is linear in the driving force:

$$j_A = P_A \left(p'_A - p''_A \right) \tag{1.1}$$

where P_A is the permeance of the gas component A and p'_A and p''_A are the partial pressures at the feed and permeate side of the membrane, respectively.

Amorphous SiO_2 membranes have been investigated and show potential for high selectivity (e.g., >100 for H_2-CO_2 separation) and high permeability due to thicknesses of only 50-200 nm reported in the literature.

Mixed ionic electronic conductors (MIECs) transport oxygen ions via vacancies in a crystal lattice. Promising materials are perovskites and flourites [11]. Barium containing perovskites show the highest permeability but are reported to be not stable in atmospheres containing CO_2, SO_2 or H_2O. The driving source for permeation is an O_2 partial pressure gradient, which leads to a directed diffusion from the high to the low pressure side of the membrane. The O_2 flux density j_{O2} in the bulk material is described by the Wagner equation:

$$j_{O2} = (RT/16F^2)\left(\sigma_{\text{amb}}/L\right)\ln(p'_{O2}/p''_{O2}) \tag{1.2}$$

where R is the gas constant, T is the temperature, F is the Faraday constant, σ_{amb} is the ambipolar conductivity, L is the membrane thickness, and p'_{O2} and p''_{O2} are the oxygen partial pressures on the oxygen rich and lean side, respectively [8]. The material related parameter ambipolar conductivity σ_{amb} is composed of the ionic and electronic conductivities. O_2 permeation increases when the membrane thickness is reduced. However, surface exchange reactions become rate limiting beneath a characteristic thickness L_c [12].Membrane modules for application of oxy-fuel combustion are under study, with consideration of several membrane geometries [13]. These membranes will be discussed in more detail in the following chapter.

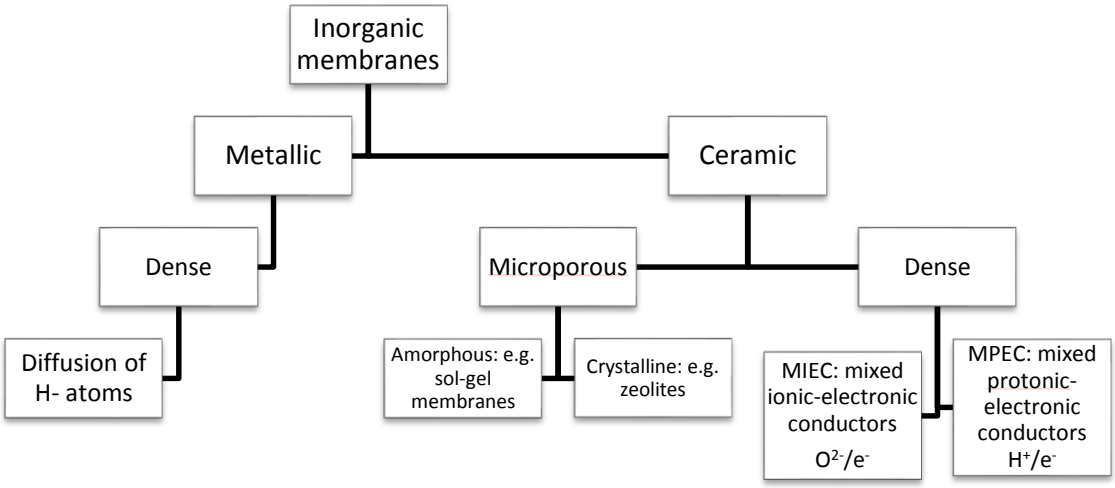

Figure 1.2 Inorganic membranes: possible application to the separation task within the capture routes

Ceramic membranes with mixed proton-electron conductivity are promising for pre combustion capture. The advantages of these membranes are their high thermal, mechanical and chemical stability. However, the mixed proton-electron conductivity, determining the hydrogen flux, has to be improved. For this purpose formation of defects in the material structure is required, either by variation of the basic component ratios or extrinsically by doping.

Metal membranes are mainly palladium or palladium alloy membranes supported by porous metallic tubes. There thickness lies in the range 1-10μm. Their H_2-CO_2 selectivity is high due to the selective transport of hydrogen atoms through the material. According to Sievert's Lawthe flux of H_2 through the membrane is

$$j_{H_2} = \left(S_{H_2} D_{H_2} / L\right)(\sqrt{p'_{H_2}} - \sqrt{p''_{H_2}} \tag{1.3}$$

where S_{H_2} is the solubility coefficient, D_{H_2} is the diffusion coefficient, L is the membrane thickness, p'_{H_2} and p''_{H_2} are the hydrogen partial pressures at the feed and permeate side of the membrane, respectively [14][15].

1.4 SCOPE AND OBJECTIVES OF CURRENT WORK

The literature review, a summary of which is presented in the Chapter 2, has pointed out that the most promising material for oxygen transporting membranes in oxy-fuel combustion is $Ba_{0.5}Sr_{0.5}Co_{0.8}Fe_{0.2}O_{3-\delta}$ (BSCF). There are, however, some issues that need attention of researchers in this area.

The amount of oxygen flux through the MIEC membranes has to be improved in order to make it a viable technology for oxygen separation at commercial scale. It is, therefore, a priority to work on improving the oxygen permeability of the disc type membranes. For BSCF, another critical issue is the chemical stability of the membrane in the flue gas stream which consists of water vapor, CO_2, O_2 and traces of SO_2 [16].

Finally, problems related to design and engineering, for example high temperature sealing, have to be solved before these membranes can be used extensively in commercial applications.

Taking these important points into consideration, the objectives of this thesis study are listed below:

1. To develop a perovskite BSCF disc type membrane for testing under high temperature conditions
2. To develop membrane sealing solutions suitable for high temperature applications.
3. To improve the permeability of the BSCF membranes by:
    a. preparing asymmetric membranes with layers of porous and dense material;
    b. coating of appropriate materials in order to enhance the permeability of the membranes
4. To improve the chemical stability of the BSCF membranes by coating of appropriate materials.

CHAPTER 2

LITERATURE REVIEW

The materials and membranes with ionic conduction have been around since many years. Initially the main concentration of major work was on the development of solid oxide fuel cells (SOFCs) and sensors [17]. Similar materials which can be used for separation of oxygen from air were discovered in the 1980s. These oxygen separating materials were capable of not only conducting the ions but also the electrons. So the oxygen passes through the membranes made of these materials in ionized form from higher to lower oxygen chemical potential side providing a selectivity of 100 percent. Meanwhile the electronic conductivity acts as an internal short circuit and a flux of electrons in the opposite direction maintains a state of neutrality. The operation of a mixed ionic electronic conducting material, in contrast to an ionic conducting material, is shown in Fig 2.1. An absence of the requirement of an external circuit makes the operations integrating membranes made out of these materials much more simple and cost effective. These membranes are now viewed as prime candidates in the processes where oxygen is separated from air for its use in production of clean energy efficiently. In the past 15 years a lot of research has been carried out in this area backed by funding from many governments, which has enabled technologies making use of these materials to the brink of commercialization.

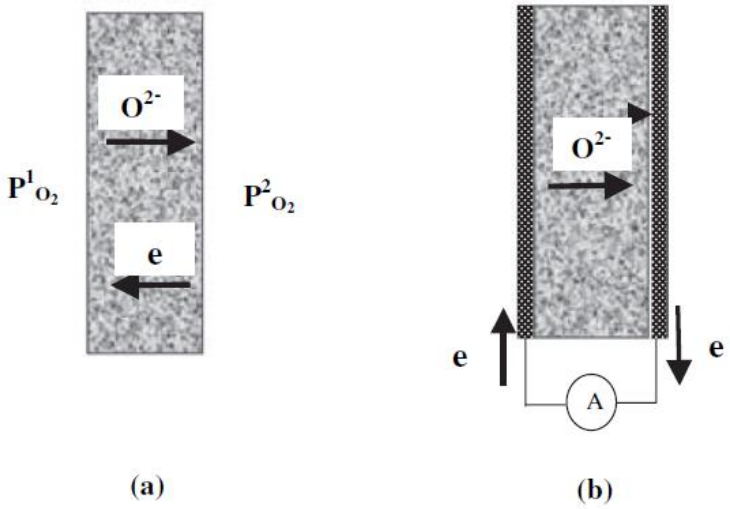

Figure 2.1 Principles for permeation of oxygen through (a) mixed ionic- electronic conductor and (b) pure ionic conductor electrolyte cell (oxygen pump) [18]

The performance of an MIEC membrane is governed by its material properties such as its composition and structure. A basic overview of these aspects is presented in the following sections:

2.1 STRUCTURE OF MIEC MATERIALS

Most of the materials capable of simultaneous electronic and ionic conduction are perovskites. Perovskites are complex oxides with general formula ABO_3, where the A site represents large ions such as lanthanides, actinides, alkali and alkaline earth elements, Pb or Bi, and the B site represents transition metal elements, Li, Mg, Ca, Al, Si,

Ga, Ge, In, Sn. Sb, Pb or Bi [19]. Hence synthetic perovskites show a wide variety of chemical composition and material properties, such as n-p conductivity, superconductivity, piezoelectricity, O^{2-} and H^{+} ion conductivity, catalytic activity and magnetism.

The perovskite structure depicted in Figure 2.2 in a polyhedral representation is characterized by a cubic close packing of large A ions together with oxygen ions, and B cations occupy the octahedral cavities furthest from A ions. The A site cation is coordinated to 12 oxygen ions forming a cuboctahedral coordination while the B site cation is coordinated to six oxygen ions with an octahedral geometry. This structure indicates the general composition and the structure of the crystal unit cell of these materials. The structure of many perovskites can deviate from the general ABO_3 unit cell type depending on the valence state of the A and B cations. Compositions such as $A^{1+}B^{5+}O_3$, $A^{3+}B^{3+}O_3$ and $A^{2+}B^{4+}O_3$ are common. The stability of the structure can be estimated according to Goldschmidt tolerance factor *t*:

$$\text{Tolerance factor} = (r_A + r_O) \;/\; \sqrt{2}\,(r_B + r_O) \qquad (2.1)$$

where r_A, r_B and r_O are the ionic radii of the A and B site cations and oxygen, respectively. A value of $t = 1$ is obtained for the idealized case when all ions are in direct contact, but cubic perovskites are also found with *t* values down to 0.9. Structures resulting from combinations of hexagonal and cubic stacking sequences of AO_3 layers occur at *t* above 1, and rombohedral, tetragonal and orthorhombic distorted structures

were observed below $t = 0.9$. It is found that a tolerance factor of around 0.96 is associated with high conductivity. The structural parameters such as tolerance factor and the specific free volume have been found to have effect on the properties of the perovskite materials. Hayashi *et al.* [20] showed the relation between these parameters and the electrical conductivity in perovskites. The effect of ionic radii of A and B site cations on the oxygen permeability of the material were studied by Yamamura et al. [21]. They suggested new materials with better ionic conductivity based on their molecular dynamic simulations.

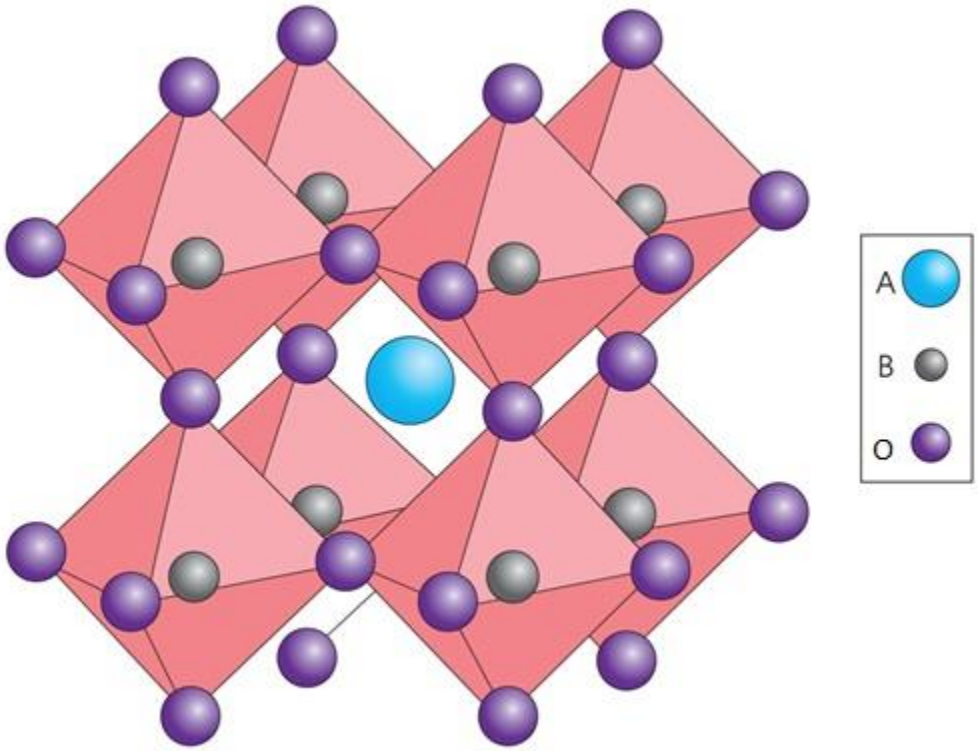

Figure 2.2 Perovskite structure [19]

An ideal perovskite is unable to conduct ionized oxygen through its lattice. For this transfer to take place, there should be a certain amount of defects or imperfections owing to nonstoichiometry. Ion defects can exist as lattice site vacancies, interstitial ions (through unoccupied sites), impurities or dopants with different charges. Electron defects can exist as ions present with charges different from the normal lattice ions, as well as due to the shifting of electrons from energy levels which are normally filled to those which are normally empty. The electron deficiency is usually called a hole (or electron hole). The vacancies and electron holes could be considered the point defects where the ions and electrons move. As a mixed ionic electronic conducting material, the overall conductivity performance depends on the contributions from both ionic and electronic defects.

The highest oxygen permeability is observed for alkaline earth cobaltites such as $Ba_{1-x}Sr_xCo_{1-y}Fe_yO_{3-\delta}$ [22][23][24][25], $BaCo_{1-y}Fe_yO_{3-\delta}$ [26][27], and $SrCo_{1-y}Fe_yO_{3-\delta}$ [28][29]. Cobalt and iron are often partly replaced by Ni, Cu, Zn, Cr, Al, Ga, In, Ce, Ti, Zr, Sn, V and Nb [30] and also by Bi, Sc, La and Y [31] and other elements. Frequently, the main target is oxygen permeability enhancement. The stabilization of the perovskite phase is also important because of the change of properties during transition to brownmillerite phases [28][29] and hexagonal perovskite [32][33]. Moreover, such phase transitions are mostly connected with significant volume changes [34] possessing the ability to destroy the ceramic membranes.

Some B ions show a strong reducibility to the metal at low oxygen partial pressures. Further, the high affinity of alkaline earth elements to CO_2 and SO_2 is accompanied by the formation of carbonate and sulfate layers on the membrane surface, blocking the oxygen flux. For that reason, stability against chemical attack is also an important aspect of material development [35][36].

2.2 STRATEGIES FOR DOPING PEROVSKITES

The physical properties of mixed conducting perovskite materials can be adapted by making use of doping of appropriate elements. For the ABO_3 type perovskite oxides, doping of B', with lower valence state, can be introduced on the B site. The new structure, $AB_{1-x}B'_xO_{3-\delta}$, forms defects with the symbol δ denoting the amount of vacancies (defects). These vacancies will be used for oxygen ions diffusion. Therefore, increasing the number of defects can have a positive effect on the permeability of oxygen. A wide range of perovskites has been investigated by either doping the A site atoms, the B site atoms or both. The resulting structure is in the form of $A_xA'_{1-x}B_yB'_{1-y}O_{3-\delta}$. Nowick and Du [37] presented other types of perovskites which also show reasonably good mixed conducting behavior. In the presence of so many choices, it is very important to adopt a proper doping strategy to obtain good results.

2.3 MATERIAL PROPERTIES

The oxygen flux of MIECs is mainly determined by the ionic and electronic conductivity. The majority of high flux MIECs are p-type semiconductors characterized by a charge carrier mobility that increases with temperature. However, the concentration of holes decreases with increasing oxygen vacancy concentration caused by increasing temperature and decreasing oxygen partial pressure. Therefore, the electronic conductivity of high-flux MIECs often show a maximum in the intermediate temperature range [38].

Ionic conductivity is determined by the oxygen vacancy diffusion coefficient and the oxygen vacancy concentration depending mainly on the material composition. An increase in temperature enhances the diffusivity and also the vacancy concentration; the latter is also increased by a decrease in oxygen partial pressure.

Therefore, the dependence on vacancy concentration differs for electronic and ionic conductivity. Accordingly, the ambipolar conductivity depends on the operating conditions in a complex manner, but in general temperature dependence dominates. According to other transport processes, an Arrhenius approach can be used in most cases to calculate the variation of the ambipolar conductivity and the related oxygen permeation with temperature. The total conductivity is expressed as the sum of both the conductivities of ions and electrons:

$$\sigma_{total} = \sigma_{ion} + \sigma_{e} \tag{2.2}$$

Often the properties of mixed ionic electronic conducting materials are defined using transport (or transference) number t_k. For any conducting specie k, t_k is defined as:

$$t_k = \sigma_k / \sigma_{total} \tag{2.3}$$

For materials with mixed electronic and ionic conduction:

$$\sigma_{total} = \sigma_{ion} + \sigma_{e} = \sigma_{total}(t_{ion} + t_{e}) \tag{2.4}$$

t_{ion} and t_e are the transport numbers which represent the ionic and electronic defects respectively. For neutrality the sum of t_{ion} and t_e is always unity. For the material to achieve good conduction properties of both ions and electrons, t_{ion} and t_e values should be close to each other. Therefore, an ideal case would have values of both t_{ion} and t_e equal to 0.5. In reality, however, in most of the materials with mixed conduction property t_e is much smaller than t_{ion}. In case of a very low value of t_e an external circuit may be required for electron conduction for the subsequent transport of ions to take place. Generally an enhancement in the t_e and t_{ion} is carried out by making use of appropriate dopants to obtain good mixed ionic electronic conducting materials.

Furthermore, most MIEC materials showing high thermal expansion are additionally superimposed with a so-called chemical expansion [39], resulting in an overall nonlinear expansion behavior. The chemical expansion is caused by a reversible adjustment of the

oxygen stoichiometry to temperature and oxygen partial pressure according to the following chemical reaction:

$$ABO_{3-\delta'} \underset{p_{O2}}{\overset{T\uparrow}{\Leftrightarrow}} ABO_{3-\delta''} + \frac{\delta' - \delta''}{2} O_2 \uparrow \tag{2.5}$$

Therefore, an increase in temperature or decrease in oxygen partial pressure results in an increase in concentration of oxygen vacancies and a decrease in reducible B ions due to an increase in their ionic radius. Further, the electrostatic repulsion between B ions is no longer compensated by an oxide ion. Correspondingly, variations in temperature and oxygen partial pressure also result in variation of the lattice constants of the crystal structure [39], atleast above a critical temperature indicating the freezing in of the system. High flux materials such as BSCF5582 ($Ba_{0.5}Sr_{0.5}Co_{0.8}Fe_{0.2}O_{3-\delta}$) show large number of unoccupied oxygen sites, for example, up to one sixth at room temperature and up to one-quarter under operating conditions [40].

Since an MIEC membrane is always located between different oxygen partial pressures under the operation conditions, there is also a gradient of oxygen vacancy concentration along the membrane thickness. The corresponding different local expansions of the crystal lattice cause a chemically induced stress dominating the whole stress situation of a working membrane. Ceramic materials tolerate high compression stress but low tensile stress caused by small oxygen partial pressure ratios is able to destroy a ceramic membrane, especially over long times. Therefore, a suitable

combination of sweep and feed gas and absolute pressure differences can be used to minimize the tensile stress, but the selection of MIEC materials with low chemical expansion coefficient and small changes in the oxygen stoichiometry under the operating conditions is also necessary.

The mechanical properties of MIECs depend distinctly on temperature and oxygen partial pressure. As an example, BSCF5582 shows a nonlinear variation of stiffness and fracture toughness with temperature with minima between 200 and 400°C [41]. Much more critical seems to be the plastic deformation due to creeping at high temperatures described for different perovskites [42] and also for BSCF5582 [43]. This has to be kept in mind for the design of thin membrane components working in an absolute pressure gradient.

2.4 TRANSPORT MECHANISM

As discussed earlier, the bulk diffusion in oxides takes place due to the existence of defects like vacancies and intersticies. Depending on the defect type, the diffusion can follow different mechanisms [44]:

(1) When an atom or ion jumps from a lattice site to a nearby lattice site which is vacant, the vacancy is shifted to the site left by the atom or ion. This is called vacancy mechanism

(2) When an atom on an interstitial site moves to one of the neighboring interstitial site. This is called the interstitial mechanism. The diffusion of the atoms following this

mechanism causes distortion in the crystal lattice. Therefore diffusion through this mechanism is likely only when the diffusing atom has a smaller size than the atoms on normal lattice positions.

(3) Sometimes an interstitial atom transfers to a lattice site which is already occupied, pushing the lattice atom to another interstitial position. This is called interstitialcy mechanism. The diffusion occurring due to this mechanism is usually negligible.

As discussed earlier, oxygen vacancies can be produced in the ceramic oxides by doping cations. The oxygen vacancies accept oxygen atoms at high temperature in oxygen rich environment. Two electron holes are produced as a result of charge neutralization:

$$\frac{1}{2}\mathrm{O}_2 + V_{\mathrm{O}}^{\bullet\bullet} \Leftrightarrow \mathrm{O}_{\mathrm{O}}^{\times} + 2h^{\bullet} \tag{2.6}$$

The charge defects are showed using the Kröger–Vink notation. $O_0^{\times}$ is the lattice oxygen (a neutral oxygen ion sitting on the oxygen lattice site), $V_{\mathrm{O}}^{\bullet\bullet}$ is oxygen vacancy (with double positive charge) and $h^{\bullet}$ is positive electron hole.

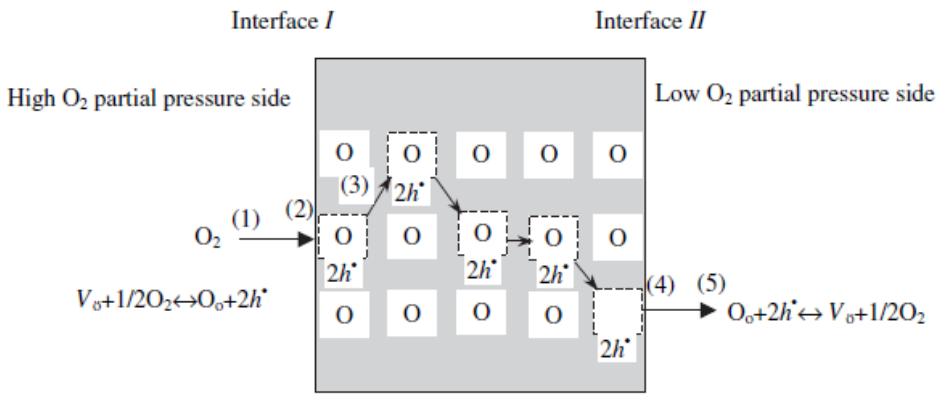

Figure 2.3 Oxygen diffusion in mixed ionic electronic conducting materials [45].

The vacancy mechanism is the most appropriate transport mechanism in the mixed conducting materials. Besides bulk diffusion, oxygen transfer through such materials also undergoes surface exchange reactions at the feed and the permeate sides of the membrane. This involves steps, such as oxygen adsorption, dissociation on the feed side and recombination and charge transfer on the permeate side. Oxygen permeation mechanism through a mixed ionic–electronic conducting ceramic membrane is schematically described in Figure 2.3. Following are the steps for the complete process:

(1) Transfer of oxygen from the feed stream to the surface of the membrane on the high pressure side.

(2) Interaction between the oxygen molecules and oxygen vacancies at the surface of the membrane on the high pressure side.

(3) Bulk diffusion of oxygen ions through the membrane by vacancy mechanism.

(4) Interaction between lattice oxygen and electron holes at the membrane surface on the low pressure side.

(5) Transfer of oxygen from the membrane surface to the permeate gas stream at the low pressure side of the membrane.

The resistance experienced in the transference of oxygen between the gas and membrane surface at high and low pressure sides (steps 1 and 5) is negligible. Therefore, only bulk diffusion and surface exchange reactions need to be considered when developing equations for oxygen transport.

2.4.1 Transport Equations

In mixed ionic–electronic conducting materials, the transport flux of charged defects (oxygen vacancy) expressed in a one dimensional model is:

$$J_V = -D_V . \frac{\mathrm{d}C_V}{\mathrm{d}x} \tag{2.7}$$

where D_v and C_v are the diffusivity and concentration of the vacancies.

Based on the relation between an oxygen molecule and the oxygen vacancy, the oxygen flux is:

$$J_{O_2} = -\frac{D_V}{2} . \frac{\mathrm{d}C_V}{\mathrm{d}x} \tag{2.8}$$

On the high pressure and low pressure side surfaces of the membranes, following reversible reactions are taking place:

$$\frac{1}{2}\mathrm{O}_2 + V_O^{\bullet\bullet} \xleftrightarrow{k_f/k_r} \mathrm{O}_\mathrm{O} + 2h^{\bullet}$$
$$\mathrm{O}_\mathrm{O} + 2h^{\bullet} \xleftrightarrow{k_f/k_r} \frac{1}{2}\mathrm{O}_2 + V_\mathrm{O} \tag{2.9}$$

where k_f and k_r are the constants for forward and reverse reaction rates of the surface reactions.

The amount of oxygen consumed at the surface high pressure side (step 2) or formed at the surface of low pressure side (step 4) can be expressed using the following two equations:

$$J_{\mathrm{O}_2} = k_f (p'_{\mathrm{O}_2})^{0.5} C'_V - k_r$$
$$J_{\mathrm{O}_2} = k_r - k_f (p''_{\mathrm{O}_2})^{0.5} C''_V \tag{2.10}$$

where p'_{O2} and p''_{O2} are the partial pressures of oxygen in the upstream and downstream. The total oxygen permeation flux in term of oxygen partial pressures as:

$$J_{\mathrm{O}_2} = \frac{k_r D_V [(p'_{\mathrm{O}_2})^{0.5} - (p''_{\mathrm{O}_2})^{0.5}]}{2Lk_f (p'_{\mathrm{O}_2} p''_{\mathrm{O}_2})^{0.5} + D_V ((p'_{\mathrm{O}_2})^{0.5} + (p''_{\mathrm{O}_2})^{0.5})} \tag{2.11}$$

It should be noted that the total resistance to oxygen permeation consists of three parts: surface reaction at high pressure membrane surface (feed side), bulk diffusion through the membrane and surface reaction at low pressure membrane surface (permeate side). In the case of tubular (hollow fiber) membranes, the local oxygen permeation rate through a membrane is [46]:

$$J_{O_2} = \frac{k_r D_V[(p'_{O_2})^{0.5} - (p''_{O_2})^{0.5}]}{2(R_o - R_{in}).k_f (p'_{O_2} p''_{O_2})^{0.5} + \frac{R_m}{R_{in}}.D_V (p'_{O_2})^{0.5} + \frac{R_m}{R_{in}}.D_V (p''_{O_2})^{0.5}} \quad (2.12)$$

where R_o is the outer radius and R_{in} is the inner radius of the hollow membrane and $R_m = (R_o - R_{in}) / \ln(R_o / R_{in})$.

2.5 OXYGEN PERMEABILITY OF MIEC MEMBRANES

The first reports on oxygen permeation through dense oxide ceramics were published in the 1960s [47]. In spite of the high temperatures, the oxygen permeation was very low due to the low electronic conductivity of the investigated oxides with a fluorite structure limiting the whole oxygen permeation in ZrO_2, HfO_2 and ThO_2. It took 30 years to demonstrate the oxygen permeation in the system $La_{1-x}Sr_xCo_{1-y}Fe_yO_{3-\delta}$ crystallizing in the perovskite structure [48][49]. Nowadays the material development of MIECs is focused on perovskites and partly on related structures, such as on brownmillerites [50], K_2NiF_4 [51], and substitutes $Sr_4Fe_6O_{13}$ [52].

The dense oxygen permeating membranes made from mixed ionic electronic conducting ceramic materials were first reported by Teraoka *et al.* [48][49]. $LaFeO_3/LaCoO_3$ were partially substituted on the A (La) site with strontium to produce $La_{1-x}Sr_xCo_{1-y}Fe_yO_{3-\delta}$. This oxide exhibited mixed conducting behavior producing oxygen with permeation flux much higher than stabilized zirconia [53]. Highest O_2 flux for 1mm thick $SrCo_{0.8}Fe_{0.2}O_{3-\delta}$ membrane was observed to be 0.023 $molm^{-2}s^{-1}$ at 850°C and 1 atm partial pressure difference between the feed side and the permeate side

Steele [54] showed that the minimum oxygen permeation flux required by the membranes to sustain most of the technological applications is around 3.5 $cm^3cm^{-2}min^{-1}$ (0.026 $molm^{-2}s^{-1}$).

Most of the oxygen conducting ceramic materials of interest are from the perovskite oxides of the families $Sr(Co,Fe)O_3$, $La(Co,Fe)O_3$ and $LaGaO_3$, etc., Some important materials also have non perovskite structures. Current research trends in the area are targeted towards improving the oxygen permeability of these materials by improving their ionic and electronic conductivities. Another task regarding these materials is to improve the stability of these materials [27][55][18][18][56][57]. A summary of the promising materials to have surfaced through recent research efforts is as follows:

2.5.1 Perovskite-type Oxides

$Sr(Co,Fe)O_{3-\delta}$ (SCFO)

Typically, the membranes prepared from materials from this group of perovskite oxides exhibit high oxygen permeability. It was found that a partial substitution of A (Sr) or B (Co/Fe) cations can change the properties of these materials significantly. This substitution is undertaken by choosing appropriate metal ions with different valance states using doping strategies.

It was found that the oxygen permeability of these materials as well as their ionic conductivities decrease when the mean radius of the A lattice site cation decreases. For instance in the solid solutions of $Sr_{0.7}M_{0.3}CoO_{3-\delta}$ (M=La, Nd, Sm, Gd) the permeability decreases when the dopants are in the order of La>Nd>Sm>Gd [58]. In the perovskite oxide $Sr_{1-x}Bi_xFeO_{3-\delta}$ (partial substitution of Sr with Bi), the increase in Bi content was found to enhance the permeability of the material [59].

Oxygen permeability of the oxides of the type SCFO also depend on the rate of exchange between the membrane surface and the gas phase [60][61]. Surface modification techniques, such as acid treatment, can be used to improve this exchange rate [62]. As the oxygen pressure increases in the SCFOs, the surface exchange kinetics and the ionic conductivity of oxygen increase and decrease respectively. This results in bulk diffusion permeation to become the rate limiting step in permeation of oxygen [63].

SCFO type perovskite oxides have been found wanting when operating under low temperature or low pressure conditions, especially under reducing atmospheres. This is due to the presence of the alkaline earth cation in the lattice. In further development of

these materials, stability remains a key issue. Ti doped $SrFeO_3$ materials were studied by Kharton et al. [64][65] for this purpose. They found that the surface exchange kinetics, and thus the overall oxygen permeability, of the membranes can be improved by either coating the dense membranes with a porous coat of the same material or by introducing a mixture of Pt and praseodymium oxide on the feed side of the membrane. The resulting oxide was found to be stable above 770K in CO_2 containing atmosphere. At lower temperatures, however, a decomposition of the perovskite structure was observed along with formation of strontium carbonate on the surface.

Partial substitution of Co with metal cations like Cr, Cu, Mn, Ni, Ti were also investigated [22], [65]–[68]. Introduction of higher valance cation e.g. Ti or Cr into B site sublattice improves stability at the cost of decreased electronic conductivity and permeability [65]. Similarly, stability of these perovskites in CO_2 containing environments can be improved by creating a moderate deficiency of cations in sublattice A, but the permeability decreases.

Shao et al. [22], [69] partially substituted the Sr sublattice in $SrCo_{0.8}Fe_{0.2}O_{3-\delta}$ with barium cation to form $Ba_{1-x}Sr_x\ Co_{0.8}Fe_{0.2}O_{3-\delta}$. The phase stability of this perovskite oxide showed improvement and the conductivities also did not experience a decrease. The oxygen permeability for this membrane was recorded to be 1.19 $cm^3cm^{-2}min^{-1}$ for a flat disc of BSCF which was 1.5mm thick operated at 850°C . It was found that the suitable barium composition was from 0.3 to 0.5 moles, 0.3 being the optimum. A long term oxygen permeability test (1000 hours) at 850°C revealed that performance of BSCF

degrades slightly with the passage of time due to surface segregation and bulk phase decomposition [22].

In order to improve the stability of BSCF, the Sr ions can be completely replaced with the larger radius Ba (same valence state) and Ti ions (higher valence state). This results in the perovskite oxide $BaTi_{0.2}Co_{0.5}Fe_{0.5}O_{3-\delta}$. Its permeability is relatively high with (0.9 $cm^3cm^{-2}min^{-1}$) at 950°C [26], [27]. Zr doped material $BaCo_{0.4}Fe_{0.6-x}OZr_xO_{3-\delta}$ is another material with high oxygen permeability (0.9 $cm^3cm^{-2}min^{-1}$ at 800°C) with good stability.

La(Co,Fe)$O_{3-\delta}$ (LCFO)

These are oxygen conducting materials with high electronic conductivities [67][70]–[73]. Their oxygen permeability is lesser than $Sr(Co,Fe)O_{3-\delta}$ based ceramics but some of the problems encountered by the SCFOs are absent in these materials.

In LCFOs, the La (A site cation) can be partially substituted with metal cations of 2+ valance state like Ba, Sr and Ca. Candidates for partial substitutions of Co (B site cation) include Ga, Cr, Fe, Pb and Ni. Kharton et al. studied the B site partial substitution of cations [70], [74]–[77]. They found that in the perovskite oxide $LaCo_{1-x}Cr_xO_3$ (x=0.1-0.4) an increase in the Cr content causes the oxygen permeability, electrical conductivity and thermal expansion to decrease. If Ni is partially substituted in the place of Co, the ionic conductivity suffers a great deal but the electrical conductivity improves [74].Substitution of Co with Ni or Cr decreased the thermal expansion while substitution of Co(Fe) with Ti led to an increase in the thermal expansion as well as the oxygen ionic and electrical

conductivities. A partial substitution of Co with both Ni and Fe causes the crystal lattice to be rhombohedrally distorted perovskite $LaCo_{1-x-y}Fe_xNi_yO_3$ (x=0.1–0.2; y=0.1–0.3) [74][76]. Presence of Ni increases the oxygen nonstoichiometry, electrical and ionic conductivities and decreases the thermal expansion but doping of Fe has the opposite effect to that.

For substitution of A site La, Sr is the best candidate [72]. Partial substitution of La with Pb enhances the catalytic and electromagnetic activities of the ceramics [78]. Pb doped perovskites also showed better stabilities as compared to the Sr doped perovskites against sulphur dioxide poisoning. In La_{1-x} $Pb_xFeO_{3-\delta}$ (x=0.1–0.3), the permeability of oxygen and the electronic conductivity both increased with an increase in x but the final permeability is still considerably lesser than $La_{1-x}Sr_xFeO_{3-\delta}$ oxides.

Double site partial substitution resulting in the perovskite $La_{1-x}Sr_xCo_{1-y}Fe_yO_{3-\delta}$ (LSCF) has high permeability and very good stability [79][80][81]. In $LaSr_3Fe_{3-x}Co_xO_{10}$ oxides, the total conductivity increased with the increase in Co content but for $T > 400$ °C conductivities are adversely affected by increasing temperature because of a loss of oxygen vacancies [82]. Xu and Thompson [81] showed that $La_{0.6}Sr_{0.4}Co_{0.2}Fe_{0.8}O_{3-\delta}$ is very stable under air upto 960°C. Other researchers have shown that LSCF shows a small deterioration in the oxygen permeability when subjected to long term permeability experiments (1100 hours) [83][84]. $La_{0.2}Sr_{0.8}Cu_{0.4}Co_{0.6}O_{3-\delta}$ perovskite has high conductivities at high temperature with oxygen permeability comparable to other cobalt containing perovskites.

$LaGaO_3$ (LGO)

Thee oxides have higher ionic conductivity but lower electronic conductivity [77]. Complete substitution of Co with Ga enhances the ionic character of the bond between cations at B site and oxygen in the perovskite lattice. This results in more stability under reducing conditions, but the electronic conductivity is compromised as a result [85]. $LaGoO_3$ type oxides have low thermal expansion coefficients [86]. Various cation dopants (Ti, Cr, Fe, Co, Ni) and their concentrations were investigated to see their effect on the transport properties of $LaGaO_3$ based materials. Cations with higher valence state (ti and Cr) cause the ionic conductivity to decrease. However, small amounts of Fe or Co (~5%) increase it. $LaGa_{1-x}Ni_xO_{3-\delta}$ (x=0.2–0.5)solid solution has been found to have good oxygen permeability flux as well as thermal expansion coefficient [77]. If La is partially substituted with an alkaline earth cation, the electron or hole conduction is decreased. Partial substitution of La with Sr at the A site, and Ga with Mg at the B site, results in electric conductivity which increases with increased Sr content (maximum x = 0.1). In the system $La_{0.9}Sr_{0.1}GaO_3$, the electrical conductivity increases when Mg, Al or In partial substitution with 0.2 mol Mg giving the best result [87]. $La_{1-x}Sr_xGa_{1-y}Mg_yO_{3-\delta}$ (LSGM) has the best ionic conductivity [88]. LSGM, however, is pure ionic conductor in nature having negligible electrical conductivity. Further dopants can make it a mixed conductor. Ullman et al. [89] studied $La_{1-x}A_xM_{1-y}B_yO_{3-\delta}$ oxides with A=Sr^{2+}, Ln^{3+}, Ce^{4+}, M=Fe, Co, Ga and B = Co, Fe, Mg (x = 0.1–1, y = 0.1–0.5). The electrical conductivity

of the LSGM can be increased by doping Co or Fe. Tables 2.1 summarizes the permeability values of all the perovskite materials discussed above.

Table 2.1 Oxygen permeability of perovskite type MIEC oxides

Composition	Oxygen Permeation (800–1000°C) $\mu mol.cm^{-2}.s^{-1}$	Ref
$SrCo_{0.8}Fe_{0.2}O_{3-\delta}$ 1.5 mm	0.43–0.93	[60]
$Sr_{0.7}M_{0.3}CoO_{3-\delta}$ (M = La,Nd,Sm,Gd) 1.4 mm	0.26–0.041 ↓	[87]
$Sr_{1-x}La_xCoO_{3-\delta}$ (x = 0.3–0.35) 1.4 mm	0.28–0.17 ↓	
$Sr_{0.97}Fe_{0.8}Ti_{0.2}O_{3-\delta}$ 1.0 mm	0.066–0.398	[90][65]
$Sr_{0.97}Fe_{0.4}Ti_{0.6}O_{3-\delta}$ 1.0 mm	0.025–0.112	
$CaFe_{0.2}Ti_{0.8}O_{3-\delta}$ 1.14 mm	$(0.32–7.9) \times 10^{-3}$	[91]
$Ba_{0.5}Sr_{0.5}Co_{0.8}Fe_{0.2}O_{3-\delta}$ 1.5 mm	0.67–1.15	[22]
$BaBi_xCo_{0.2}Fe_{0.8-x}O_{3-\delta}$ (x = 0.1–0.5) 1.5 mm	0.223–0.744	[92]
$LaCo_{0.9}Cr_{0.1}O_{3-\delta}$ 1.4 mm	0.04–0.08	[74]
$LaCo_{0.7}Ni_{0.3}O_{3-\delta}$ 1.0 mm	0.04–0.12	
$LaFe_{1-x}Ni_xO_{3-\delta}$ (x = 0.2–0.5) 1.0 mm	0.0043–0.086	[75]
$LaCo_{0.8}Fe_{0.1}Ni_{0.1}O_{3-\delta}$ 1.0 mm	$(0.46–1.08) \times 10^{-3}$	[76]
$LaCo_{0.7}Fe_{0.1}Ni_{0.2}O_{3-\delta}$ 1.0 mm	$(1.68–3.2) \times 10^{-3}$	

Composition	Oxygen Permeation (800–1000°C) μmol.cm^{-2}.s^{-1}	Ref
$LaCo_{0.6}Fe_{0.2}Ni_{0.2}O_{3-\delta}$ 1.0 mm	$(0.27–1.17) \times 10^{-3}$	
$LaCo_{0.5}Fe_{0.2}Ni_{0.3}O_{3-\delta}$ 1.0 mm	$(1.57–3.11) \times 10^{-3}$	
$La_{0.3}Sr_{0.7}CoO_{3-\delta}$ 1.15 mm	0.32–1.0	[72]
$La_{0.2}Sr_{0.8}CoO_{3-\delta}$ 0.5 mm	0.644 at 850°C	[93]
$La_{0.9}Pb_{0.1}FeO_{3-\delta}$ 1.0 mm	(0.001–0.002 at 1000°C	[78]
$La_{0.6}Sr_{0.4}Co_{0.2}Fe_{0.8}O_{3-\delta}$	0.03–0.3	[94][83] [84]
$La_{0.2}Sr_{0.8}Co_{0.2}Fe_{0.8}O_{3-\delta}$	0.11–0.89	
$La_{0.8}Sr_{0.2}Co_{0.8}Fe_{0.2}O_{3-\delta}$ 0.5mm	0.25–0.83	[86]
$La_{0.6}Sr_{0.4}Co_{0.8}Fe_{0.2}O_{3-\delta}$	4.46×10^{-3} at 850°C	[80]
$La_{0.2}Sr_{0.8}Co_{0.6}Cu_{0.4}O_{3-\delta}$0.8mm	0.12–0.60	[95]
$LaGa_{1-x}Ni_xO_{3-\delta}$ (x = 0.2–0.6) 1.0 mm	0.019–0.066	[75]
$LaGa_{0.8}Ni_{0.2}O_{3-\delta}$ 1.0mm	0.0447–0.0891	[70][96]
$LaGa_{0.4}Mg_{0.2}Co_{0.4}O_{3-\delta}$ 1mm	0.050–0.0631	[86]
$LaGa_{0.3}Mg_{0.1}Co_{0.6}O_{3-\delta}$ 1 mm	$(0.4–10) \times 10^{-3}$	
$LaGa_{0.4}Mg_{0.25}Co_{0.35}O_{3-\delta}$ 1mm	0.038–0.05	
$La_{0.8}Sr_{0.2}Ga_{0.8}Fe_{0.2}O_{3-\delta}$ 0.5 mm	0.35–0.52	
$La_{0.8}Sr_{0.2}Ga_{0.7}Fe_{0.3}O_{3-\delta}$ 0.5 mm	0.41–1.03	
$La_{0.8}Sr_{0.2}Ga_{0.7}Ni_{0.3}O_{3-\delta}$ 0.5mm	0.37–0.73	
$La_{0.8}Sr_{0.2}Ga_{0.7}Co_{0.3}O_{3-\delta}$ 0.5mm	0.23–1.1	

2.5.2 Non-perovskite-type Oxides

All the mixed conductivity carrying materials discussed thus far have been perovkite oxides in their structure. In addition to these materials, there are some non perovskite materials as well that exhibit mixed ionic electric conduction properties. $SrFeCO_{0.5}O_x$ is one such material [97]. It was found to have excellent phase stability when it was tested for more than 1000 hours in reducing environment [98]. In another such material, $Sr_4Fe_{6-x}Co_xO_{13+\delta}$ ($1 \leq x \leq 3$), the oxygen flux increased with increase in Co content [99]. $Sr_4Fe_4Co_4O_{13+\delta}$ was found to have better structural and chemical stability than the perovskite $SrFe_{0.2}Co_{0.8}O_{3-\delta}$ at high temperature and low oxygen partial pressure [100].

Another type of non-perovskite MIEC is $La_2Cu_{1-x}Co_xO_{4+\delta}$ ($0 \leq x \leq 0.3$) was found to have K_2NiF_4 structure [101]. It had very good electric conductivity and the partial substitution of cobalt in copper sublattice site resulted in elevated permeability ($x = 0.02 - 0.1$). Above $x = 0.1$, the permeation starts to decrease. Due to absence of alkaline earth metal cation these materials exhibit significant stability with no phase change observed even after being in operation for more than 12 months.

2.6 DUAL PHASE MEMBRANES

As discussed already, the overall oxygen permeability of a good mixed conducting material should have high ionic as well as high electronic conductivity. It is often very hard to find this condition fulfilled in a single material. A solution to this problem can be found in dual phase membranes. The first reported instance of such material involved the use of yttrium stabilized zirconia (YSZ) as an ion conductor and a metal (silver or gold)

as electronic conductor [102]. In dual phase membranes, the ionic conductor normally forms the continuous phase whereas the electronic conductor is interspersed consistently forming a network. These types of membranes give a wide variety of options in terms of material selection and membrane fabrication.

Figure 2.4 shows a schematic of a dual phase membrane with a continuous ion conducting phase and a uniformly distributed electronic conductor phase. Several researchers have tried different combinations like yttria stabilized zirconia palladium and, erbia stabilized bismuth silver or gold [103][104][105]. It was found that a mixture of about 40 vol. % of metal in the ceramic material is sufficient to obtain significant electron conductivity. The limiting step in the permeability of oxygen was found to be the bulk diffusion for down to 1mm thick membranes. Below that both surface exchange kinetics and bulk diffusion are believed to be limiting factors.

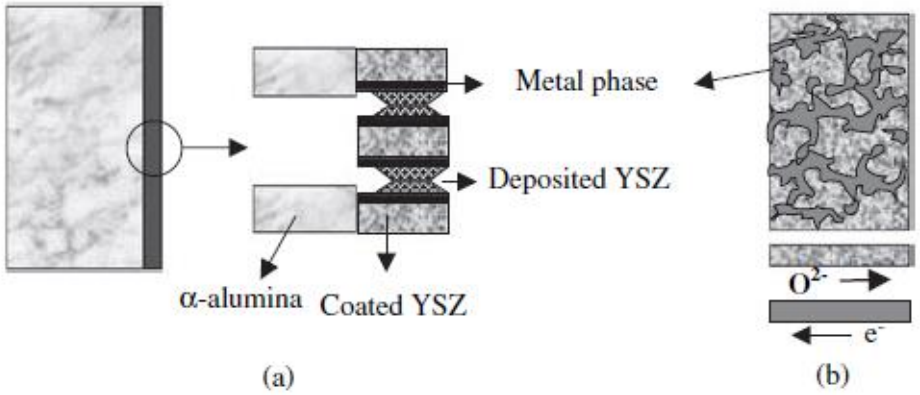

Figure 2.4 Depiction of dual phase membranes: (a) structure; (b) oxygen transport mechanism[45].

In addition to dual phase membranes comprising of ceramic and metallic phases, they have also been prepared from two different ceramic materials. One of these ceramic materials has high ionic conductivity whereas the second one has good electronic conductivity [106][107]. The examples of such membranes include the membranes prepared from gadolinia doped ceria electrolyte $Ce_{0.8}Gd_{0.2}O_{2-\delta}$ perovskite-type $La_{0.8}Sr_{0.2}Fe_{0.8}Co_{0.2}O_{3-\delta}$ and $La_{0.15}Sr_{0.85}Ga_{0.3}Fe_{0.7}O_{3-\delta}$-$Ba_{0.5}Sr_{0.5}Fe_{0.2}Co_{0.8}O_{3-\delta}$.

2.7 ENHANCEMENR OF THE OXYGEN PERMEABILITY

2.7.1 Increasing Partial Pressure Difference

In addition to improving inherent material properties, there are further opportunities to enhance the oxygen permeation. One of these is to increase the difference in the oxygen partial pressures at the feed and permeate side. Obviously, very low oxygen partial pressure at the permeate side increases the oxygen drive through the membrane. Therefore, the use of sweep gases that consume oxygen enhances the permeation significantly, but the material demands are very high as using such sweep gases generally has unwanted side effects. Real industrial gases such as flue gas contain CO_2, NO_x, SO_2, and dust. Therefore, majority of high flux materials cannot be used with recirculating flue gas and stable materials have to be developed [36]. Otherwise the driving force has to be realized by compression of feed air, also an energy consuming process. Therefore, high feed overpressures must be avoided, but this also limits the level of oxygen enrichment. The production of pure oxygen is possible in the absence of a sweep gas, which also

makes the gas management simpler. However, the whole driving force has to be realized by compression of air or extraction of oxygen with vacuum. The energy demand for compression of an excess of feed air is much higher than the extraction of oxygen by vacuum due to a much lower gas volume. [108].

2.7.2 Asymmetric Membranes

A second opportunity for a distinct enhancement of the oxygen flux for a given material under fixed operating conditions is a decrease in the separation layer thickness. Obviously the mechanical stability required for the separation membrane, for example against different absolute pressures, can be achieved by a porous support coated with a dense MIEC separation layer. This concept, called an asymmetric membrane. Such membranes were developed by different groups and significant enhancements of oxygen permeation were described [109][110][111][112][110].

The structure of asymmetric membrane comprises of a thin dense membrane layer supported on a maqcroporous membrane layer for mechanical strength and stability. Interlayers of graded porosity can be used between the macroporous support and the thin dense layer. Catalytically active material can also be incorporated in these layers. In some cases a porous catalytic layer is also deposited on top of the dense layer. One of the problems with the asymmetric membranes is that a disparity in the thermal expansion behavior of support membrane and dense membrane materials can cause the failsure of the thin layer. Perovskite materials have unique thermal expansion behavior, so asymmetric perovskite membranes are normally prepared by supported a thin dense

perovskite on a porous perovskite membrane of the same material or one having similar composition.

Li et al. [113] prepared an asymmetric BSCF membrane with a dense layer on top of a porous BSCF membrane. The thickness of the substrate was 0.9mm and that of the dense layer was 20μm. The oxygen permeability flux of the asymmetric membrane reaches a maximum value of 32.5mlmin^{-1}cm^{-2} with pure oxygen at feed side and vacuum on the permeate side. In comparison, a dense BSCF membranes shows an oxygen flux of less than 5 mlmin^{-1}cm^{-2} when the pressure gradient $ln(pO_{2,\,feed} / pO_{2,permeate})$ was kept at 4 at a temperature of 900°C). Menzler et al. tried preparing the asymmetric BSCF membranes with the tape casting technology [114].

In a study by Kovalevsky et al. [115] an asymmetric BSCF membrane was prepared using uni-axial compaction. The flat three-layer asymmetric membranes were fabricated by a three-stage uniaxial compaction procedure. In order to prepare the porous support, BSCF powder mixed with 4 wt.% of Degalan P24 and 27 wt.% of graphite was compacted using a press. Then an dense layer was formed on top of the compact by adding BSCF powder with 3 wt.% of the binder. This powder was also flattened and compacted in the press. The third layer, a porous activation layer, was prepared by adding a calculated amount of the powder similar to that in the first case (BSCF, Deggalan and Graphite) and the whole structure was compacted to form a three layer asymmetric membrane. The oxygen fluxes through these membranes at 1223 K were ~1.5 times higher than those for a 1.00 mm thick symmetric membrane

Haworth et al. [116] prepared yttrium doped BSCF membranes coated with silver. They reported no particular improvement in the oxygen permeation flux of silver coated membranes with respect to uncoated membranes when flat membranes of thicknesses greater than 0.5mm were tested. Hollow fiber membranes of 0.3mm wall thickness, however, showed an improvement between 20-55% in temperature range of 600-900°C. They also calculated the average critical thickness of the BSCFY membranes to be 0.4mm.

Recently Shen et al. [117] tried coating BSCF membranes with double layer perovskite structure materials $RBaCo_2O_{5+\delta}$ (R112, R=Y, Pr, Nd, Sm, Gd). The mixtures of 60 wt% of R112 powders, 20 wt.% glycerol and 20 wt.% ethanol were coated on both surfaces of BSCF membranes using a spin-coating apparatus which was operated at 4000 rpm for 30 s. The oxygen permeation fluxes increased according to the order of Pr112 < Nd112 < Sm112 < Gd112.

$La_{0.7}Sr_{0.3}CoO_3$ powders were screen-printed on both surfaces of BSCF membrane to result in ~20m-thick layer by Hong and Choi [118]. The JO_2 values of all membranes increased with surface coating regardless of membrane thickness.

Kim et al. [119] proposed a method to improve permeability of oxygen and stability of BSCF tube membrane by coating a layer of $La_{0.6}Sr_{0.4}Ti_{0.3}Fe_{0.7}O_{3-\delta}$ (LSTF). The oxygen permeation fluxes at the starting time were 2.31 and reached a value of 1.67 ml/cm^2 min ($\Delta \cong -28\%$) at the ending time of stability test. In comparison the uncoated

BSCF tubular membrane decreases from 2.14 to 1.16 ml/cm^2 min ($\Delta \cong -46\%$) in similar conditions.

Lobera et al. [120] prepared a membrane with a thin layer of $Ce_{0.9}Gd_{0.1}O_{1.95-\delta}$ (CGO), on a porous CGO substrate. The top of the membrane was also coated using two different porous layers of BSCF and CeTbO+Co, respectively, aiming to improve the oxygen activation rate on the permeate side. Zhu et al. [121] coated BSCF porous layer on the membrane surfaces made from $BaCe_{0.15}Fe_{0.85}O_{3-\delta}$. They showed that such coating could effectively accelerate the surface oxygen exchange rate, thus greatly improve the oxygen permeability of the membrane

A lot of R&D is also in progress to make metallic supports for perovskite thin membranes [122]. If these efforts prove to be successful, it will be possible to choose the substrate material from ceramics other than perovskites or metals. This would make it easier to have oxygen transport membranes with much better mechanical stability and joining technology and lower cost. The greatest issue with such membranes seems to be leakage of the thin crystalline separation layer due to bad selectivity. In many cases these leakages were caused by the use of porous ceramic supports with an expansion behavior not well adjusted to the complex expansion behavior of the MIEC separation layer [123]. Therefore, the use of identical material compositions for the porous support and the dense separation layer were recommended.

Oxygen permeation values of thin MIEC membranes fall well below the expectations from the Wagner equation. This is caused by the surface exchange reactions limiting the oxygen transport for thin membranes. This means that no further increase in the oxygen permeation takes place below a critical membrane thickness L_c [12] given by the following equation:

$$L_c = D_V / k_s \tag{2.13}$$

The state of the art in large scale oxygen production using asymmetric membranes is currently represented by Air Products and Chemicals (APC) (Allentown, PA, USA) [124].

2.7.3 Hollow Fibre Membranes

Some researchers have preferred using membranes in the shape of hollow fibres over planar disc shaped membranes. A major advantage of hollow fibers is high package density of membrane area per unit reactor volume together with relatively low membrane thicknesses [125][126][127]. In principle, small reactors with high oxygen fluxes can be realized as demonstrated by Tan et al. [128]. They used LSCF6428 hollow fibers for a demonstration unit producing oxygen at 1070°C; oxygen was extracted by a vacuum pump. However, the joining of hollow fibers was effected with a silicon polymer sealant that did not withstand temperature of more than 350°C. Therefore, the reactor design was not suitable for use with hot gases preheated in a heat exchanger and did not utilize the whole built-in membrane area.

2.8 SEALING PROCEDURES FOR ION TRANSPORT MEMBRANES

The operational temperature for this oxygen separation process through ion transport membranes is typically from 700-1100°C depending on the material used to prepare the ITM. Sealing the membranes at such high temperature is a critical issue. If the membrane is not sealed perfectly, the air from the surroundings will mix with the separated oxygen on the permeate side of the membrane. Sealing systems able to withstand the high operating temperatures has been recognized as a key area in the commercialization of ITM technology for oxy-fuel processes [129].

During the initial years of the ITM technology, many researchers tried to seal the ceramic membranes between metallic support tubes by brazing. Standard reactive metal brazing technology using titanium as an active element cannot be used due to the high vacuum required at high temperatures during brazing [130]. These conditions destroy the required crystal structure in the membranes. A more promising solution is reactive air brazing (RAB) based on Ag–CuO brazes, which is performed in atmospheric air instead of a high vacuum [131]. The bond thus formed becomes a permanent one upon cooling. Finding a sealing material with good thermal and chemical compatibility with the ITM as well as the support tubes made of appropriate material is a critical issue here. Moreover in the laboratory experiments the support tubes are usually made from ceramic materials like alumina or quartz instead of metal due to high operating temperatures.

To address these problems some researchers sealed the membranes using silver paste [116][132][133][134][135]. The membrane edges were coated with silver paste and then the membrane was placed inside the ceramic tubes and heated to around 925°C to soften the silver and form a seal. Silver being an inert metal doesn't react with the membrane or the support surface but this type of sealing limits the experimental temperature to be below the melting point of silver (~965°C). Silver rings, instead of silver paste have also been successfully used as a seal [121]. In order to be able to do experiments at higher temperature, gold rings [81][113][118][120][136][137][138][139] or gold paste [140][141][142][143][144] was also employed as sealing materials. Using gold is obviously more expensive but it has the advantage of having a higher melting temperature, so the permeability setup temperature can be increased as high as 1050°C.

Several researchers have also attempted to use glass in the form of rings or paste to seal the membrane/support tube setup [133]. The setup seals when the glass melts to fill the gaps between the membrane and the tube. However at temperatures above the softening point of the glass, it continues to flow which may result in a loss of sealing. Also glass may react at high temperatures with the membrane causing the seal to break. It also tends to diffuse towards the center of the membrane from the edges which causes the effective area available for permeability to reduce and errors in the calculation of oxygen flux occur. Some researchers have opted for a mixture of glass and ceramic powders to form a paste which seals at high temperature. One such method is to mix strontium cerate

powder with Pyrex glass. Sodium aluminate and boron oxide are added and then this mixture is used as a sealant in paste form [145][146].

Normally when a seal made of materials other than the constituent materials of membranes and support tubes are employed, they cause the membranes to crack upon cooling due to a difference of thermal expansion coefficients. Wetting of these materials with the membrane and support tube is another issue to be looked at.

2.9 OXYGEN SEPARATION WITH O_2 TRANSPORT MEMBRANES IN POWER PLANTS

The membrane based oxy-fuel power plant process is considered to be the most energy efficient carbon capture and storage technology, but its efficiency strongly depends on the process integration of the membrane unit. Compared with the currently available post-combustion process, in which CO_2 is separated from the flue gas at the very end of the process, the energy penalty of the oxy-fuel technology is considered to be lower.

Nevertheless, there is still a high energy demand for the production of pure oxygen required by the process. The state of the art production process for oxygen is cryogenic air separation, in which total efficiency losses of 8-12% have been estimated for a Greenfield oxy-fuel power plant [147], mainly caused by the cryogenic air separation unit (ASU). Ceramic MIEC membranes used for oxygen separation can give infinite

selectivity at high temperatures. The required operating temperature is achieved by efficient integration of the membrane into the power plant process.

2.9.1 MIEC Membrane Operating Concepts in Power Plants

Membranes used for separating oxygen from air in oxy-fuel processes can be functioned with a ***four-end*** [148]or ***three-end design*** [149]. In a four end membrane concept, a stream of sweep gas is introduced to the permeate (low pressure) side in order to remove the oxygen produced by the membrane. Thereby the concentration of oxygen on this side of the membrane is reduced, increasing the partial pressure difference and hence the oxygen transport across the membrane. In the three end concept, the partial pressure difference to maintain the driving potential of the oxygen across the membrane is maintained by increasing the oxygen pressure on the feed side or by decreasing it on the permeate side by applying vacuum (Figure 2.5). The chemical stability demands put on the membrane materials for these membrane operating concepts are dissimilar as shown in Figure 2.6. In the three end membrane operation, the membrane material only interacts with air (Process routes A and B in Figure 2.6). This allows the use of a variety of materials for membrane development that can be enhanced and improved for high flux of oxygen without many limitations. On the other hand, in the four end concept the membrane material is directly exposed to the flue gas on the permeate side, so the membrane material has to be selected such that it is able to resist all components of the flue gas without compromising on an acceptable flux of oxygen (Process routes C and D in Figure 2.6). For the three end concept, BSCF is widely used material, since the oxygen

flux is much higher than the materials considered appropriate for interaction with the flue gas. The heat required to run at the operating temperature is delivered by the sweep gas in the four-end concept or the air in the three-end concept.

The specific O_2 permeation of the membrane is calculated by the Wagner equation, a simplified form of which is:

$$j_{O2} = C_{\text{Wagner}} \frac{T_{\text{Mem}}}{d_{\text{Mem}}} e^{-\frac{k_{\text{Wagner}}}{T_{\text{Mem}}}} \ln \Pi_{O_2} \tag{2.14}$$

where j_{O2} is the specific flux of oxygen ($molm^{-2}s^{-1}$) and C_{Wagner} and k_{Wagner} are inherent material constants for the membrane which are found experimentally (values for perovskites such as BSCF were determined as 1.004×10^{-6} mol $m^{-1}s^{-1}K^{-1}$ and 6201 K, respectively), T is the operating temperature, and d is the active thickness of the membrane in meters.

The mean O_2 partial pressure ratio Π_{O_2} depends on the process variant and the chosen boundary conditions. It is influenced by

- The O_2 separation ratio ξ, defining the ratio of the separated O_2 flow to the entering O_2 flow of the air, influencing the oxygen partial pressure in the retenate
- The applied feed pressure
- The mean O_2 partial pressure on the sweep and permeate side.

$$\text{Four End:} \quad \Pi_{O_2} = \frac{p\left(O_{2,\text{feed}}\right) + p\left(O_{2,\text{retenate}}\right)}{p\left(O_{2,\text{sweep}}\right) + p\left(O_{2,\text{permeate}}\right)} \tag{2.15a}$$

$$\text{Three End:} \quad \Pi_{O_2} = \frac{p\left(O_{2,\text{feed}}\right) + p\left(O_{2,\text{retenate}}\right)}{2p\left(O_{2,\text{permeate}}\right)} \tag{2.15b}$$

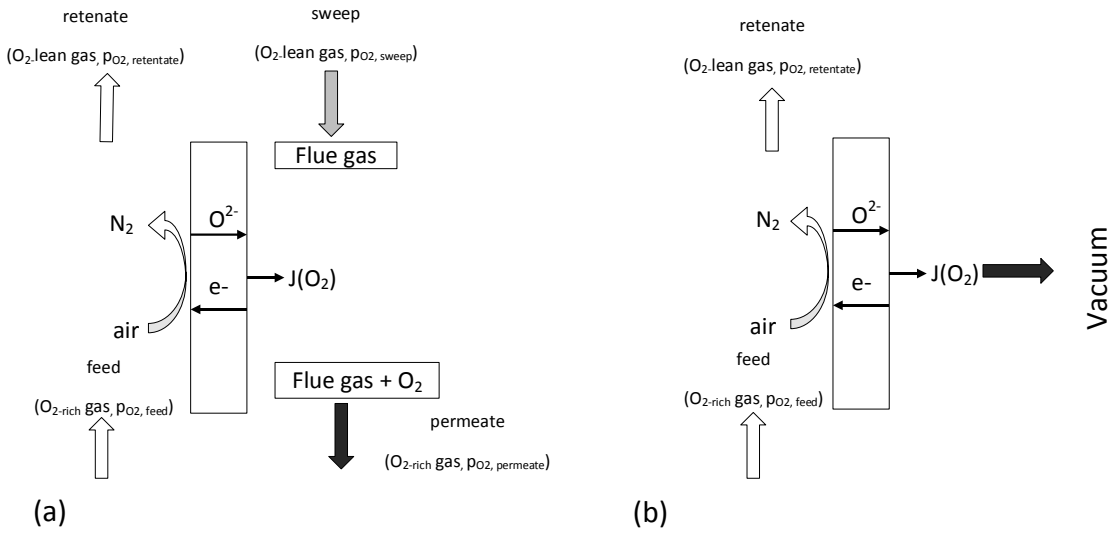

Figure 2.5 Oxygen separation by MIEC membranes: (a) four-end operation; (b) three-end operation. Adapted from [148].

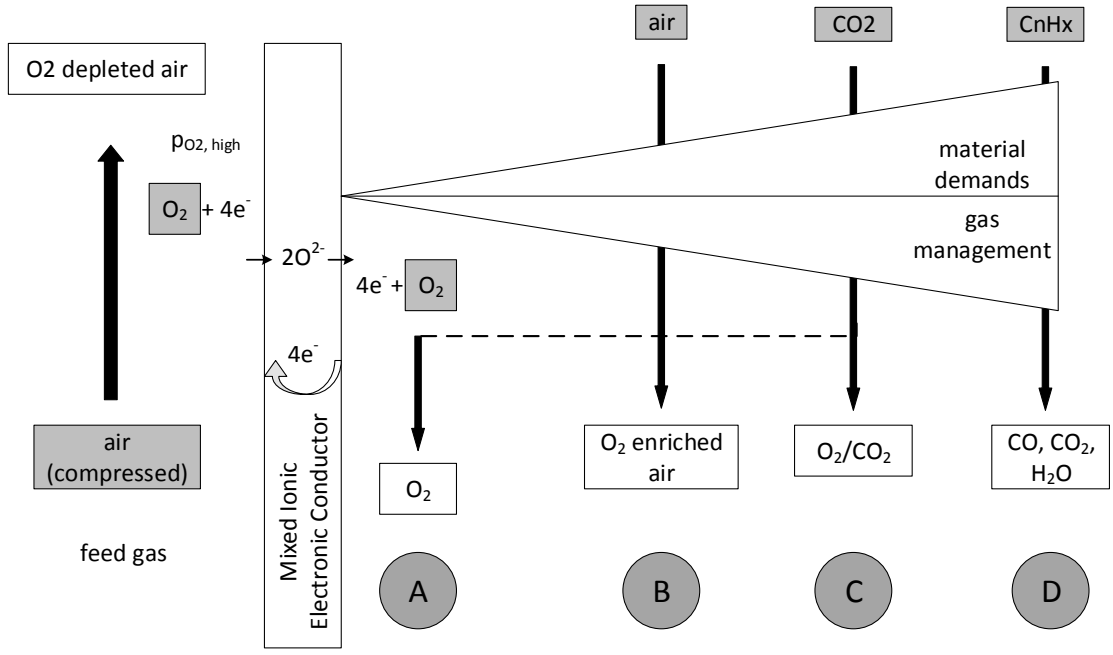

Figure 2.6 Oxygen separation with MIEC membranes: functional principle and process variants [150].

2.10 STABILITY ISSUES WITH ION TRANSPORT MEMBRANES IN POWER PLANT ENVIRONMENT

One of the major contributors to the CO_2 emissions (40%) is Power plants, that operate with fossil fuel[151]. There are three possible technical solutions for CO_2 capture in fossil-fuel power plants: post-combustion, pre-combustion, and oxy-fuel combustion[152][153]. In the oxy-fuel combustion fuel is burnt in a pure oxygen atmosphere and produces high concentration of CO_2 and water steam, which can be

easily condensed. Pure oxygen environment, inside the reactor, can be generated by either external oxygen supply or internal oxygen extraction using ion transport membranes (ITM). It has been validated [154][155] that ITMs are excellent candidates for oxy-fuel combustion because of their low energy consumption and their easy integration into membrane reactors.

It has been demonstrated that the efficiency of oxy-fuel power plants based on Oxygen-ion Transport Membranes (OTMs) is higher than those operating with cryogenic distillation [156]. Kunze and Spliethoff [157] evaluated the efficiency of the three carbon capture routes (post-combustion, pre-combustion and oxy-fuel combustion) in Integrated Gasification Combined Cycle (IGCC). They concluded that the process using OTMs revealed better net efficiency and had excellent long term potential.

Since Teraoka et al. [49] first reported the remarkable high oxygen permeation flux through membranes from the $La_{1-x}Sr_xCo_{1-y}Fe_yO_{3-\delta}$ (LSCF) perovskite oxides, cobalt-containing perovskite membranes have been widely investigated. The cobal containing perovskites have been reported to have poor chemical stability but are found to act stably under strict partial oxidation conditions[7,8]. It has already been discussed that among these membranes, $Ba_{0.5}Sr_{0.5}Co_{0.8}Fe_{0.2}O_{3-\delta}$ (BSCF) membranes have the highest oxygen permeability. Some researchers have tried to prepare perovskite membranes from cobal free compositions to improve upon the chemical stability. Examples include perovskites prepared from La–Sr–Ga–Fe [86], Be–Ce–Fe [159] and Ba–Sr–Zn–Fe [160]. However,

so far, no cobalt free material has been able to match the oxygen permeation fluxes of BSCF.

In a power plant environment, the flue gas stream volume consists of about 25 to 30% water vapor, 70 to 75 % CO_2, 1-3 % O_2, and 400 ppm SO_2 concentration [16]. BSCF membranes, with the highest oxygen permeability [153], are one of the best membrane candidates for oxygen separation in power plant reactors. However, recent studies have shown that BSCF is not an ideal material for long-term service in CO_2 containing environment. This is due to its high reactivity and the formation of $(Ba,Sr)CO_3$ compounds at the operating temperatures[140], [161]. These instability issues lead to severe degradation in the performance of the BSCF membranes [32], [162].

Many researchers have tried to investigate the performance of the ITMs by measuring oxygen permeability while using CO_2 (pure or mixture) as a sweep gas [16][140][115]. The results show that as soon as the inert carrier gas is switched to CO_2 at the sweep side, the permeability of BSCF membranes deteriorate greatly. Other researchers have exposed the BSCF membranes to CO_2 rich environment and used various characterization techniques like XRD, TG/DSC, SEM/EDS etc. to determine the reason for this deterioration [161][32][163]. A reaction zone was observed to be formed on the surface of BSCF membranes when annealed in CO_2 containing atmosphere [16]. This layer was determined to be a mixed barium and strontium carbonate of the form $(Ba_xSr_{1-x})CO_3$. It was found that this carbonate layer covers the complete surface of the BSCF pallet when annealed at 700°C and 800°C, but for 600°C only few spots of the surface were covered.

In order to solve the stability issue with BSCF, researchers have tried to modify the membrane materials by doping or replacing the A or the B site of the perovskite structure with other elements. For example, Kim et al. [164] showed that Lanthanum doped BSCF showed good stability under air, CO_2 containing atmosphere, and low oxygen partial pressure. Wang et al. [165] showed that Nb doping could improve the stability of BSCF against CO_2. Efimov et al. [166] considered different calcium containing perovskite materials and concluded that $La_{0.6}Ca_{0.4}Co_{0.8}Fe_{0.2}O_{3-\delta}$ (LCCF) was one material which, not only retained perovskite structure at high temperatures but also showed constant oxygen flux in CO_2 rich environment without showing any formation of carbonates. Another material investigated for its use as ITM in oxy-fuel combustion was $La_{0.6}Sr_{0.4}Ti_{0.3}Fe_{0.7}O_{3-\delta}$ (LSTF) which showed strong resistance and durability for CO_2 environment but its oxygen flux was found to be relatively low[167]. A cobalt free composition $BaFe_{0.55}Nb_{0.45}O_{3-\delta}$ was tested for oxygen permeability by Yi et al. [168] with CO_2 as sweep gas. It did not show any significant degradation. Similarly, Engels et al. [16] showed that the compositions $Sr_{0.5}Ca_{0.5}Mn_{0.8}Fe_{0.2}O_{3-\delta}$ (SCMF) and $La_2NiO_{4+\delta}$ (LNO) had high chemical stability in the presence of CO_2 but they do display instability when 360ppm SO_2 was introduced in the sweep. All of these materials, discussed so far, have better chemical stability than BSCF but considerably low oxygen permeability. Chen et al. [169] measured the oxygen permeability of perovskite-type oxide $SrCo_{0.8}Fe_{0.2}O_{3-\delta}$ (SCF). They showed that using pure CO_2 as sweep gas, the membrane starts to degrade immediately. A summary of chemical stability of ITM materials is presented in Table 2.2,

which confirms that most OTMs with high oxygen permeability flux show relatively poor stability in CO_2 environment; whereas, all stable OTMs have low permeation flux.

Table 2.2 Summary of oxygen permeability and chemical stability of OTMs

Membrane composition	Thickness	Temperature (°C)	O_2 permeation flux using inert sweep-gas (μmol.cm^{-2}.s^{-1})	O_2 flux in presence of 100% CO_2 in the sweep-gas (μmol.cm^{-2}.s^{-1})	Ref.
$Ba_{0.5}Sr_{0.5}Co_{0.8}Fe_{0.2}O_{3-\delta}$	30μm asymmetric	900	1.58	0.02 after 200 hours	[115]
$Ba_{0.5}Sr_{0.5}Co_{0.8}Fe_{0.2}O_{3-\delta}$	1mm	875	1.27	0.017 after ½ hour	[140]
$Ba_{0.5}Sr_{0.5}Co_{0.8}Fe_{0.2}O_{3-\delta}$	1.15 mm hollow tube	900 (air at 10 bar)	1.91	0.07 after 1 hour	[16]
$Sr_{0.5}Ca_{0.5}Mn_{0.8}Fe_{0.2}O_{3-\delta}$	1.0 mm hollow tube	900 (air at 20 bar)	0.085	0.082 after 20 hours	[16]
$La_2NiO_{4+\delta}$	1.0 mm hollow tube	900 (air at 5 bar)	0.075	0.075 after 100 hours	[16]
$La_{0.6}Ca_{0.4}Co_{0.8}Fe_{0.2}O_{3-\delta}$	1.0 mm	900	0.18	0.10 after 100 hours	[166]
$La_{0.6}Sr_{0.4}Ti_{0.3}Fe_{0.7}O_{3-\delta}$	1.6 mm	900	0.06	XRD shows stable phase after 170 hours	[167]
$BaCo_{0.7}Fe_{0.2}Nb_{0.1}O_{3-\delta}$	NA	900	0.89	Nil after 25 hours	[168]
$BaFe_{0.55}Nb_{0.45}O_{3-\delta}$	NA	900	0.008	0.007 after 6 hours	[168]
$SrCo_{0.8}Fe_{0.2}O_{3-\delta}$	1.0 mm	950	0.82	Nil after 25 hours	[169]
$(Pr_{0.9}La_{0.1})_2(Ni_{0.74}Cu_{0.21}Ga_{0.05})O_{4+\delta}$	0.8 mm	975	0.23	0.22 after 250 hours	[40]

OTM based oxy-fuel power plants could be operated with either a four-end or a three-end design [170]. In a four-end design an oxygen consuming sweep (syngas or methane) is delivered to the permeate (low pressure) side of the membrane. In this way the partial pressure difference across the membrane is maintained, hence continuous oxygen supply

through the membrane [170]. The membrane, in this case, is in a state of a direct contact with the flue-gas; therefore, the material has to resist all components of the flue-gas while producing an acceptable flux of oxygen. Stadler et al. have shown that a power plant based on the four-end concept has better efficiency than that of the three-end concept. On the other hand, in a three-end concept, the production of oxygen is sustained by either applying higher pressure on the feed side or by removing the permeated oxygen using vacuum [11]. The membrane, in this case interacts only with air, can be made from many different materials of high oxygen flux. For this reason, a three-end design concept is considered to be more suitable due to the absence of rigorous chemical stability of the membrane [156]. Castillo [171] has studied BSCF material in three-end membrane concept and has shown that the overall plant efficiency could be 4% higher than that based on cryogenic technology. Gupta et al. [172] have used a tubular OTM device consisting of three layers (oxygen incorporation, oxygen separation, and fuel oxidation layers). The performance of these OTM tubes has been tested in a coal derived syngas fuel. The material used in this process was 40 vol% $(La_{0.825}Sr_{0.175})_{0.94}Cr_{0.72}Mn_{0.26}V_{0.02}O_{3-\delta}$ and 60 vol% $Zr_{0.802}Sc_{0.18}Y_{0.018}O_{1.901}$. The oxygen flux of the membrane was relatively low but stable for 80 hours of continuous operation. Another case of CO_2 capture via direct oxy-fuel combustion was reported using methane [173]. The membranes were made in the form of U-shaped hollow fiber of $(Pr_{0.9}La_{0.1})_2$ $(Ni_{0.74}Cu_{0.21}Ga_{0.05})$ $O_{4+\delta}$ (PLNCG). These membranes were operating for 450 hours with good stability but the oxygen flux values were much lower than that of BSCF membranes.

2.11 TOWARDS REALIZATION – MODULE DESIGN

Process calculations indicate that the membrane-based oxy-fuel technology is the most promising carbon capture and storage measure. Various efforts have been started towards the realization of membrane technology for oxy-fuel combustion. Since most of the process components are adaptable state of the art power plant processes, current research is focused on the membrane material and how to integrate it into a fossil fuel-fired power plant.

Figure 2.7 shows the most important issues for the application of MIEC membranes in a power plant process. All the requirements interact with or even contradict each other. For instance the membranes providing the highest flux are chemically unstable and unacceptable for operation in the four-end module. Similarly, raising the operating temperature, or making thinner membranes enhances the oxygen production but they have, amongst others, influences on the thermal stability and mechanical strength. Some research and development activities in this field are presented in this section.

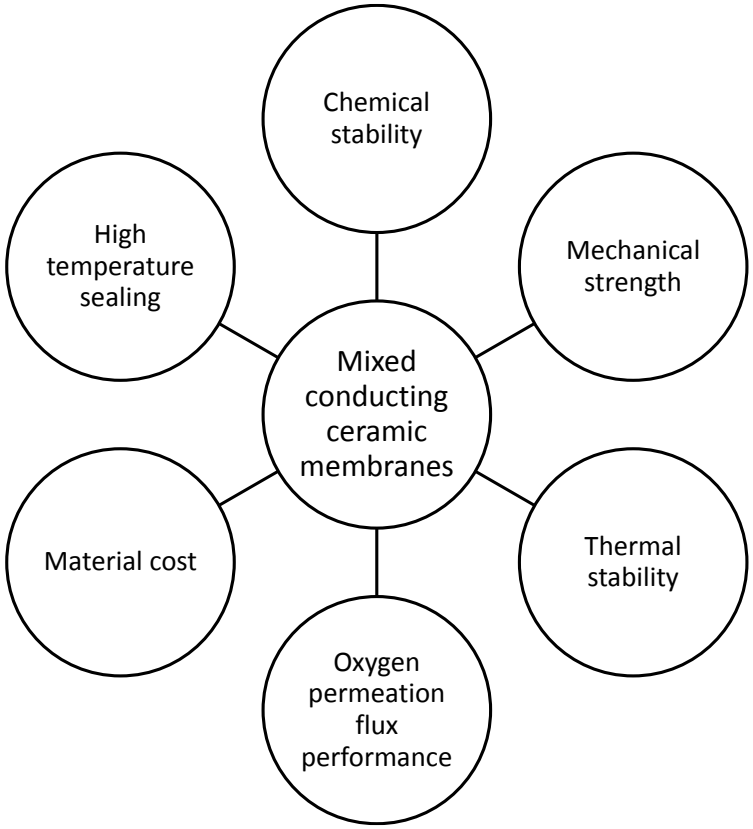

Figure 2.7 Critical issues in mixed conducting ceramic membranes. Adapted from [19]

2.11.1 Air Products ITM Technology

In collaboration with the US Department of Energy (DOE), Air Products is developing their ITM Technology with the aim of reducing capital and running costs for oxygen production. Compared with cryogenic air separation, Air Products expects savings in both the power demand and capital cost of more than 30%. [174].

In the oxygen production process, air is compressed to 10-34 bar and then heated via direct combustion of H_2 fuel gas (Figure 2.8). This feed stream enters the membrane unit, where oxygen is separated from the air stream. The depleted air is reheated by additional

combustion and then enters a turbine expander for electricity production. Thermal energy of the retentate stream is partly recovered in a steam generator.

The membrane unit itself (Figure 2.9) consists of a pressure vessel in which a number of planar ion transport membranes are installed and arranged in series. Each of these modules consists of several wafers having planar parallel surfaces as shown in Figure 2.10. Oxygen can diffuse through the outside dense, thin, active membrane layer that is fixed to a porous support and enters the interior of the wafer, which consists of a channeled support to let the oxygen flow to the central collection tube. Via this manifold, the oxygen is delivered to the outside of the pressure vessel [124].

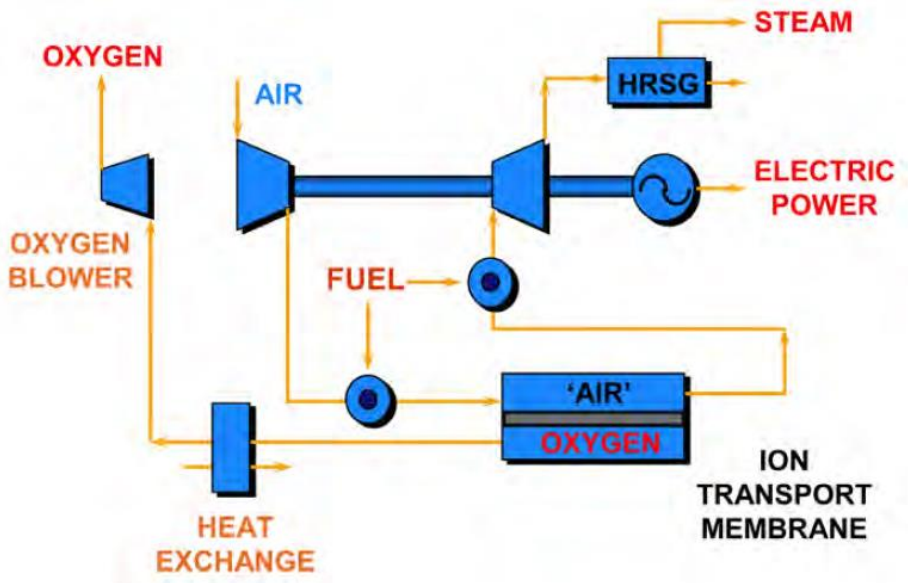

Figure 2.8 Scheme of Air Products process for ITM oxygen production [175]

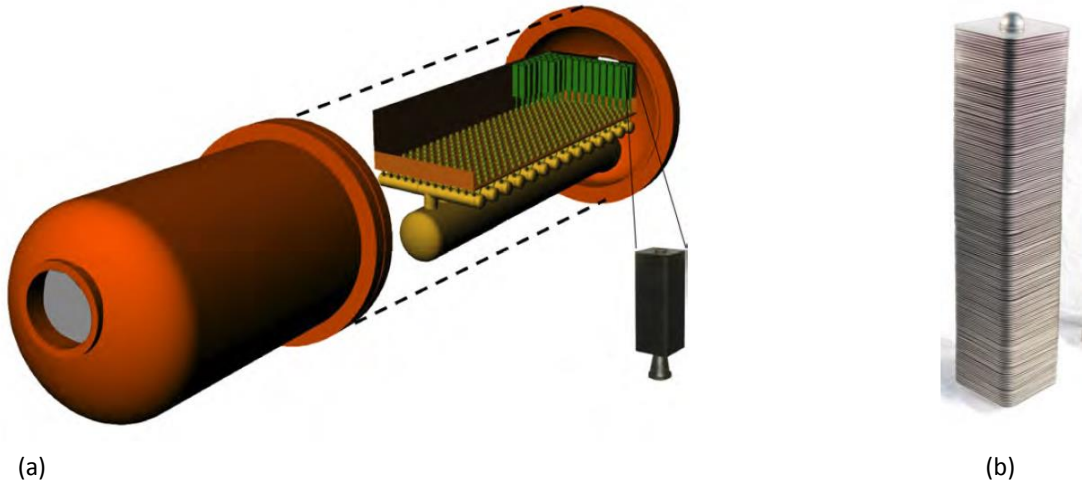

Figure 2.9 Air Products membrane unit (a) and single 0.5 t d^{-1} membrane module (b) [175]

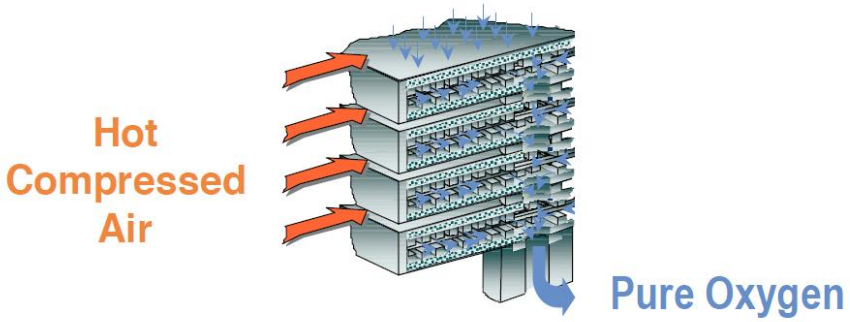

Figure 2.10 Assembly for Air Products membrane wafer stack [175].

One stacked module reaches an oxygen production capacity of $0.5td^{-1}$. A pilot plant in Maryland is already delivering $5td^{-1}$ of oxygen [175]. In the next phase, scale-up to $150td^{-1}$ is planned.

2.11.2 Praxair OTM Boiler

Also supported by the DOE, Praxair is concentrating on the development of an "oxygen transfer membrane" (OTM) system. By utilizing an oxygen-consuming reaction on the membrane permeate side, the oxygen partial pressure ratio is enhanced (Figure 2.11). The OTM system delivers oxygen to a power cycle where gasified coal is used for electricity generation[176]. In conceptual design the tubular membranes are integrated directly into the boiler (Figure 2.12). Due to the combustion reaction between oxygen and fuel occurring on the permeate side of the membrane, the partial pressure of oxygen becomes much lower than the partial pressure on the feed side. This difference helps the transport of oxygen through the membrane without the requirement to compress the air on feed side or apply vacuum on the permeate side. As an additional advantage, the membrane doesn't have to withstand high mechanical stress caused by large pressure differences.

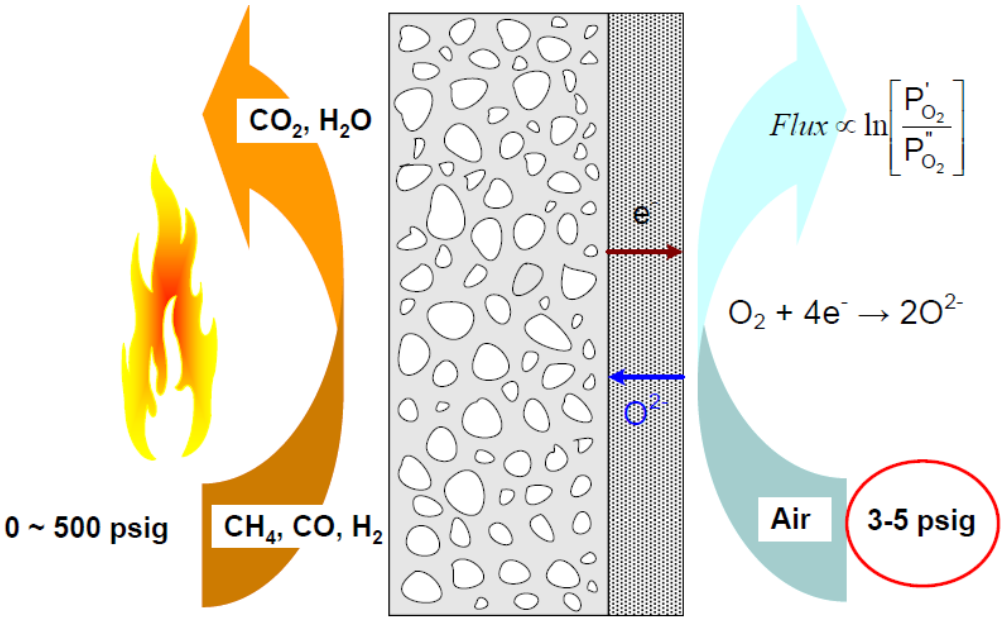

Figure 2.11 Principle of the Praxair OTM system [176]

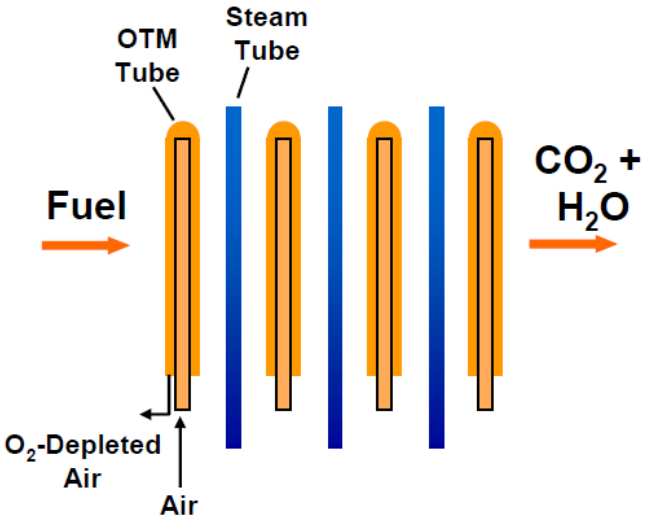

Figure 2.12 Principle of the OTM boiler [176]

Test results have indicated the potential for a 70% decrease in auxiliary power consumption for supplying oxygen on a $kWht^{-1}$ O_2 basis

The steam generator pipes are located in the combustion chamber in addition to the membrane tubes. Due to the direct heat release to the steam generator pipes during combustion, no recycled exhaust gas is necessary. For the membrane, a tubular design is chosen. The tubes consist of a zirconia porous support and a dual-phase zirconia and metal oxide separation layer at the inner side of the tube.

Laboratory scale OTM reactors have been built for natural gas and for hard coal combustion. Laboratory tests demonstrate that the natural gas-fired reactor shows good combustion and a stable membrane at 1020°C. During coal combustion, problems in attaining the required temperature have emerged.

2.11.3 OXYCOAL-AC Pilot Module

The working principle of this pilot scale module is shown in Figure Figure 2.13. The symmetrical assembly consists of a pressure vessel with closed-ended tubular membranes enclosed in a flange between the two parts of the vessel

Compressed and preheated air at up to 20 bar and 900°C flows around the membrane tubes, forcing the oxygen to permeate through the membrane. The oxygen is collected in the flange and conveyed by means of a vacuum pump. To avoid high temperature sealing, the flange is cooled by water. Under optimized process conditions, which mean high feed air pressure and low permeate pressure, the capacity exceeds $0.5td^{-1}$ of oxygen.

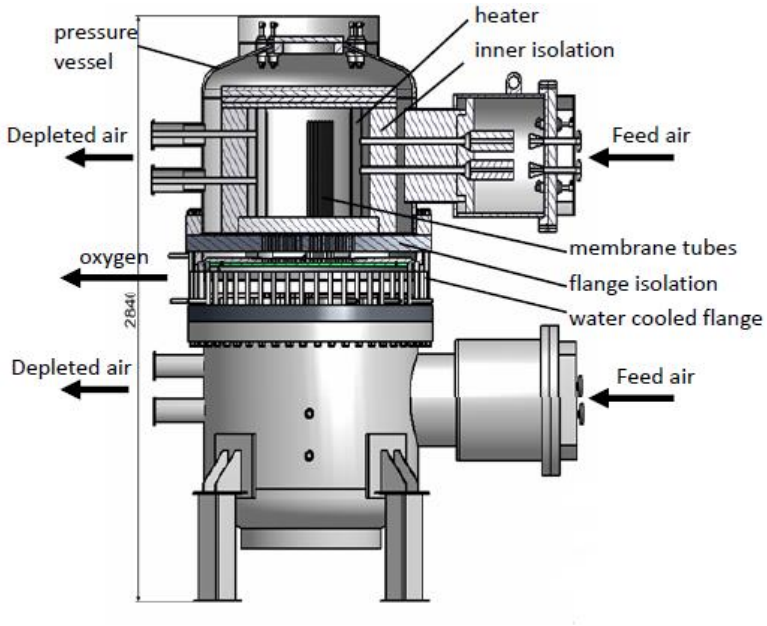

Figure 2.13 Pilot-scale module of the OXYCOAL-AC project [177]

CHAPTER 3

EXPERIMENTAL PROCEDURES

This chapter describes the methods and processes undertaken in order to manufacture mixed ionic electronic conducting ceramic membranes. The steps involved as well as the issues encountered during the manufacturing are detailed. Once the membranes are prepared, it is essential to be able to characterize the membranes in order to correlate between the performance and the properties of the membranes. Various characterization techniques employed throughout the work of this thesis are also introduced in this chapter. The design of the ion transport membrane reactor to measure the permeability of the BSCF membranes is discussed. Experimental procedures involved in undertaking the major objectives of this study, i.e. permeability and stability enhancement of BSCF membranes and the development of sealing material for ion transport membranes are also explained in detail in this chapter.

3.1 MANUFACTURING OF DENSE MEMBRANES

3.1.1 Powder Preparation

Different methods for the preparation of ceramic oxide powders have been reported in the literature. To prepare the powders for MIEC membranes, solid state reaction method,

co-precipitation method and sol-gel methods are widely used. The $Ba_{0.5}Sr_{0.5}Co_{0.5}Co_{0.8}Fe_{0.2}O_{3-\delta}$ and other ceramic powders used throughout this work were prepared by Pechini method which is a modified sol-gel method [178]. Barium nitrate, strontium nitrate, cobalt nitrate and iron nitrate were used as the starting salts. The stoichiometric amounts of these nitrates were mixed in deionized water. Citric acid ($C_6H_8O_7$) and ethylene glycol ($C_2H_6O_2$) were added to obtain an organic-polymeric complex containing the metal cations. Citric acid was added as a chelating agent while ethylene glycol was added to this solution to promote polymerization of the mixed citrate. The solution was stirred for some hours on a magnetic stirrer. This solution is dehydrated by heating slowly onto the stirrer to obtain a viscous gel. The gel was then calcined at a temperature of 250°C for about half an hour to obtain a foamy lump. This lump was crushed to get the powder and was kept for heat treatment at temperature of 600°C to obtain the final black colored $Ba_{0.5}Sr_{0.5}Co_{0.5}Co_{0.8}Fe_{0.2}O_{3-\delta}$ powder.

3.1.2 Manufacturing of Flat Membranes

The BSCF powder obtained was mixed with few drops of ethylene glycol (added as a binder). After mixing the binder thoroughly the powder was sieved through a fine mesh in order to ensure a homogeneous distribution of particles. This sieved powder was then compacted in a die of 25mm diameter at a force of 10000lb for 10 minutes using a Carver Auto Pellet Press. The membranes thus prepared were found to be porous in nature, so the BSCF powder was ball milled before compacting it into discs. This will be further explained in the next sub section. The compacted membrane was sintered at a

temperature of 1120°C for 5 hours. In order to guard against cracking of the membrane during heating and cooling process, the rates for heating and cooling during the sintering process were maintained at 1 and 2°C/min respectively. The sintered membrane was polished using silicon carbide (SiC) papers with different grits (120, 180, 240, 320, 400 and 600) to control the final thickness of the membrane. Figure 3.1 shows the BSCF disc prepared from this method in its final form before its permeability is measured.

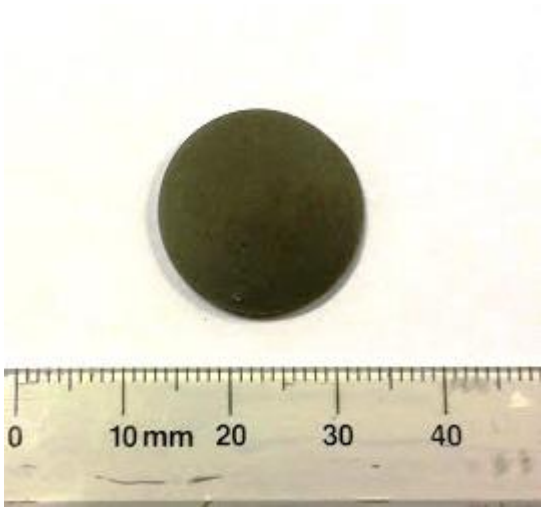

Figure 3.1 BSCF Membrane ready for oxygen permeability test

3.1.3 Ball Milling

As stated earlier, the membranes prepared directly from the calcined and heat treated powder were found to be porous in nature. This was evident from the SEM of the cross section of the membrane as well as the low densification value given by the density measurement. In order to see the effect of the temperature of the heat treatment of the powder on the final densification of the membrane after sintering, membranes were

prepared from the powders heat treated at 600, 700, 800 and 900°Ct. All of these membranes still had high porosity, but the membranes heat treated at 600 and 700°C were found to be slightly better than others Figure 3.2. To resolve this problem of high porosity it was decided to ball mill the powder heat treated at 600°C. The technique of wet milling was used inside a jar mill (LABMILL-8000). Ethanol and BSCF powders, equal in volumes, were placed inside the jar. Both the balls and milling jar were made of alumina. The number of balls to be used was selected such that the ration of weight of powder to that of the balls was 1:10. The milling time was varied and the revolutions were kept fixed at about 60 rpm. Figure 3.3 shows the SEM images of the BSCF powder particles after 24 hours of milling. It can be easily seen that the particle seize has reduced to values below 1 micron. The membranes prepared from the powders thus milled showed much lower porosities. The densification value for all membranes prepared after ball milling is above 90%. Figure 3.4 and Figure 3.5 show the cross sections of these membranes with small disconnected pores and possessing good densification.

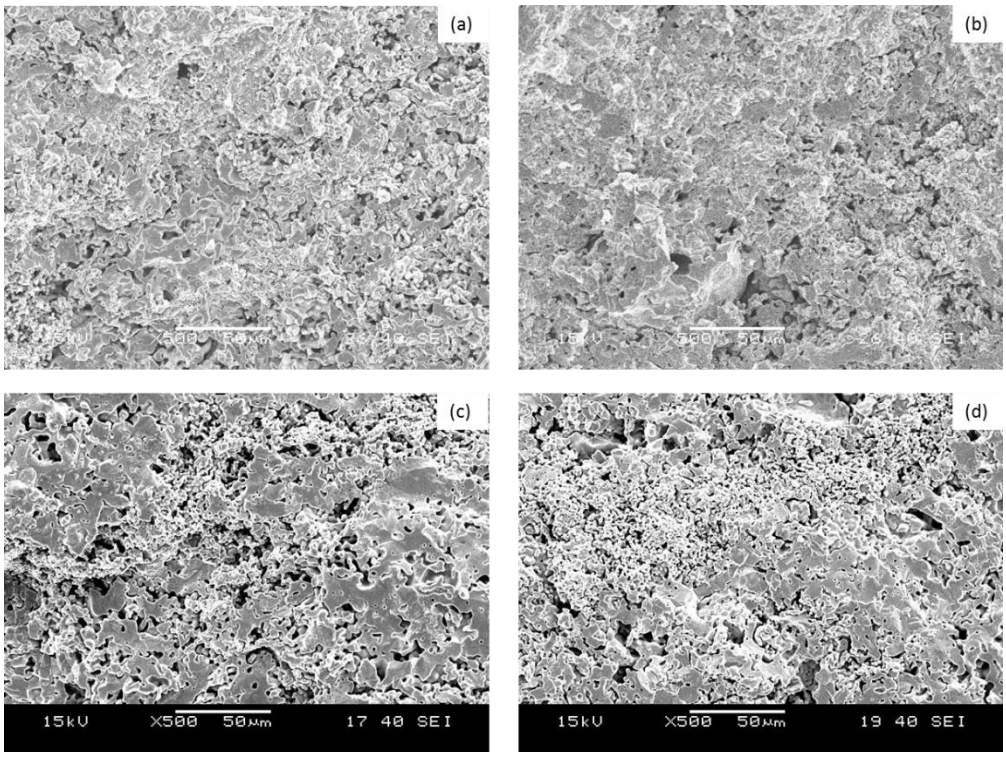

Figure 3.2 Cross section of BSCF discs prepared by pressing powder after heat treatment at (a) 600°C (b) 700°C (c) 800°C and (d) 900°C.

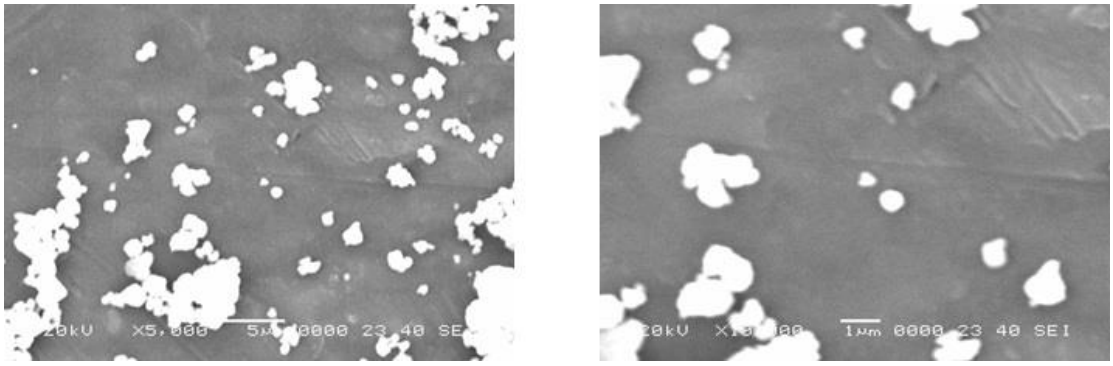

Figure 3.3 SEM of particles of BSCF powder after ball milling for 96 hours.

Figure 3.4 shows the surface and the cross section of the membranes prepared from dry milled powder whereas Figure 3.5 shows the surface and cross section of membranes prepared from wet milled powders. The wet milling results in much better densification as shown by the SEM images. The density measurements also show that membranes prepared from wet milled powder always reach a densification value in excess of 95%.

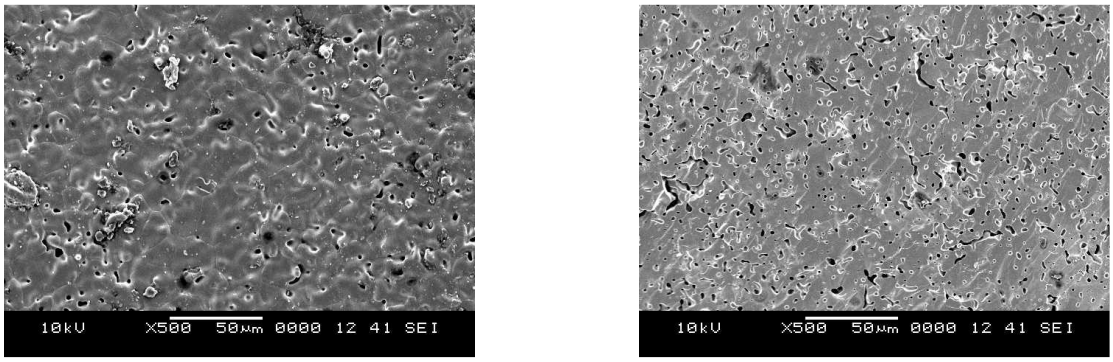

Figure 3.4 Surface and cross section of membrane prepared from dry milling BSCF powder for 96 hours.

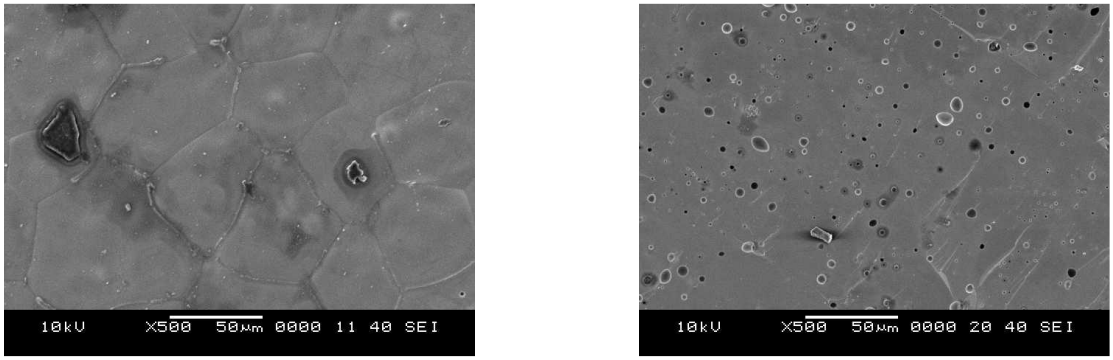

Figure 3.5 Surface and cross section of membrane prepared from wet milling BSCF powder in ethanol for 96 hours

3.2 PREPARATION OF ASYMMETRIC MEMBRANES

In Chapter 2, it was explained that the dense membranes used for separation purpose are limited by bulk diffusion and surface exchange kinetics of the membrane. The bulk diffusion of the membrane is dependent on the temperature and the thickness of the membrane. As the thickness of the membrane is decreased the flux increases proportionally. At a critical value of thickness for a membrane prepared by a particular material operating at a certain temperature, further reduction in thickness does not increase the permeability of the membrane appreciably. This is because at this stage the surface exchange kinetics increasingly becomes the permeability limiting factor. To overcome this problem, the best solution is to prepare ultra-thin membranes for countering limited bulk diffusion and then use methods such as catalyst deposition or

surface modification to increase the surface exchange kinetics. An ultra-thin membrane made from BSCF, however, would have very low mechanical strength and would not serve this purpose. The solution of this problem is to make membranes with graded porosities. This can be done by depositing a very thin dense layer of membrane material on top of a porous substrate which would act as a support for the dense layer. Such membranes are called asymmetric membranes. In order to match the thermal and chemical properties of the substrate and the top layer, it is advisable to use the same material for both layers. Two methods have been used in order to come up with such membranes

3.2.1 Uniaxial Pressing of Dense and Porous Layer

In this method both the BSCF powder without ball milling (coarse particles) was used to make the porous layer whereas the ball milled powder (fine particles) was used for making the dense layer. Initially a certain amount of fine powder (0.05g -0.2g depending on the thickness required) was dissolved in ethanol, thus making BSCF slurry. This slurry was poured in the same die which is used to press the membranes. Upon evaporation, a uniform thin layer of BSCF powder with very fine particles is left at the bottom of the die. About 2g of powder with coarse particles is poured into the die and the membrane is pressed at 1000lbf for 10 minutes as before. The membrane is removed from the die and sintered t 1120°C. In this way both the dense and porous layers are formed during a single sintering step which saves a lot of time. Figure 3.6 shows an asymmetric membrane with a 50μm dense layer prepared using this method.

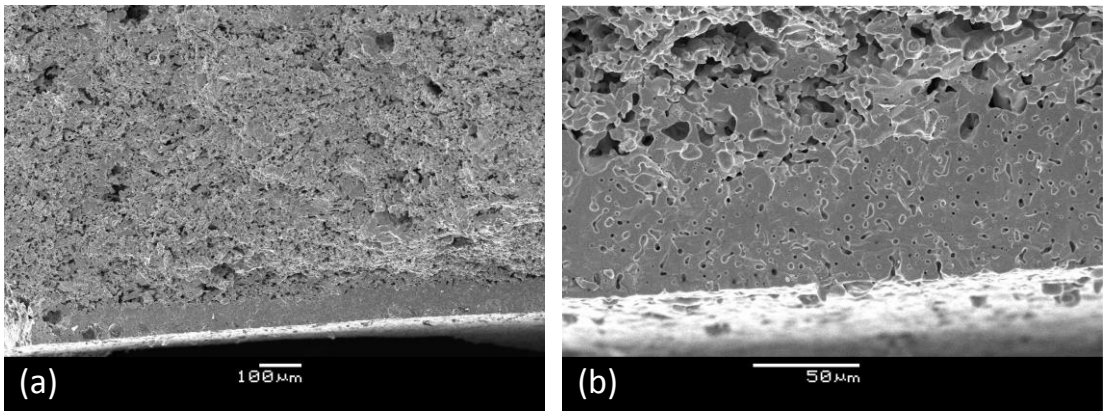

Figure 3.6 Asymmetric BSCF membrane prepared by uniaxial compaction of fine and coarse powder in a single step. (a) 500X and (b) 1000X

3.2.2 Coating of Dense Layer

In this technique, 2g of powder with coarse particles was pressed and sintered using the same parameters as before. The sintered membrane was spin coated with the ethanol based BSCF slurry. The spin coating procedure was done at least three times. In between each spin coating run, the membrane was allowed to dry in air for some time. After the coating is finished the membrane is sintered again so that the top layer has good density and the required phase. Similar membrane can also be prepared by dip coating the membrane in the BSCF slurry.

3.3 CHARACTERIZATION TECHNIQUES FOR MEMBRANES

3.3.1 Scanning Electron Microscopy (SEM) with Energy Dispersive Spectroscopy (EDS)

The scanning electron microscope (SEM) is widely used to examine microscopic structure by scanning the surface of materials. An SEM image is formed by a focused electron beam that scans over the surface area of a specimen. In addition, an SEM system enables us to obtain chemical information from a specimen by equipping it with X-ray energy dispersive spectrometer (EDS). EDS is separately introduced as a technique for chemical analysis in the next section. JEOL JSM-6460LV Scanning Electron Microscope was used to study the morphology of the surface and the cross-section of the membranes. Samples were coated with gold using a sputtering instrument to make them conductive.

3.3.2 X-Ray Spectroscopy for Elemental Analysis

X-ray spectroscopy is a technique of using characteristic X-rays to identify chemical elements. X-ray spectroscopy determines presence and quantities of chemical elements by detecting characteristic X-rays that are emitted from atoms irradiated by a high-energy beam. From the characteristic X-rays emitted from sample atoms, chemical elements can be identified either from the X-ray wavelength, as in X-ray wavelength dispersive spectroscopy (WDS), or from the X-ray energy, as in X-ray energy dispersive spectroscopy (EDS).

The most commonly used spectrometers for X-ray spectroscopy include X-ray fluorescence spectrometers (XRF) and microanalyzers in electron microscopes. The X-ray fluorescence spectrometer is stand-alone equipment for elemental analysis. It uses X-ray radiation to excite the emission of characteristic X-rays from sample atoms. A microanalyzer is an EDS type of X-ray spectrometer that is commonly found in a

scanning or a transmission electron microscope. The EDS microanalyzer in an electron microscope uses a primary electron beam to excite the emission of characteristic X-rays from the sample atoms. Since the electron beam can be readily focused on a microscopic area on a sample, the EDS microanalyzer can examine chemical compositions in a microscopic area; while the X-ray fluorescence spectrometer is mainly used to examine overall chemical compositions in a sample. Bruker S8 Tiger XRF was used to confirm the overall compositions of the materials during and after the powder preparation process. Microanalyzed EDS **(**OXFORD Instruments INCAx-sight**)** provided with the SEM was used to inspect the chemical compositions at particular areas of the membranes during the analysis.

3.3.3 X-Ray Diffraction (XRD)

As discussed in Chapter 2, the development of perovskite phase is essential for oxygen transport in BSCF membranes. X-ray Diffraction technique is used to analyze the phases occurring in the powder samples as well as the sintered pallets. Information about the crystallite size in the sample can also be acquired from the XRD spectrum. As the process of synthesis of ceramics is dependent on both the sintering temperature and dwell time, a heating chamber provided with the Bruker D8 Advance X-Ray Diffractometer was used.

3.3.4 X-Ray Photoelectron Spectroscopy (XPS)

X-ray Photoelectron Spectroscopy is a technique in which characteristic electrons emitted from a solid sample are used for its elemental analysis. The characteristic

electrons show distinct binding energies, which are used to find the chemical composition of the samples under inspection. Photoelectrons can only escape from the uppermost layers of the solid specimen (a depth of 10 nm or less) because of their low mean free path. Thus, electron spectroscopy is an excellent technique for chemical and elemental analysis of the surface. The XPS analysis was done using a Thermos Scientific X-Ray Photoelectron Spectrometer (Model # Escalab 250Xi) equipped with an Al x-ray source.

3.3.6 Density Measurement

The density of the membrane samples was measured using the Buoyancy method based on the Archimedean Principle. A precision balance was used to measure the weight of the sample reduced by the buoyancy force (apparent weight) in a reference liquid whose density was already known. The weight of the sample in air and the weight of the sample in the reference liquid were measured and used in the following equation to evaluate the density.

$$\rho = \frac{A}{A-B}(\rho_O - \rho_L) + \rho_L \tag{3.1}$$

where ρ is the sample density, A and B are the masses of sample in air and reference liquid respectively, ρ_0 and ρ_L are the densities of reference liquid and air (0.0012g/cm^3) respectively.

3.4 MEMBRANE REACTOR DESIGN AND PERMEABILITY MEASUREMENT

In this section the experimental setup built at King Fahd University of Petroleum and Minerals in order to deploy the BSCF membranes for the purpose of oxygen separation at high temperatures is described. With some modifications, this experimental setup was also used as an ITM reactor with oxy-fuel combustion taking place at the membrane surface, which is also discussed here.

Initially the BSCF membranes were tested for their oxygen permeability with respect to time and temperature. The experimental set up for such measurements is shown in Figure 3.7. This apparatus consisted of two aligned sets of alumina tubes separated with the ion transport membrane inside a split furnace. Each alumina set was considered as a chamber composed of two coaxial ceramic tubes. In each ceramic chamber, the gas entered from the inner tube towards the membrane and escaped through the outer tube. The membrane was placed between the two alumina chambers and sealed there. A thermocouple was placed in the upstream chamber and used to measure the actual temperature near the membrane's surface. The membrane was heated in the split furnace to the final temperature at a heating rate of 2°C/min. Three different methods were used to seal the membranes with the outer alumina tubes during the heating.

1. The membrane was placed inside a glass ring between the two alumina chambers. The top set of alumina tubes was free to move vertically so that it will seal the

membrane during the heating of the system using the gravitational force to squeeze the glass sealant between the membrane and the alumina tubes. This type of sealing was found to be effective for a limited temperature range (up to 700°C)

2. For permeability measurements at high temperatures a paste made from mixture of BSCF ceramic powder and borosilicate glass was used to seal the membrane with the alumina tubes. Permeability data could be collected in the temperature range of 700-1100°C using this seal. A more detailed description of these two sealing solutions is presented in a later section.
3. Silver rings were placed between the membrane and outer alumina tubes (top and bottom). When the system was heated close to the melting point of silver (960°C) the system sealed inside blocking air from outside to enter. This type of sealing was preferred for experiments which were carried out at fixed temperatures below 960°C.

Once the sealing was done properly, natural air was introduced in the upstream chamber using a mass flow controller. Helium was used as a sweep gas in the downstream chamber which was connected to a Gas Chromatograph (GC) for quantitative gas analysis. A GC is an analytical instrument that measures the content of various components in a gas sample. The sample is injected into the system and the carrier or sweep gas (helium in our case) takes the sample into the separation column. The constituents of the gas stream are separated here. A detector measures the quantity of each constituent exiting the column. Quantities in a gas sample with unknown

concentration can be measured by first calibrating the instrument with standard sample of known concentrations. The retention time of the peaks (appearance time) from standard sample and the area under the peaks are equated with the known concentrations. The appearance time and the areas from a sample of unknown concentration can then be compared with those of the standard sample to calculate the required concentrations. Gas Chromatograph (BRUKER 450-GC) was used for the permeability analysis of the membranes.

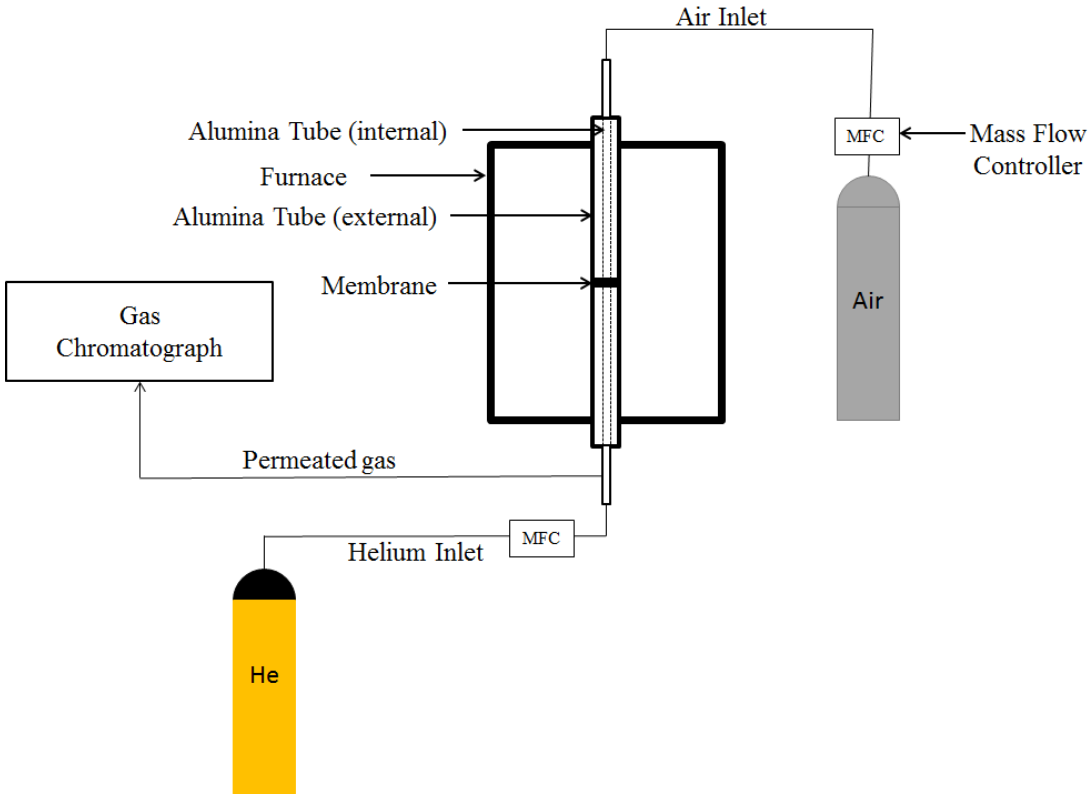

Figure 3.7 Membrane permeability measuring setup for operation under inert environment

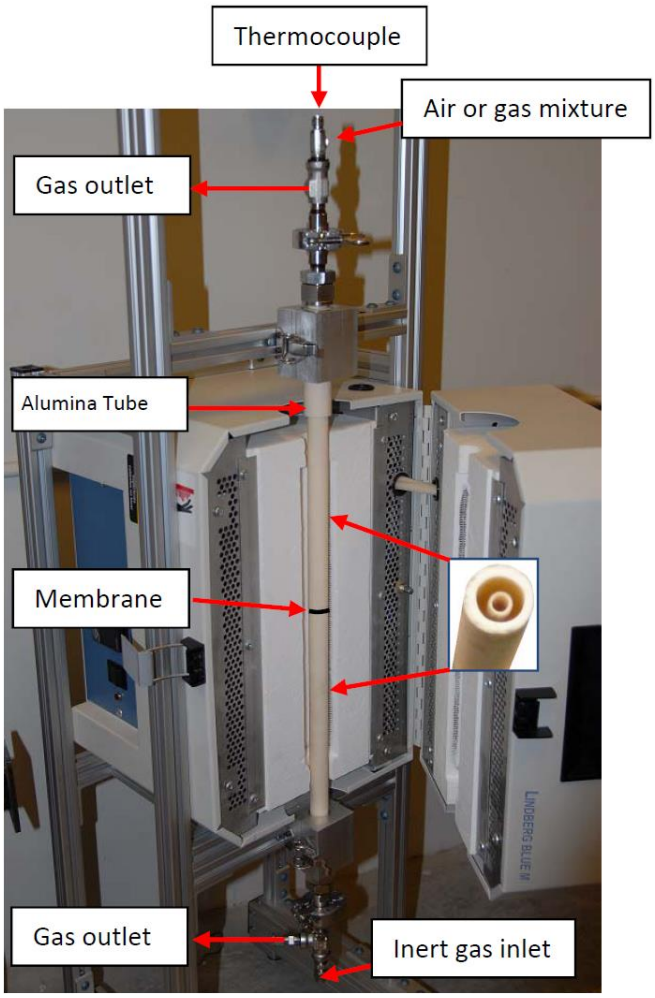

Figure 3.8 High temperature vertical setup for testing gas permeability of an ion transport membrane

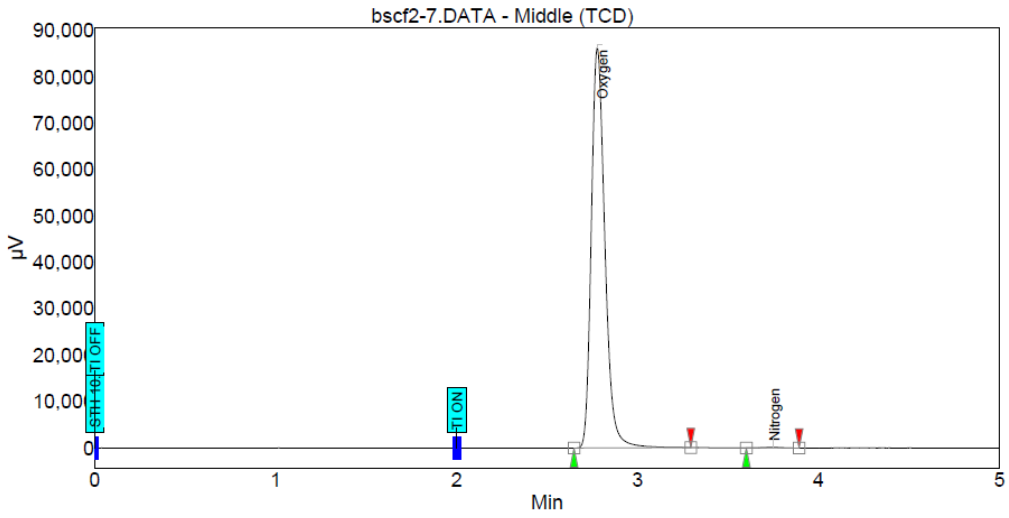

Peak results :

Index	Name	Time [Min]	Quantity [%]	Height [µV]	Area [µV.Min]	Area % [%]
1	Oxygen	2.78	99.77	86280.1	7504.9	99.778
2	Nitrogen	3.75	0.23	130.6	16.7	0.222
Total			100.00	86410.6	7521.6	100.000

Figure 3.9 A sample gas chromatogram obtained for oxygen permeated from a BSCF membrane

In order to evaluate the stability of the BSCF membranes, it was necessary to test them under power plant conditions. To accomplish that, it was decided to inject controlled volumes of methane gas from the sweep side. The GC was calibrated with a standard sample containing all the possible products from reaction of methane with oxygen i.e. carbon dioxide, carbon monoxide and methane in addition to oxygen and nitrogen. Water also being a product of combustion reaction, it was necessary to remove it from the permeate stream before injecting it into the GC. This was done by passing the permeate through a condenser which was constantly supplied with coolant from a

circulating cold bath at 5°C. The volume of the water being obtained as condensate could be measured accurately, hence giving us another yardstick by which to monitor the condition of the reaction. The volume of gas entering the GC for analysis was precisely measured by using high resolution Mass Flow Meters (Model number). The complete setup used for carrying out combustion inside the ITM reactor is shown in Figure 3.10.

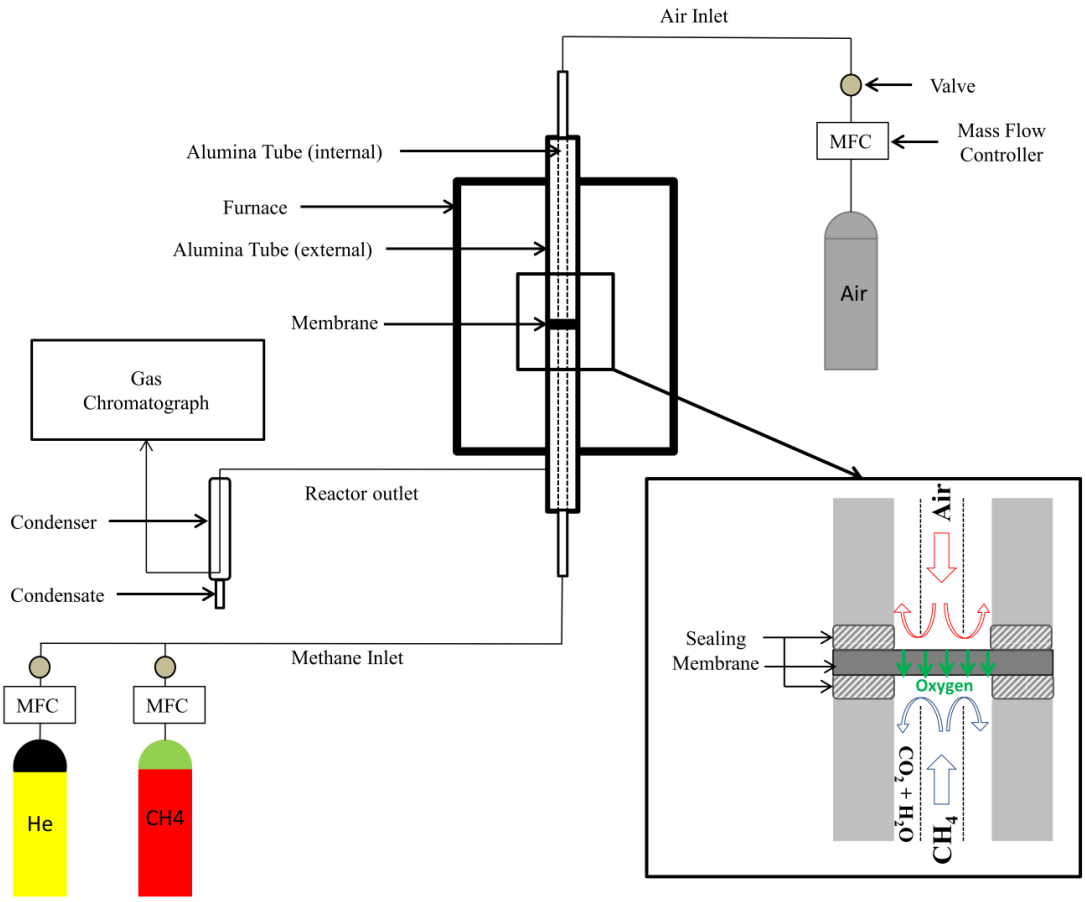

Figure 3.10 Complete setup for carrying out laboratory scale oxy-fuel combustion with the ion transport membrane reactor

3.5 SEALING OF ION TRANSPORT MEMBRANES

In this study a sealing material is proposed, made from a mixture of Pyrex in fine powder form with the powder of the same material from which the ITM is made from (BSCF in this case). The Pyrex glass powder is obtained from crushing a Pyrex beaker and then ball milling it for 24 hours in an alumina jar mill using alumina balls. BSCF powder was made from sol-gel process and ball milled as discussed earlier. Mixtures of BSCF powder and Pyrex glass were prepared in four different compositions (60 wt. % BSCF-40 wt. % Pyrex, 70 wt. % BSCF-30 wt. % Pyrex, 80 wt. % BSCF-20 wt. % Pyrex and 90 wt. % BSCF-10wt. % Pyrex). The mixtures were ball milled again for 5 hours to achieve homogeneity. In order to apply this mixture to a membrane for sealing, it was converted into paste form. This was done by adding three drops of distilled water in 1 gram of BSCF-Pyrex mixture. The paste, thus prepared, is enough for application to a single membrane with a diameter of 20mm. The surfaces of the membrane and the alumina support tube, where this paste is to be applied, are polished with 600 grit size abrasive paper. The uniform layer of about 1mm thickness of this glass ceramic paste was then applied with a spatula on the alumina tube as shown in Figure 3.11 Some weight was applied on top of the setup to improve the bonding adhesion of the paste. The setup was heated inside the gas permeation measuring setup. Air was supplied from the top tube and He was introduced as the sweep gas in the lower tube which carried the permeated oxygen to the gas chromatograph which measured the percentage of O_2 and any other gases present in the stream. Any presence of nitrogen in the permeate gas

stream would indicate an improper sealing. Both BSCF and LNO membranes were sealed using the above mentioned procedures and the permeability of oxygen was measured through these membranes to showcase the versatility of this sealing method.

Membranes of materials BSCF and LNO were also sealed using glass rings as sealants. After carrying out the permeability experiments for extended period of time with both glass and BSCF-Pyrex mixture as the sealant, the spread of silicon on the membrane surface was analyzed using energy dispersive x-ray spectroscopy (EDS).

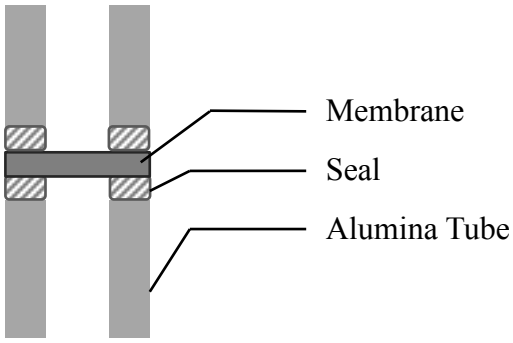

Figure 3.11 Configuration of seal between membrane and support tubes

3.6 PERMEABILITY AND STABILITY STUDIES OF BSCF MEMBRANES

There were various studies conducted in order to investigate the permeability and the stability of BSCF membranes. The effect of microstructure of the BSCF membranes over

the oxygen flux that is produced was studied by preparing membranes with different grain sizes. This was achieved by varying the dwell time at 1120°C during the sintering of the membranes. The dwell times selected for this purpose were 5, 10, 15 and 48 hours. All the other parameters i.e. the thickness and effective area of the membranes, feed and sweep flow rates etc. were kept identical. In order to determine the effect of thickness on the oxygen permeability as well as to find the critical thickness of the BSCF membranes, three membranes of thicknesses 1.3, 1.1 and 0.9mm were prepared. The thickness of these membranes was controlled by polishing them with SiC abrasive paper. The effect of oxygen partial pressure difference was studied by changing the oxygen concentration on the feed side. The different feeds were composed of 10%, 20%, 40%, 60%, 80% and 100% oxygen. The balance was nitrogen. All these experiments were conducted in the permeability measuring setup shown in Figure 3.7.

For the stability tests of the BSCF membranes, the test setup of Figure 3.8 was used with pure methane or a mixture of helium or methane being used as the sweep on the permeate side. This makes our setup as an oxy-fuel combustion reactor with four end membrane operation. The sweep rates were finalized by analyzing the results of various runs as described in the next chapter. The air flow rate on the feed side, however, was always kept constant at 20ml/min. In order to improve the stability and permeability of the BSCF membrane during oxy-fuel combustion, different materials were coated on the permeate side of the dense membranes. Platinum was coated using a sputter coating instrument. A mixture of BSCF and $La_2NiO_{4+\delta}$ (LNO) powders was also prepared for the

purpose of coating. This mixture was prepared by adding BSCF and LNO powders in equal weight percentage in ethanol and sonicating it for 2 hours. This mixture was then coated on the permeate side of the BSCF membranes in slurry form using spin coating technique.

CHAPTER 4

RESULTS AND DISCUSSIONS

4.1 CHARACTERIZATION OF BSCF MEMBRANES

4.1.1 Elemental Analysis by XRF and EDS

In order to confirm the composition of the BSCF powder, its elemental analysis was done using the XRF instrument. This analysis was done right after the heat treatment step during the manufacturing of the powder. Table 4.1 shows that the weight and atomic percentages of Ba, Sr, Co and Fe in the powder are very close to the desired composition $Ba_{0.5}Sr_{0.5}Co_{0.8}Fe_{0.2}O_{3-\delta}$.

Table 4.1 Elemental analysis of BSCF powder from Wavelength Dispersive Spectroscopy using XRF instrument

Element	Wt. %	At. % (Calculated)	Composition
Ba	39.14	24.19	0.48
Sr	26.26	25.44	0.51
Co	27.97	40.29	0.81
Fe	6.63	10.08	0.20

After compaction of the powder into discs and their subsequent sintering, the surface and cross section of the membranes were examined under SEM. The membranes were found to be dense with very small disconnected pores. Density measurements of the membranes also indicated densification values in excess of 90% for all the membranes. The EDS elemental analysis was also performed along with the electron microscopy of the membranes. The spectrum obtained from BSCF membranes is shown in Figure 4.1 along with the atomic percentages of elements in Table 4.2. Again the actual composition of elements is very close to the desired composition.

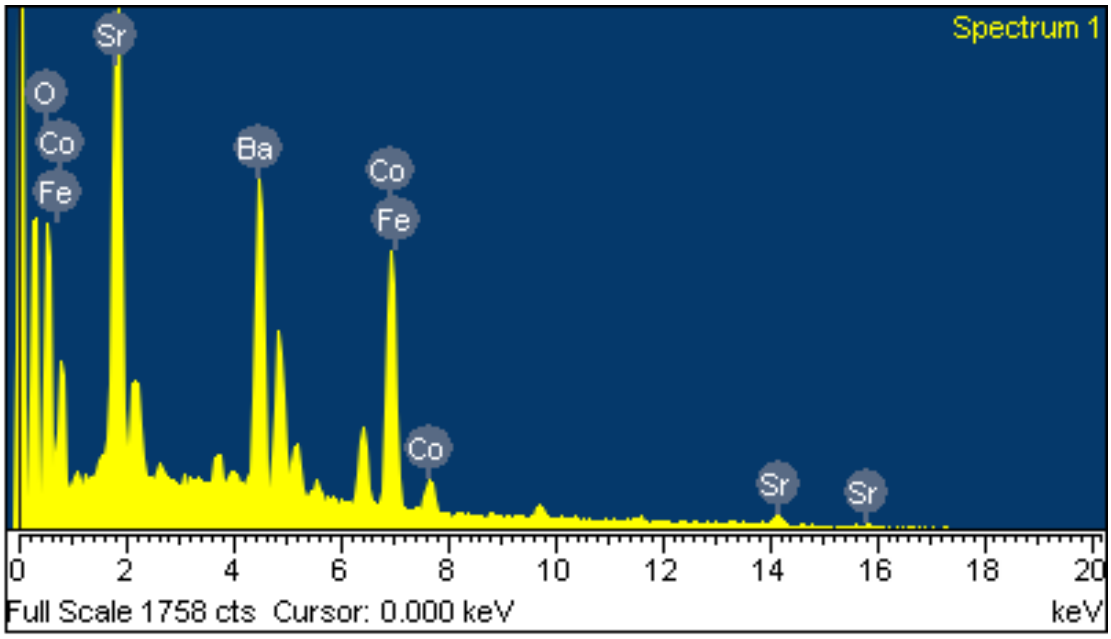

Figure 4.1 EDS spectrum obtained from BSCF membrane

Table 4.2 Elemental analysis of BSCF using Energy Dispersive Spectroscopy using SEM

Element	Atomic %	Composition
Barium	25.32	0.51
Strontium	24.38	0.49
Cobalt	39.95	0.80
Iron	10.34	0.20

4.1.2 X-Ray Diffraction

As described in earlier chapters, the pure perovskite phase of a BSCF membrane is absolutely critical for its oxygen permeability. To verify the phase, the X-ray diffraction of a BSCF membrane sintered at 1120°C for 5 hour was done and is shown in Figure 4.2. The spectrum obtained confirms that the membrane has single perovskite phase.

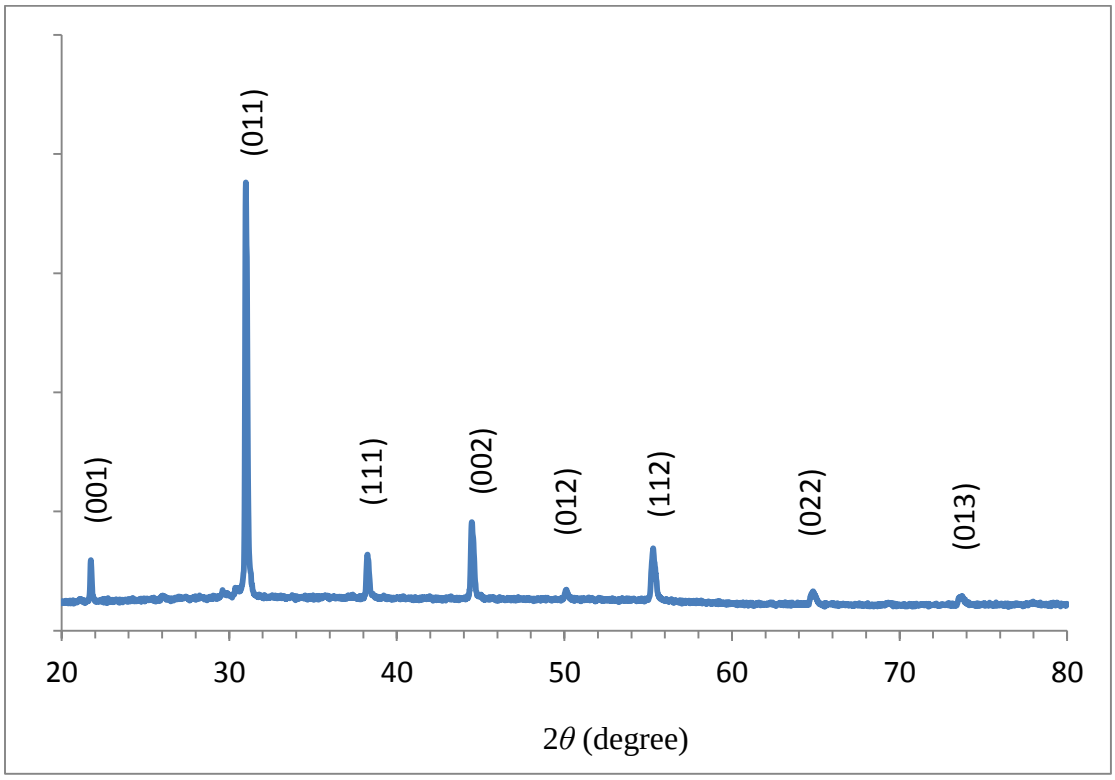

Figure 4.2 XRD of the BSCF membrane at room temperature

4.2 PERMEABILITY TESTS OF ITM WITH PROPOSED SEAL

In this section a method is described to develop an inexpensive, easy to create sealing material which can be used with a variety of ITMs in the complete operating range of temperature without experiencing any of the problems mentioned above. The proposed materials were used to successfully seal $Ba_{0.5}Sr_{0.5}Co_{0.8}Fe_{0.2}O_{3-\delta}$ (BSCF) and $La_2NiO_{4+\delta}$ (LNO) ion transport membranes during the oxygen separation process in a temperature range of 700-1100°C.

4.2.1 Sealing ITMs with Glass Rings

Oxygen permeability results with respect to time for BSCF and LNO membranes sealed using glass rings are shown in Figure 4.3 and Figure 4.4 respectively. These tests were carried out at a temperature of 700°C, which is lower than the temperature at which these membranes operate best. The reason for undertaking tests at a lower temperature is that the glass sealing cannot withstand a higher temperature and is bound to melt and flow. Although the sealing withstood for the complete duration of the tests, a decrease in the oxygen flux through the membrane was observed in both cases. A sharp decrease of oxygen flux at the start of the experiment was followed by a steadier decline. In BSCF the value of oxygen permeating through the membrane decreased from an initial value of 0.64 µmol $cm^{-2}s^{-1}$ to a final value of 0.13 µmol $cm^{-2}s^{-1}$ in 90 hours. The initial oxygen flux through the LNO membrane was recorded to be 0.062 µmol $cm^{-2}s^{-1}$ which decreased to a value of 0.019 µmol $cm^{-2}s^{-1}$ after almost 70 hours of continuous operation. The reason for this could be the wetting or reacting of the membrane surface with glass sealing. With time this glass flows and spreads on the membrane surface and thus reduced the effective membrane surface area exposed for permeation. Hence a decrease in the permeation was observed, as a good portion of the membrane became ineffective. Moreover, it is also possible that glass might have reacted with the membrane to form secondary phases. This phenomenon was also observed by other researchers where they observed the formation of these secondary phases [179]. The profile EDS analysis of the

membrane surface is shown in Figure 4.5. The analysis was done starting from the edge of the membrane and moving towards its center. It can be clearly seen that the concentration of silicon at the edge of the membrane was quite high. Around 30-35% silicon (glass) was observed at the edge of the membrane. Silicon was quite abundant on the membrane surface up to 3-3.5mm from the membrane edge. At around 3.5mm from the membrane edge the concentration of silicon dropped to 2-3% and then it was found to be constant throughout the membrane surface.

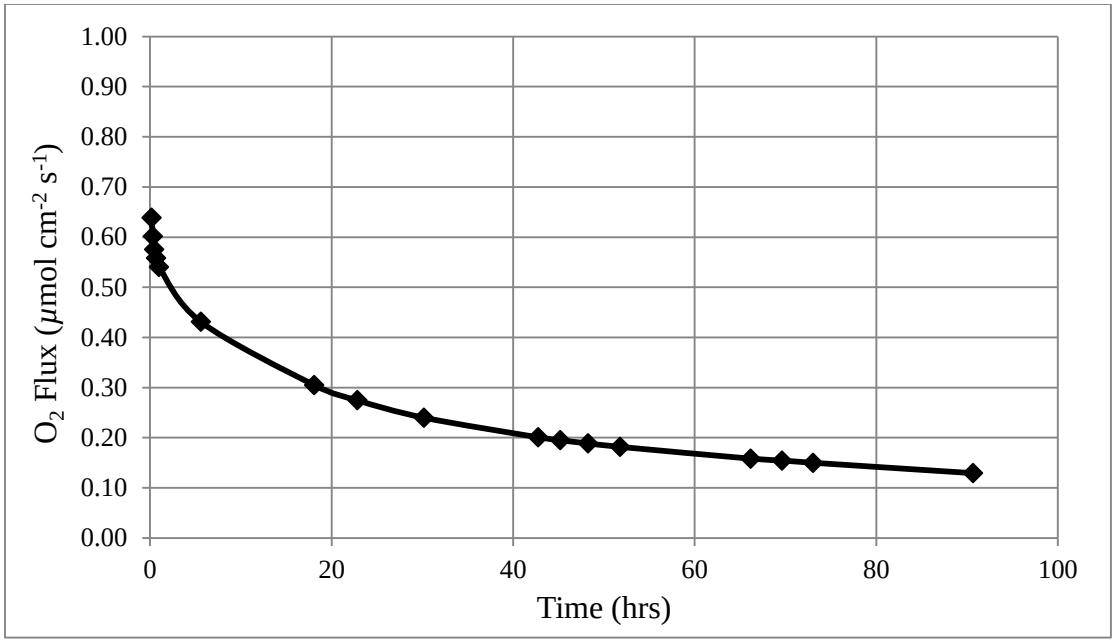

Figure 4.3 Oxygen Permeability of a 1mm thick BSCF membrane sealed using glass rings at 700°C.

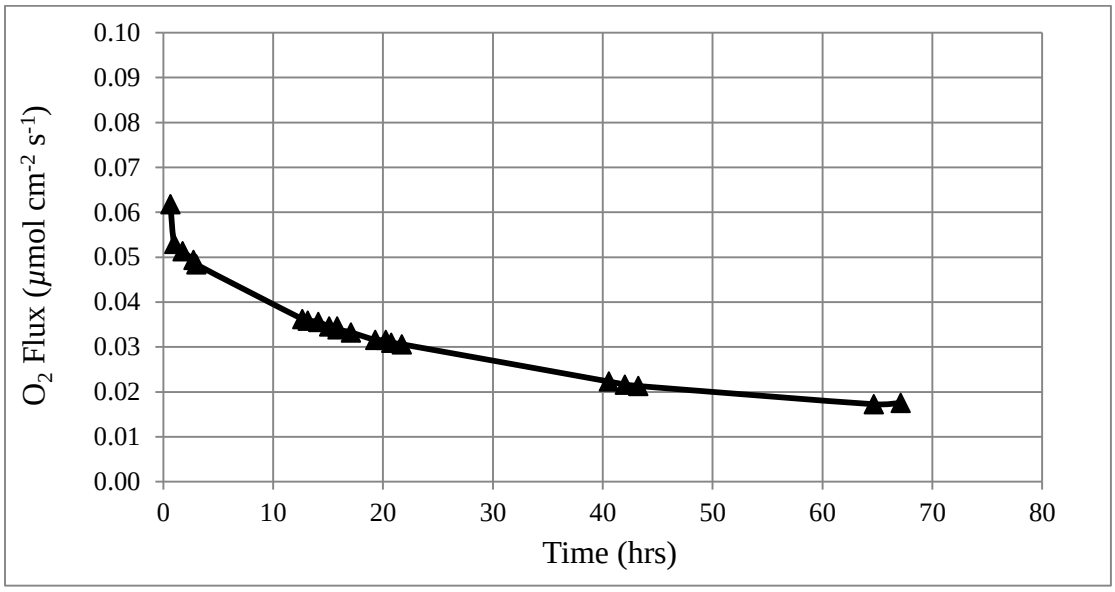

Figure 4.4 Oxygen Permeability of a 1mm thick LNO membrane sealed using glass rings at 700°C.

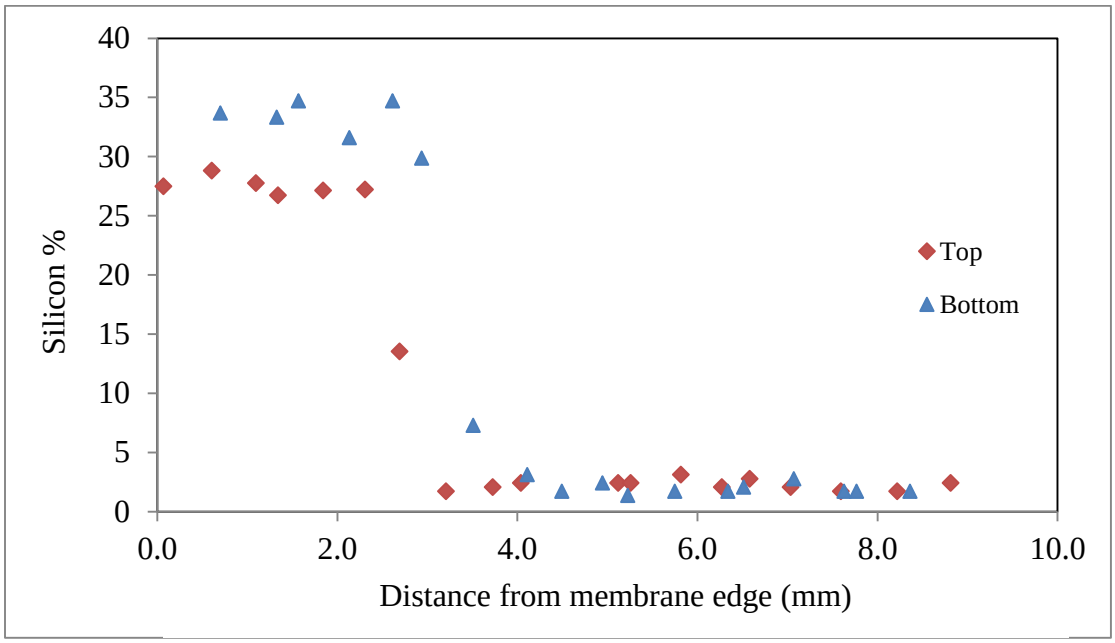

Figure 4.5 Profile EDS analysis of the surface of LNO membrane (from edge towards center) after permeation. The membrane was sealed using glass rings

4.2.2 Sealing ITMs with BSCF Powder Mixed with Pyrex

To overcome this problem mixtures of BSCF and Pyrex powders were prepared as discussed in the previous section. A total of four mixtures of BSCF and Pyrex powders as shown in Table 4.3, varying the glass content in the BSCF powder from 40 wt.% to 10wt.%. It was found that the mixtures with 30 and 40 wt.% pyrex always sealed the membrane between the support tubes but this seal is not suitable due to strong reaction with the membrane material. The bond was also found to be too strong. Due to this, the membrane cannot be removed from the setup without breaking it after the test. On the other hand, the seal with 10 wt. % Pyrex glass formed a weak bond between the tube and the membrane. As a result it was unable to seal the setup on a consistently regular basis.

Table 4.3 Summary of test results of seals of Ion Transport Membranes

Sr #	BSCF powder (wt.%)	Pyrex glass (wt.%)	Observation
1	60	40	Good wetting, very strong bond, considerable reaction between glass and membrane
2	70	30	Good wetting, very strong bond, slight reaction between glass and membrane
3	80	20	Good wetting, desirable bond strength, no reaction between glass and membrane
4	90	10	Poor wetting, weak bond, no reaction

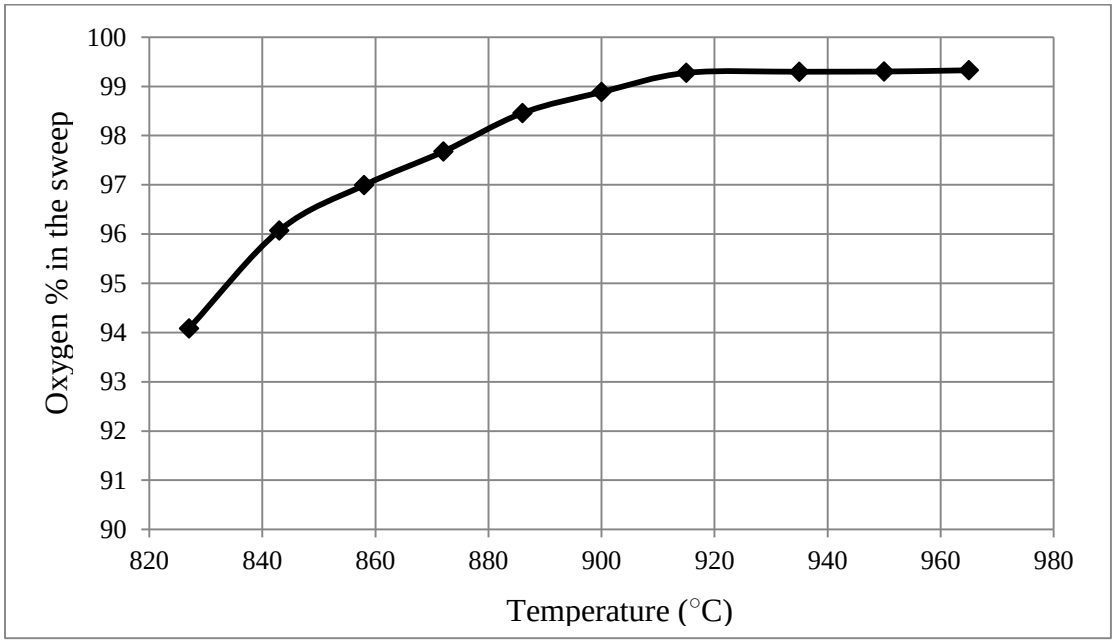

Figure 4.6 Percentage of oxygen at the permeate side of the membrane during heating of the setup

The seal with 80 wt. % BSCF powder and 20 wt. % Pyrex was found to be the best sealing material in all of our experiments. Using this mixture, setup was properly sealed in all runs with desirable bond strength and no visible reaction with the membrane material. So this composition is proposed as the best sealing material for the ITM based gas separation applications.

The membrane to be sealed with the above mentioned procedure starts to seal at around 830°C during heating at a rate of 2°C/min. (Figure 4.6). By the time temperature crosses 900°C the amount of oxygen in the permeate is above 99%. In all the experiments the system was heated to 950°C and kept there for 30 minutes for perfect sealing. Afterwards the system can be steered to the desired temperature value at which the permeability measurements have to be done. This seal has been tested with a 0.9mm thick BSCF membrane in the temperature range of 800-1100°C and found to be working very well (Figure 4.7). The glass ceramic mixture prepared from the technique described above has very good wetting with both the membrane and the alumina tube.

As the glass content is only 20% hence there is no considerable chemical reaction with the membrane material. Also the presence of ceramic particles trap the glass once it melts and stops it from diffusing towards the center of the membrane. This is shown by the excellent stability in the flux of oxygen through the 0.9mm thick BSCF membrane for 80 hours at 900°C (Figure 4.8). Similar test done with a 1.0 mm thick LNO membrane also reveals constant flux for 90 hours at 900°C (Figure 4.9). Further evidence of the limited spread of glass on the surface of the membranes was obtained from the profile

EDS analysis of the surface of the BSCF and LNO membranes tested with the proposed sealing (Figure 4.10). Similar to the EDS analysis done with glass sealing (Figure 4.5), the analysis was started from the edge of the membranes and readings were taken at regular intervals, moving away from the edge, till the center of the membrane was reached at around 6mm from the edge. The silicon content was found to be around 20% at the edge for both BSCF and LNO membranes and drops to values below 1 wt. % as close as about 1mm from the edge of the membrane. The silicon percentage drops to values lower than 0.1 wt. % after a distance of 2.5mm from the edge. This proves that the use of this sealing inhibits the spread of glass and ensures that most of the membrane area is effective for carrying out oxygen separation. In contrast, the membrane sealed with glass rings was having a silicon weight percentage of around 30 wt. % at around 1mm and continued to show high silicon percentage till 3.5 mm distance from the edge of the membrane. A consistent value of around 2 wt. % was detected further towards the center (Figure 4.5).

Due to presence of a large quantity of ceramic powder BSCF, which is same as the membrane material, the thermal expansion of the sealing material becomes comparable to the membrane itself. So the membrane doesn't experience thermally induced stresses during heating and cooling of the setup and hence does not break. This means that after the permeability test the membrane is removed undamaged from the setup and can be used for characterization or further experiments.

The strength of bond between the seal, membrane and the alumina tube was found to be desirable when the proposed percentages of the Pyrex glass and ceramic powder were used. Moreover, the seal is simple and easy to develop. The ceramic powder required to make the seal comes from the same material as the membrane and the Pyrex glass powder is obtained from crushing Pyrex beakers which are inexpensive. The proposed seal can be used with multiple ITM membranes. The oxygen permeability of an LNO membrane is also measured and is shown to be very stable with this seal at 900°C as shown in Figure 4.9.

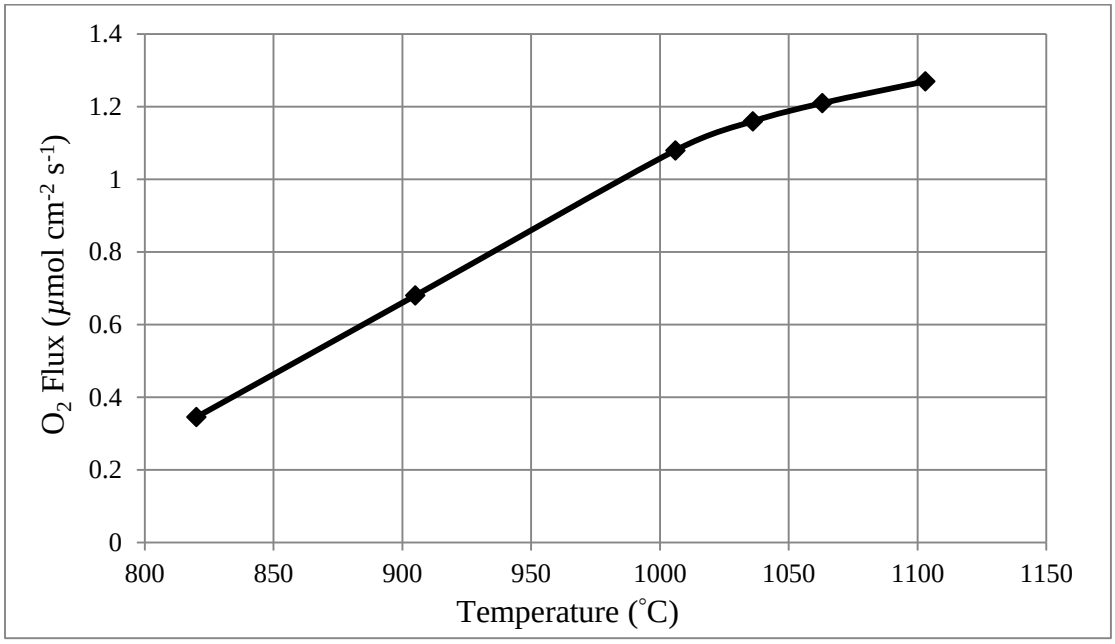

Figure 4.7 Oxygen permeability of a 0.9mm thick BSCF membrane with respect to temperature (membrane sealed using BSCF-Pyrex mixture)

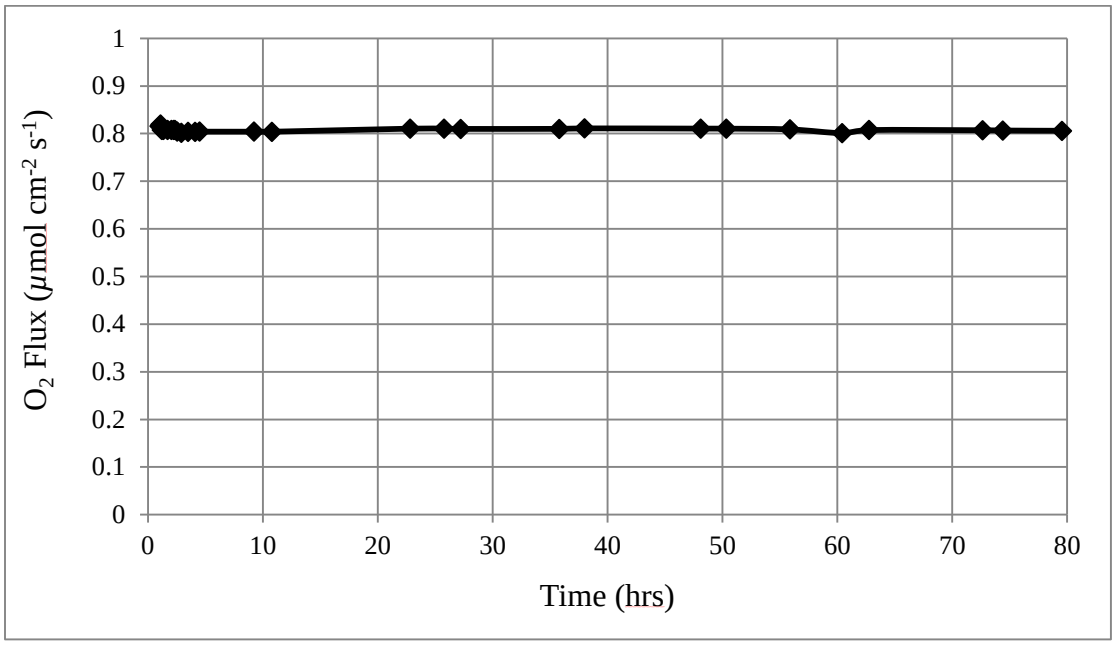

Figure 4.8 Oxygen permeability of a 0.9mm thick BSCF membrane at 905°C sealed with the BSCF-Pyrex mixture

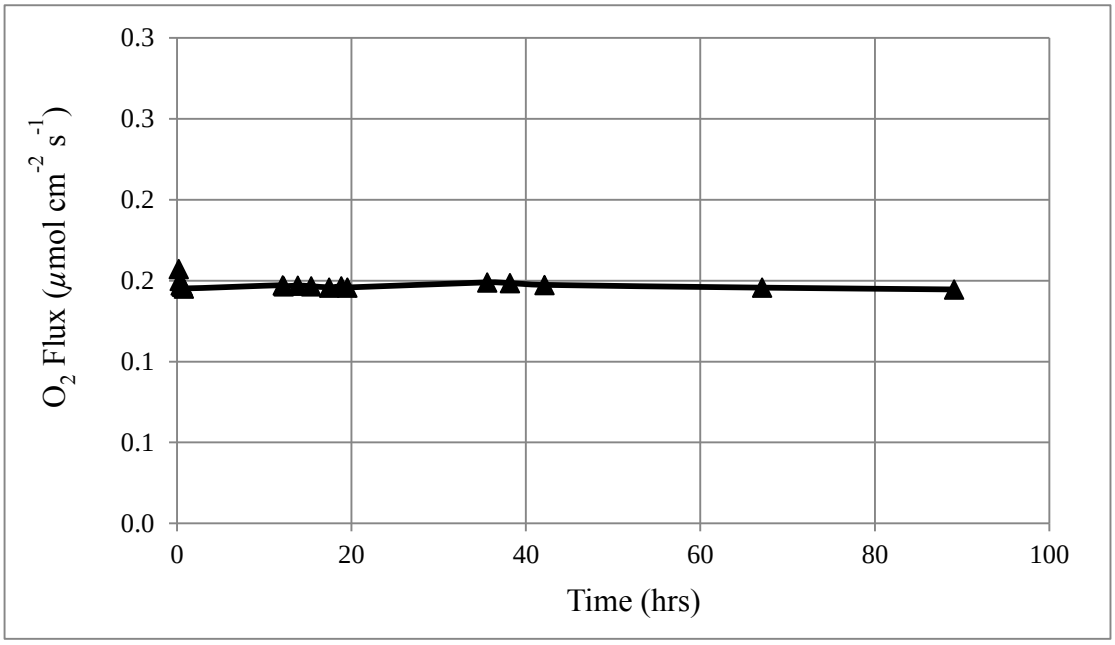

Figure 4.9 Oxygen permeability of a 1mm thick LNO membrane at 900°C sealed with the BSCF-Pyrex mixture

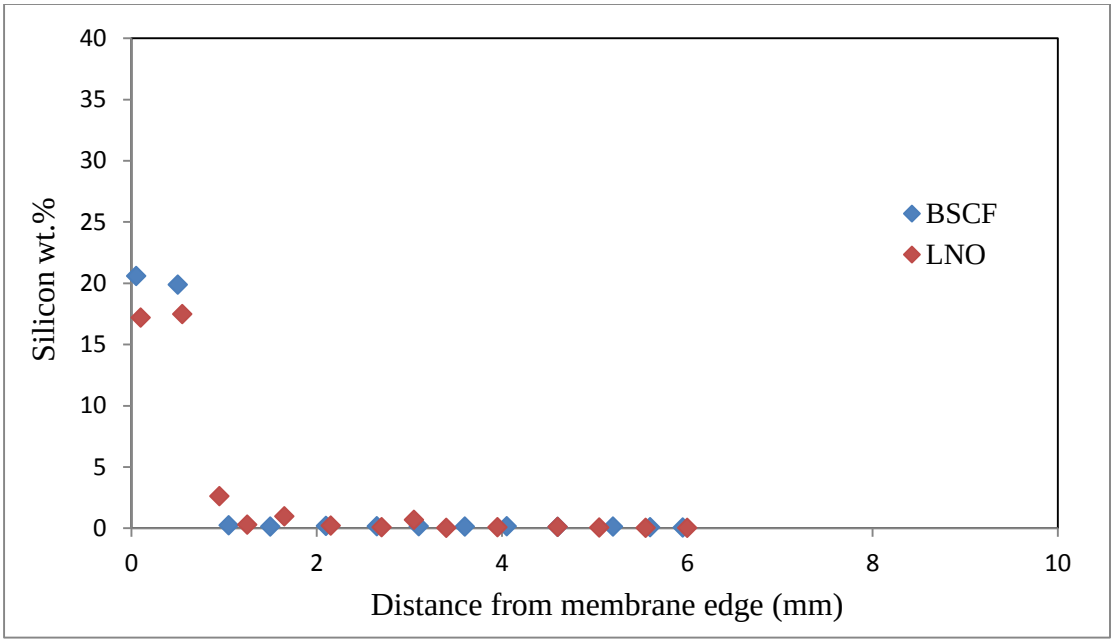

Figure 4.10 Profile EDS analysis of the surface of BSCF and LNO membranes (from edge towards center) after permeation. The membranes were sealed in the setup using mixture of 20% Pyrex and 80% BSCF powders.

4.2.3 Summary of Proposed Sealing Solution for ITMs

The Ion Transport Membranes BSCF and LNO, when sealed with glass rings during the oxygen separation process, lose considerable performance due to the spreading of glass. Preparing a mixture of BSCF powder (80 wt. %) and Pyrex powder (20 wt. %) solves this problem. BSCF and LNO membranes sealed with this material showed constant oxygen permeability values when tested for more than 80 hours. The glass was also found to be

contained on the surface of the membranes within 1mm from the edge. The proposed seal allows operating the membranes within an extended temperature range (800°C - 1100°C). The sealing material results in desirable bond strength between the membrane and the alumina support tubes in the experimental setup, and there is no chemical reaction between the glass and the membrane due to limited quantity of the former. The sealing material is inexpensive and easily prepared. These advantages make our proposed material an excellent choice to be used as a sealing material during ITM operation.

4.3 PERMEABILITY INVESTIGATIONS OF BSCF MEMBRANES IN INERT SWEEP

In this section various aspects of the oxygen permeability of a BSCF membrane are discussed when this membrane is operated under an inert environment on the permeate side. All the membranes used for this purpose were prepared using the BSCF powder as discussed in Chapter 3. The characterization of the membranes is discussed in the opening sections of this chapter after which the effect of sintering conditions on the microstructure and permeability of the BSCF membranes is investigated. The effect of changing thickness of the BSCF membrane on its permeability is examined and a critical thickness of the BSCF membrane is determined for the temperature range of interest. The long term stability and the permeability of BSCF membrane with respect to oxygen partial pressure is also studied.

4.3.1 Effect of Microstructure on Permeability of BSCF

To obtain improved membranes one of the areas in focus is to optimize microstructure and processing parameters. Arnold et al. prepared perovskite-type membranes $Ba_{0.5}Sr_{0.5}Fe_{0.8}Zn_{0.2}O_{3-\delta}$ (BSFZ) using boron nitride (BN) as sintering aid [141]. They studied the average grain size of these membranes as a function of the amount of BN used. They concluded that a lower grain size lowers the oxygen permeability. Diethem et al. showed that the membranes prepared from $La_{0.5}Sr_{0.5}FeO_{3-\delta}$ with larger grains (i.e fewer grain boundaries) had smaller oxygen permeation than the ones with smaller grains. Shaula et al., on the other hand concluded the exact opposite in their study on $CaTi_{0.8}Fe_{0.2}O_{3-\delta}$ membranes suggesting that grain boundaries act as barriers for oxygen permeation [180]. Klande et al. prepared BSCF and SCF membranes of varying grain sizes by using different dwell times during the sintering step of membrane preparation [144]. They have determined that the flux in BSCF membranes was independent of the grain size in the range of 24-42μm, but smaller grains showed a decreased oxygen flux. However for SCF, the oxygen flux was showed to be decreasing with larger grains. Zeng et al. studied the effects of sintering temperature on phase structure, microstructure, oxygen nonstoichiometry, electrical conductivity and oxygen permeation of $La_{0.6}Sr_{0.4}Co_{0.2}Fe_{0.8}O_{3-\delta}$ membranes [133]. They suggested that although the phase structure and oxygen nonstoichiometry of the membranes largely remained unchanged, there was significant effect on the microstructure and the electrical

conductivity, which in turn would have an effect on the oxygen permeability. They showed that the grain boundaries have a much lower electrical conductivity than the bulk.

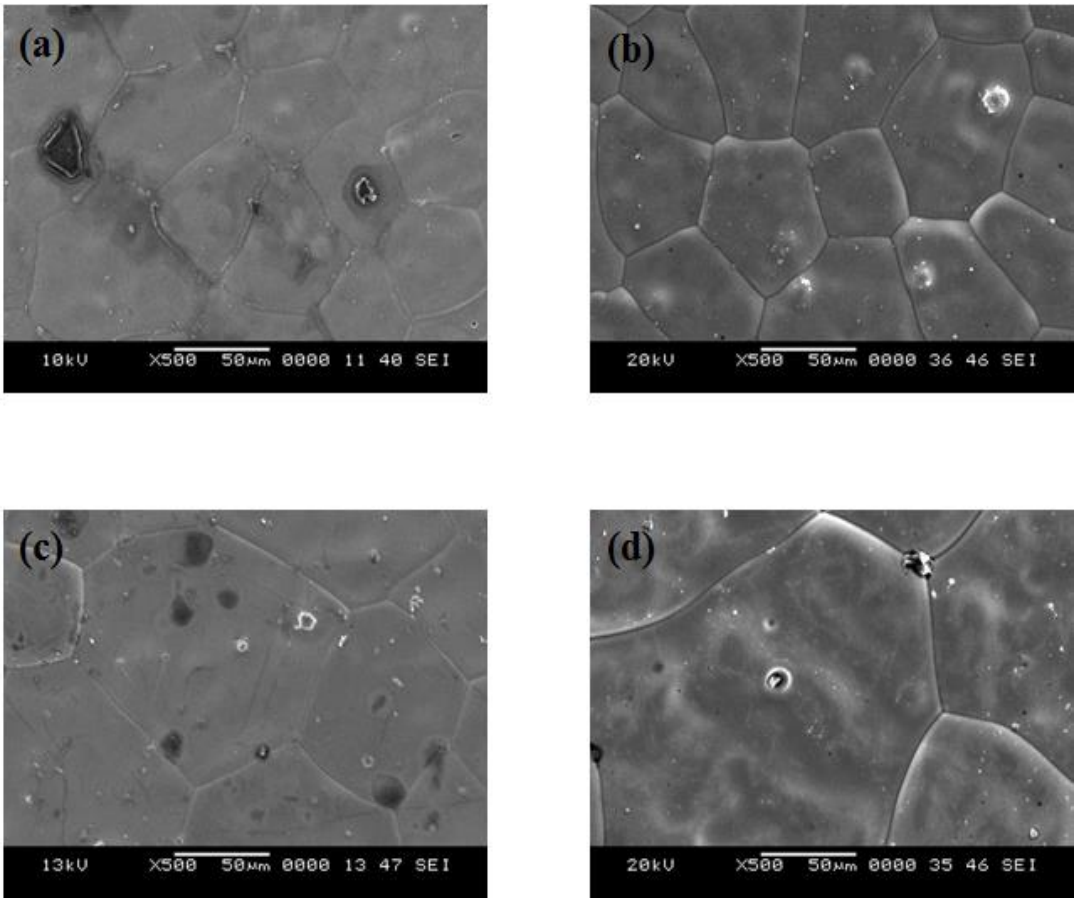

Figure 4.11 SEM micrographs of BSCF membranes sintered at 1120°C for (a)5 hours, (b) 10 hours, (c)15 hours and (d)48 hours

In order to study the effect of varying dwell times during sintering on the microstructure and the permeability of the BSCF membranes, four types were prepared

using sintering times of 5, 10, 15 and 48 hours. SEM images of the surfaces of these membranes clearly show that an increase dwell time during sintering results in larger grains (Figure 4.11). To obtain the average grain size of the samples, more than 400 grains from membranes prepared with each sintering time were analyzed from the SEM micrographs. The average grain size increased from a value of 57.57μm for the membrane sintered for 5 hours to a value of 125.52μm for the membrane sintered for 48 hours (Table 4.4). The grain size of BSCF membranes is plotted as a function of sintering time in Figure 4.12 The growth of grains is found to follow a power law $d = kt^{1/n}$ where k is the constant for grain growth and n is the grain growth exponent. These constants for BSCF were estimated to be 32.98 and 2.85 respectively.

To see the effect of this variation on the performance of the membranes, the permeability tests were conducted. First all the membranes were polished to a final thickness of 1.2mm using SiC abrasive paper. The membranes were sealed inside the experimental setup using the paste prepared from 20%BSCF powder and 80% Pyrex. Once the membrane was sealed, 20 ml/min air was introduced from the feed side and 30 ml/min Helium from the sweep side which carried the permeate oxygen to the GC. The tests were conducted in the temperature range of 800°C to 1070°C and their result is shown in Figure 4.13. The membrane sintered for 5 hours shows better permeability although the rest of the membranes show identical results.

Table 4.4 Average Grain size of the BSCF membranes prepared by sintering at 1120°C for different dwell times.

Dwell Time	5 hrs	10 hrs	15 hrs	48 hrs
Avg. Grain size (μm)	57.57	71.10	90.91	125.52

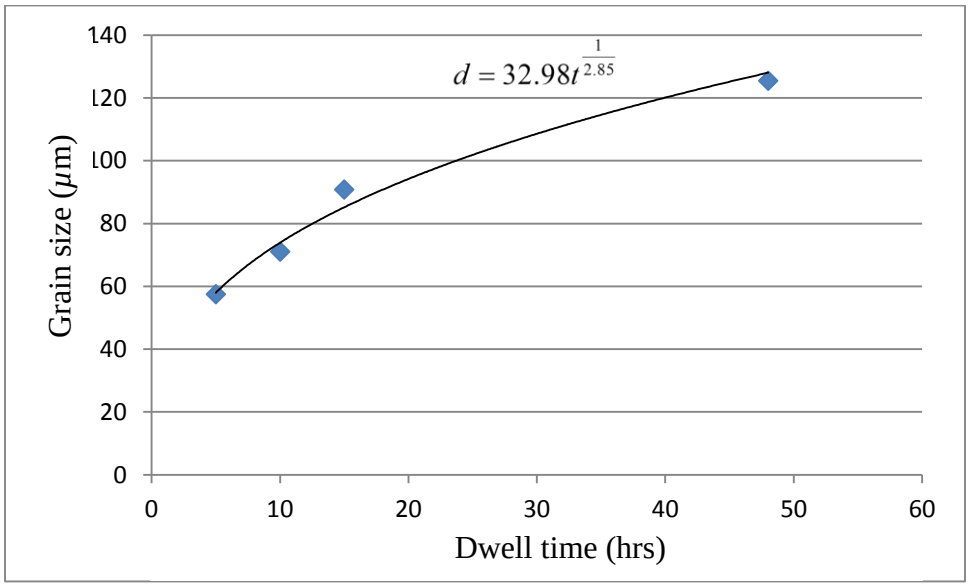

Figure 4.12 Average grain sizes of BSCF membranes as a function of dwell time during sintering at 1120°C. Experimental data is fitted using power law.

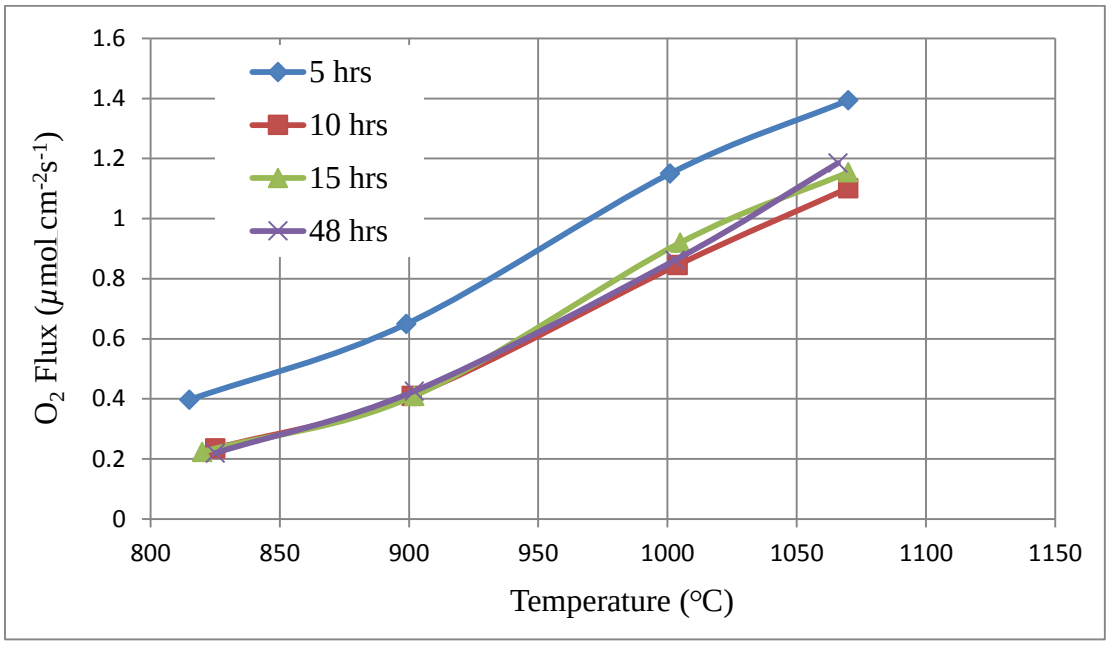

Figure 4.13 Oxygen permeability of the 1.2mm thick BSCF membranes sintered for 5, 10, 15 and 48 hours with respect to the operating temperature.

4.3.2 Effect of Thickness on Permeability of BSCF Membranes

In order to increase the oxygen flux, the thickness of the membrane is often reduced. When this thickness becomes lower than a certain value, the surface kinetic reactions start to limit oxygen permeation more than the bulk diffusion [118]. This thickness value (often called the 'critical thickness' or ***Lc***) of these rival factors becomes a very significant factor. This is a temperature dependent quantity and has been reported to vary from 20 to 3000μm in mixed conducting materials depending on the composition and oxygen partial pressure [181][182]. Li et al. prepared BSCF membranes of varying thicknesses (1.5 to 2.5mm) and observed an increase in the oxygen flux with decreasing length at 800°C and 900°C under vacuum [20]. However they did not further decrease the

thickness of the membrane in order to get to the critical thickness of the membranes. Haworth et al. determined the critical thickness of BSCFY hollow fibre membrane to be around 0.4mm [116]. They deposited silver catalyst in order to further enhance the permeation flux, once the critical thickness was achieved. (temperature range is 650-900°C). Wiik et al. studied the critical thickness of $SrFe_{1\_x}Co_xO_{3\_\delta}$ as a function of cobalt content and found out that L_c decreased from 2mm to 0.7mm when 67% cobalt was added [183]. Zhu et al. prepared cobalt free perovskite $BaCe_{0.15}Fe_{0.85}O_{3-\delta}$ and found its critical thickness to be 0.78mm in the temperature range of 750-950°C [121].

In order to determine the critical thickness of the BSCF membranes in the temperature range of 800-1100°C, three membranes of different thickness were prepared. Figure 4.14 shows the oxygen permeability of the BSCF membranes with 0.9, 1.1 and 1.3mm thickness. It can be inferred looking at the result that the oxygen transport through a 1.3mm thick membrane is limited by the bulk diffusion. That is why a reduction in membrane thickness to 1.1mm enhances the permeability. A further reduction of thickness to 0.9mm has almost no effect on the oxygen flux between 900 and 1100°C which means that the surface kinetic reactions have taken over as the limiting factors at 1.1mm thickness. Thus it can be concluded that the critical thickness of the BSCF membrane is close to 1.1mm in the temperature range of interest for the application of BSCF membranes.

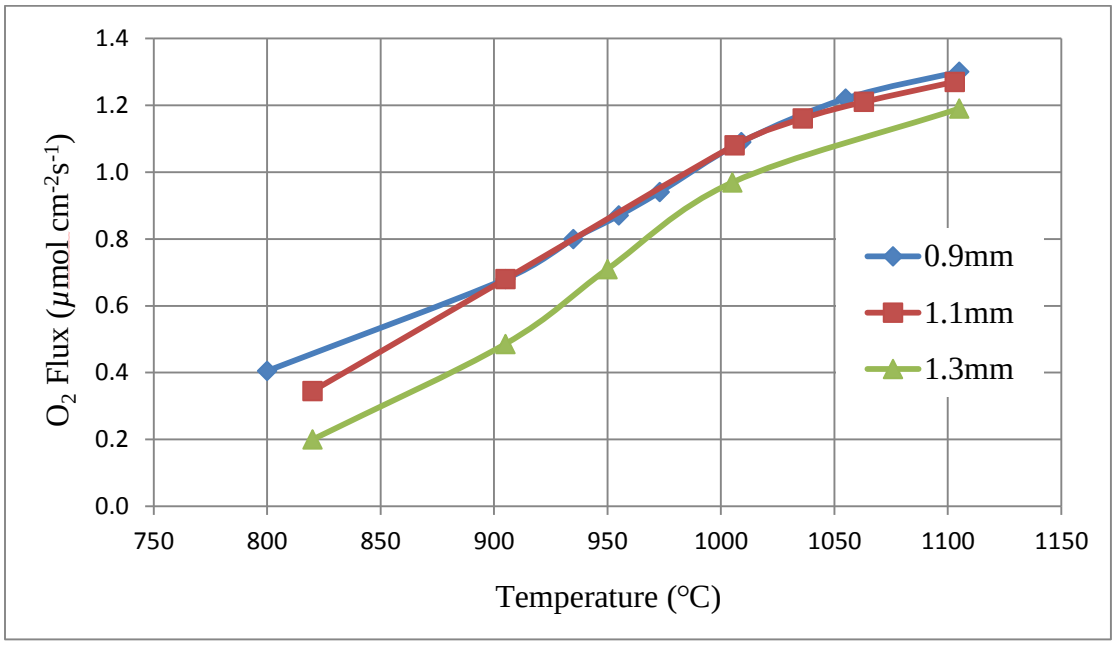

Figure 4.14 Oxygen Permeability of BSCF membranes of 1.3, 1.1 and 0.9mm thicknesses with respect to operating temperature.

4.3.3 Long term Stability Test of BSCF

In order to validate the long-term stability of the BSCF material, the oxygen permeability of a 1.4 mm thick BSCF membrane has been measured for more than 1000 hours. Silver rings were used to seal the membrane between the alumina tubes of the ITM reactor and the test was carried out at 920°C. The oxygen permeated by the membrane was carried from the reactor to the gas chromatograph using Helium supplied at a rate of 30ml/min. Even for such a prolonged time the BSCF membrane showed excellent stability with a consistent oxygen flux value of around 0.83μmol.cm^{-2}.s^{-1} (Figure 4.15). Similar values were reported in the literature [153]. For example, Menzler et al. [114] has measured the oxygen permeability of a 1.0 mm thick BSCF membrane at 900°C to be

1.45 ml min^{-1} cm^{-2} (0.98μmol cm^{-2} s^{-1}). Shen et al. [117] has studied a 1.5mm thick BSCF membrane at 850°C and has found the oxygen flux to be 0.92 ml min^{-1} cm^{2} (0.627µmol cm^{-2} s^{-1}). This result is very encouraging as it proves the suitability of BSCF as a material of choice for commercial oxygen separation applications as it can provide undiminished performance for extended period of time.

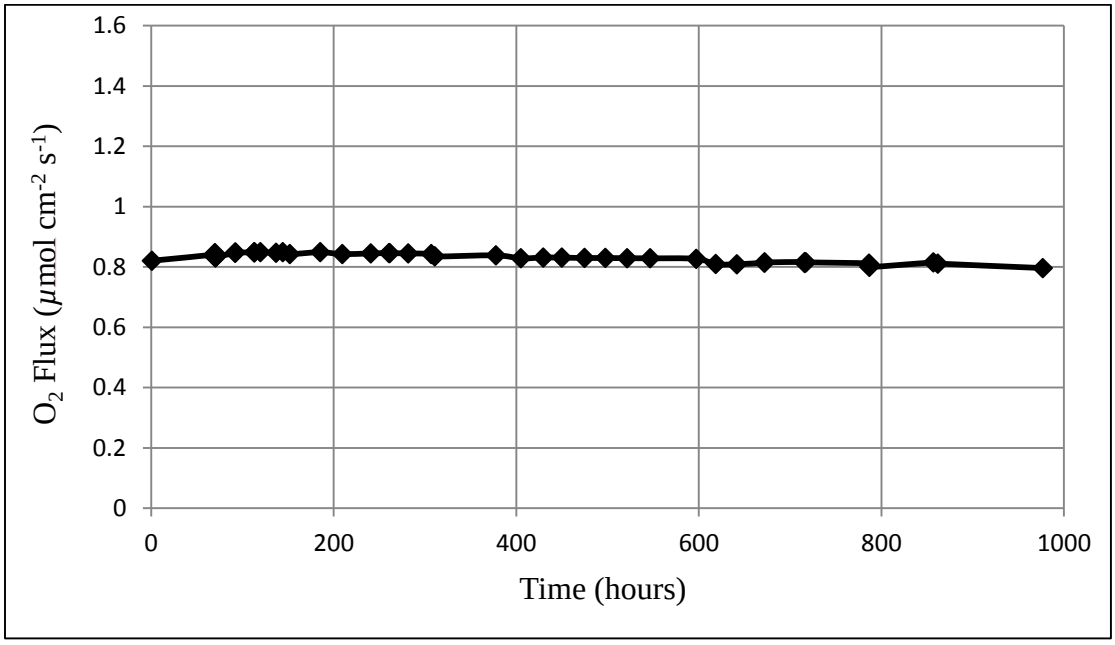

Figure 4.15 Oxygen permeability of a 1.4mm thick BSCF membrane at 920°C with respect to time

4.3.4 Oxygen Permeability of BSCF with respect to Partial Pressure of Oxygen

In order to study the effect of change in the partial pressure on feed side on the permeability of the membrane, the percentage of oxygen was varied in the feed from 10% to 100%. This test was conducted using a 1.4mm thick BSCF membrane at 920°C and the

result is shown in Figure 4.16. The permeability of the membrane was close to 0.82μmolcm^{-2}s^{-1} when the air was used as the feed but for pure oxygen in the feed, this value increases to 1.57 μmolcm^{-2}s^{-1}, which is an increase of more than 90%.

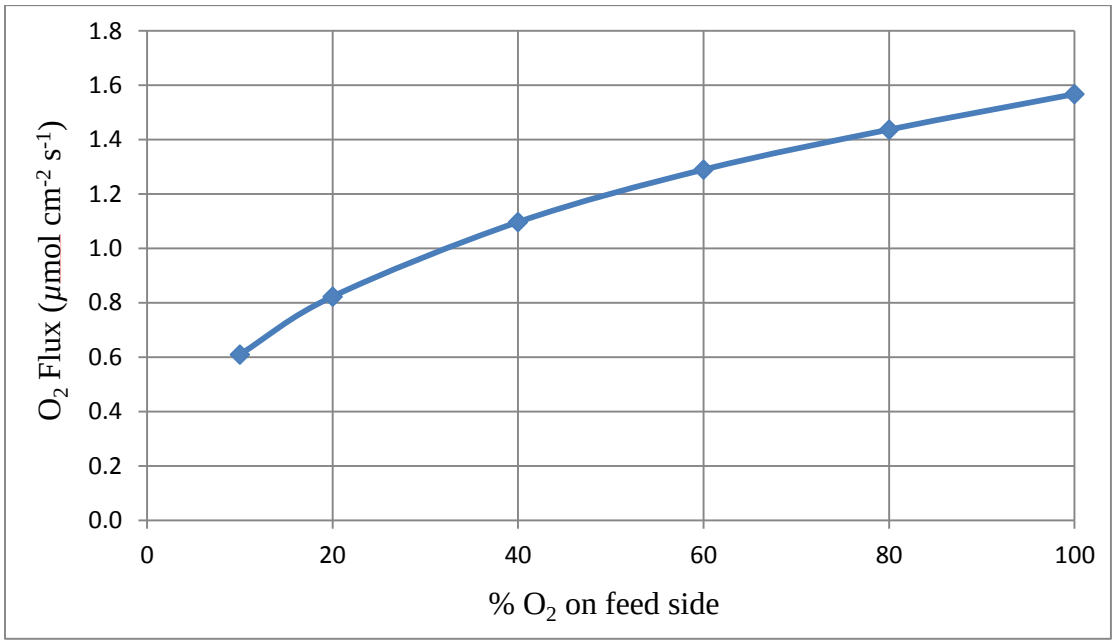

Figure 4.16 Oxygen permeability of a 1.4mm thick BSCF membrane at 920°C with respect to oxygen concentration in feed.

4.3.5 Summary

$Ba_{0.5}Sr_{0.5}Co_{0.8}Fe_{0.2}O_{3-\delta}$ powders were prepared by modified Pechini method. Membranes were prepared using uniaxial compaction and sintering. These membranes were found to have the desired pure perovskite phase and good densification values.

The effect of grain size of the BSCF membranes on its oxygen permeability was studied by preparing membranes with varying sintering time. The grain size was seen to increase from 57.57μm for 5 hours dwell time to 125.52μm for 48 hours dwell time. This increase in the grain size was found to be following power law. The BSCF membranes sintered for short time (5 hrs) showed better oxygen permeability. BSCF membranes with longer sintering durations (10, 15 and 48 hours) had similar oxygen permeability values. Permeability tests of membranes varying in thickness from 0.9mm to 1.3mm were carried out which revealed that the BSCF membrane has a critical thickness of around 1.1mm in the temperature range of 800-1100°C. A long term permeability test of the BSCF membrane showed excellent stability with respect to time producing a constant oxygen flux for an operation of 1000 hours. When the partial pressure of oxygen at the feed side was increased, the permeability showed significant improvement. A feed of 100% oxygen increased the membrane permeability by 90% compared to the permeability when air was being used as the feed.

4.4 APPLICATION OF BSCF MEMBRANE IN OXY-FUEL COMBUSTION REACTOR

The approach that has been taken in evaluating ITM stability, in the reported literature, is a CO_2 rich environment. This approach is good for quick membrane screening for ITM stability; however, it over estimates the real operating conditions of oxy-fuel reactors. Therefore, this approach might eliminate good candidates that are

relatively stable in a less harsh environment. In this study, a new approach has been taken, where the ITM is being subjected to actual reactor condition of pure fuel-gas flow. In this section the performance of BSCF membranes has been evaluated for oxygen separation under power plant conditions using methane gas as fuel. The volume of the methane gas has been optimized to the value where all methane and oxygen gases are consumed by the combustion reaction. Quantitative analysis of all gases (CH_4, O_2, CO, CO_2, N_2) have been studied using an online gas chromatograph. The membrane permeability and stability have been evaluated for long runs, up to 200 hours.

4.4.1 Oxy-Fuel ITM Reactor

BSCF flat discs were prepared with final diameter of 19mm. The membrane thickness of 1.0 mm and 1.4 mm were achieved using polishing grits. The oxygen permeability was measured in an ITM reactor explained in detail in Chapter 3. The membranes were sealed to the alumina support tubes of the setup using silver rings. All the tests were carried out at 920°C.

The reactor was first used to measure the oxygen permeability of the BSCF membrane in the absence of any fuel. On the top surface of the membrane, air was continuously supplied at a flow rate of 20ml/min. On the bottom surface of the membrane, permeate side, helium was used as the sweep gas to carry permeated oxygen to the gas chromatograph (GC). In order to evaluate the performance of the membranes in oxy-fuel conditions, methane/helium mixture and pure methane were applied as the sweep gas. The GC was calibrated to measure all possible gas species present in the

sweep after combustion i.e. carbon dioxide, carbon monoxide, methane, oxygen and nitrogen. The water steam, produced by the combustion reaction, was condensed before the permeate passes to the GC.

4.4.2 Stability of BSCF Membrane during Oxy-Fuel Combustion

The real issue with the BSCF stability arises when the membrane is operating inside a combustion reactor where the CO_2 is a major product of the reaction. Therefore, one of the most adopted methods to test the stability of ITM membranes is the use of CO_2 as a sweep gas. It has been reported that when the CO_2 percentage in the sweep is more than 25% the oxygen permeability of the BSCF membrane decreases considerably, and when pure CO_2 is used as the sweep gas, the BSCF membrane completely fails immediately [140]. Engels et al. [16] used BSCF tube membranes and showed that when 5% CO_2 was used as sweep there was a drop of 6% in oxygen permeability but the performance of the membrane was stable. When the CO_2 concentration in the sweep gas was increased by 15%, the oxygen permeability was decreased by 80%, within 200 min.

In this study, instead of using the above mentioned method to evaluate BSCF membranes, a more direct approach has been adopted by introducing fuel (methane) in the reactor at high temperature and carrying out actual combustion. As a first step, a constant volume flow rate of 1.5ml/min methane was added to the helium sweep gas. Different flow rates (10, 20 and 30ml/min) of the mixture were studied. Since the methane flow was maintained at a constant rate of 1.5ml/min, the change of the total flow rate of the mixed gas (helium and methane) from 30 to 10 ml/min has changed the

methane concentration from 5 to 15%, respectively. It was evident from the results of Figure 4.17 that high flow rate (30 ml/min) or low methane concentration (5%), only 0.02 ml/min of methane has reacted; the remaining 1.48 ml/min did not have a chance to contact oxygen molecules for reaction. Also for the same flow rate, negligible amount of CO_2 and CO were detected. Decreasing the quantity of Helium while keeping methane quantity fixed has improved the combustion. The amounts of oxygen and methane have decreased from 1.30 and 1.48ml/min to 0.24 and 0.83ml/min, respectively, when the flow rates were decreased from 30ml/min to 10ml/min. On the other hand, CO_2 has increased from being negligible in the sweep to 0.65 ml/min. Nevertheless, the presence of both methane and oxygen in the sweep revealed that the reaction was not completed.

It can be concluded from this experiment that the methane concentration in the sweep gas and the total flow rate have affected the combustion reactions. Accordingly, the combustion reactions prefer low flow rate of the gas mixture and high concentration of methane in the sweep gas.

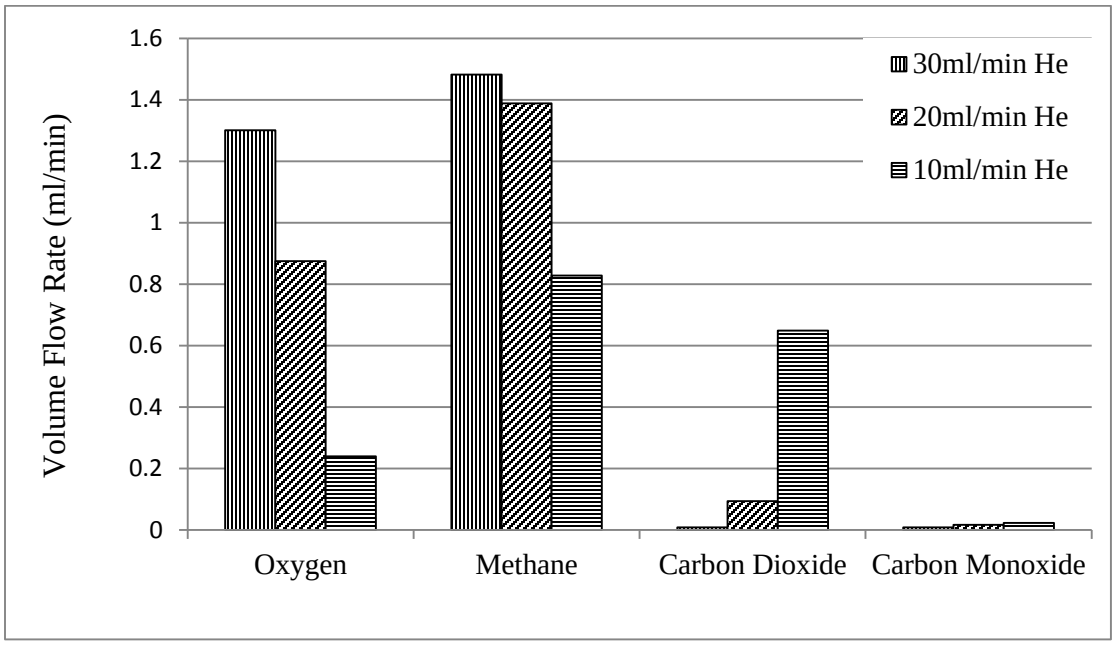

Figure 4.17 Effect of sweep-gas flow rate on combustion reaction at 920°C using 1.4 mm thick BSCF membrane and constant methane flow rate of 1.5ml/min. Different helium flow rates have been added to accumulate the total flow rates of 10, 20, and 30 ml/min.

Based on the previous conclusion, if pure methane has been used as a sweep gas then there would have been a better chance for a complete combustion reaction to take place. For this reason, the following experiments were conducted without using helium as the sweep gas and only pure methane was flowing into the reactor from the permeate side. It should be noted that Helium gas played two major roles in the ITM reactor. Firstly, it created low oxygen partial pressure at the sweep side of the membrane. Usually, for higher flow rates lower oxygen partial pressures would be generated, leading to higher membrane permeability[153]. Secondly, the helium flow was needed to carry the oxygen to the online GC instrument for gas analysis. Here also, higher flow rates were preferred

for faster data collection. In the absence of helium, as a sweep gas, the methane gas had to accomplish the two tasks that used to be carried out by helium; i.e. creating low oxygen partial pressure and delivering the gas mixture to the GC for analysis. The first task could be easily accomplished by methane as it reacted with oxygen near or at the membrane surface; therefore, it created low oxygen partial pressure. In addition, if all available oxygen molecules at the membrane surface reacted with methane then lower partial pressure could be created with low flow rates of methane compared to the partial pressure produced using high flow rates of helium. The second task could also be accomplished using pure methane gas; however, for low flow rates, longer time was needed to deliver the gas mixture to the online GC instrument. As a matter of fact, the gas-sample collection time has increased from few minutes using helium (at 30ml/min) to few hours using pure methane at 1.5 ml/min. Large portion of the sampling time was required for flashing the reactor chamber and the delivering tubes.

The effect of methane flow rate on the combustion reaction has been studied in the range of 0.65 to 1.0 ml/min at constant temperature of 920°C. The results of Figure 4.18 show that for 1.0 ml/min methane, there is a presence of both oxygen and methane in the permeate stream. This means that not all oxygen has been consumed even when the methane is present in excess. Upon reduction of the methane quantity in the sweep (0.9, 0.89 and 0.88 ml/min methane), both the oxygen and methane diminish after combustion, whereas the amount of CO_2 increases. This means that all produced oxygen by the BSCF membrane is consumed by the combustion reaction and there is no excess of unburned

methane. A further reduction of methane (0.87 and 0.85 ml/min) in the sweep causes the amount of oxygen to rise, meaning the methane was not enough to consume all produced oxygen. In addition, the presence of small quantities of carbon monoxide indicates there is a slight occurrence of either an incomplete reaction or syngas reaction.

Taking all of the above observations into account, a long-term study using 0.88ml/min methane has been implemented. This flow rate would ensure nearly complete consumption of both oxygen and methane during the combustion and yield maximum amount of carbon dioxide. Furthermore, the small traces of CO detected in the gas stream with this flow rate (Figure 4.18) indicates that a close to complete combustion reaction is taking place. The membrane and setup used for this experiment is the same as the previous experiment i.e. 1.4 mm thick BSCF membrane operating at 920°C. Figure 4.19 shows that the performance of the membrane deteriorates with the passage of time, evident by the decreasing amount of CO_2 and increasing methane. However, the rate of deterioration is much slower than what is claimed in the literature. According to Figure 4.19, the BSCF membrane has operated under reactive condition for about 2 days without showing signs of deterioration. Even after 92 hours there is enough oxygen being supplied by the BSCF membrane to consume 0.61 ml/min methane. As expected, during the oxy-fuel combustion, the volume concentration of CO_2 in the sweep gas is consistently detected to be over 33%. The deterioration in the presence of such large percentage of CO_2 is only 30% after more than 90 hours continuous reaction. In the

literature it is shown that even 20% concentration of CO_2 in the sweep gas reduces the membrane performance by 80% within 3 hours [16][36].

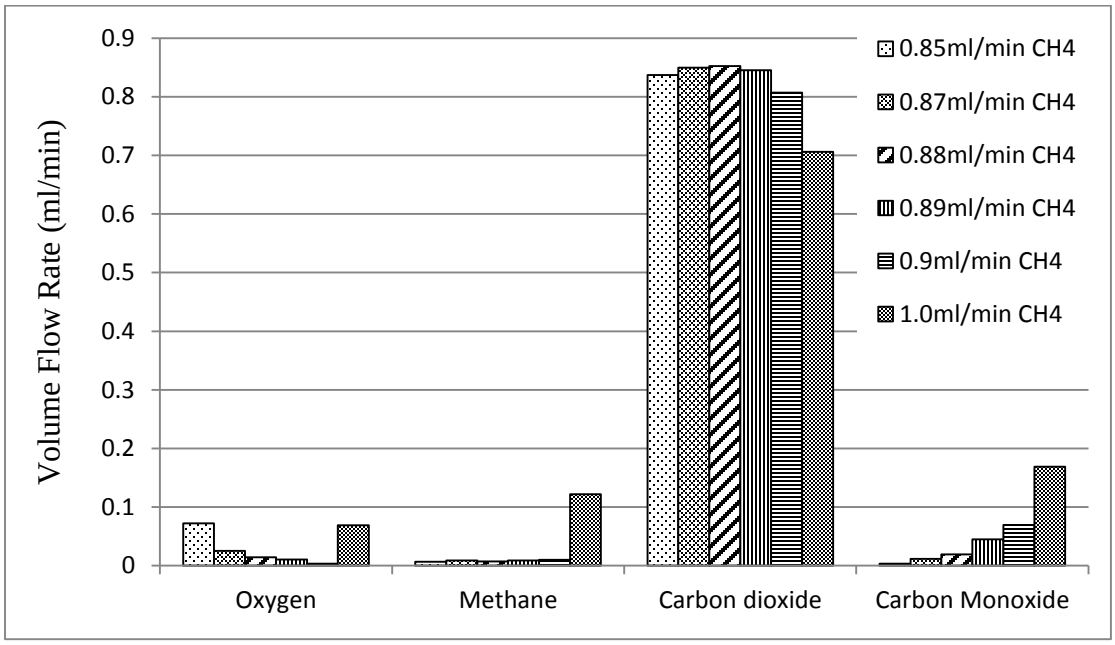

Figure 4.18 Effect of methane flow rate on combustion reaction at 920°C using 1.4mm thick BSCF membrane.

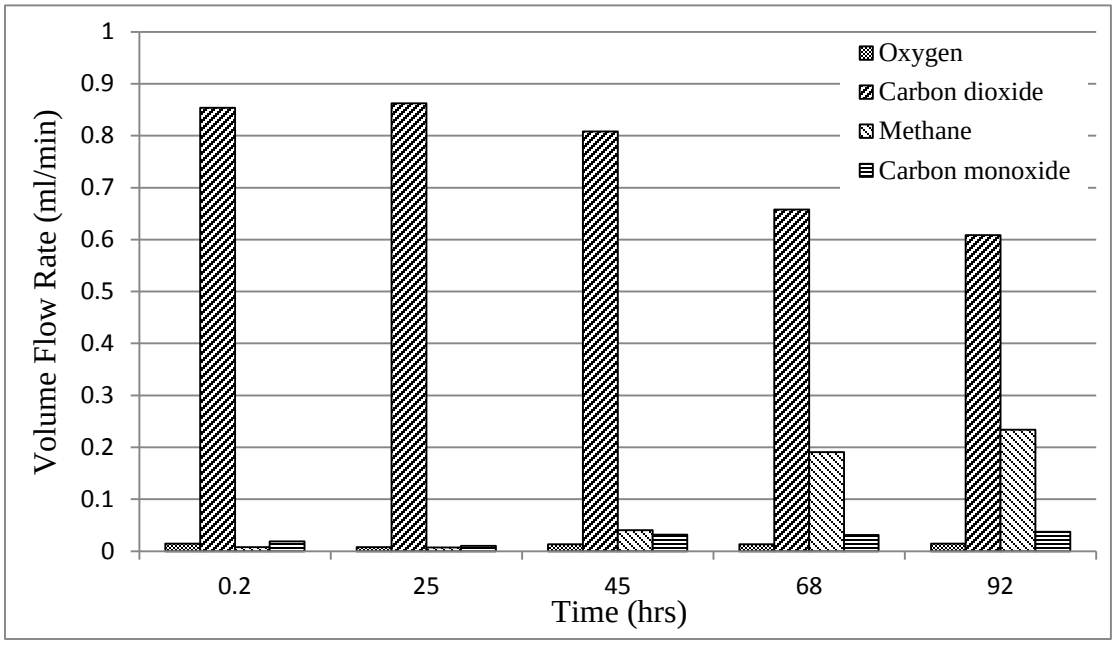

Figure 4.19 Quantitative analysis of gases detected in the sweep during long-term combustion with 0.88ml/min CH_4 at 920°C. (Helium is not used in this test)

After 100 hours of combustion at the methane flow rate of 0.88 ml/min, the fuel flow rate has been adjusted in order to determine the optimum fuel quantity needed for 100 hour operation. Figure 4.20 shows that a fuel volume of 0.65ml/min produces maximum CO_2 with nearly complete consumption of both oxygen and methane. In addition, CO gas has not been detected, which is another good indication of a close-to-perfect combustion reaction.

The next test has been performed using the newly determined rate of fuel (0.65ml/min) for the long term combustion reaction (Figure 4.21). As expected, initially

the amount of methane is completely consumed and very little amount of oxygen is remained. However, for longer durations, the amount of CH_4 gradually increases and that of CO_2 decreases. It is worth noting that this membrane has already been subjected to previous tests, more than 150 operating hours. For this reason, a new identical membrane was prepared and tested with 0.65ml/min CH4 sweep in order to see the performance of a fresh membrane. The experimental test has run for in excess of 200 hours and the results are shown Figure 4.22. According to the Figure 4.22, it is evident that the BSCF membrane shows a good performance using 0.65ml/min CH_4 for an extended period of time. Theoretically, if all methane is to be consumed, the membrane should produce a minimum oxygen flow of 1.3 ml/min. Figure 4.22 shows that initially the membrane is producing excess of oxygen of 0.097 ml/min (7.5% excess). However, the excess-oxygen decreases with time and becomes negligible after 190 hours of combustion. It can be predicted that if the test is kept running for a longer period of time the trend seen in Figure 4.21 will be followed.

Figure 4.23 shows the oxygen permeability flux through the membrane during continuous oxy-fuel combustion reaction for nearly 200 hours. The initial flux value at the startup of the reactor is 0.827μmol $cm^{-2}s^{-1}$, and the flux value after 190 hours is 0.762 μmol $cm^{-2}s^{-1}$. This is a decrease of only 7.9% under a continuous oxy-fuel combustion reaction at the membrane's surface for more than a week of operation.

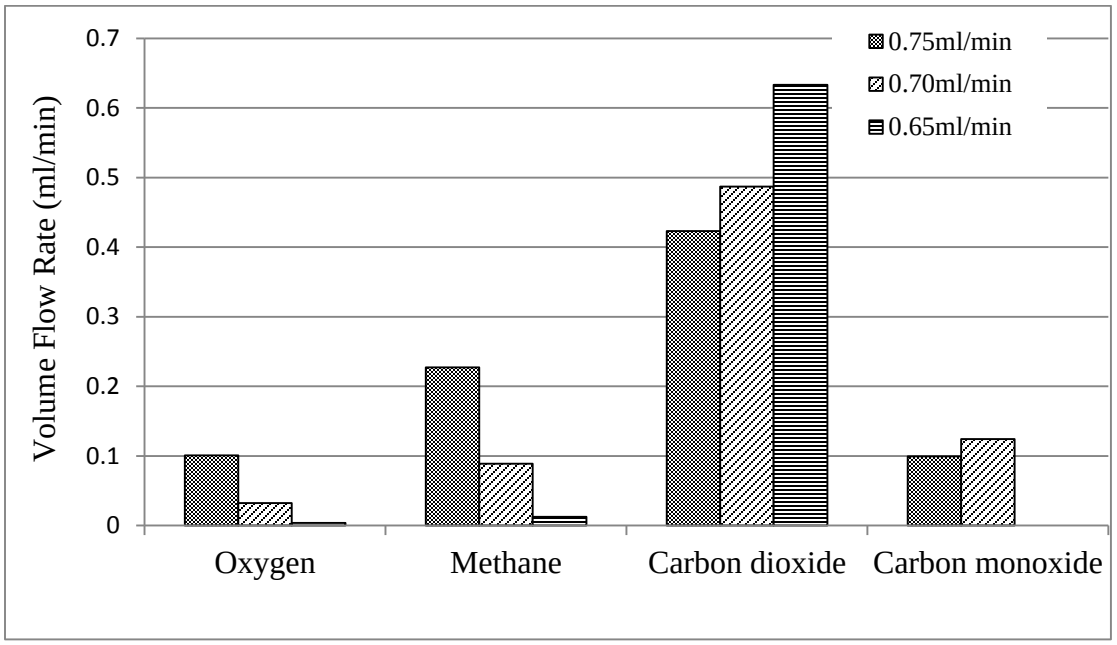

Figure 4.20 Quantitative analysis of gases detected in the sweep after 100 hours of combustion with various methane flow rates at 920°C.

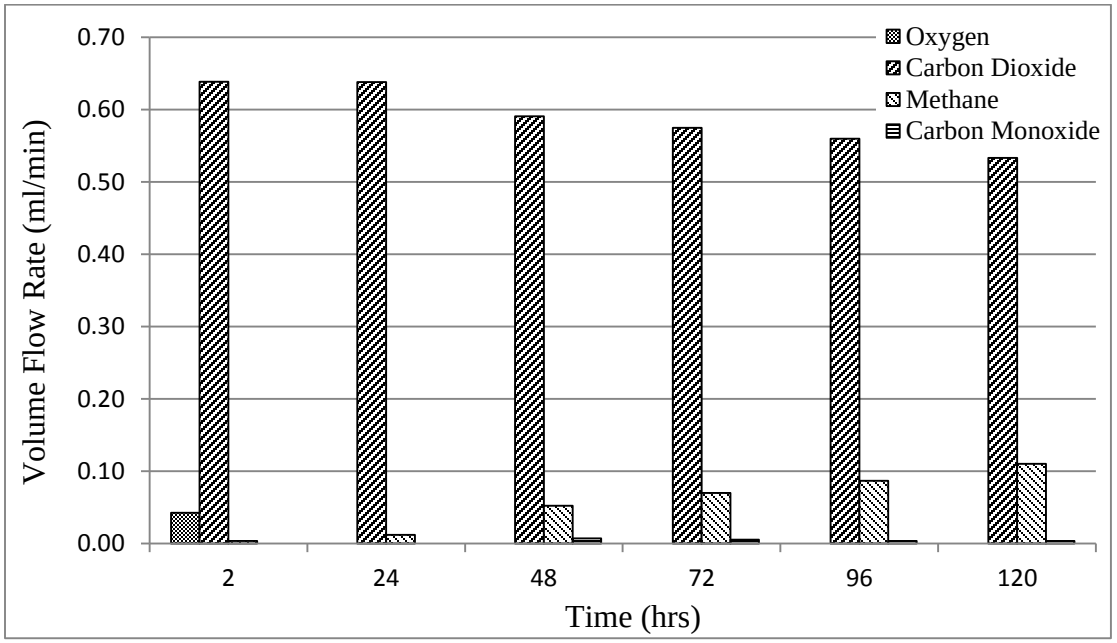

Figure 4.21: Gas analysis of a long term combustion reaction at 920°C and 0.65ml/min CH_4.The membrane is a 1.4mm thick BSCF after being used in previous experiments of Figure 4.20

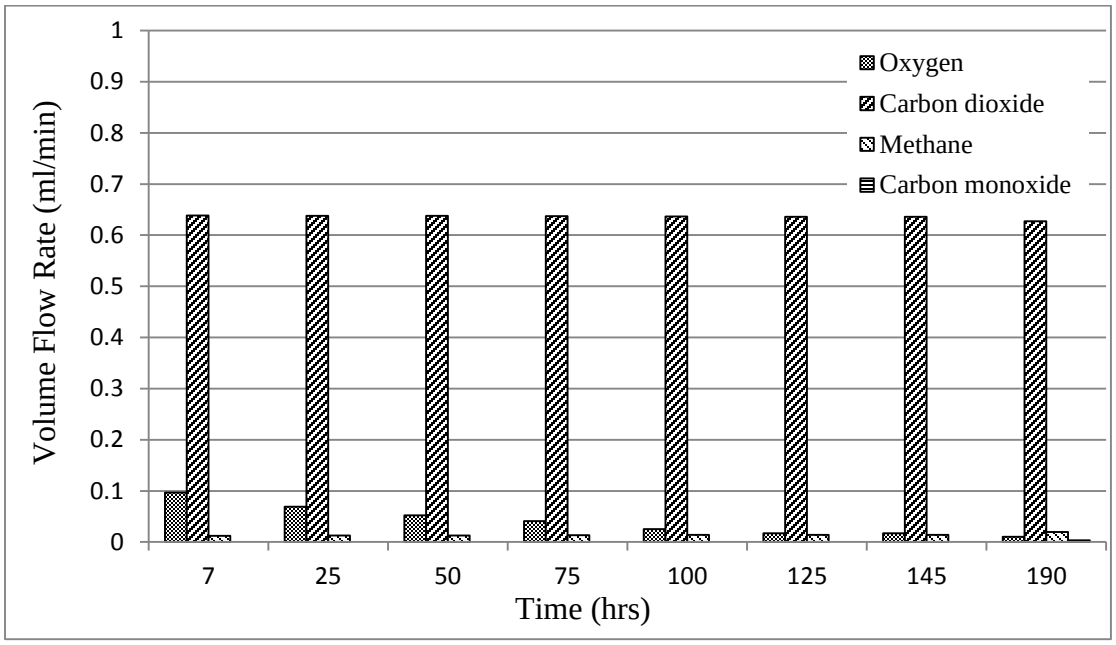

Figure 4.22: Gas analysis of a long-term combustion reaction at 920ºC using a new 1.4mm thick BSCF membrane and constant methane flow rate of 0.65ml/min.

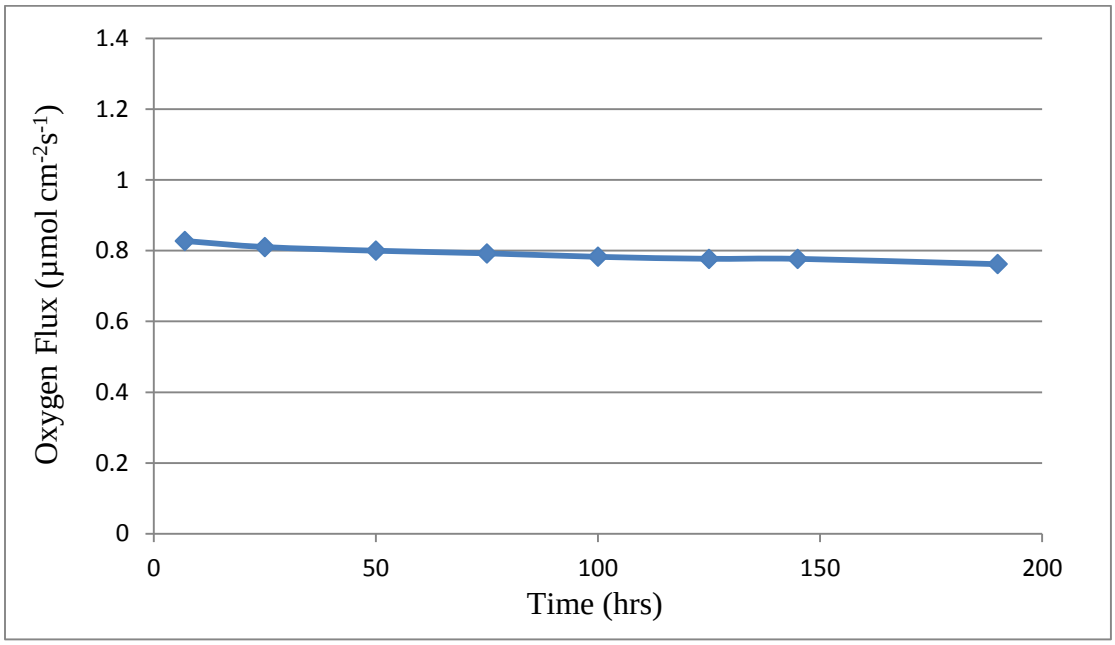

Figure 4.23: Oxygen Flux through the membrane during combustion calculated using complete combustion equation $CH_4 + 2\ O_2 \rightarrow CO_2 + 2\ H_2O$

Figure 4.24 shows that the oxygen permeability of the BSCF membranes decreases 11.7% from a value of 0.94μmolcm^{-2}s^{-1} during inert operation to a value of 0.83μmolcm^{-2}s^{-1} at the beginning of the combustion reaction. This drop in permeability flux is due to the effect of differences in partial pressure at the permeate side. Apparently, the helium gas flow rate, 30 ml/min, generates higher partial pressure difference than that when using methane at 0.65 ml/min. As a matter of fact, right after the first measurement of the permeability flux under combustion reaction, the system was switched back to inert gas process (30ml/min of helium), and the flux was measured to be the same as the first measured flux of 0.94μmolcm^{-2}s^{-1}. Therefore, the membrane did not show any deterioration at the early stage of oxy-fuel combustion. However, after 190 hours of

continuous oxy-fuel combustion reaction, the permeability of the membrane was measured again under helium gas flow rate of 30 ml/min, and the permeability flux was found to be 0.80μmolcm^{-2}s^{-1}. Compared to the initial value of 0.94μmolcm^{-2}s^{-1} before the start of combustion, there is a 15% loss. In order to refresh the membrane it was kept under air flow on both feed and permeate sides for 12 hours at 920ºC. The oxygen permeability flux was measured after this recovery and found to be 0.84μmolcm^{-2}s^{-1}. This indicates that the membrane has endured a permanent damage of about 10%. It is worth noting that initially, under methane combustion, the membrane was producing 0.097 ml/min excess of oxygen (Figure 4.22). After 190 hours of combustion, the excess of oxygen has dropped to 0.01 ml/min.

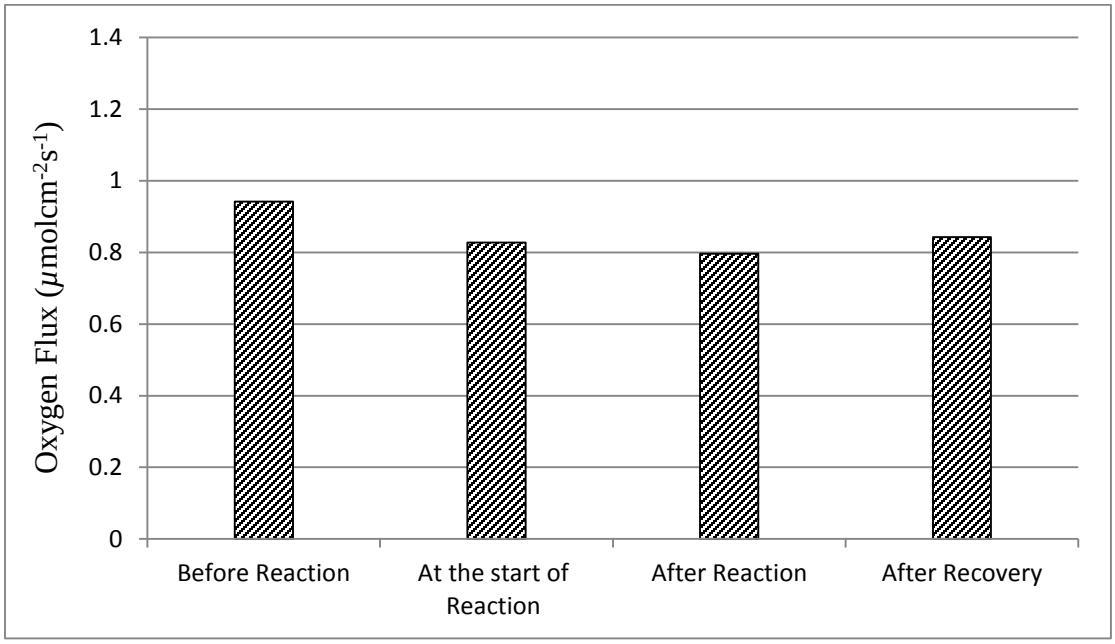

Figure 4.24: Effect of combustion reaction on oxygen permeation flux. The reaction temperature is 920ºC; BSCF membrane thickness is 1.4 mm; and methane flow rate is

0.65ml/min. Before and after reaction the sweep gas is pure helium at 30ml/min. The recovery is set for 12 hrs under air flow on both sides of the membrane.

Up till this point, BSCF membranes of 1.4mm thickness were used to investigate the permeability and chemical stability. It is understood that a decrease in the thickness of the BSCF membrane would enhance the oxygen flux. This holds true until the membrane reaches a critical thickness value (L_c) after which surface kinetics of the membrane start to limit the permeability of oxygen. A further decrease in the thickness doesn't appreciably increase the oxygen flux. Hong and Choi [118] determined L_c of BSCF membranes operating at a temperature of 900°C to be 1.1 mm. Our results presented in Section 4.3.2 of this chapter also confirm this. Considering this, a membrane of 1.0 mm thickness was produced and tested in identical conditions as before. This membrane was found to have a constant oxygen permeability of 1.26μmolcm^{-2}s^{-1} for a period of 100 hours when tested with 30ml/min helium as sweep (Figure 4.25) at 920°C. The helium sweep-gas was then replaced with 0.65ml/min methane gas in order to determine the stability and permeability of this membrane when subjected to combustion reaction. Figure 4.26 showed that, in this case, all of the methane gas reacted with oxygen to convert to carbon dioxide and water in a complete combustion reaction. In addition, there was excess oxygen of 0.20 ml/min (15% excess), measured from the sweep side. No traces of methane or carbon monoxide were detected. The experiment was kept running for more than 200 hours while taking regular readings. Even after 200 hours the amount of excess oxygen remains 0.20 ml/min with no decrease in the amount of carbon dioxide.

This is a remarkable result which showed that a carefully controlled fuel volume introduced into a BSCF ITM reactor provided high oxygen output and excellent stability for long period of time.

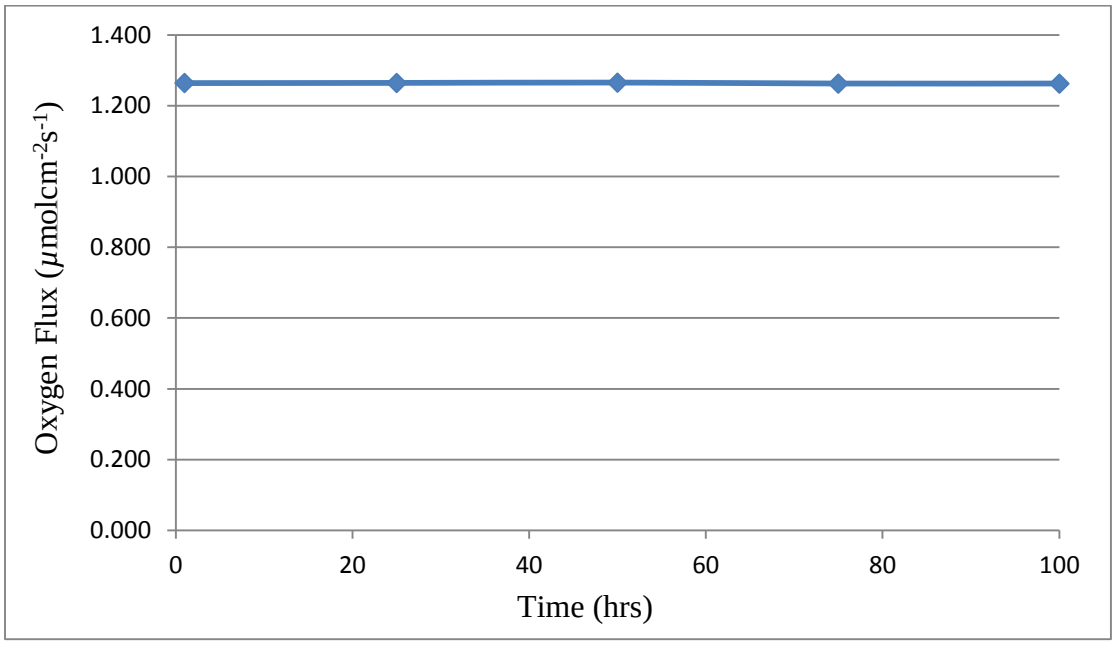

Figure 4.25: Oxygen permeability of a 1.0 mm thick BSCF membrane at 920°C. Helium is used as a sweep gas at a flow rate of 30ml/min.

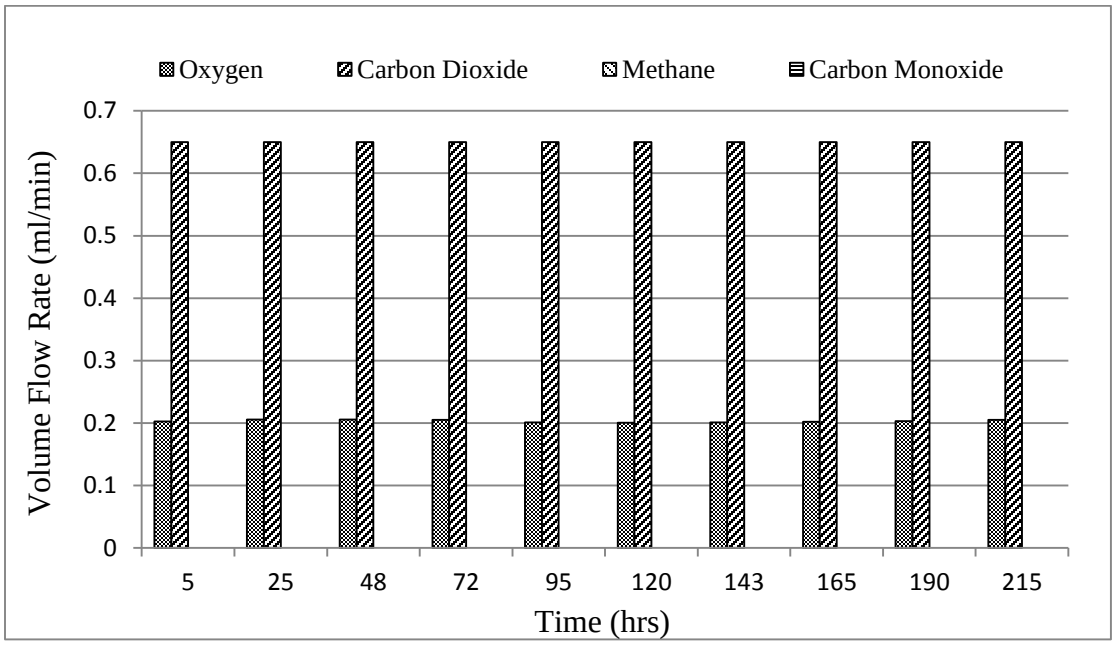

Figure 4.26: Gas analysis of a long-term combustion reaction at 920ºC using a 1.0 mm thick BSCF membrane and constant methane flow rate of 0.65ml/min.

Figure 4.27 shows that the permeability of oxygen during the combustion reaction is constant at about 0.91μmol cm^{-2} s^{-1} for the whole duration of the experiment. Once the combustion has ended the permeability of the membrane is analyzed using 30ml/min helium as sweep (Figure 4.28). The membrane immediately returns a permeability of 1.25μmol$cm^{-2}s^{-1}$ which is the same value as that before combustion. This further confirms that there is no temporary or permanent damage to the membrane as a result of the combustion reaction with methane.

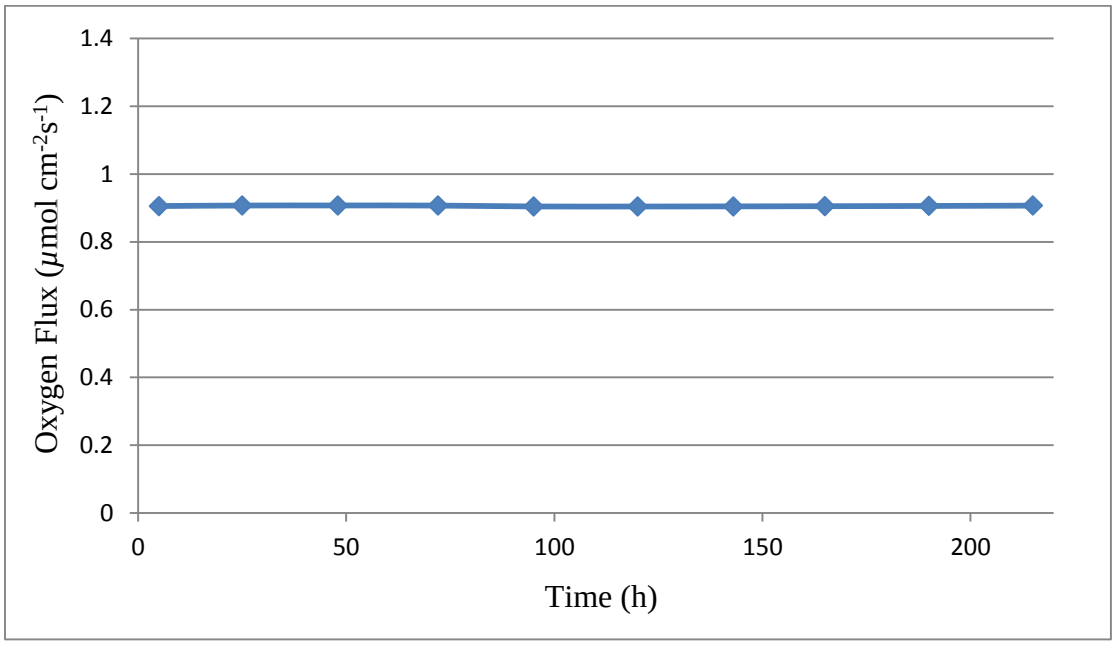

Figure 4.27: Oxygen Flux through the 1mm thick BSCF membrane during combustion calculated using complete combustion equation $CH_4 + 2O_2 \rightarrow CO_2 + 2H_2O$

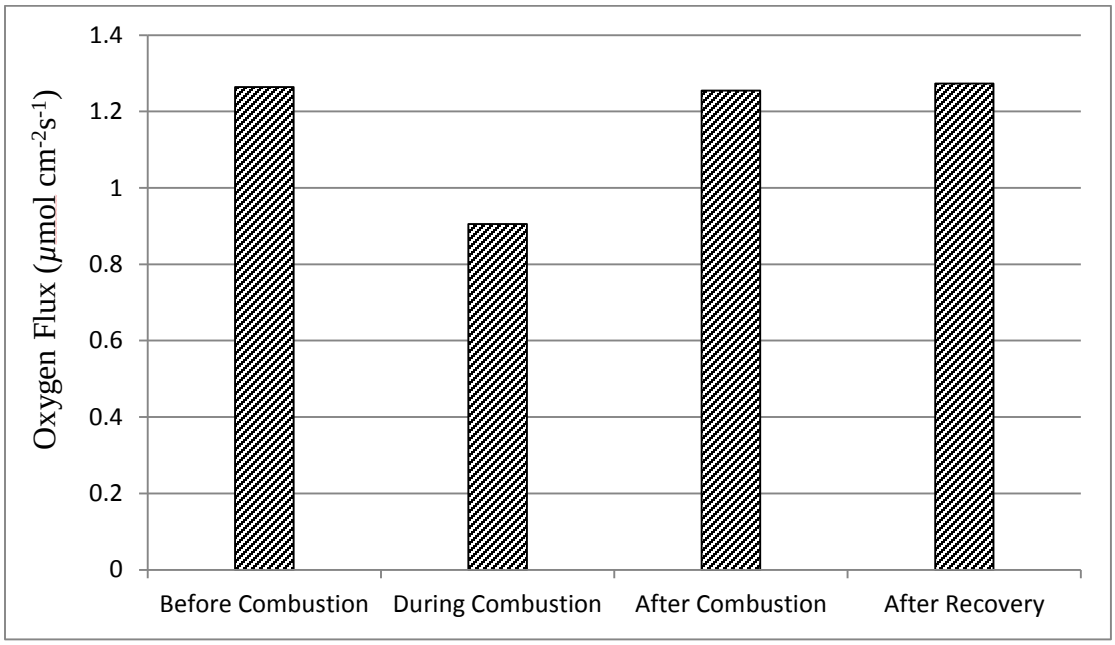

Figure 4.28: Effect of combustion reaction on oxygen permeation flux. The reaction temperature is 920ºC; BSCF membrane thickness is 1.0 mm; and methane flow rate is 0.65ml/min (during combustion). Before and after combustion the sweep gas is pure helium at 30ml/min. The recovery is set for 12 hours under air flow on both sides of the membrane.

4.4.3 Determination of Optimal Fuel for Long Term Reactions

It is evident from the previous experiments that a 1mm thick BSCF membrane is stable giving a constant oxygen permeability flux when a fixed volume of 0.65ml/min methane is used for oxy-fuel combustion on the permeate side of the membrane. In order to further build up on this result, it was decided to carry out combustion reactions increasing the methane flow rate into the reactor in various steps. In each step the methane flow rate will be increased by 0.1ml/min and the gas analysis of the permeate

side will be done for at least 100 hours before moving on to the next step. Another 1mm thick membrane was prepared for this purpose and tested with the methane flow rates of 0.65, 0.75, 0.85, 0.95 and 1.05ml/min. The gas analysis and the total oxygen permeability of the membrane for these experiments are showed in Figure 4.29 to Figure 4.38. The oxygen permeability of this membrane with respect to methane flow rate and time is shown in Figure 4.39. These results show that the permeability of the membrane improves when the methane flow is increased. This is because an increase in the fuel causes greater consumption of oxygen increasing the difference in the partial pressure between the feed and permeate side. As a result the value of oxygen permeability, which was 0.91μmol $cm^{-2}s^{-1}$ for 0.65ml/min methane, increases to 1.0, 1.09, 1.16 and 1.21μmol $cm^{-2}s^{-1}$ for methane flow rates of 0.75, 0.85, 0.95 and 1.05ml/min respectively. The gas analysis and the oxygen permeability values were found to be constant for 100 hour operation for all the methane flow rates except the last one i.e. 1.05ml/min. In this case the oxygen permeability of the membrane experienced a small but steady drop of 4.13% in 115 hours.

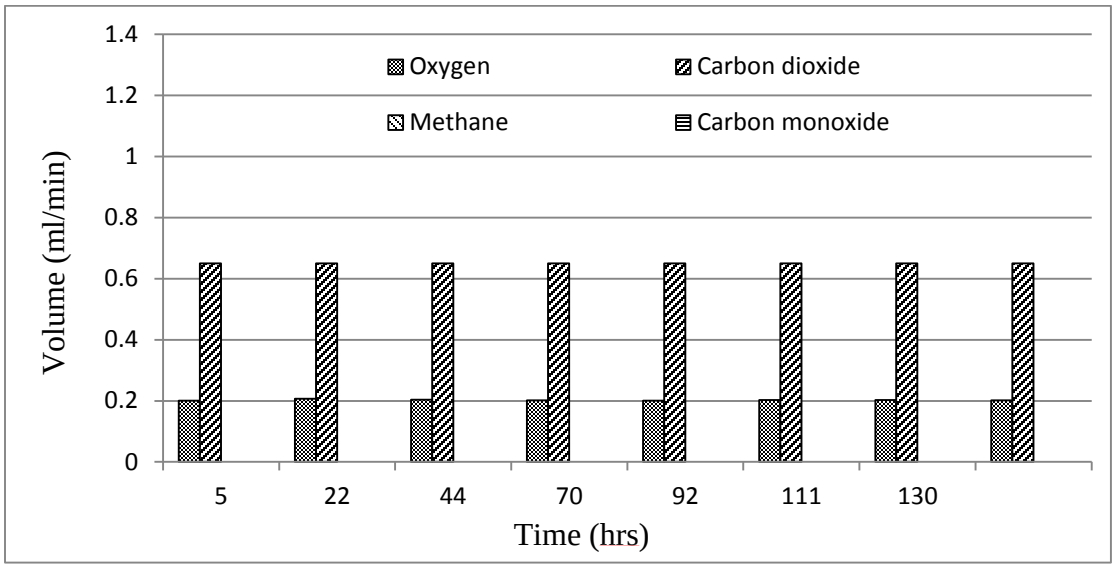

Figure 4.29 Gas analysis of a combustion reaction at 920ºC using a 1 mm thick BSCF membrane at constant methane flow rate of 0.65ml/min.

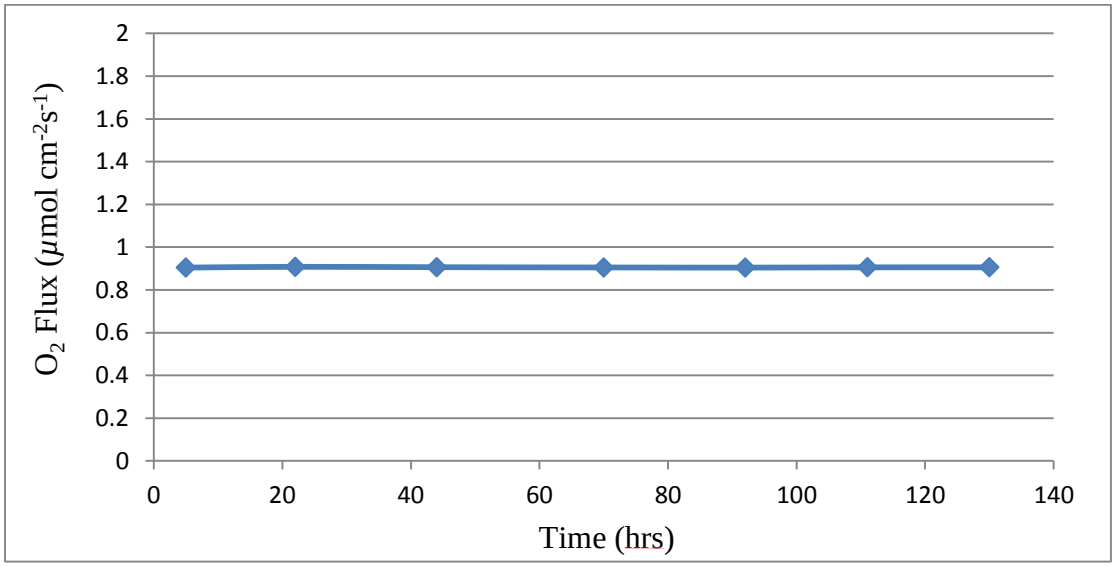

Figure 4.30 Oxygen Flux through the 1mm thick BSCF membrane during combustion with 0.65ml/min methane at 920°C.

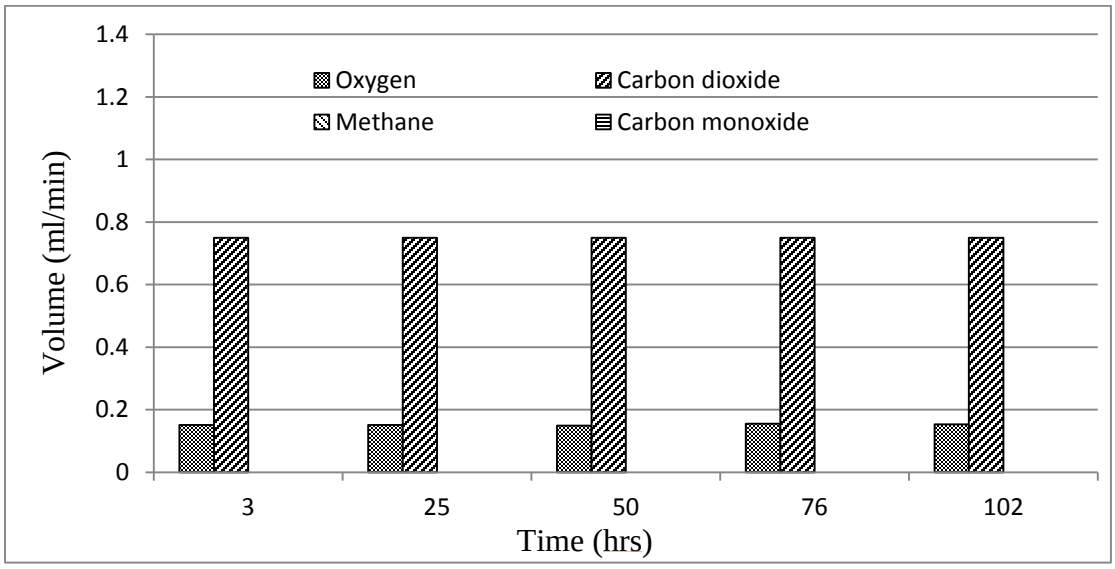

Figure 4.31 Gas analysis of a combustion reaction at 920ºC using a 1 mm thick BSCF membrane at constant methane flow rate of 0.75ml/min.

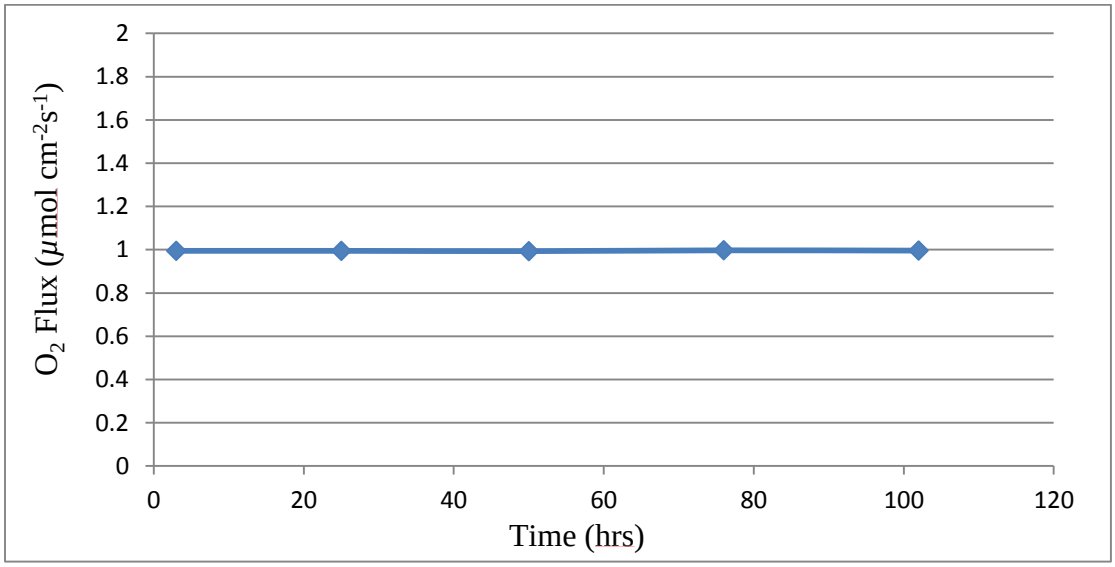

Figure 4.32 Oxygen Flux through the 1mm thick BSCF membrane during combustion with 0.75ml/min methane at 920°C.

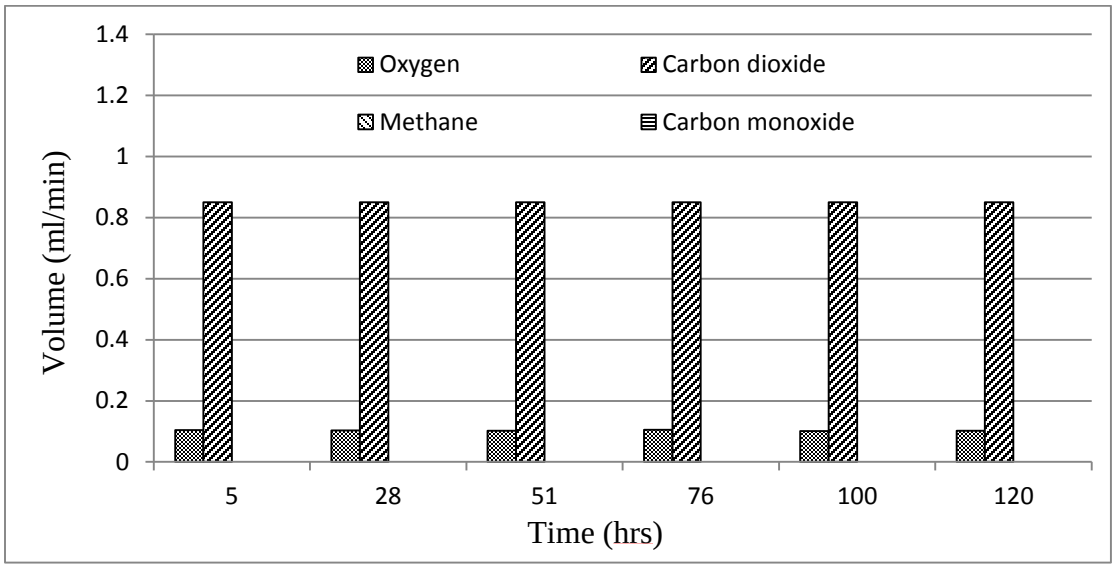

Figure 4.33 Gas analysis of a combustion reaction at 920ºC using a 1 mm thick BSCF membrane at constant methane flow rate of 0.85ml/min.

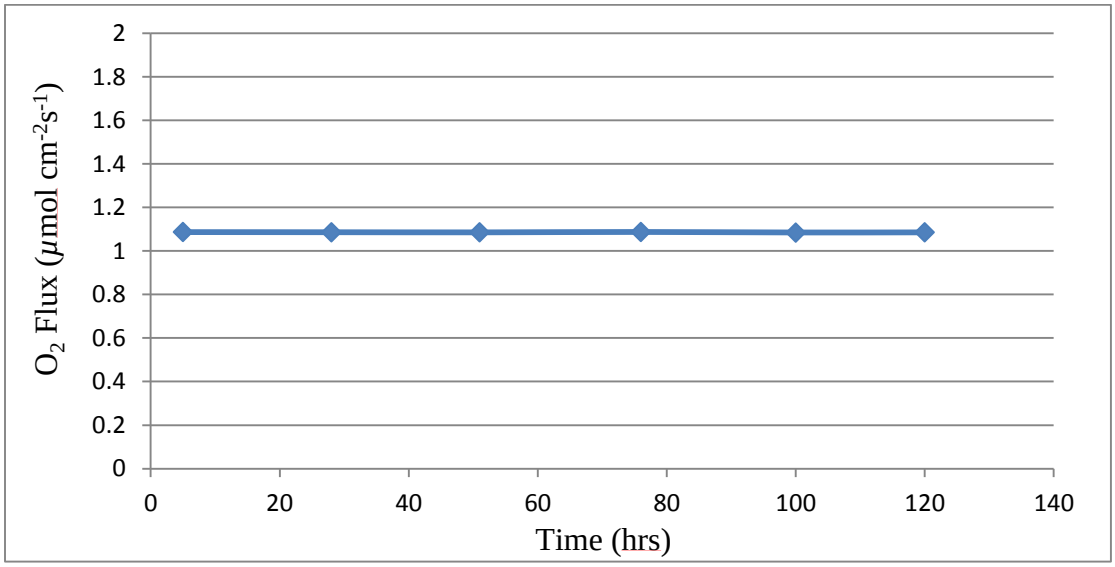

Figure 4.34 Oxygen Flux through the 1mm thick BSCF membrane during combustion with 0.85ml/min methane at 920°C.

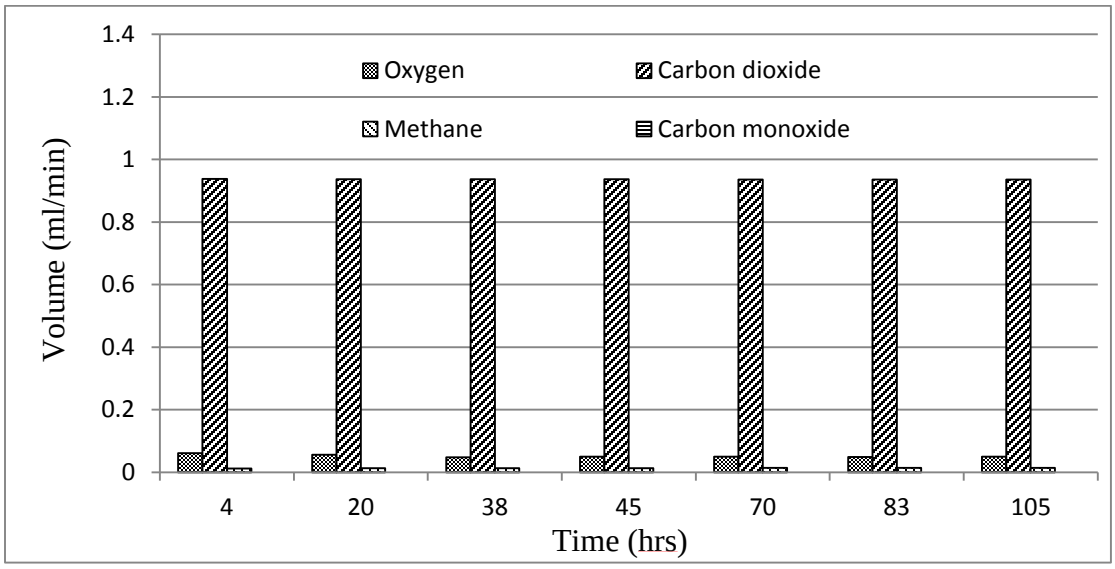

Figure 4.35 Gas analysis of a combustion reaction at 920ºC using a 1 mm thick BSCF membrane at constant methane flow rate of 0.95ml/min.

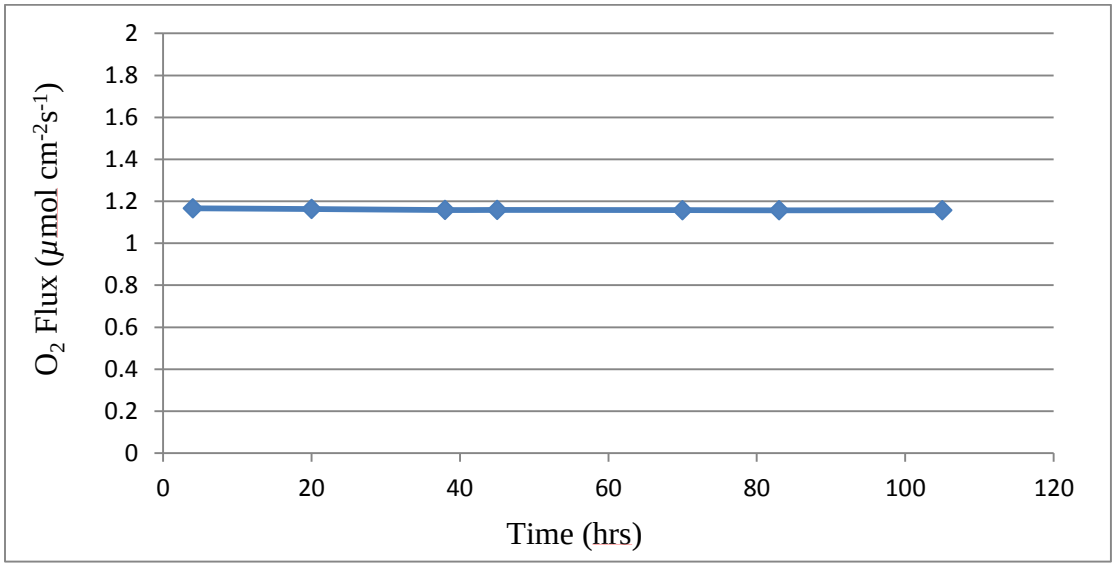

Figure 4.36 Oxygen Flux through the 1mm thick BSCF membrane during combustion with 0.95ml/min methane at 920°C.

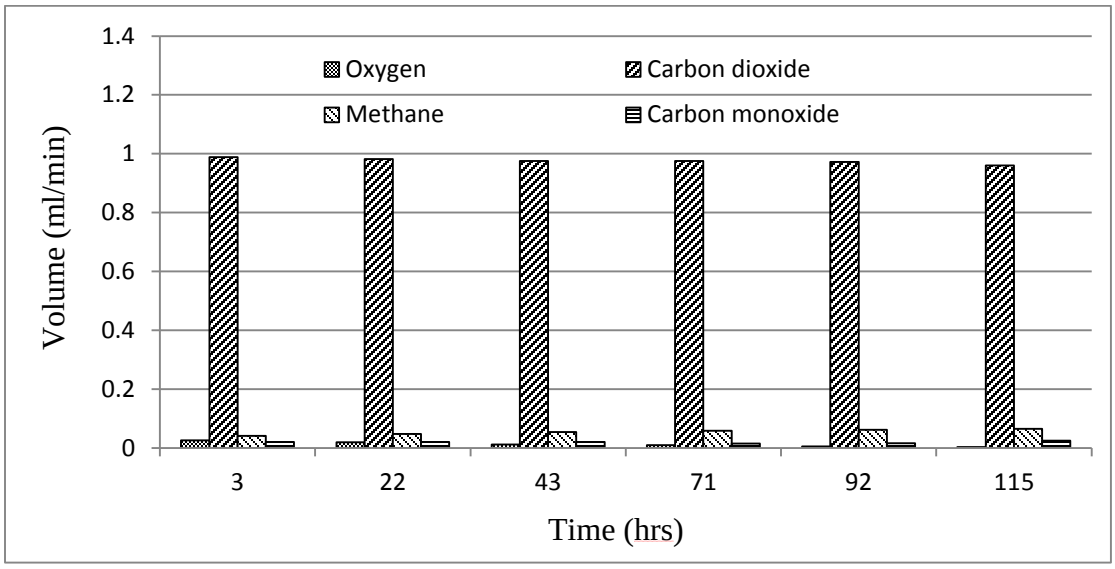

Figure 4.37 Gas analysis of a combustion reaction at 920ºC using a 1 mm thick BSCF membrane at constant methane flow rate of 1.05ml/min.

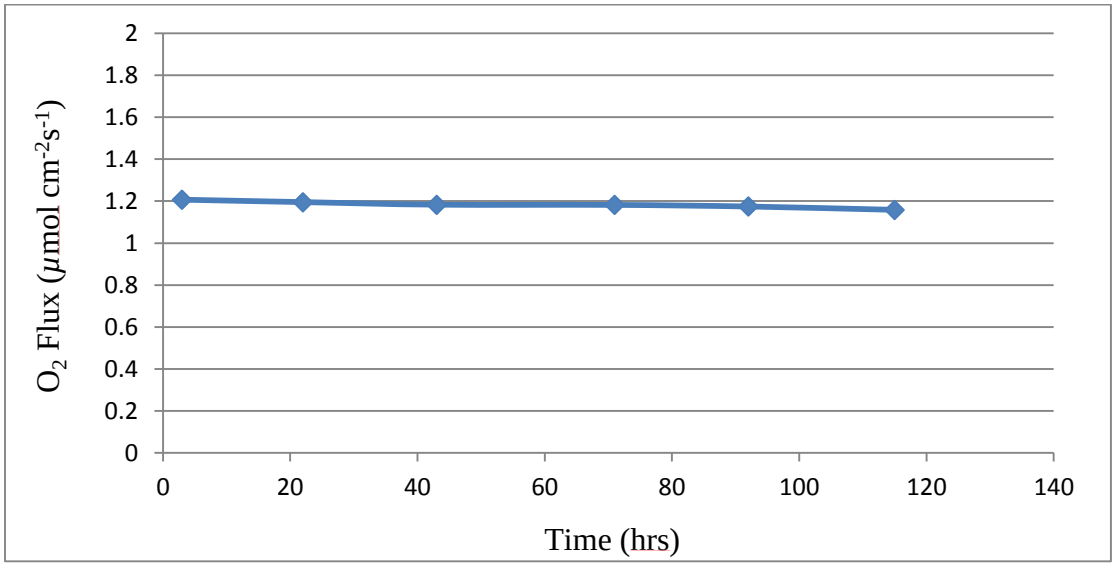

Figure 4.38 Oxygen Flux through the 1mm thick BSCF membrane during combustion with 1.05ml/min methane at 920°C.

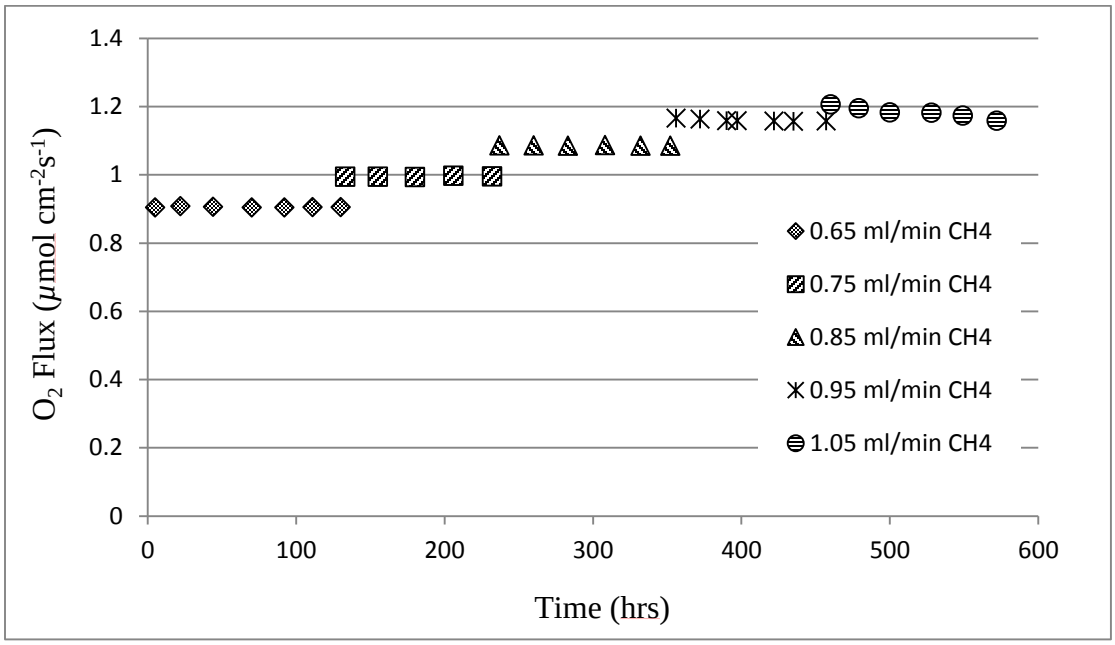

Figure 4.39 Oxygen Flux through the 1mm thick BSCF membrane during combustion with methane at 920°C. The methane flow rate varies from 0.65ml/min to 1.05ml/min.

4.4.4 Surface Analysis of the Post Reaction Membrane Surface

During the test this side of the membrane had been exposed to combustion reaction for more than 550 hours in total. The membrane had also experienced slight degradation at the last stage of the test. Before the start of the test both permeate and feed sides of the membrane were identical. The SEM of permeate side after the combustion reaction (Figure 4.40) is quite different looking than the SEM of the feed side of the membrane (Figure 4.41). The surface looks to have undergone some sort of chemical change.

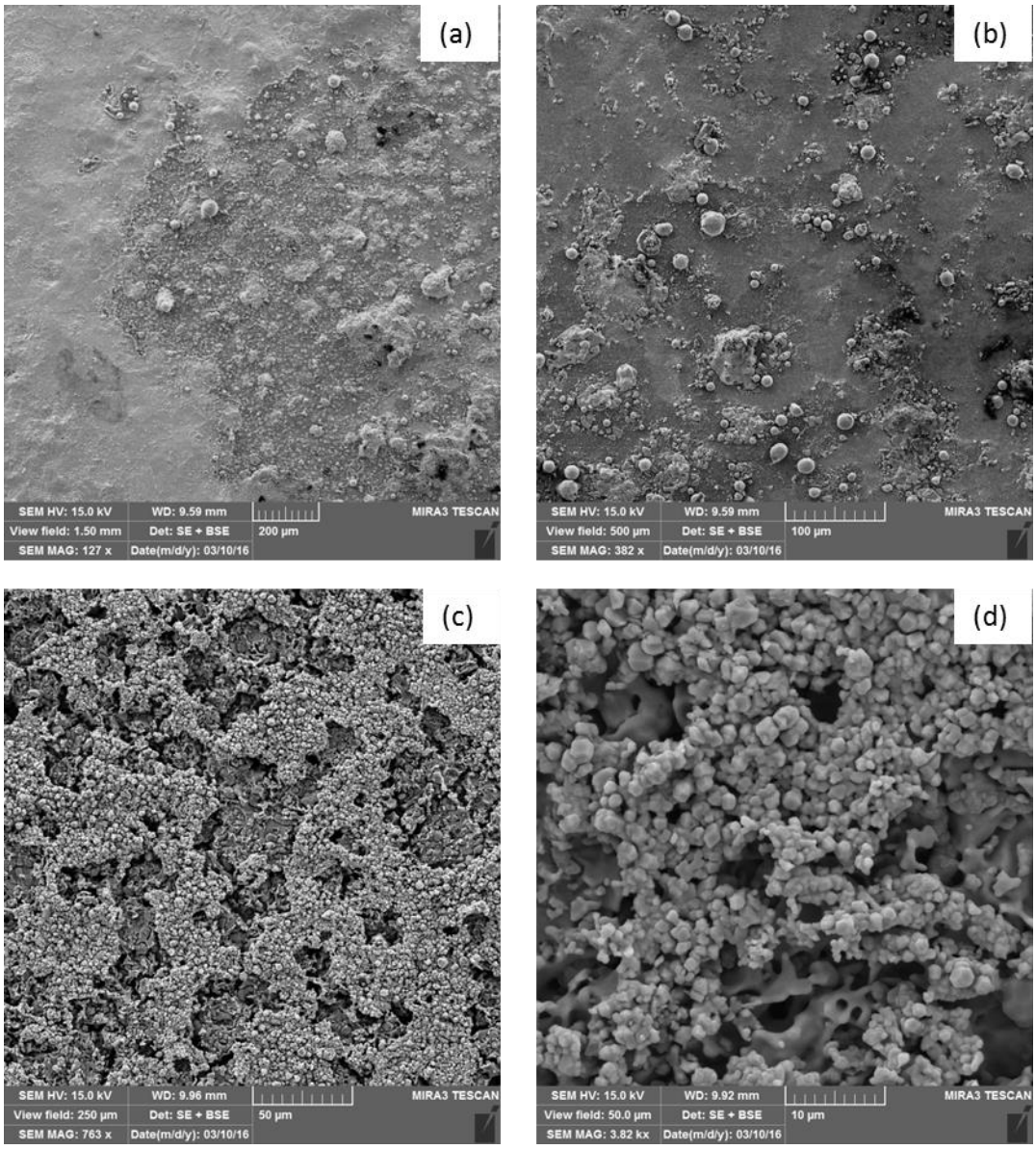

Figure 4.40 SEM analysis of the permeate side of the BSCF membrane after it was subjected to oxy-fuel combustion reaction for 572 hours

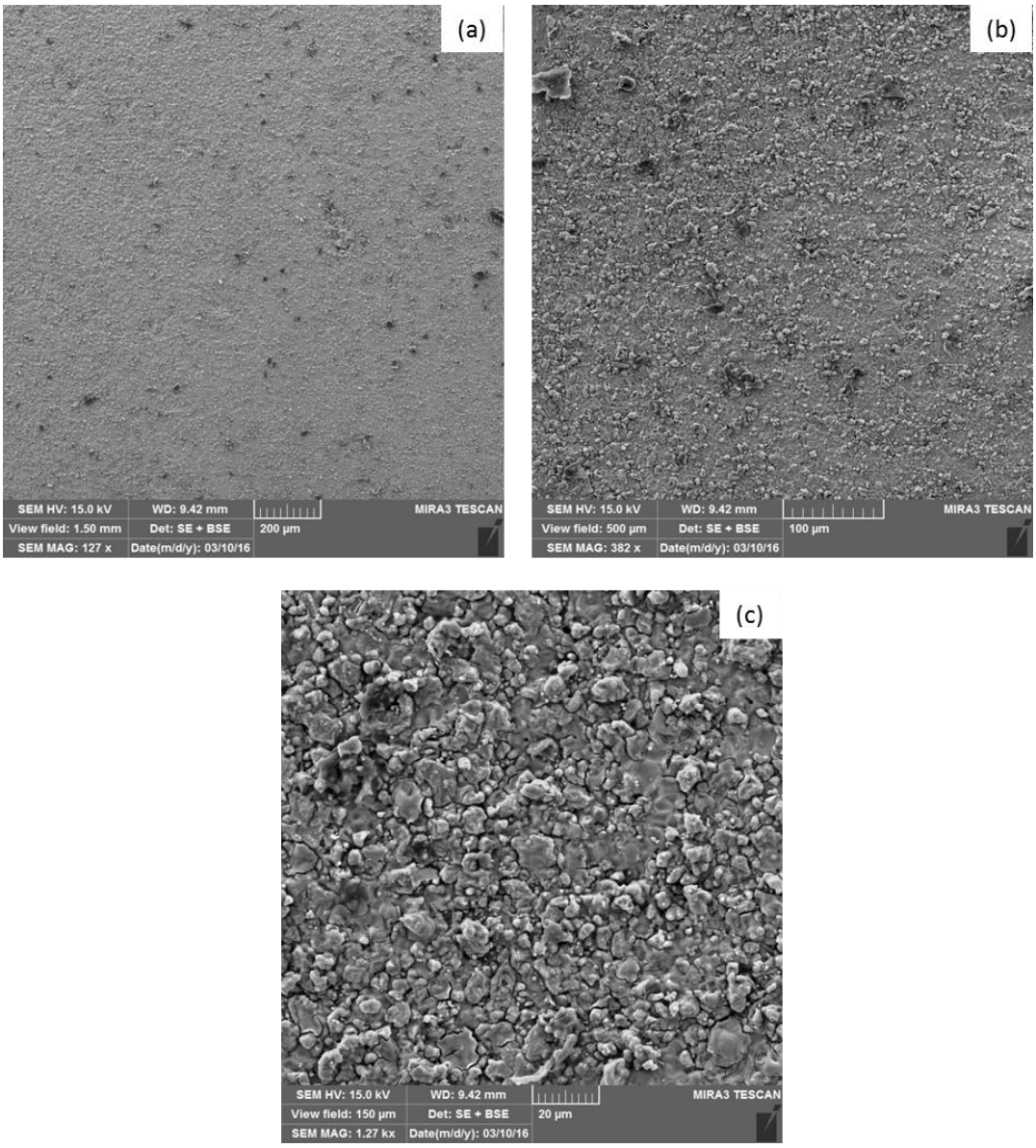

Figure 4.41 SEM analysis of the feed side of the BSCF membrane after completion of oxy-fuel combustion reaction.

Table 4.5 EDX elemental analysis of the permeate side of the BSCF membrane after undergoing oxy-fuel combustion for 572 hours

Element	At. %
Barium	30.99
Strontium	39.98
Cobalt	24.14
Iron	4.89

The EDX analysis was carried out to see if this observation could be verified. The area shown in Figure 4.40(d) was selected for this purpose. The atomic percentages of the elements show that the surface of the membrane is rich in barium and strontium as their values have increased from 25% each in unused membrane to 30.99% and 39.98% respectively. This is possibly due to a reaction zone forming at the surface which includes barium and strontium possibly reacting with CO_2.

The XPS analysis of the permeate side of the BSCF membrane after the test clearly shows that the surface of the membrane is enriched in barium and strontium whereas iron and cobalt seem to be buried beneath the top layer (Figure 4.42). In order to investigate this we take a closer look at the peaks. Clearly the oxygen, carbon and strontium have chemical shifts corresponding to carbonate formation (Figure 4.43). In fact the relative intensity of the carbonate peaks in all of these elements was found to be greater than the oxide peak. This confirms that there is a layer of barium and strontium carbonate that has

formed on the surface of the BSCF membrane on the side where it was interacting with the flue gas. This layer is responsible for the decrease in the permeability of the BSCF membrane when the volume of fuel is increased.

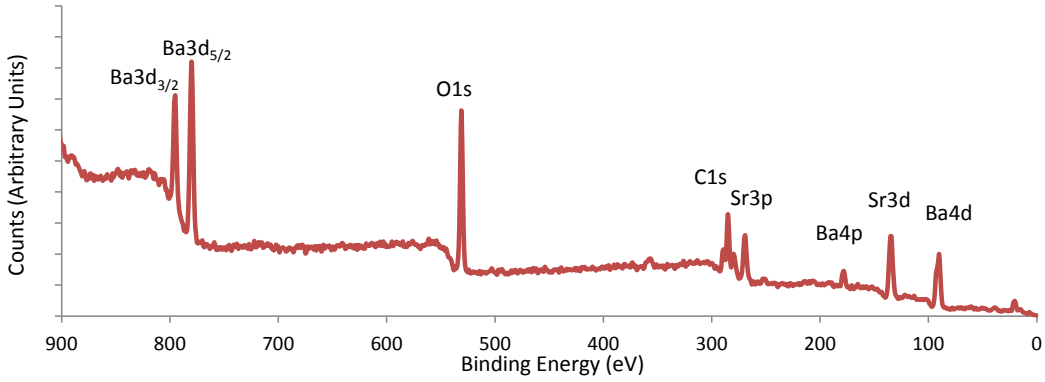

Figure 4.42 XPS scan of the permeate side of the BSCF membrane after combustion reaction with methane

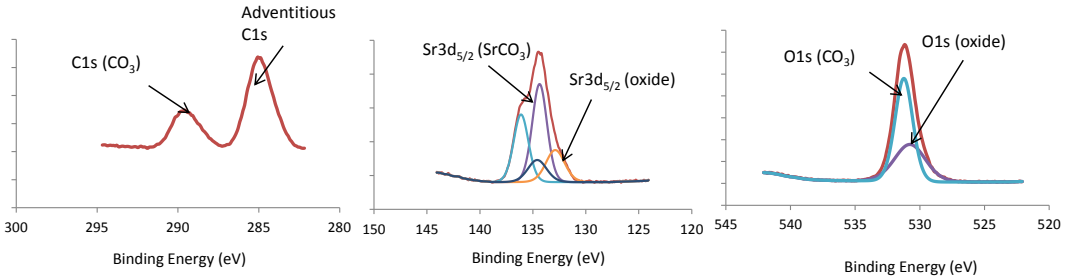

Figure 4.43 Detailed XPS scan of the Carbon, Strontium and Oxygen peaks from the permeate side of the BSCF membrane after combustion reaction with methane

4.4.5 Summary

In this section the performance of BSCF membranes employed inside a laboratory scale oxy-fuel combustion reactor was evaluated. To create the conditions necessary for the reaction to take place, the sweep gas used earlier (helium) was replaced to methane. Initially the quantity of methane used was carefully adjusted so that all of oxygen produced by a 1.4mm thick membrane was utilized without leaving any excess of methane in the sweep. A methane quantity of 0.65 ml/min was found to be appropriate for running the experiment in excess of 200 hours. The quantities of carbon dioxide produced as a result of the reaction and any excess of oxygen or methane were measured. It was shown that with such optimized combustion taking place, the degradation of BSCF membranes was much slower than expected. During an operation of nearly 200 hours the quantity of oxygen produced by the membrane reduced only by 7.9%. A 1.0 mm thick BSCF membrane tested under identical conditions was found to produce 1.26 μmol cm^{-2} s^{-1} and 0.91 μmol cm^{-2} s^{-1} oxygen under 30ml/min He and 0.65 ml/min methane sweep, respectively. During combustion reaction, this membrane was found to be consuming all of the methane provided into carbon dioxide, in addition to excess oxygen of 0.20 ml/min (15% excess oxygen). Both levels of oxygen and carbon dioxide were found to be constant for an operation of above 200 hours indicating excellent stability. After finishing the combustion, a return to helium gas as sweep produced 1.25μmol cm^{-2} s^{-1} oxygen, further providing evidence of stable membrane operation under combustion reaction. Moreover, it was found that the permeability of the membrane improves if the amount of methane provided for combustion is increased. A methane flow rate of 0.95ml/min

enabled the membrane to produce a stable oxygen flux of 1.16μmol cm^{-2} s^{-1} which is very close to the value produced under inert sweep. A further increase in the methane flow rate starts to have an adverse effect on the performance of the membrane. A drop of 4.13% of oxygen permeability was measured over a period of 115 hours in this case. EDX analysis of the permeate side of the membrane after test showed a presence of almost 5 wt.% of carbon indicating some carbonate formation on the surface. This was confirmed by the XPS analysis of the permeate surface of the membrane.

4.5 IMPROVEMENT IN STABILITY AND PERMEABILITY USING COATING MATERIALS

4.5.1 Effect of Platinum and Palladium Coating on BSCF Membranes

In order to improve the permeability of the BSCF membrane, the surface kinetic reaction of membranes with thickness below the value of critical thickness has to be enhanced. In order to do so, it was decided to coat platinum and palladium on the feed side of the membrane and observe its effect on the oxygen permeability. The coating on the surface of BSCF membranes was accomplished using a sputter coater (Quorum Q300T T). When a 5nm thick platinum layer was coated on the feed side of the membrane it reduced the oxygen flux to a value of 1.12 µmol $cm^{-2}s^{-1}$ (Figure 4.44). So it was decided to use palladium as the catalyst on the feed side surface of the 0.9mm thick membrane. Different thicknesses of the palladium coat were achieved by sputter coating the 0.9mm thick BSCF membrane using different times while keeping the voltage and

current of the instrument constant. The oxygen permeability flux of these membranes with Pd coating time durations of 30, 90, 180 and 300 seconds are shown in Figure 4.45. It is clear that the membrane coated for 180 seconds gives the best permeability among them at 1.39 μmol $cm^{-2}s^{-1}$.

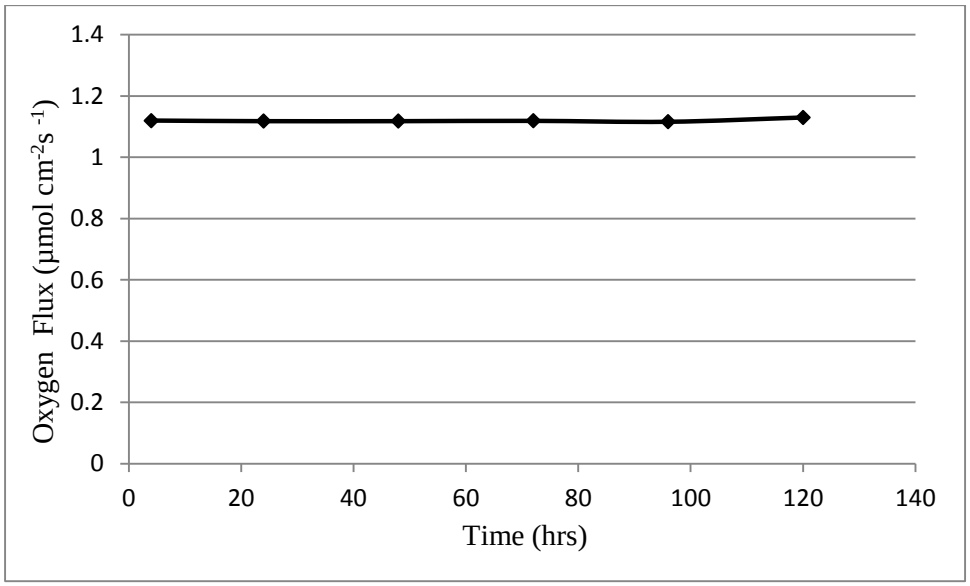

Figure 4.44 Oxygen permeability of 0.9mm thick BSCF membrane coated with 5nm thick platinum on the permeate

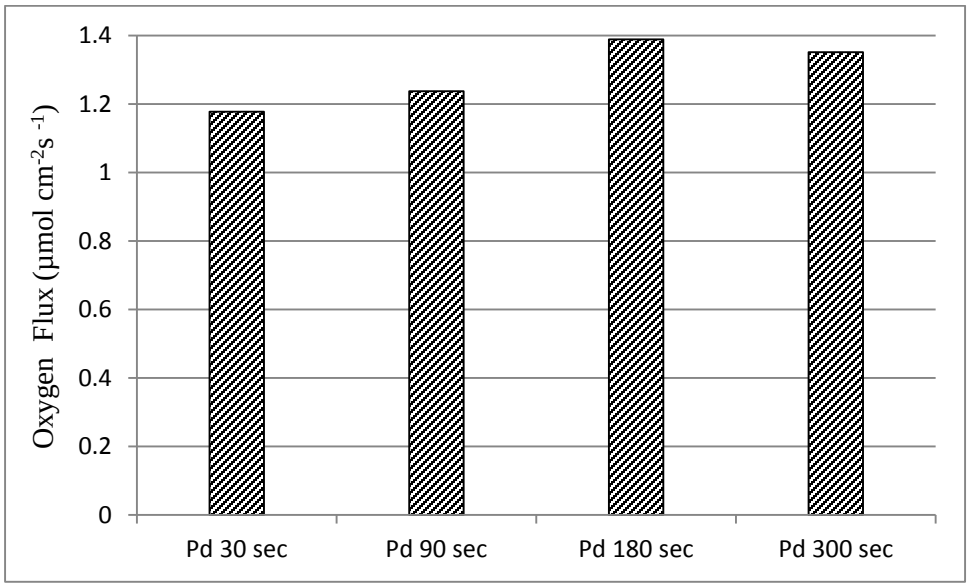

Figure 4.45 Oxygen permeability fluxes of 0.9mm thick BSCF membranes with palladium coated on the feed side for 30, 90, 180 and 300 seconds using sputter coater

In order to improve the chemical stability of the BSCF membrane during combustion, it was first coated with platinum on the permeate side. Platinum was chosen as the coating material because of its inertness and high melting temperature. Later this membrane was sealed in the ITM reactor with silver rings. To verify the stability of this membrane with respect to time, its oxygen permeability was measured with helium as sweep (Figure 4.46). A constant flux of around 0.80μmolcm^{-2}s^{-1} was achieved. This flux is lower than that of the uncoated membrane or the membrane coated with the same material on the permeate side. This flux reduction is mainly due to the coating effect on surface area exposure. Nevertheless, the flux of this coated membrane is much higher

than that of any chemically stable ITMs proposed in the literature, such as: LNO, LCF, LCCF, SCMF, CGO etc.

Similar to the experiments presented in the last section, 0.65ml/min methane is introduced to the reactor on the sweep side of the membrane. Figure 4.47 shows the quantitative analysis of gases in the sweep. The results show that the level of CO_2 produced by the reaction is almost constant. A lack of oxygen and a small amount of methane are detected in the sweep which indicates that there was a slight excess of methane. This is understandable as the permeability of this membrane is less than that for which the quantity of methane was optimized. Nonetheless, it is very encouraging to note that the level of methane in the sweep has remained constant throughout the 100 hour operation under oxy-fuel combustion. Hence it is concluded that a Platinum coated BSCF membrane is stable and suitable for oxy-fuel combustion applications.

Figure 4.48 shows a comparison between the oxygen permeability flux of the Pt coated membrane before, at the start of and after the reaction. The decrease in the permeability of the membrane during combustion is around 5.3% which is less than half of the decrease experienced by the uncoated membrane shown in Figure 4.23. As the membrane was delivering stable quantities of oxygen during combustion, so it is expected that the membrane did not undergo any deterioration. This is confirmed when the oxygen permeability is measured with helium sweep after finishing the combustion. The value of oxygen permeability in this case is $0.76 \mu molcm^{-2}s^{-1}$, which is almost identical to the permeability measured before starting the combustion. Similar to the

experiment with uncoated membrane, it was left to recover overnight and then its permeability was measured again which came out to be 0.765μmolcm^{-2}s^{-1}.

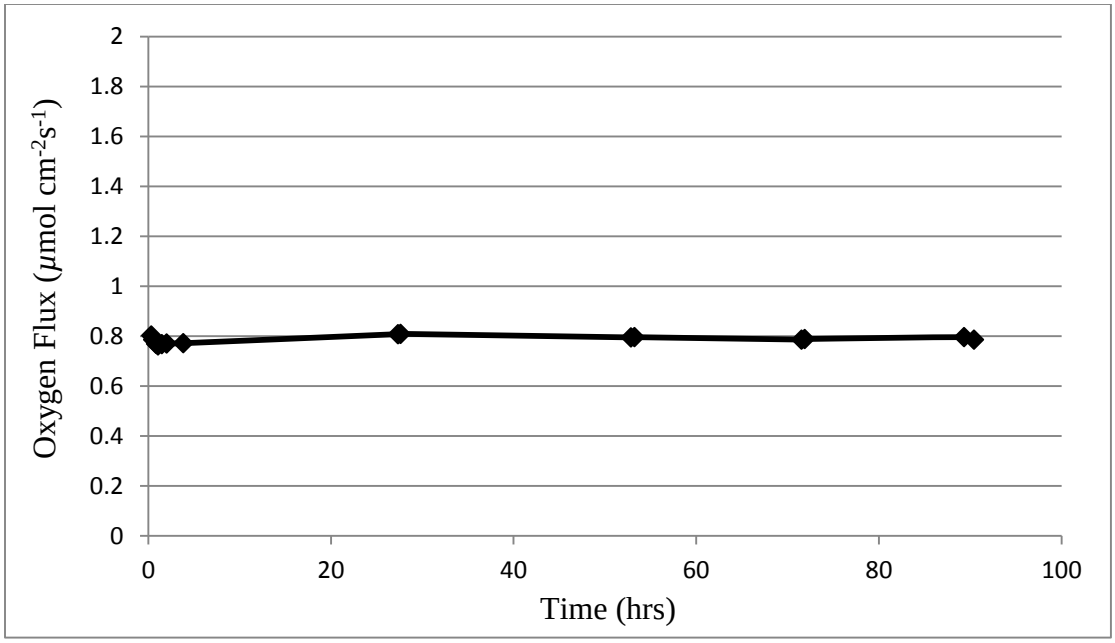

Figure 4.46 Oxygen permeation flux from a 1.0 mm thick BSCF membrane coated with Platinum (permeate side) under inert environment

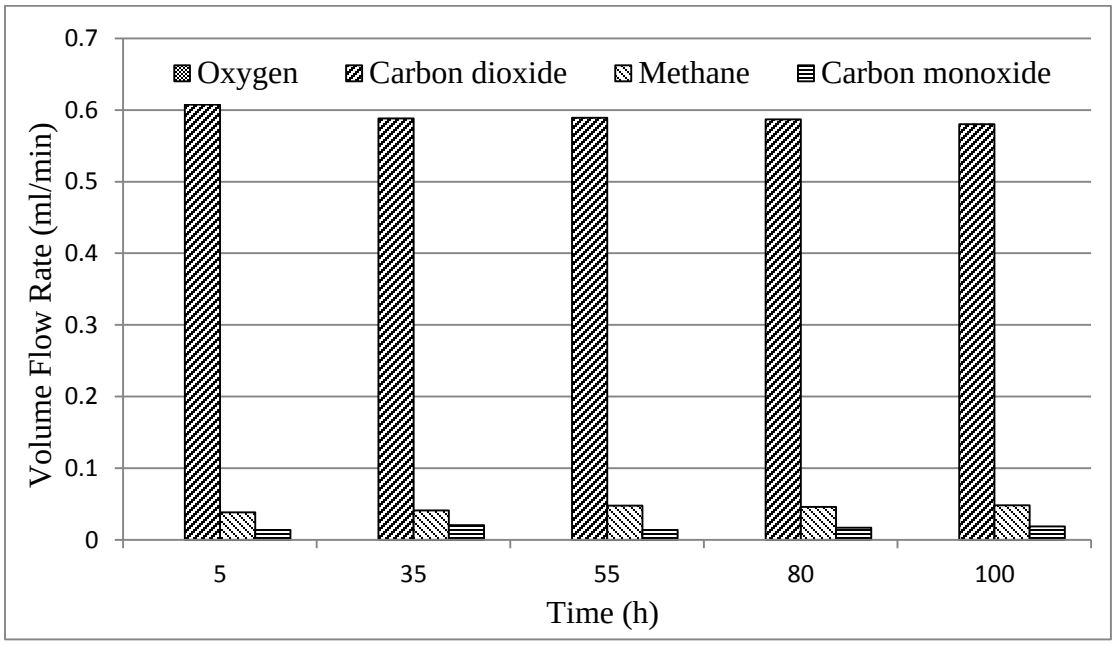

Figure 4.47: Effect of platinum coating on BSCF membrane for long-term stability during combustion reaction at 920ºC and constant methane flow rate of 0.65ml/min. Membrane thickness is 1.0 mm.

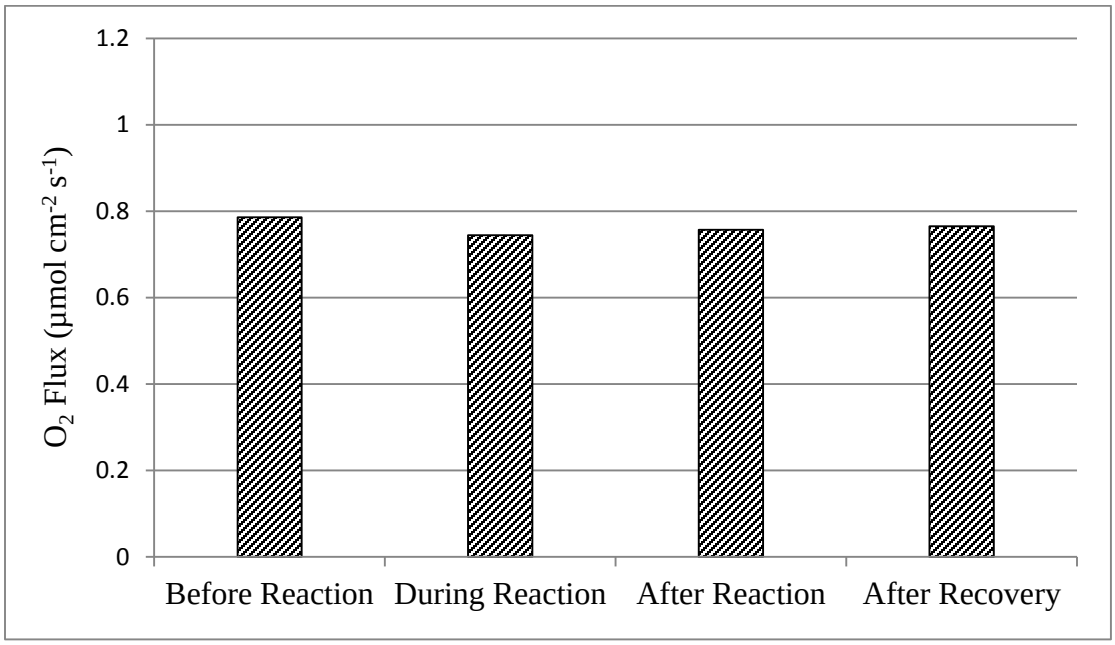

Figure 4.48: Oxygen permeation flux from the 1.0mm thick platinum coated BSCF membrane before, during and after reaction with 0.65 ml/min methane flow rate.

As shown previously, coating palladium on the feed side of the membrane had a better effect on the oxygen permeability of the BSCF membranes and Pd coating done for duration of 180 seconds provided the best results. So the same coating and thickness was chosen to be applied on the permeate side of the membrane and its effect on the stability of the BSCF membrane was observed. This membrane produced an oxygen flux of 1.14 µmol $cm^{-2}s^{-1}$ when operated in inert environment on the permeate side (30ml/min He). This was much higher than the Pt coated membrane, so it was decided to use the fuel rate of 0.85ml/min methane instead of 0.65ml/min in order to maintain a rigorous environment with excess fuel on the permeate side. Figure 4.49 shows that the fluxes of CO_2 and CH_4 remain constant with trace amounts of CO appearing. The corresponding

oxygen flux also remains constant at a value of 0.92 µmol $cm^{-2}s^{-1}$. So the Pd coated membrane is stable with much better performance than the Pt coated BSCF membrane. When the methane flow rate was increased to 1.05ml/min on the permeate side of the membrane the oxygen flux increased to a value of 1.06 µmol $cm^{-2}s^{-1}$ (Figure 4.50). With the passage of time the level of CO_2 started to increase and that of the CH_4 started to decrease instead of remaining constant. Correspondingly the oxygen flux also increased. After 216 hours the level of oxygen flux had risen to a value of 1.18 µmol $cm^{-2}s^{-1}$. The reason of this behavior is under investigation.

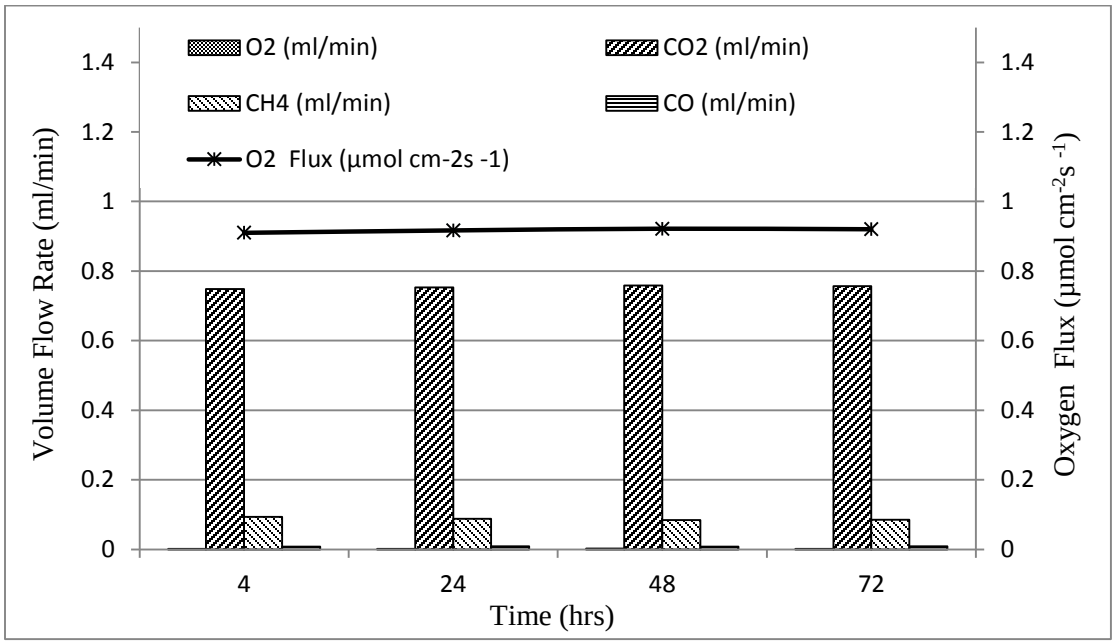

Figure 4.49 Gas analysis of a combustion reaction at 950°C using a 0.9 mm thick BSCF membrane sputter coated with palladium for 180 seconds on permeate side and constant methane flow rate of 0.85ml/min.

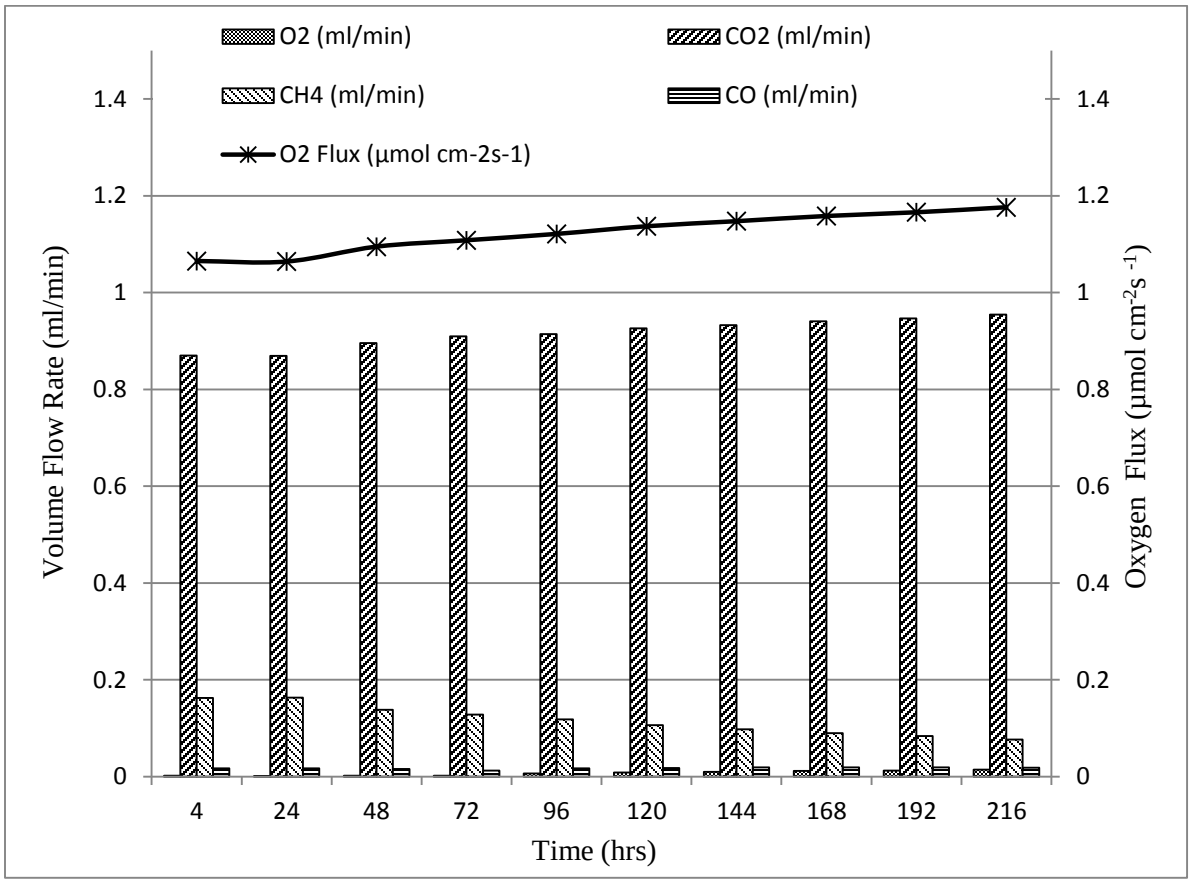

Figure 4.50 Gas analysis of a combustion reaction at 950°C using a 0.9 mm thick BSCF membrane sputter coated with palladium for 180 seconds on permeate side and constant methane flow rate of 1.05ml/min.

4.5.2 Attempts to Coat LNO on Permeate Side of the BSCF Membrane

Various materials have been discussed in Chapter 2 which have high chemical stability in the presence of CO_2. Unfortunately, all such materials have permeability at least one order of magnitude lower than that of BSCF. Nevertheless the possibility of using such materials was examined in this work. One such material which has excellent

stability and relatively better oxygen permeability is $La_2NiO_{4+\delta}$. In Section 4.2 it was shown that a 0.9mm thick LNO membrane produces a stable oxygen flux of $0.15\mu mol.cm^{-2}.s^{-1}$(Figure 4.9) when 30ml/min Helium was used as sweep. The powder for this LNO membrane was prepared from modified Pechini method and the pressed discs were sintered for 10 hours at 1500°C. Similar LNO membrane (1mm thick) were also tested at 920°C with both helium and CO_2 used as the sweep gas alternatively (Figure 4.51). It is evident that the LNO membranes would perform very well in CO_2 containing atmosphere as there is no degradation observed when the membrane when it was exposed to 100% CO_2. Keeping this in mind it was decided to use the advantages of permeability of BSCF and stability of LNO together. For this, a 1mm thick BSCF membrane was prepared and coated with slurry containing ethanol and LNO powder. The slurry was coated using the spin coating technique. Once the coating was done the membrane was heat treated at a temperature of 1150°C. As the sintering temperature for LNO and BSCF differ greatly, it was decided to keep the membrane at 1150°C for 50 hours. It was found that the LNO powder had not properly merged with the surface of the BSCF membrane leading to abandonment of this idea.

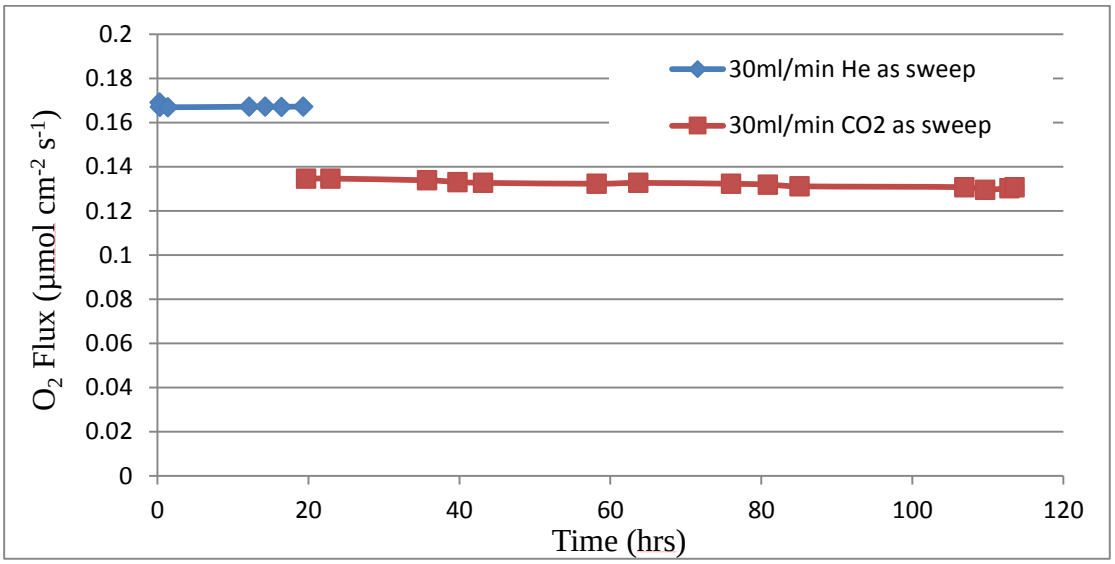

Figure 4.51: Oxygen permeation flux through 1mm thick LNO membrane with helium or carbon dioxide as sweep gas.

4.5.3 Coating of BSCF-LNO Mixture on the Permeate Side of BSCF Membrane

In order to use the good chemical stability of the LNO material in CO_2 environment, it was decided that a mixture of BSCF and LNO will be made use of. Equal proportions by weight of both the materials were taken and mixed them using ball milling. This mixture was coated on one side of a dense BSCF membrane which was 1mm thick. The coating was done using the dip coating technique. The BSCF membrane was placed in the oxy-fuel combustion reactor in such a way that the coated side would become the permeate side and the uncoated side would act as the feed side.

4.5.3.1 Analysis of the Permeate during Oxy-fuel Reaction

The membrane was first tested with 30ml/min helium introduced as sweep on the permeate side. 20ml/min air was introduced on the feed side of the membrane. The test was conducted at 920°C. The permeability of the membrane for this test is showed in Figure 4.52. The membrane produces a constant oxygen flux of 1.15μmolcm^{-2}s^{-1}. In comparison, the flux produced by an uncoated 1mm thick BSCF membrane acting at the same temperature produced 1.26μmolcm^{-2}s^{-1} (Figure 4.25). So coating the membrane at the permeate side with a BSCF-LNO mixture caused a slight decrease in the permeability of the membrane (8.7%). The stability of the membrane, however, was not found to be affected as the flux was constant for more than 120 hours. On the other hand coating a similar membrane with platinum on the permeate side caused a much more significant drop in the oxygen flux returning a permeability value of 0.8μmolcm^{-2}s^{-1} as shown in Figure 4.46 (a decrease of 36.5%). In order to evaluate the performance of this membrane under oxy-fuel combustion, 0.65ml/min of methane was introduced from the permeate side of the membrane. A continuous operation of 75 hours showed constant values of carbon dioxide and excess oxygen detected by the GC. The value of the oxygen permeability calculated from this was also found to be consistent at 0.83μmolcm^{-2}s^{-1}. So the decrease in the flux resulting from coating BSCF-LNO mixture 8.7% and 7.7% for operation under inert environment and 0.65ml/min of methane respectively.

It is worth noting that when the pure BSCF membranes were being tested under 0.65ml/min methane, the 1mm thick membrane was showing an excess of 0.2ml/min of oxygen which was maintained for the whole duration of the experiment i.e. 200 hours

(Figure 4.26). On the other hand a 1.4mm thick BSCF membrane was able to produce only half of that excess which was found to diminish over the duration of experiment done for 190 hours (Figure 4.22). Similar to the study described in the last section, the behavior of the BSCF-LNO coated BSCF membrane was evaluated while increasing the amount of methane on the permeate side in steps. During each step volume rate of methane was increased by 0.1ml/min and the gas analysis at the permeate side was carried out for 80-120 hours. The oxygen permeability from each step was also measured. The gas analysis and oxygen permeability measurements for each step are shown in Figure 4.53 to Figure 4.70. It was shown that for the methane inflow of 0.65, 0.75 and 0.85 ml/min methane there was some excess of oxygen present in the permeate. The value of this excess was 0.1, 0.06 and 0.03ml/min respectively. The level of the excess oxygen as well as that of CO_2 was found to be constant throughout the measurement. As a result the oxygen permeability for individual steps was also constant. If the oxygen permeability for different flow rates of methane is compared, a clear increase can be seen in the permeability as the methane flow rate increases. This clearly indicates that a BSCF-LNO coated BSCF membrane can sustain the oxy-fuel combustion at higher values of methane by giving higher oxygen outputs which are stable as well. The average values of oxygen permeability for the 0.65, 0.75 and 0.85ml/min methane sweep are 0.84, 0.94 and 1.04μmolcm^{-2}s^{-1} respectively.

In the next two steps, with the methane flow rates of 0.95 and 1.05ml/min, all of the oxygen is consumed and the level of carbon dioxide in the sweep continues to rise but

still excess methane or carbon monoxide remains negligible. This means that the membrane is still producing more and more oxygen for each step resulting in conversion of the extra methane provided in each step to carbon dioxide. This is evident from the average oxygen permeability values which are 1.14 and 1.25μmolcm^{-2}s^{-1} for 0.95 and 1.05ml/min methane respectively. All the gases appearing in the analysis of permeate are still maintaining their levels for the duration of running each step.

A further increment in the methane level (1.15, 1.15, 1.25 and 1.35ml/min) resulted in further increase in the oxygen permeability of the membrane (1.35, 1.45 and 1.52μmolcm^{-2}s^{-1} respectively). But this increase was not sufficient enough to consume all of the methane provided. As a result little amounts of methane and carbon monoxide start appearing in the permeate gas analysis. However, the membrane is still found to be operating very stably. The stability starts to get affected slightly only when the methane flow rate is increased to 1.45ml/min. During this step, the oxygen permeability was found to decrease from 1.6μmolcm^{-2}s^{-1} to 1.53μmolcm^{-2}s^{-1} during 100 hours (a decrease of 4.3%). It is to be noted that at this point the membrane had already operated continuously for close to 1000 hours with oxy-fuel combustion occurring at its surface.

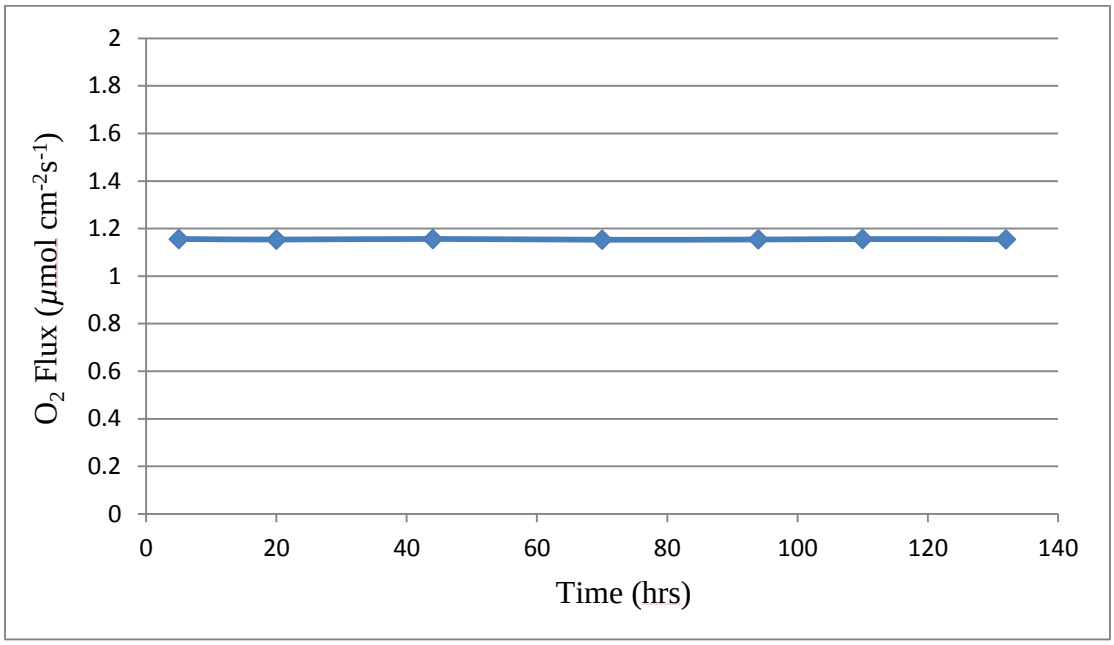

Figure 4.52: Inert Reaction with 30 ml/min Helium in sweep

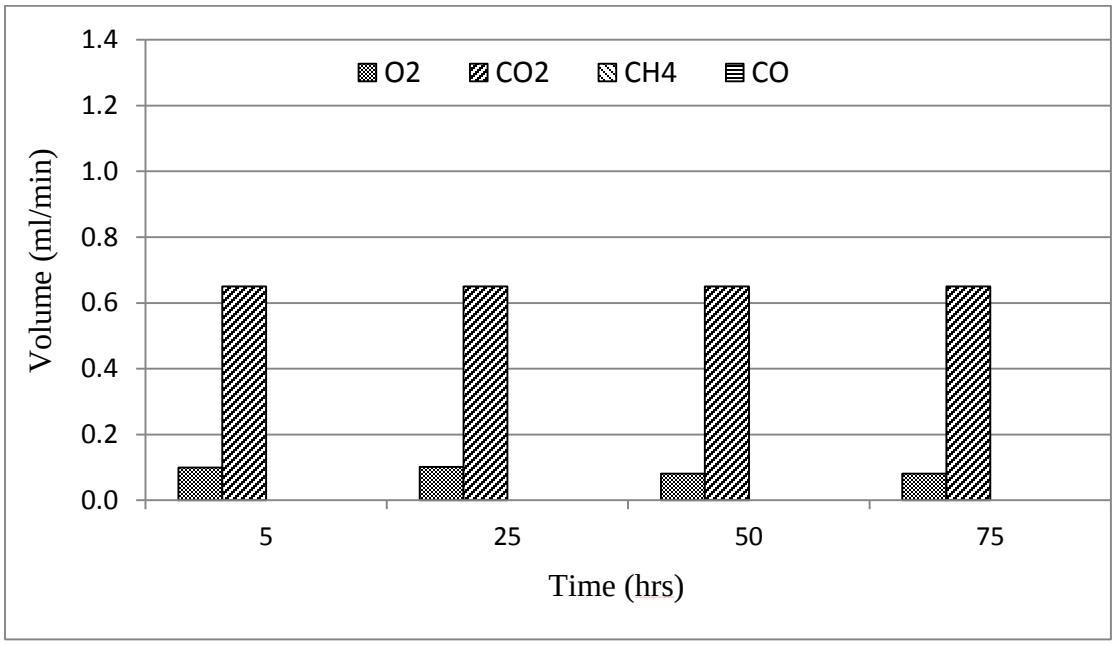

Figure 4.53 Gas analysis of a combustion reaction at 920ºC using a new 1 mm thick BSCF membrane coated with BSCF-LNO mixture on permeate side and constant methane flow rate of 0.65ml/min.

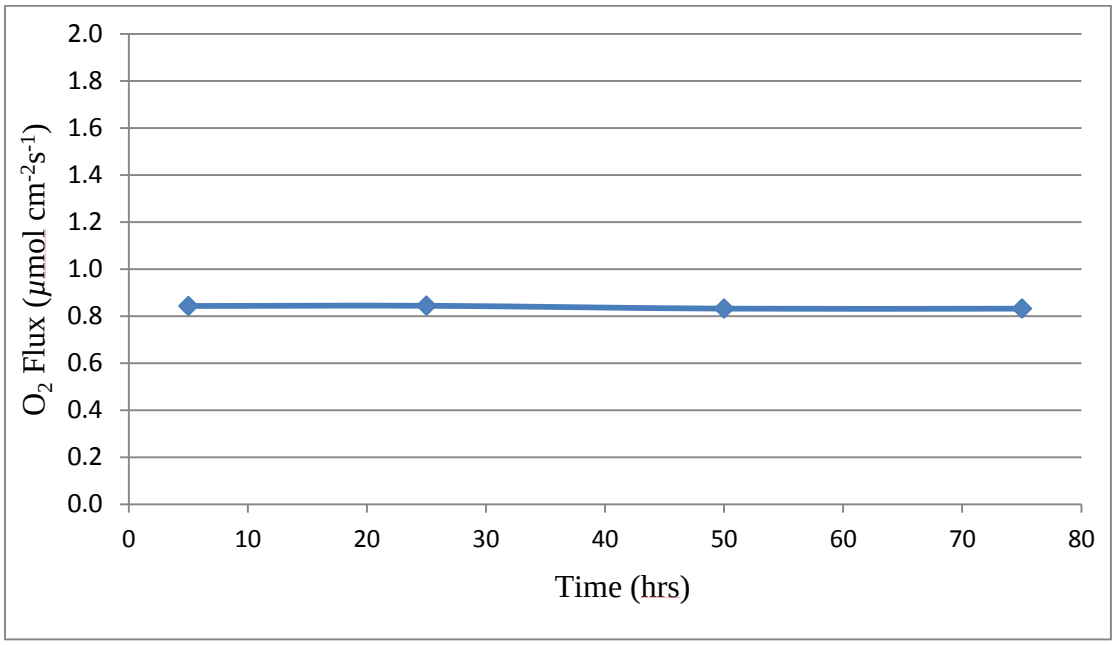

Figure 4.54 Oxygen Flux through the 1mm thick BSCF membrane coated with BSCF-LNO mixture at the permeate side during combustion with 0.65ml/min methane at 920°C.

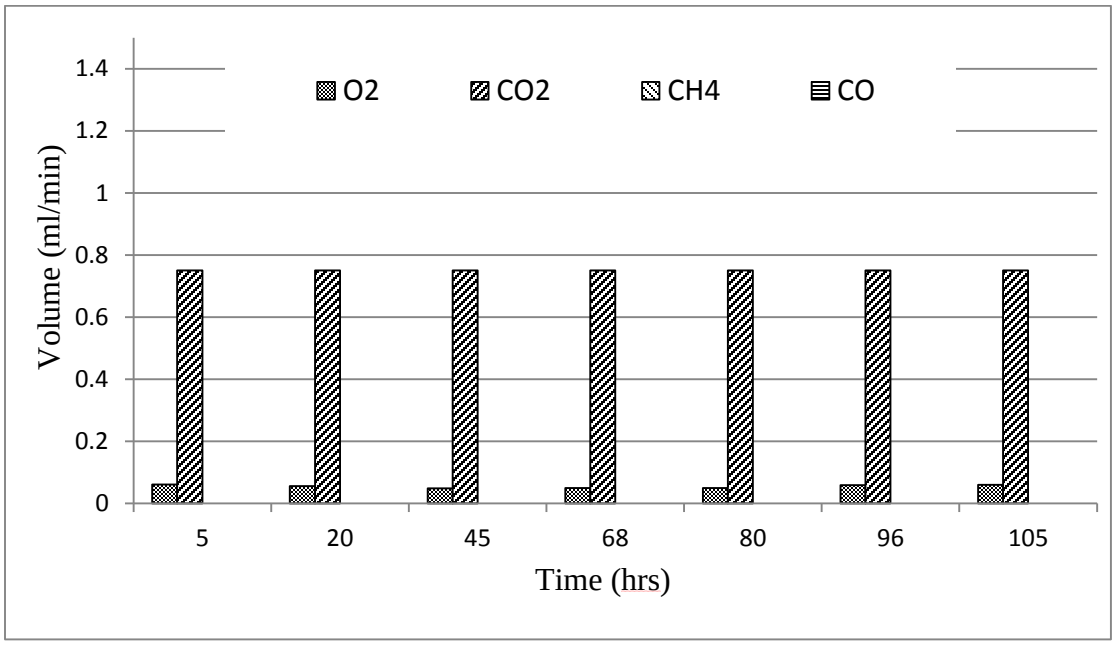

Figure 4.55 Gas analysis of a combustion reaction at 920ºC using a new 1 mm thick BSCF membrane coated with BSCF-LNO mixture on permeate side and constant methane flow rate of 0.75ml/min.

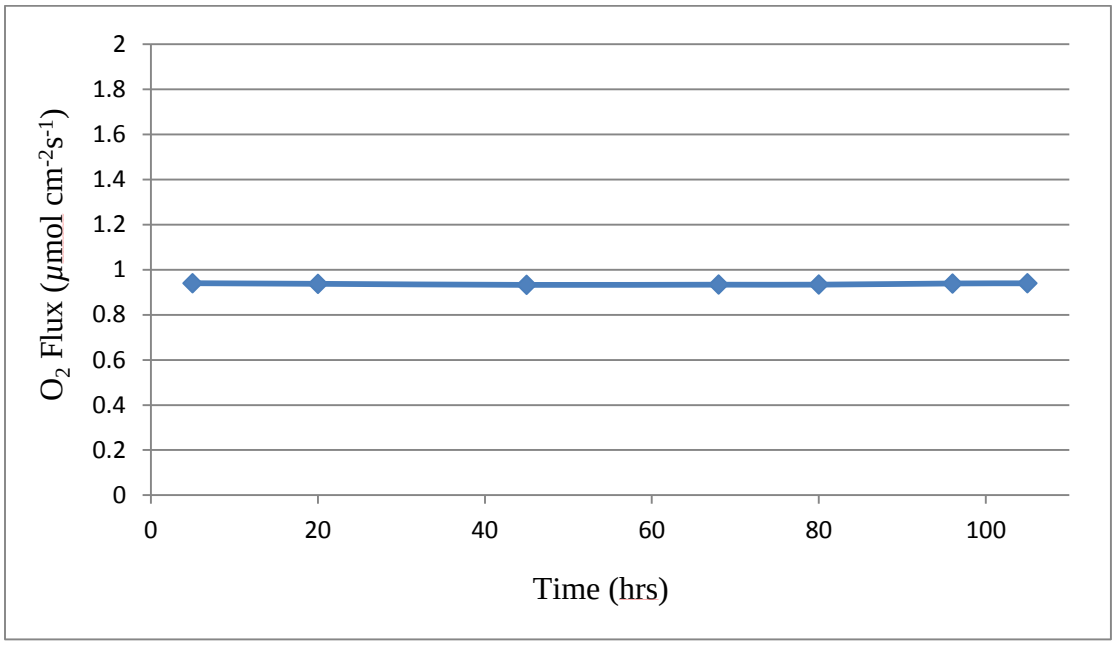

Figure 4.56 Oxygen Flux through the 1mm thick BSCF membrane coated with BSCF-LNO mixture at the permeate side during combustion with 0.75ml/min methane at 920°C.

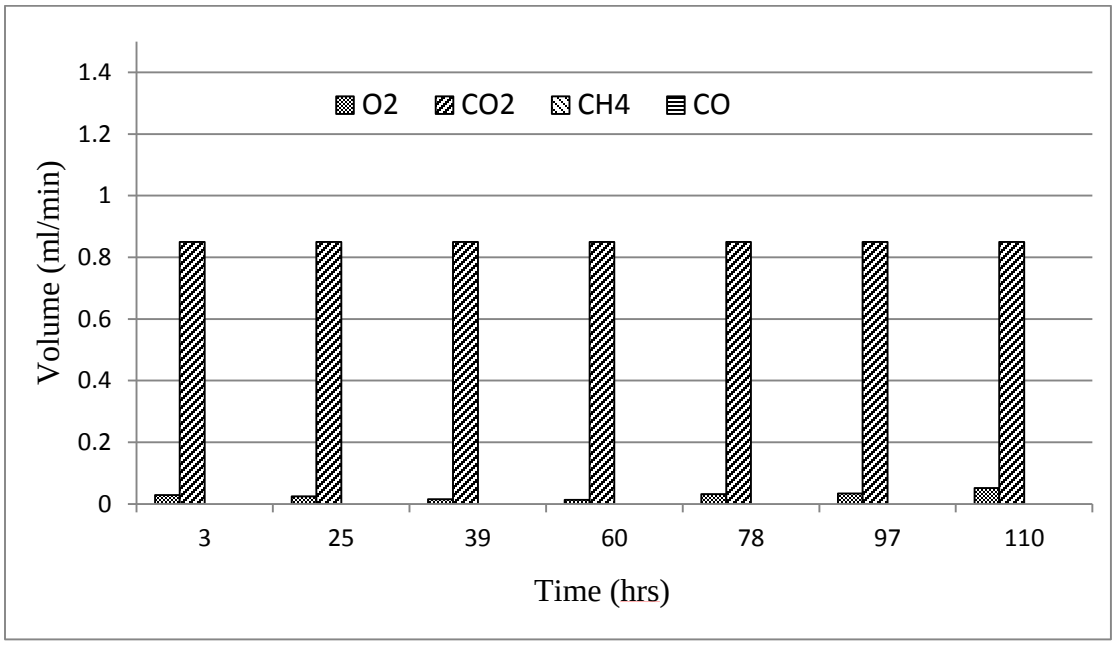

Figure 4.57 Gas analysis of a combustion reaction at 920ºC using a new 1 mm thick BSCF membrane coated with BSCF-LNO mixture on permeate side and constant methane flow rate of 0.85ml/min.

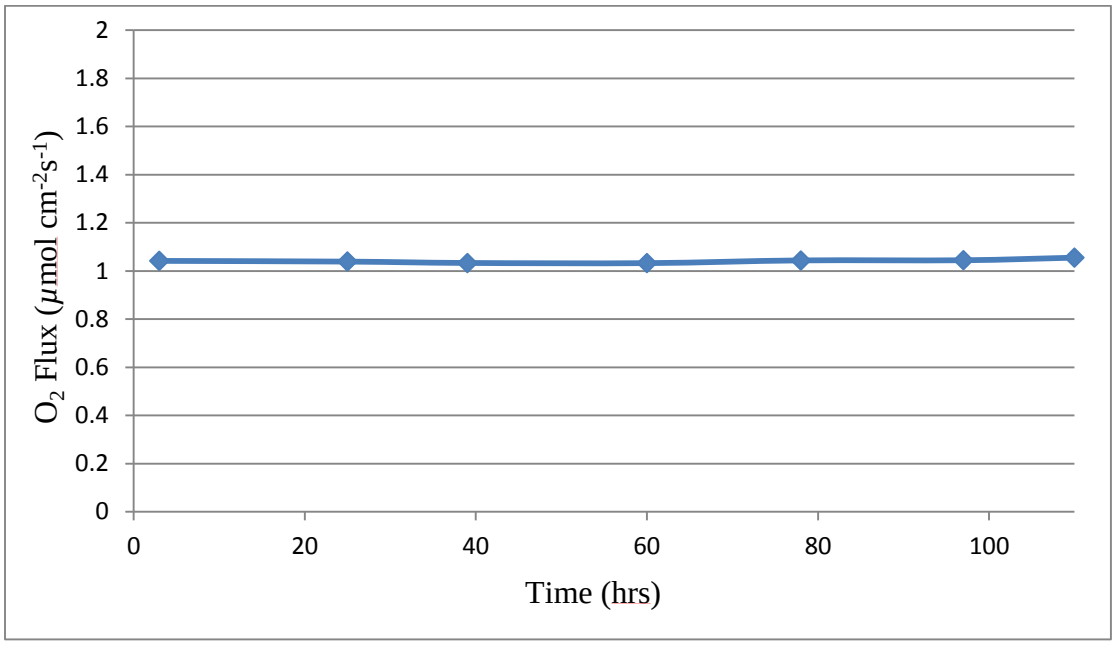

Figure 4.58 Oxygen Flux through the 1mm thick BSCF membrane coated with BSCF-LNO mixture at the permeate side during combustion with 0.85ml/min methane at 920°C.

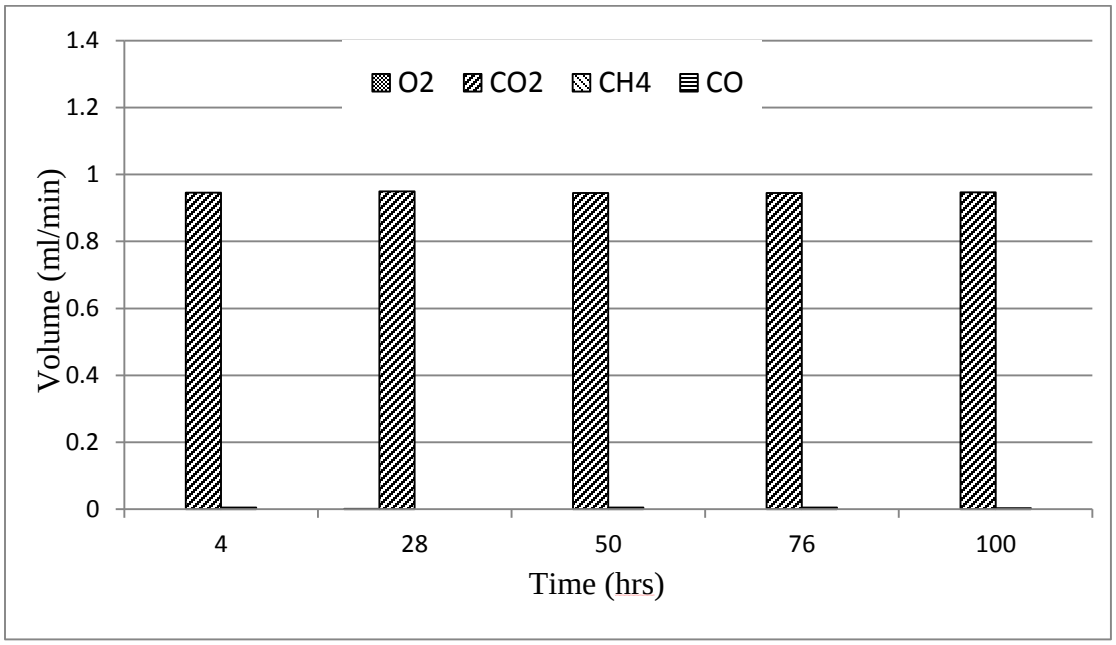

Figure 4.59 Gas analysis of a combustion reaction at 920ºC using a new 1 mm thick BSCF membrane coated with BSCF-LNO mixture on permeate side and constant methane flow rate of 0.95ml/min.

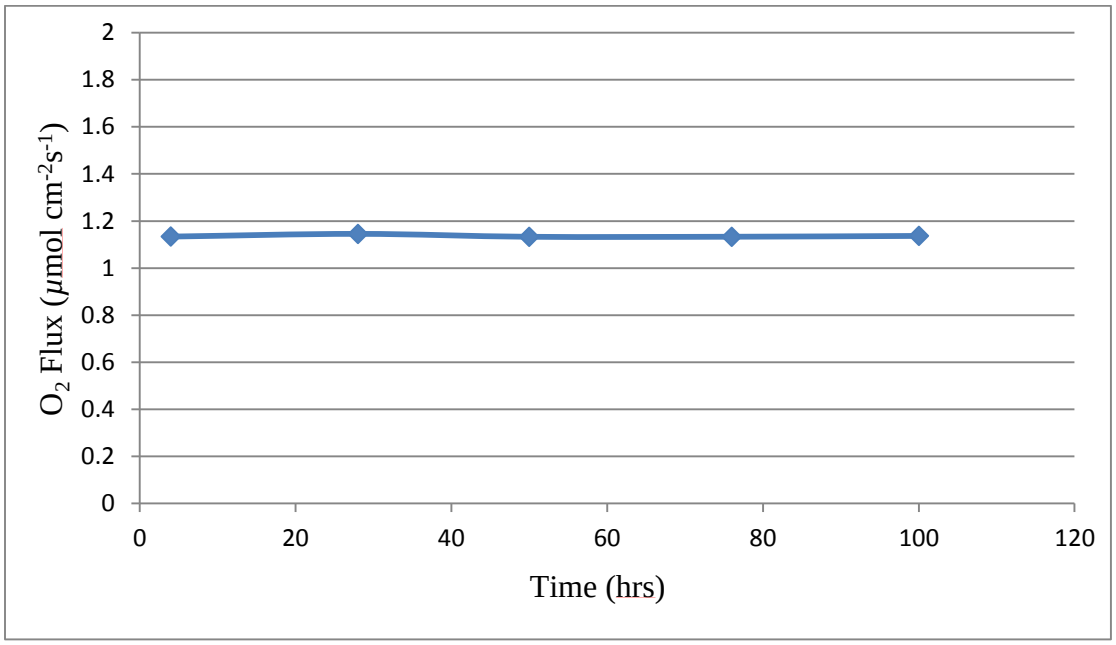

Figure 4.60 Oxygen Flux through the 1mm thick BSCF membrane coated with BSCF-LNO mixture at the permeate side during combustion with 0.95ml/min methane at 920°C.

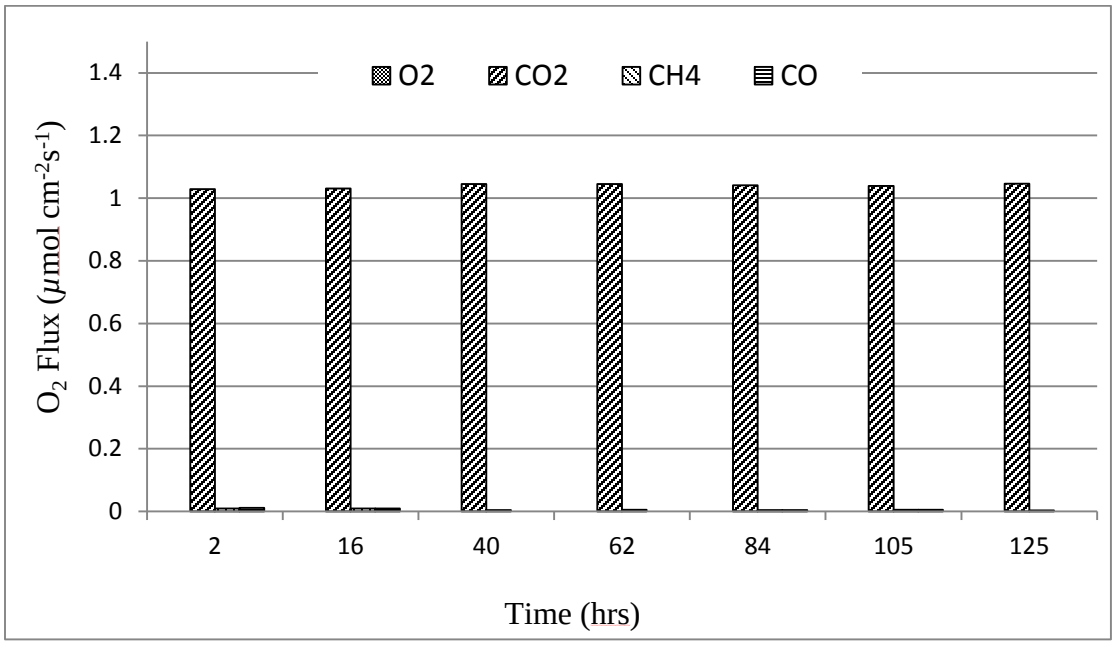

Figure 4.61 Gas analysis of a combustion reaction at 920ºC using a new 1 mm thick BSCF membrane coated with BSCF-LNO mixture on permeate side and constant methane flow rate of 1.05ml/min.

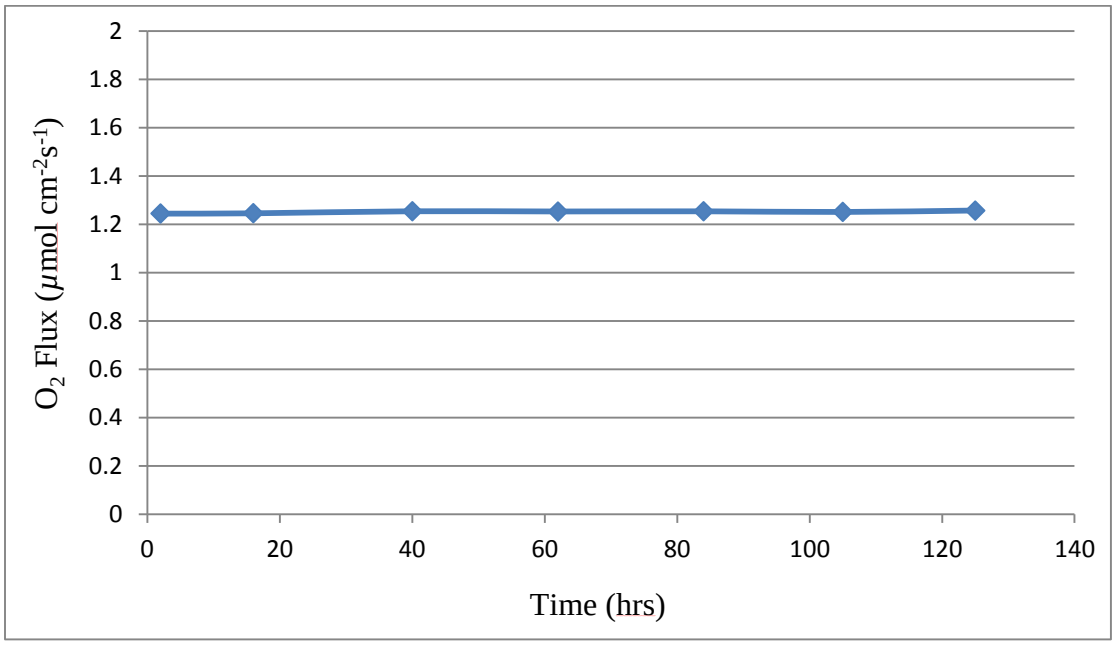

Figure 4.62 Oxygen Flux through the 1mm thick BSCF membrane coated with BSCF-LNO mixture at the permeate side during combustion with 1.05ml/min methane at 920°C.

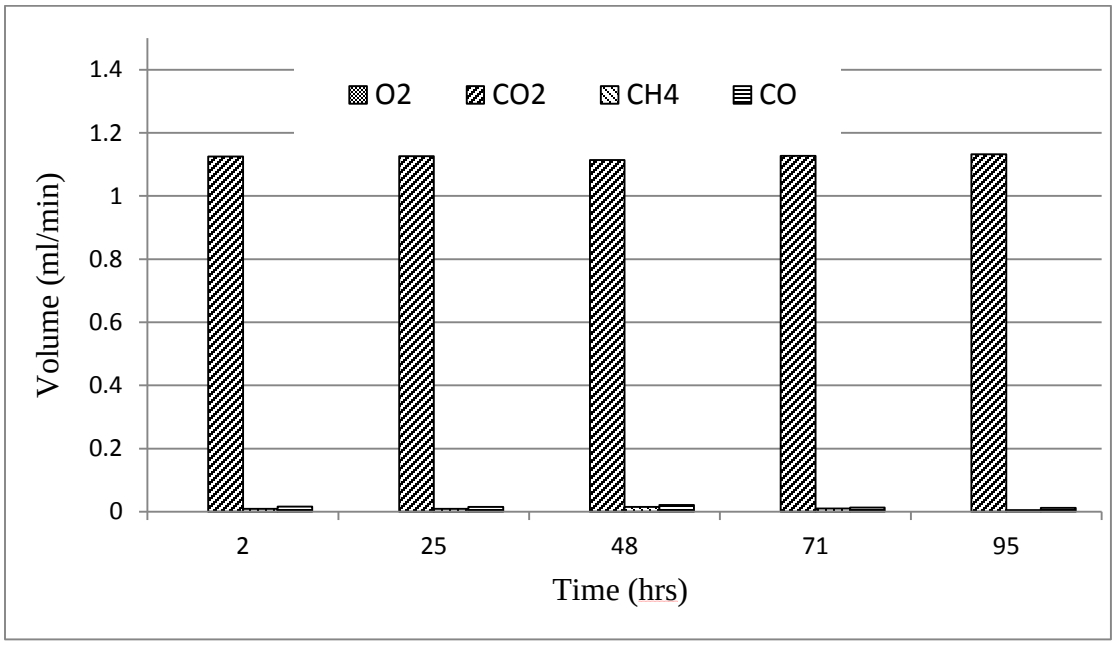

Figure 4.63 Gas analysis of a combustion reaction at 920ºC using a new 1 mm thick BSCF membrane coated with BSCF-LNO mixture on permeate side and constant methane flow rate of 1.15ml/min.

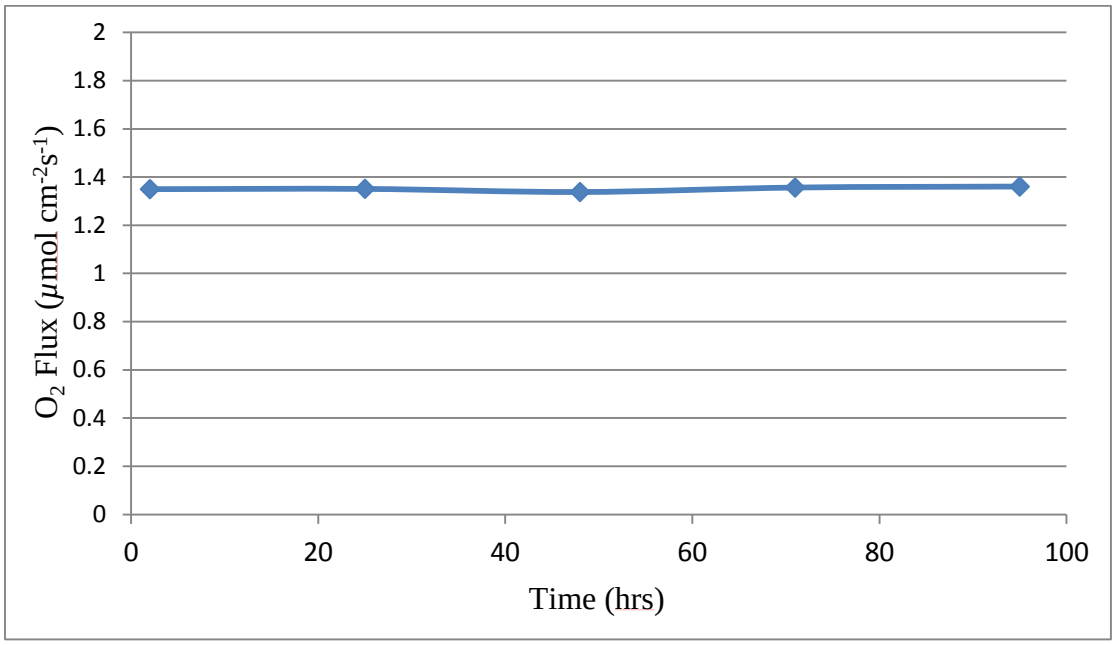

Figure 4.64 Oxygen Flux through the 1mm thick BSCF membrane coated with BSCF-LNO mixture at the permeate side during combustion with 1.15ml/min methane at 920°C.

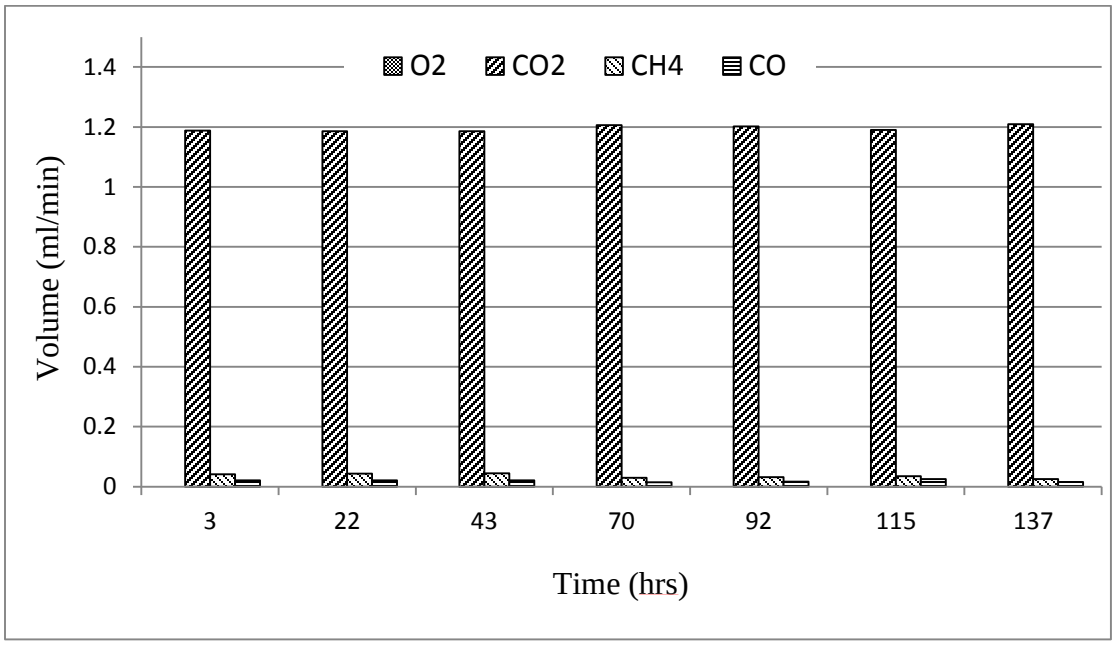

Figure 4.65 Gas analysis of a combustion reaction at 920ºC using a new 1 mm thick BSCF membrane coated with BSCF-LNO mixture on permeate side and constant methane flow rate of 1.25ml/min.

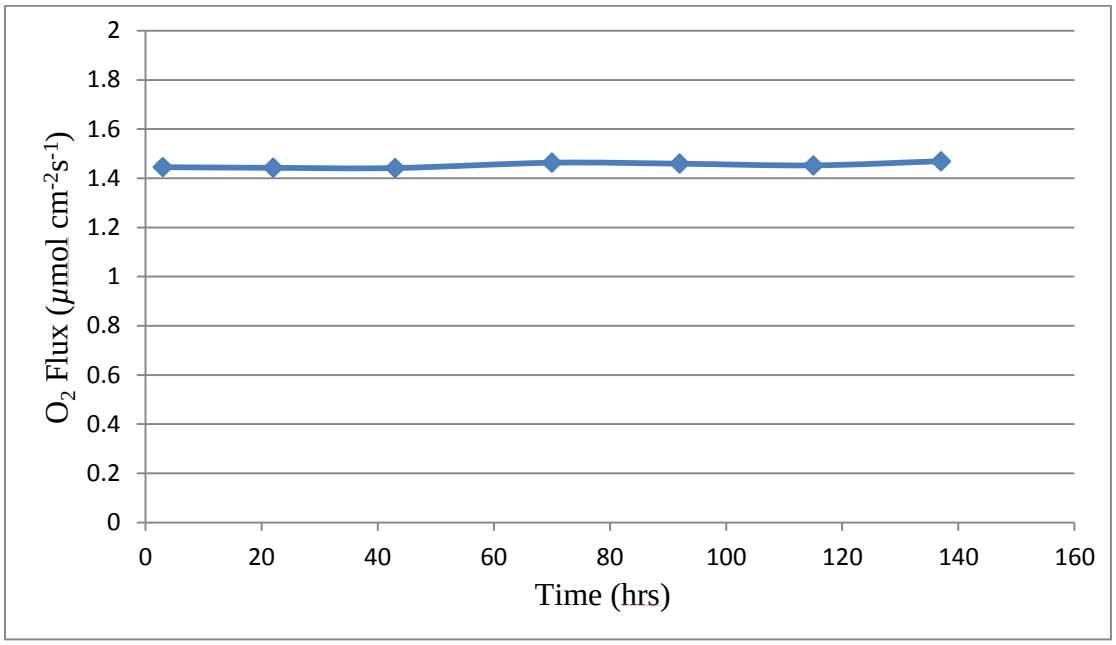

Figure 4.66 Oxygen Flux through the 1mm thick BSCF membrane coated with BSCF-LNO mixture at the permeate side during combustion with 1.25ml/min methane at 920°C.

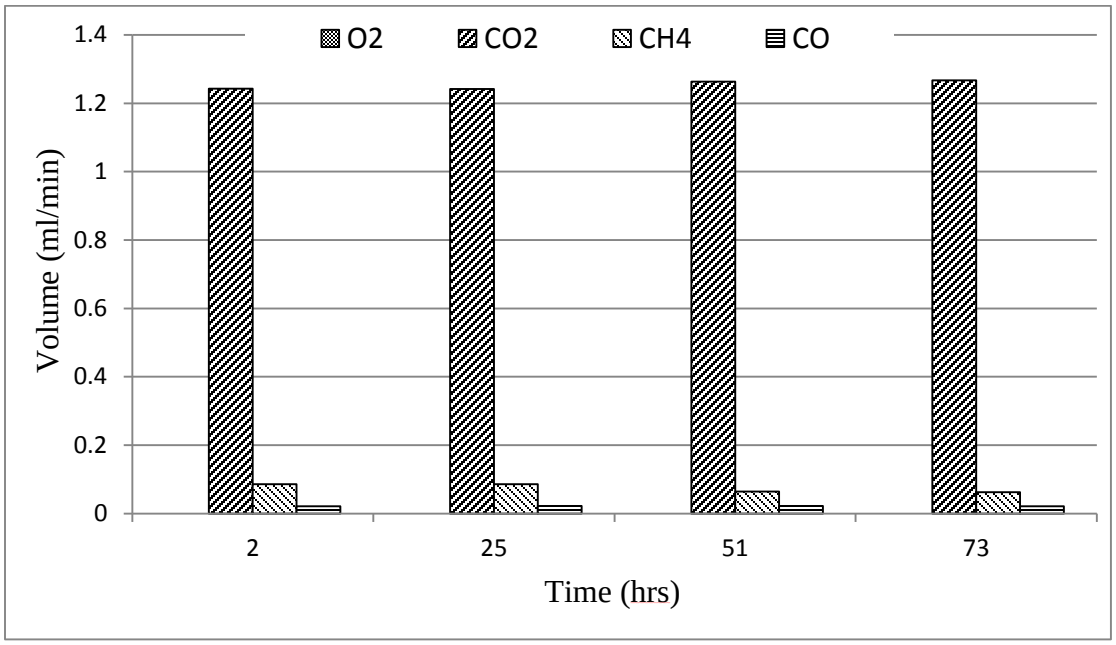

Figure 4.67 Gas analysis of a combustion reaction at 920ºC using a new 1 mm thick BSCF membrane coated with BSCF-LNO mixture on permeate side and constant methane flow rate of 1.35ml/min.

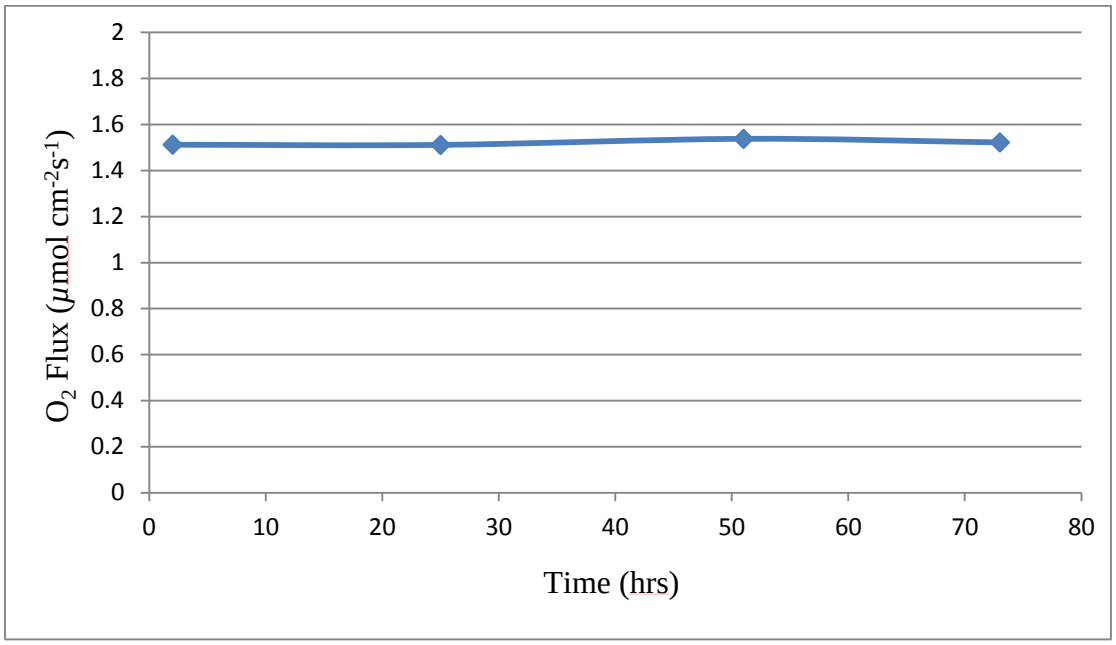

Figure 4.68 Oxygen Flux through the 1mm thick BSCF membrane coated with BSCF-LNO mixture at the permeate side during combustion with 1.35ml/min methane at 920°C.

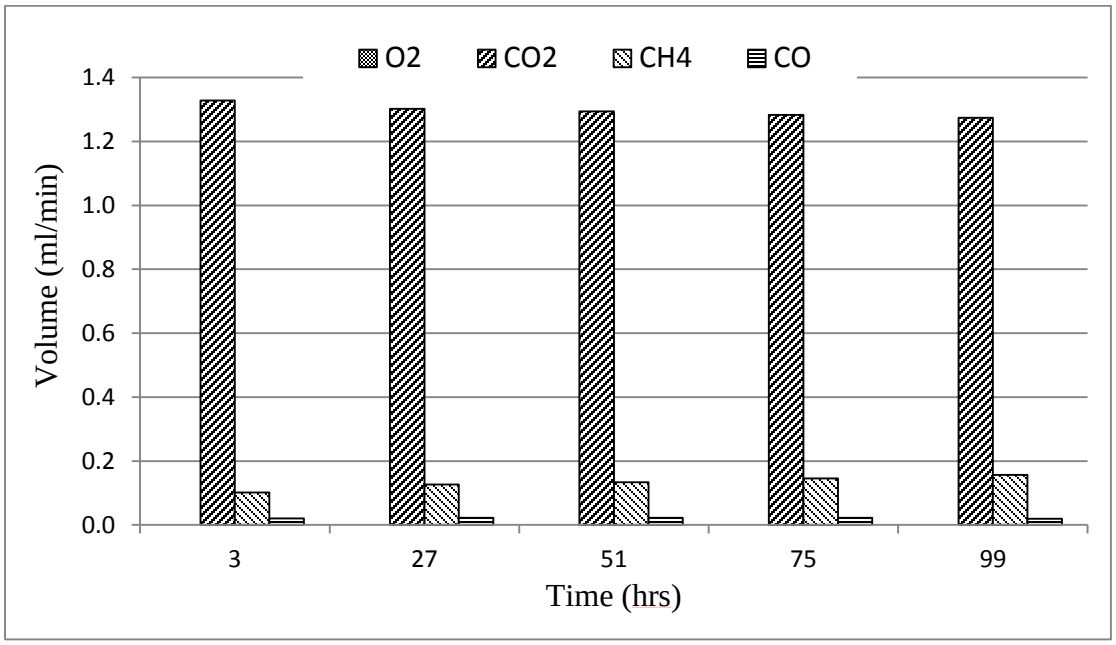

Figure 4.69 Gas analysis of a combustion reaction at 920ºC using a new 1 mm thick BSCF membrane coated with BSCF-LNO mixture on permeate side and constant methane flow rate of 1.45ml/min.

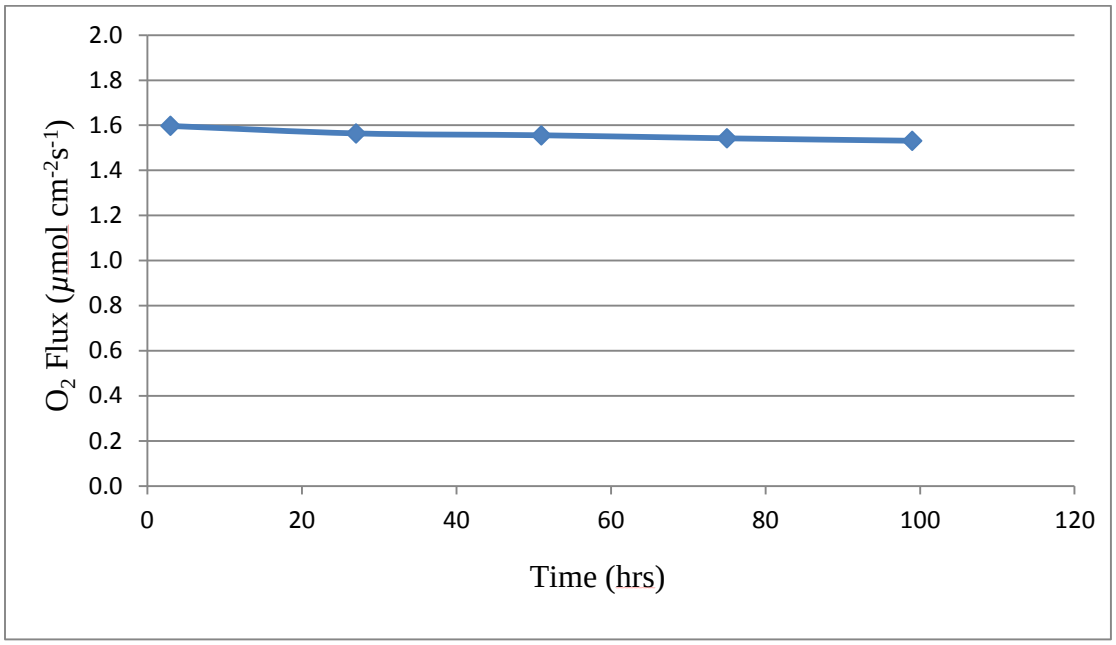

Figure 4.70 Oxygen Flux through the 1mm thick BSCF membrane coated with BSCF-LNO mixture at the permeate side during combustion with 1.45ml/min methane at 920°C.

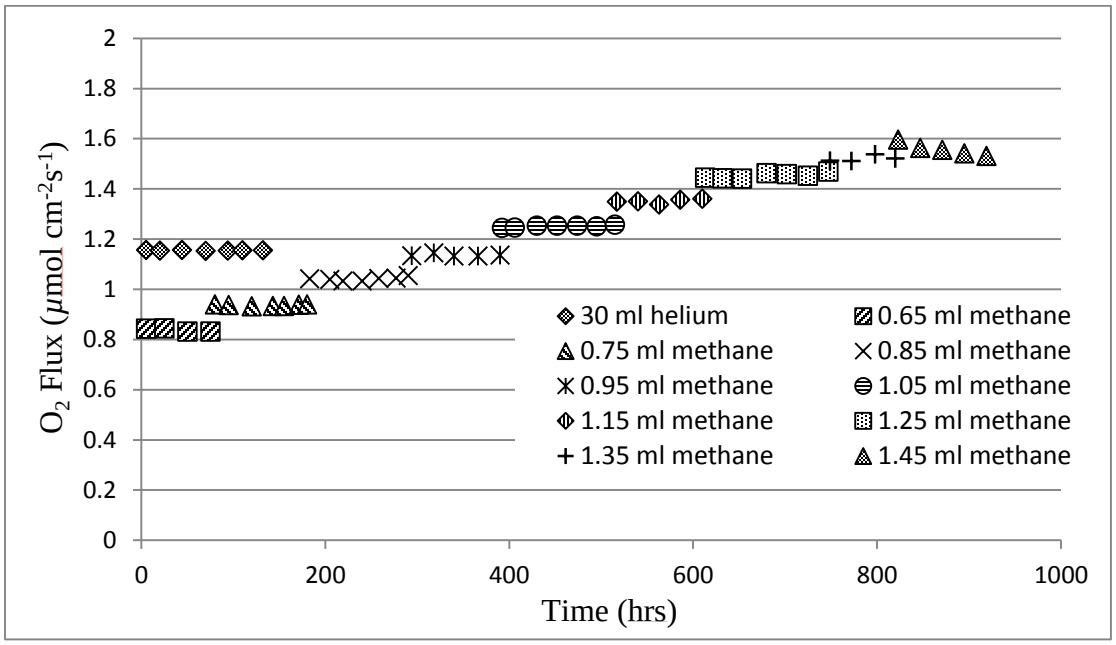

Figure 4.71 Oxygen Flux through the 1mm thick BSCF membrane coated with BSCF-LNO mixture at the permeate side during combustion with methane at 920°C. The methane flow rate varies from 0.65ml/min to 1.45ml/min.

4.5.3.2 Analysis of the Membrane Surface

The permeate side of the BSCF-LNO coated BSCF membrane is shown in Figure 4.72 after completion of combustion reaction lasting 919 hours. The change of surface color suggests that the membrane has undergone some chemical change. The central area of the membrane which was directly over the inner tube of the reactor carrying the methane gas has assumed white color whereas the area towards the edge appears to be pinkish in color. There are other regions on the membrane which are black (unchanged color). It seems that the BSCF-LNO coating is non-existent in these areas exposing the surface of the BSCF membrane. This indicates that the coating has played a part in

shielding the BSCF membrane as the surface beneath the coating appears to be clean. The results have also indicated that this membrane can support a higher flow rate of methane than the uncoated BSCF membrane used in a similar experiment explained in Section 4.4.

Figure 4.73 shows the SEM of the permeate side of the coated membrane. In Figure 4.73(a), it can be seen that the area with pinkish color in Figure 4.72 is in the form of a layer on the surface of the membrane. A closer look at higher magnification Figure 4.73d) reveals that needle like structures have formed in this layer. This structure was not found in the membrane before the test was conducted. The EDX of the membrane was conducted on selected areas from the central whitish region of the membrane as well as on the pinkish and black regions towards the edge of the membrane (Figure 4.74-Figure 4.76).

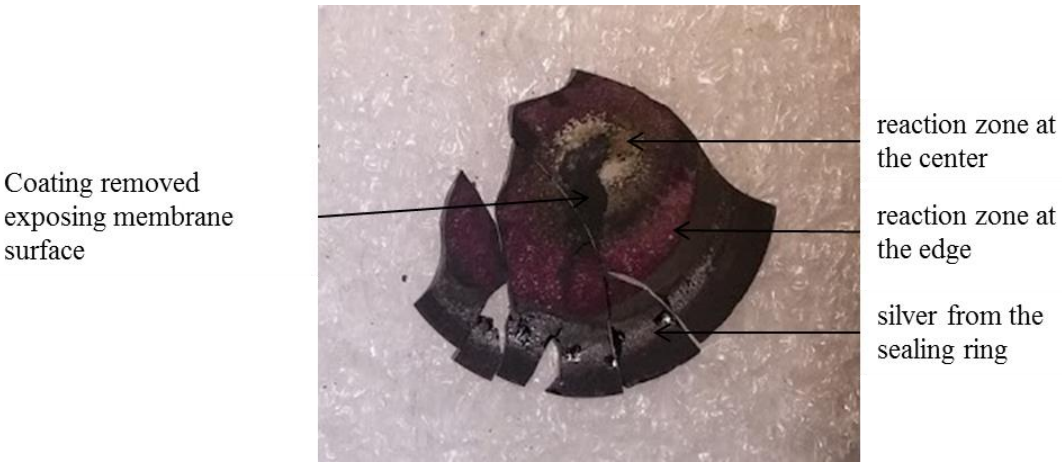

Figure 4.72 Permeate side of the BSCF-LNO coated BSCF membrane after undergoing combustion reaction for 919 hours.

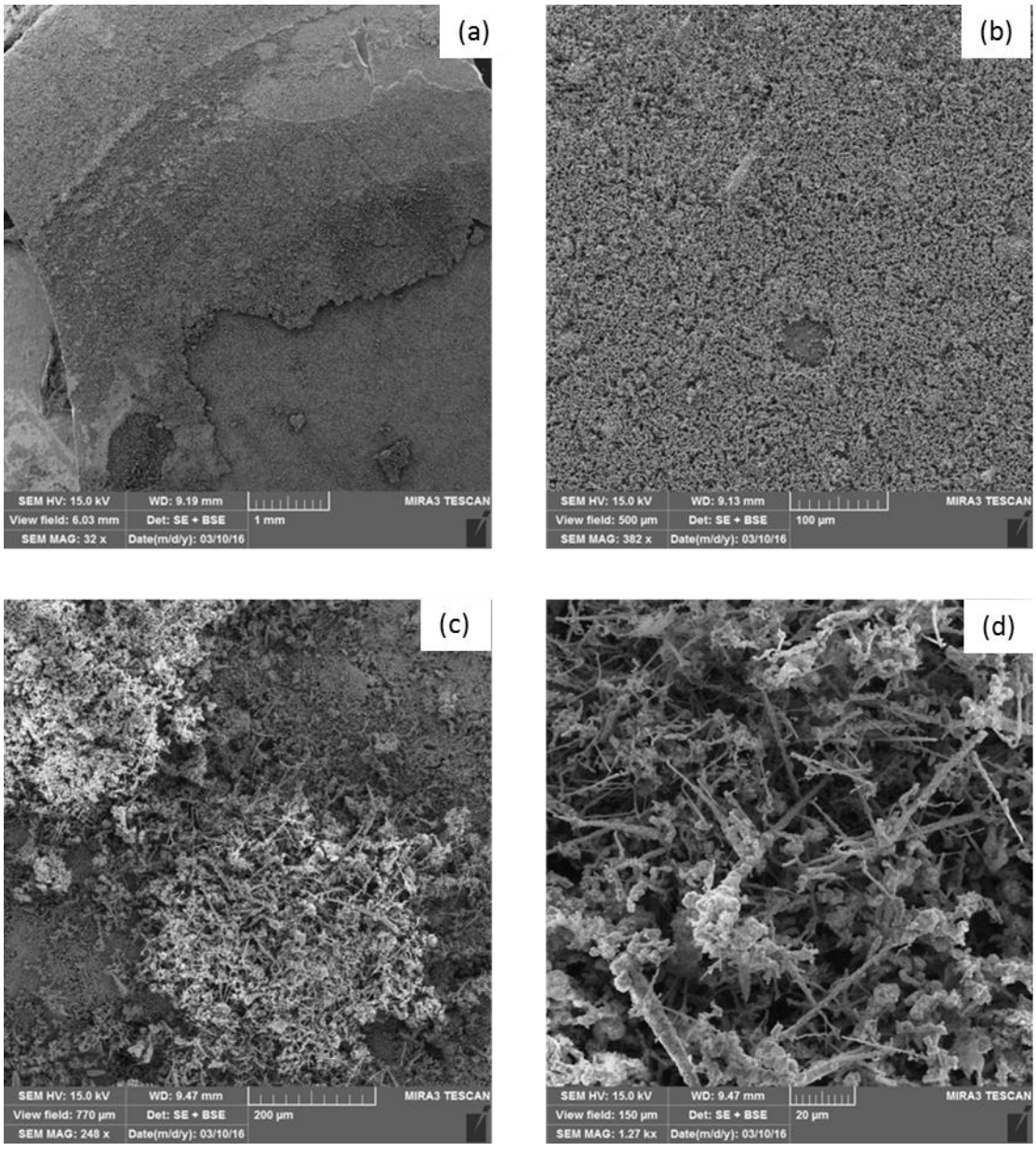

Figure 4.73 SEM of the permeate side of the BSCF-LNO coated BSCF membrane after undergoing combustion reaction for 919 hours.

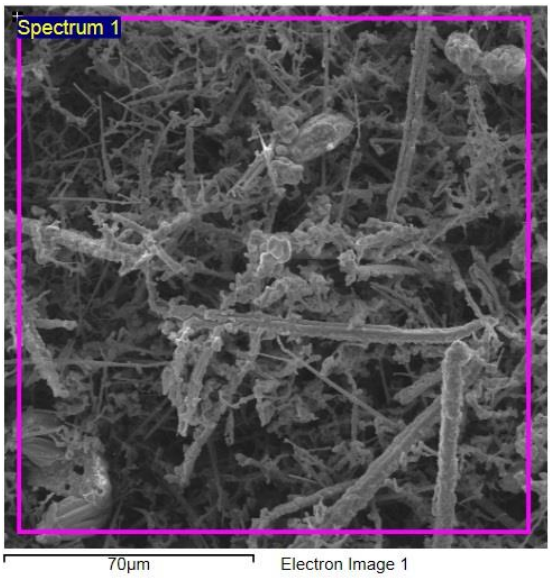

Figure 4.74 Area selected for EDX from the center of the membrane surface (white region)

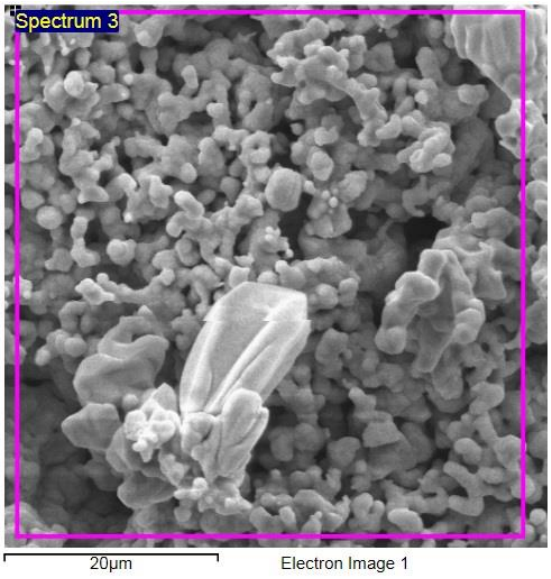

Figure 4.75 Area selected for EDX from the surface of the membrane where the coating is nonexistent (black region)

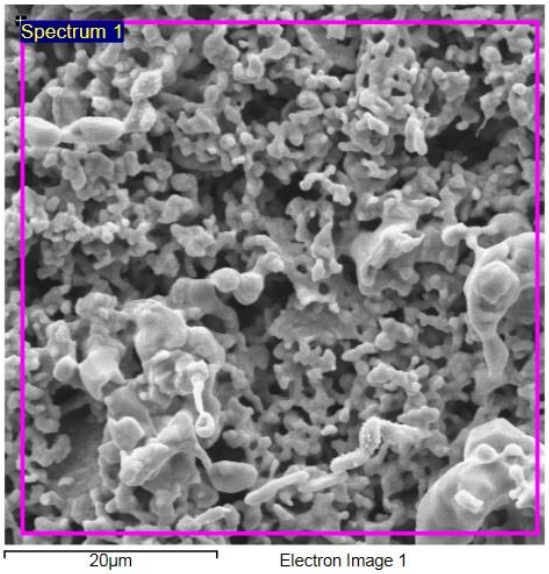

Figure 4.76 Area selected for the EDX from the edge of the membrane surface (pink region)

In Figure 4.74, Figure 4.75 and Figure 4.76 areas were selected from the central region (white), region without coating (black) and the region towards the edge of the membrane (pink) for EDX analyses. The results are presented in

Table 4.6. In the central region, which should be the area most affected, a large amount of barium was found to exist. The cobalt and iron quantities were found to be largely diminished. This indicates a chemical change in this region possibly due to the formation of a compound of barium (possibly carbonate) which has covered the surface. EDX analysis of the black colored area in the center of the membrane (see Figure 4.72) where the coating seems to be nonexistent was done next. Absence of La and Ni confirm that the BSCF-LNO protective coating was removed possibly during the removal of the

membrane from the reactor after finishing the test. Although the Ba and Sr content is found to be a little bit higher, the overall composition of Ba, Sr, Co and Fe in this region are found to be closest to the stoichiometric composition of BSCF out of all the analyses done on coated and uncoated membranes. For instance here we have 11.9% of Fe which was found to completely missing in the central white region of this membrane. In the membrane used for combustion in the previous section (uncoated membrane) Fe content was found to be 4.89% (Table 4.5). This clearly shows that coating of BSCF-LNO mixture has protected the membrane surface beneath with limited formation of carbonates on it. The area outside the perimeter of the inner tube carrying the methane gas (pink region) has a high Sr and Ba content with lower values of Co and Fe. The presence of La indicates that the protective coating is still there on the surface and is perhaps responsible for the better stability of this membrane.

Table 4.6 Elemental analysis of the three regions on the permeate side of BSCF-LNO coated BSCF membrane after the combustion reaction

Atomic % of Elements	Central white region	Black region without coating	Pink region towards the edge
Ba	66.53	33.51	36.78
Sr	17.44	28.72	37.68
Co	7.91	25.86	14.85
Fe		11.91	4.19
La	4.89		6.50
Ni	3.23		

The XPS analysis of the permeate side of the BSCF-LNO coated BSCF membrane after the test (Figure 4.77) shows that similar to the uncoated membrane, the surface of this membrane is also rich in barium and strontium. However traces of iron, cobalt, lanthanum and nickel can also be seen here. The detailed analysis of oxygen and carbon peaks shows the formation of carbonates (Figure 4.78). These are the carbonates of barium and strontium as these are elements present at the surface in considerable quantities with chemical shifts corresponding to carbonates of the elements. Lanthanum and nickle from LNO have not reacted and are therefore playing their part in improving the stability of this membrane.

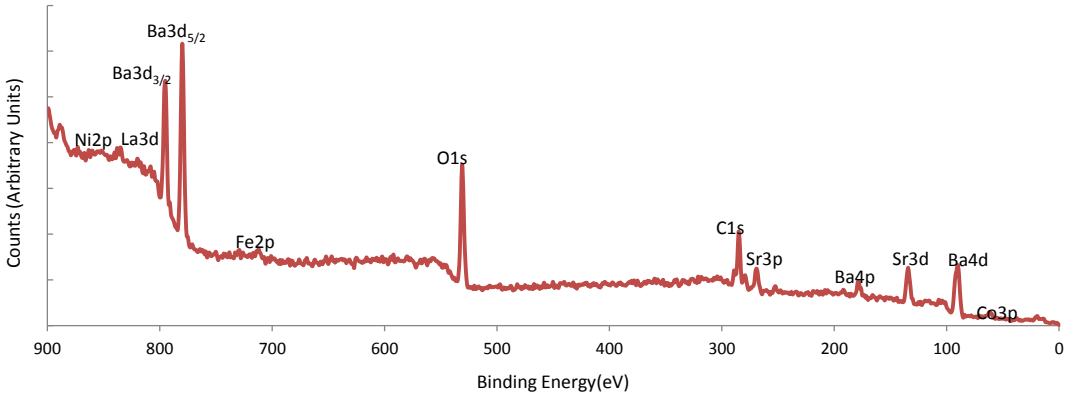

Figure 4.77 XPS scan of the permeate side of the BSCF-LNO coated BSCF membrane after combustion reaction with methane.

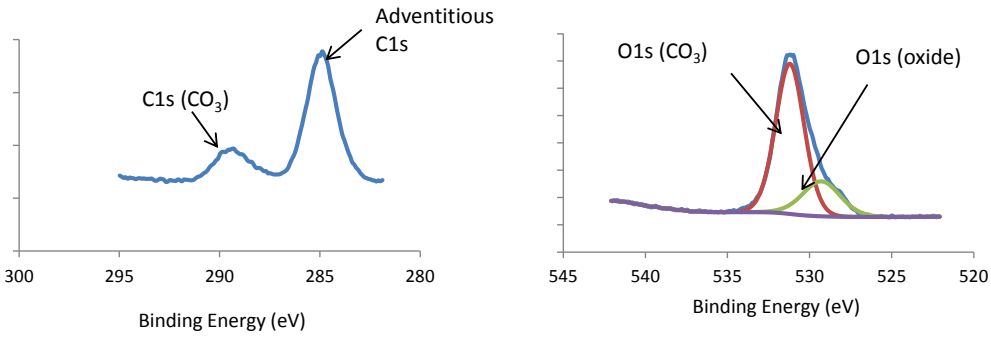

Figure 4.78 Detailed XPS scan of the Carbon and Oxygen peaks from the permeate side of the BSCF-LNO coated BSCF membrane after combustion reaction with methane.

4.5.4 Asymmetric membrane in the oxy-fuel reactor

In order to further improve the oxygen permeability of the BSCF membrane an asymmetric membrane was prepared. The porous support of this membrane was produced by pressing and sintering BSCF powder that was not ball milled. The large grain size of this powder ensured that the membrane had high porosity. The ball milled BSCF powder was mixed in acetone. A layer of this slurry was deposited on one side of the porous membrane by dip coating. The membrane was again sintered to make the top layer dense. This membrane was placed in the ITM reactor in such a way that the porous side was dense side was facing the feed side and the dense layer was facing the sweep side. The membrane was sealed from the bottom (dense side) using silver rings. The test was performed with both methane and helium used as the sweep gas alternatively. Figure 4.79 shows that when 0.65ml/min methane was used, there was excess oxygen amounting to 0.77 ml/min detected in permeate. This means that the asymmetric BSCF membrane produces more oxygen than a 1mm thick dense BSCF membrane which produced

0.2ml/min excess oxygen in similar conditions. Following this observation, the methane supply was increased to 1.35ml/min and still a small amount of oxygen (0.07ml/min) could be detected in permeate after the combustion had taken place. A further increase of methane to 1.95ml/min resulted in appearance of 0.2ml/min methane with a small amount of carbon monoxide to appear.

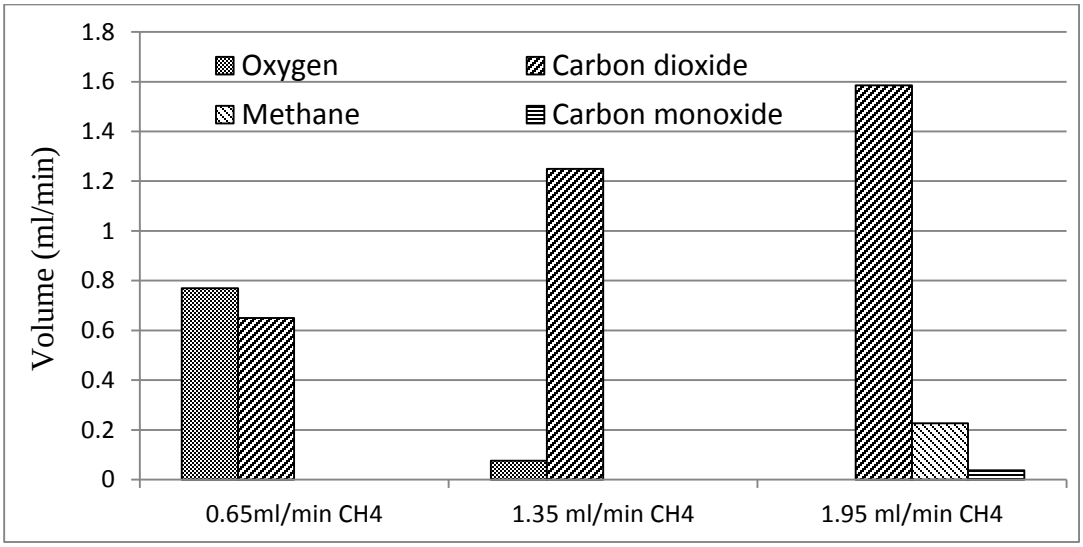

Figure 4.79 Gas analysis of permeate side of an asymmetric membrane employed in oxy-fuel combustion reaction at 920°C. The flow rates of methane used for the experiment are 0.65, 1.35 and 1.95ml/min.

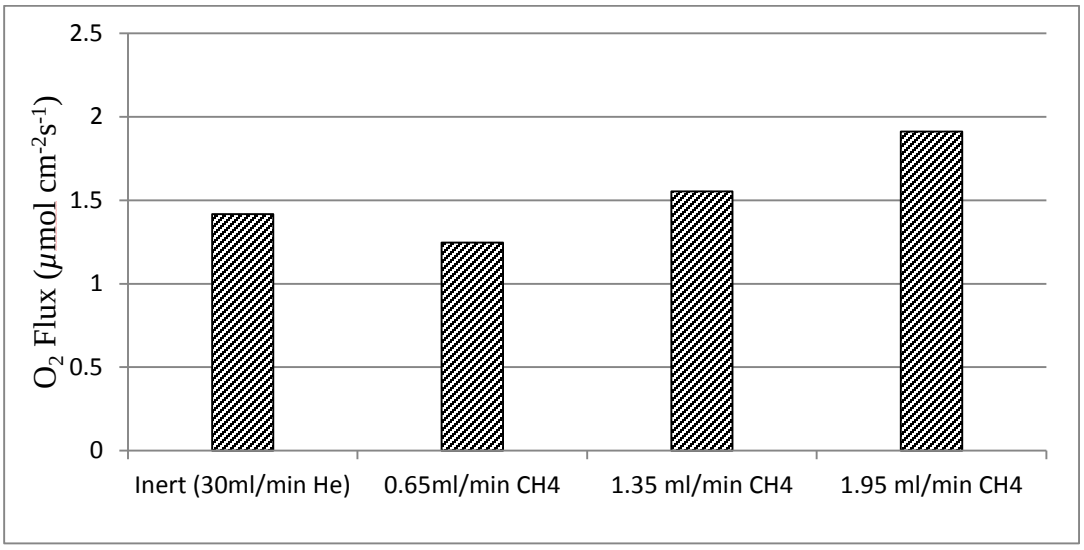

Figure 4.80 Oxygen permeability of the asymmetric membrane with helium (30ml/min) or methane (0.65, 1.35 and 1.95 ml/min) sweep gas

The oxygen permeability of the asymmetric BSCF membrane corresponding to these methane flow rates is shown in Figure 4.80. In addition, the oxygen permeability of this membrane was also measured with 30ml/min helium supplied as the sweep gas. These results show that the permeability of asymmetric membrane is 1.46μmol $cm^{-2}s^{-1}$ in helium sweep as compared to 1.26 μmol $cm^{-2}s^{-1}$ for a dense BSCF membrane. It can be expected that this permeability will further improve upon improvement of surface exchange kinetics of the membrane by deposition of appropriate catalyst. This will be further discussed in detail later. The oxygen permeability under 0.65, 1.35 and 1.95ml/min methane sweep was found to be 1.25, 1.55 and 1.91μmol$cm^{-2}s^{-1}$ respectively. These flux values are quite high as compared to dense membrane. For instance the 1mm thick dense membrane produced 0.91μmol $cm^{-2}s^{-1}$ oxygen with 0.65ml/min methane

(Figure 4.27). The maximum flux it could manage without deteriorating was 1.16μmol $cm^{-2}s^{-1}$ for 0.95ml/min methane (Figure 4.39). Looking at these results it can be concluded that an asymmetric BSCF membrane coated with a catalyst on the feed side would further improve the oxy-fuel combustion results. The permeate side of such membrane can also be coated with a protective layer such as BSCF-LNO mixture used earlier to enhance the stability of the membrane under carbon dioxide containing environment.

4.5.5 Summary

In this section the enhancement of the permeability and stability of the BSCF membrane separating oxygen for an oxy-fuel combustion reaction taking place in close proximity to the permeate side of the membrane is demonstrated. In order to investigate the effect of catalyst coating on the feed side of a BSCF membrane, the coating materials chosen were platinum and palladium. Palladium was found to be ineffective in increasing the permeability but palladium was found to enhance it. A study conducted on the thickness of these coatings revealed that palladium sputter coated for 180 seconds on the feed side of the 0.9mm thick BSCF membrane produced an oxygen flux of 1.39μmolcm^{-2}s^{-1}. These noble metals are also expected to shield the membrane from chemical changes during contact with flue gas when coated on the permeate side. For this purpose the permeate side of membrane was first coated with platinum using a sputter coater. Although this resulted in a reduction of the permeability of the membrane but the membrane operation was found to be stable even in the absence of excess oxygen and

presence of methane in the permeate stream. The membrane coated with palladium showed a much better oxygen flux to start with and this flux was found to be increasing steadily with the passage of time.

As LNO membranes are believed to be very stable, a 1mm thick LNO membrane was prepared and tested with CO_2 as the sweep gas. The membrane was found to be very stable even in 100% CO_2. An attempt was made to coat LNO layer on BSCF material to protect it under oxy-fuel combustion. This attempt was unsuccessful because of the large temperature difference at which BSCF and LNO densification occurs. This problem was solved by preparing a mixture of 50% LNO and 50% BSCF powders and coating this mixture on the permeate side of a 1mm thick BSCF membrane. The coated membrane was tested at 920°C both under helium and methane as sweep gas. Under 30ml/min helium the loss of permeability was very small. The membrane was found to be stable under methane flow rate of up to 1.35ml/min. It was observed that increasing the methane flow rate in the sweep increases the overall permeability of the membrane significantly. For instance, the oxygen permeability at 1.35ml/min methane sweep had risen to a value of 1.51μmolcm^{-2}s^{-1} which is much higher than the permeability when helium was used as sweep (1.15μmol cm^{-2}s^{-1}). A further increase in the methane flow rate to 1.45ml/min caused the oxygen permeability to reduce by 4.3% during 100 hours of operation. Using an asymmetric membrane under similar conditions was found to further enhance the oxygen permeability. The oxygen flux under inert operation was measured to be 1.42μmol cm^{-2}s^{-1}. Under 1.35ml/min and 1.95ml/min methane sweep, this value had risen

to 1.55 and 1.91μmol $cm^{-2}s^{-1}$ respectively. It can be concluded from the results presented in this section that the best way forward would be to employ an asymmetric membrane in oxy-fuel combustion reactor. This membrane should have a catalyst coating on the feed side to enhance the oxygen permeability by improving the surface exchange kinetics. On the permeate side the membrane should be coated with a protective layer such as BSCF-LNO mixture.

CHAPTER 5

CONCLUSIONS AND FUTURE WORK

The principal goals laid out for the study carried out in this thesis were to improve certain aspects of the performance and application of an Oxygen Transport Membrane (OTM) in oxy-fuel combustion reaction for carbon capture. The material selected for this purpose was the mixed ionic electronic conducting ceramic material $Ba_{0.5}Sr_{0.5}Co_{0.8}Fe_{0.2}O_{3-\delta}$ (BSCF). From the literature review it was concluded that membranes prepared from this material are by far the best in terms of oxygen permeability flux among all inorganic membranes considered for oxygen separation. Poor chemical stability of this material under operating conditions of an oxy-fuel power plant, however, has been the major hindrance in using this material for the said application. Another issue is the sealing of these membranes at high operating temperatures.

In Chapter 3 detailed procedure for preparation of dense and asymmetric BSCF membranes was discussed. It was shown that the powder synthesized using the modified Pechini method could be directly used to prepare porous BSCF membranes. For preparation of dense membranes the powder had to be ball milled. Asymmetric membranes could be prepared by simultaneously pressing and sintering a thin layer of fine powder and thick layer of coarse powder simultaneously. Another method was to sinter the porous membrane first and then coating this with BSCF slurry made from the fine powder using spin coating or dip coating techniques.

The reactor to test the oxygen permeability of the membrane was designed such that helium or methane could be chosen as the sweep on the permeate side of the membrane. When methane was being used, the oxy-fuel combustion reaction would take place very close to the membrane with the pure oxygen being produced by it. The quantity of all the possible products from this oxy-fuel combustion were measured by Gas Chromatography technique after water was condensed from the permeate stream.

A new sealing method was presented in order to seal ITM membranes to the reactor setup. It was found that a mixture of Pyrex and BSCF powder in the form of a paste, applied between the membrane and the alumina support tubes of the reactor, gives perfect sealing. Various compositions of this mixture were prepared and tested with BSCF and $La_2NiO_{4+\delta}$ (LNO) membranes and it was found that 80 wt.% Pyrex and 20 wt.% BSCF mixture provided the best results. Using this mixture the oxygen detected in the permeate was above 99.9% pure for the temperature range 700-1100°C and the sealing did not react with the membrane. No deterioration in the performance of the membrane was detected when this sealing was used for long duration experiments.

The microstructure and permeability properties of the BSCF membranes were investigated. The sintering time variation in BSCF membranes was found to significantly affect the grain size. The oxygen permeability of membrane with relatively smaller grain size was prepared by sintering it for 5 hours. It showed better permeability than the membranes prepared by sintering for 10, 15 and 48 hours having larger grains. The effect of thickness of BSCF membrane on its permeability was also studied. It was revealed that

the oxygen flux produced by membranes with thickness 1.1mm and 0.9mm were very close to each other in the temperature range 800-1100°C. From this the critical thickness of the BSCF membrane was estimated to be close to 1.1mm. The partial pressure difference between the feed side and the permeate side was also found to play an important role in the permeability of the BSCF membranes. When the partial pressure on the feed side was increased by supplying pure oxygen as feed the oxygen flux of the membrane increased by 90% as compared to when air was supplied as feed. The membrane was found to have excellent stability with respect to time producing constant oxygen permeability flux at 920°C for an operation of over 1000 hours.

The application of 1.4mm and 1mm thick BSCF membranes to produce oxygen at 920°C for oxy-fuel combustion was investigated. It was found that a complete combustion reaction took place when 0.65ml/min methane was introduced on the permeate side of the 1.4mm thick BSCF membrane. At the start of this reaction there was 7.5% excess oxygen detected along with CO_2 in the sweep. The test was run for 190 hours. Throughout the duration of this test the decrease in oxygen permeability was found to be only 7.9%. It can be concluded that the deterioration in the membrane BSCF membrane is very slow under carefully adjusted fuel volume during oxy-fuel combustion. A 1mm thick BSCF membrane was also tested under identical conditions. This membrane produced higher oxygen flux, therefore the excess oxygen was found to be greater than before (15%). This membrane produced constant oxygen flux throughout 200 hours of oxy-fuel combustion with no deterioration observed in the permeability of

the membrane. The methane flow rate provided to the membrane was increased to 0.75, 0.85 and 0.95ml/min. At these flow rates the oxygen flux also increased and still the membrane did not show any deterioration for up to 100 hours at each flow rate. The membrane was producing 1.16μmolcm^{-2}s^{-1}. The membrane only started to degrade when the flow rate of methane was increased to 1.05ml/min.

The effects of coating materials on permeability and stability of BSCF membranes were investigated. First the BSCF membranes were sputter coated with noble metals platinum and palladium on the feed side. The platinum did not have any positive effect on the permeability of the membrane. The palladium coating, however, was seen to enhance the oxygen flux. A study on different sputtering times, and hence the coating thicknesses, of palladium showed that the best permeability could be achieved by coating the membrane for 180 seconds. Next the same two coating materials were used on the permeate side of the membrane to enhance the stability of the membrane. With platinum the permeability of the membrane was seen to drop under inert operation as well as during oxy-fuel combustion as compared to the uncoated membrane. However this membrane was found to perform stably even in the absence of any excess oxygen at the permeate side. BSCF membranes coated with palladium on the permeate side performed better. The oxygen flux was only slightly reduced while maintaining the stability even under higher rates of methane. Ceramic materials were also used for protective coatings on the permeate side of the BSCF membranes. LNO membranes have been found to operate stably in CO_2 sweep. However attempt to coat a layer of this material on BSCF

membrane proved unsuccessful due to mismatch in the sintering temperatures of both the materials. A mixture of equal weight percentages of LNO and BSCF was prepared for this purpose. Slurry of this mixture was prepared to dip coat it on the permeated side of the membrane. The loss of the permeability of the membrane, in this case, was much lower than the platinum coated membrane. It produced an oxygen permeation flux of 1.15µmolcm^{-2}s^{-1} in inert sweep. This membrane also showed excellent stability during oxy-fuel combustion with 0.65ml/min methane. Due to the presence of the protective coating, the amount of methane could be increased to 1.35ml/min without causing deterioration in the flux. The oxygen permeability of the membrane at this flow rate of methane was found to be stable at 1.51μmol cm^{-2}s^{-1} which is 20% higher than what a 1mm thick BSCF membrane (without coating) could produce with helium as sweep. A further increase in the methane flow rate to 1.45ml/min caused a decrease of 4.3% in oxygen flux during 100 hours of operation. Similar tests were performed for asymmetric membrane as well. It produced 1.41μmol cm^{-2}s^{-1} oxygen under inert sweep which is 12% higher than 1mm thick dense membrane. The oxygen flux produced with methane sweep also increased. An appropriate coating of catalyst on the feed side and a protective layer on the permeate side of the asymmetric membrane should further improve the permeability and stability of these membranes.

In future focus of research in this area should be on the asymmetric membranes for the purpose of oxygen separation prior to the oxy-fuel combustion. Palladium was the material found to have maximum impact on the oxygen permeation flux when coated on

a dense BSCF membrane. Its flux almost matched that produced by an asymmetric membrane. So it is very promising to try and coat palladium on the feed side of the asymmetric BSCF membranes. The oxygen flux is expected to rise well above the usual values produced by BSCF membranes. In order to improve the stability of these palladium coated asymmetric membrane, they can be coated them with the same material (palladium) on the permeate side as well. We have shown during this study that the membranes with palladium on the permeate side have performed very well in the presence of flue gas. Another method which allowed us to enhance both the stability and permeability of the dense membranes during oxy-fuel combustion reaction was coating a mixture of BSCF-LNO powder on the permeate side. It would be a worthy effort to try and prepare asymmetric membranes coated with palladium on the feed side and BSCF-LNO mixture on the permeate side and try to enhance the permeability and stability of the BSCF membranes to the maximum.

Another area where the researchers should focus in the future is the introduction of liquid fuel in the ion transport membrane reactor for the purpose of oxy-fuel combustion. In various studies undertaken during the course of this thesis, methane gas was being used as fuel. While this was a unique endeavor in itself, most of the CO_2 emission in power sector is from oil and coal fired power plants. For instance, in 2007 the total CO_2 emissions from power sector was 30Gt. Out of this oil and coal accounted for 12Gt of CO_2 each and natural gas produced 6Gt of CO_2. Kingdom of Saudi Arabia is dependent on oil for almost all of its power generation. Considering this, it will be a worthwhile

effort to try and produce oxygen separation membranes and reactor designs capable of handling liquid fuel for the purpose of carbon capture through oxy-fuel combustion.

REFERENCES

[1] K. S. Lackner and J. D. Sachs, “A Robust Strategy for Sustainable Energy,” *Brookings Pap. Econ. Act.*, vol. 36, no. 2, pp. 215–284, 2005.

[2] K. S. Lackner, “The Case for Carbon Capture and Storage,” in *Efficient Carbon Capture for Coal Power Plants*, D. Stolten and V. Scherer, Eds. Weinheim: Wiley-VCH, 2011, pp. 3–9.

[3] J. Hansen, M. Sato, P. Kharecha, D. Beerling, R. Berner, V. Masson-Delmotte, M. Pagani, M. Raymo, D. L. Royer, and J. C. Zachos, “Target atmospheric CO2: Where should humanity aim?,” *Open Atmos. Sci. J.*, vol. 2, pp. 217–231, 2008.

[4] M. T. and Solomon, S., D. Qin, M. Manning, Z. Chen, M. Marquis, K.B. Averyt and H. L. Miller, “IPCC - Intergovernmental Panel on Climate Change,” *Contribution of Working Group I to the Fourth Assessment Report of the Intergovernmental Panel on Climate Change*, 2007. [Online]. Available: https://www.ipcc.ch/publications_and_data/publications_ipcc_fourth_assessment_report_wg1_report_the_physical_science_basis.htm. [Accessed: 18-Jan-2016].

[5] K. House, *Carbon Dioxide in Terrestrial: On the Physics and Chemistry of Carbon Dioxide Capture and Storage in Terrestrial and Marine Environments*. Lambert Academic Publishing, 2009.

[6] R. Bredesen, “High-temperature membranes in power generation with CO2 capture,” *Chem. Eng. Process.*, vol. 43, no. 9, pp. 1129–1158, 2004.

[7] H. LIU, R. ZAILANI, and B. GIBBS, “Comparisons of pulverized coal combustion in air and in mixtures of O/CO,” *Fuel*, vol. 84, no. 7–8, pp. 833–840, May 2005.

[8] E. Riensche, J. Nazarko, S. Schiebahn, M. Weber, L. Zhao, and D. Stolten, “Capture Options for Coal Power Plants,” in *Efficient Carbon Capture for Coal Power Plants*, D. Stolten and V. Scherer, Eds. Weinheim: Wiley-VCH, 2011, pp. 45–81.

[9] C. E. Powell and G. G. Qiao, “Polymeric CO2/N2 gas separation membranes for the capture of carbon dioxide from power plant flue gases,” *J. Memb. Sci.*, vol. 279, no. 1–2, pp. 1–49, 2006.

[10] L. Pauling, “The nature of the chemical bond—1992,” *J. Chem. Educ.*, vol. 69, no. 7, p. 519, 1992.

[11] J. Sunarso, S. Baumann, J. M. Serra, W. a. Meulenberg, S. Liu, Y. S. Lin, and J. C. Diniz da Costa, “Mixed ionic-electronic conducting (MIEC) ceramic-based membranes for oxygen separation,” *J. Memb. Sci.*, vol. 320, no. 1–2, pp. 13–41, 2008.

[12] H. J. M. Bouwmeester and A. J. Burggraaf, “Dense ceramic membranes for oxygen separation,” in *Fundamentals of Inorganic Membrane Science and Technology*, A. J. Burggraaf and L. Cot, Eds. Elsevier, 1996, pp. 435–527.

[13] J. Vente, W. Haije, R. Ijpelaan, and F. Rusting, “On the full-scale module design

of an air separation unit using mixed ionic electronic conducting membranes," *J. Memb. Sci.*, vol. 278, no. 1–2, pp. 66–71, 2006.

[14] A. Bhargav and G. S. Jackson, "Thermokinetic modeling and parameter estimation for hydrogen permeation through Pd0.77Ag0.23 membranes," *Int. J. Hydrogen Energy*, vol. 34, no. 12, pp. 5164–5173, 2009.

[15] A. Bhargav, G. S. Jackson, R. J. Ciora Jr., and P. T. K. Liu, "Model Development and Validation of Hydrogen Transport Through Supported Palladium Membranes," *J. Memb. Sci.*, vol. 356, no. 1–2, pp. 123–132, 2010.

[16] S. Engels, T. Markus, M. Modigell, and L. Singheiser, "Oxygen permeation and stability investigations on MIEC membrane materials under operating conditions for power plant processes," *J. Memb. Sci.*, vol. 370, no. 1–2, pp. 58–69, Mar. 2011.

[17] P. Dyer, "Ion transport membrane technology for oxygen separation and syngas production," *Solid State Ionics*, vol. 134, no. 1–2, pp. 21–33, 2000.

[18] B. Ma, J. P. Hodges, J. D. Jorgensen, D. J. Miller, J. W. Richardson Jr., and U. Balachandran, "Structure and Property Relationships in Mixed-Conducting Sr4(Fe1−xCox)6O13±δMaterials," *J. Solid State Chem.*, vol. 141, no. 2, pp. 576–586, 1998.

[19] S. M. Hashim, A. R. Mohamed, and S. Bhatia, "Current status of ceramic-based membranes for oxygen separation from air.," *Adv. Colloid Interface Sci.*, vol. 160, no. 1–2, pp. 88–100, Oct. 2010.

[20] J. D. Way and D. L. Roberts, “Hollow Fiber Inorganic Membranes for Gas Separations,” *Sep. Sci. Technol.*, vol. 27, no. 1, pp. 29–41, 1992.

[21] Y. Yamamura, C. Ihara, S. Kawasaki, H. Sakai, K. Suzuki, S. Takami, M. Kubo, and A. Miyamoto, “Materials design of perovskite-based oxygen ion conductor by molecular dynamics method,” *Solid State Ionics*, vol. 160, no. 1–2, pp. 93–101, 2003.

[22] Z. Shao, W. Yang, Y. Cong, H. Dong, J. Tong, and G. Xiong, “Investigation of the permeation behavior and stability of a Ba0.5Sr0.5Co0.8Fe0.2O(3-δ) oxygen membrane,” *J. Memb. Sci.*, vol. 172, no. 1–2, pp. 177–188, 2000.

[23] H. Lu, J. H. Tong, Y. Cong, and W. S. Yang, “Partial oxidation of methane in Ba0.5Sr0.5Co0.8Fe0.2O3-delta membrane reactor at high pressures,” *Catal. Today*, vol. 104, no. 2–4, pp. 154–159, 2005.

[24] J. F. Vente, S. McIntosh, W. G. Haije, and H. J. M. Bouwmeester, “Properties and performance of BaxSr1−xCo0.8Fe0.2O3−δ materials for oxygen transport membranes,” *J. Solid State Electrochem.*, vol. 10, no. 8, pp. 581–588, May 2006.

[25] J. F. Vente, W. G. Haije, and Z. S. Rak, “Performance of functional perovskite membranes for oxygen production,” *J. Memb. Sci.*, vol. 276, no. 1–2, pp. 178–184, 2006.

[26] J. Tong, W. Yang, B. Zhu, and R. Cai, “Investigation of ideal zirconium-doped perovskite-type ceramic membrane materials for oxygen separation,” vol. 203, pp.

175–189, 2002.

[27] J. Tong, W. Yang, R. Cai, B. Zhu, G. Xiong, and L. Lin, “Investigation on the structure stability and oxygen permeability of titanium-doped perovskite-type oxides of BaTi0.2CoxFe0.8−xO3−δ (x=0.2–0.6),” *Sep. Purif. Technol.*, vol. 32, no. 1–3, pp. 289–299, 2003.

[28] H. Kruidhof, H. Bouwmeester, R. Vdoorn, and a Burggraaf, “Influence of order-disorder transitions on oxygen permeability through selected nonstoichiometric perovskite-type oxides,” *Solid State Ionics*, vol. 63–65, pp. 816–822, 1993.

[29] L. Qiu, “Oxygen permeation studies of SrCo0.8Fe0.2O3 − δ,” *Solid State Ionics*, vol. 76, no. 3–4, pp. 321–329, 1995.

[30] T. Nagai, W. Ito, and T. Sakon, “Relationship between cation substitution and stability of perovskite structure in SrCoO3-??-based mixed conductors,” *Solid State Ionics*, vol. 177, no. 39–40, pp. 3433–3444, 2007.

[31] P. Zeng, Z. Shao, S. Liu, and Z. P. Xu, “Influence of M cations on structural, thermal and electrical properties of new oxygen selective membranes based on SrCo0.95M0.05O3−δ perovskite,” *Sep. Purif. Technol.*, vol. 67, no. 3, pp. 304–311, 2009.

[32] S. Švarcová, K. Wiik, J. Tolchard, H. J. M. Bouwmeester, and T. Grande, “Structural instability of cubic perovskite BaxSr1 - xCo1 - yFeyO3 - δ,” *Solid State Ionics*, vol. 178, no. 35–36, pp. 1787–1791, 2008.

[33] M. Arnold, T. M. Gesing, J. Martynczuk, and A. Feldhoff, “Correlation of the formation and the decomposition process of the BSCF perovskite at intermediate temperatures,” *Chem. Mater.*, vol. 20, no. 12, pp. 5851–5858, 2008.

[34] R. Kriegel and N. Preuss, “Dilatometric determination of phase transition temperatures and oxidation temperatures on the compounds srmno3-y and sr2mno4-y’,” *Thermochim. Acta*, vol. 285, pp. 91–98, 1996.

[35] Q. Zeng, Y. Zuo, C. Fan, and C. Chen, “CO2-tolerant oxygen separation membranes targeting CO2 capture application,” *J. Memb. Sci.*, vol. 335, no. 1–2, pp. 140–144, 2009.

[36] M. Schulz, R. Kriegel, and A. Kämpfer, “Assessment of CO2 stability and oxygen flux of oxygen permeable membranes,” *J. Memb. Sci.*, vol. 378, no. 1–2, pp. 10–17, Aug. 2011.

[37] a Nowick, “High-temperature protonic conductors with perovskite-related structures,” *Solid State Ionics*, vol. 77, pp. 137–146, 1995.

[38] J.-I. Jung, S. T. Misture, and D. D. Edwards, “The electronic conductivity of Ba0.5Sr0.5Co x Fe1−x O3−δ (BSCF: x = 0 ∼ 1.0) under different oxygen partial pressures,” *J. Electroceramics*, vol. 24, no. 4, pp. 261–269, Apr. 2009.

[39] A. Atkinson and T. M. G. M. Ramos, “Chemically-induced stresses in ceramic oxygen ion-conducting membranes,” vol. 129, pp. 259–269, 2000.

[40] R. Kriegel, R. Kircheisen, and J. Töpfer, “Oxygen stoichiometry and expansion

behavior of Ba0.5Sr0.5Co0.8Fe0.2O3 - δ," *Solid State Ionics*, vol. 181, no. 1–2, pp. 64–70, 2010.

[41] B. X. Huang, J. Malzbender, R. W. Steinbrech, and L. Singheiser, "Discussion of the complex thermo-mechanical behavior of Ba0.5Sr0.5Co0.8Fe0.2O3-delta," *J. Memb. Sci.*, vol. 359, no. 1–2, pp. 80–85, 2010.

[42] J. L. Routbort, K. C. Goretta, R. E. Cook, and J. Wolfenstine, "Deformation of perovskite electronic ceramics — a review," *Solid State Ionics*, vol. 129, no. 1–4, pp. 53–62, 2000.

[43] J. X. Yi, H. L. Lein, T. Grande, S. Yakovlev, and H. J. M. Bouwmeester, "High-temperature compressive creep behaviour of the perovskite-type oxide Ba0.5Sr0.5Co0.8Fe0.2O3 - δ," *Solid State Ionics*, vol. 180, no. 36–39, pp. 1564–1568, 2009.

[44] C. K. M. Shaw, "Mass transport in mixed conducting perovskite related oxides," Imperial College London (University of London), 2001.

[45] Y. Liu, X. Tan, and K. Li, "Mixed Conducting Ceramics for Catalytic Membrane Processing," *Catal. Rev.*, vol. 48, no. 2, pp. 145–198, 2006.

[46] X. Tan and K. Li, "Modeling of air separation in a LSCF hollow-fibre membrane module," *Am. Inst. Chem. Eng. J.*, vol. 48, pp. 1469–1477, 2002.

[47] A. W. SMITH, F. W. MESZAROS, and C. D. AMATA, "Permeability of Zirconia, Hafnia, and Thoria to Oxygen," *J. Am. Ceram. Soc.*, vol. 49, no. 5, pp.

240–244, May 1966.

[48] Y. Teraoka, H.-M. Zhang, S. Furukawa, and N. Yamazoe, “Oxygen permeation through perovskite-type oxides.,” *Chemistry Letters*. pp. 1743–1746, 1985.

[49] Y. Teraoka, H. M. Zhang, K. Okamoto, and N. Yamazoe, “Mixed ionic-electronic conductivity of La1−xSrxCo1−yFeyO3−δ perovskite-type oxides,” *Materials Research Bulletin*, vol. 23, no. 1. pp. 51–58, 1988.

[50] M. T. Anderson, J. T. Vaughey, and K. R. Poeppelmeier, “Structural similarities among oxygen-deficient perovskites,” *Chem. Mater.*, vol. 5, no. 33, pp. 151–165, 1993.

[51] D. M. Bochkov, V. V Kharton, A. V Kovalevsky, A. P. Viskup, and E. N. Naumovich, “Oxygen permeability of La2Cu(Co)O4+ solid solutions,” *solid state ionics*, vol. 120, no. January, pp. 281–288, 1999.

[52] B. Ma, U. Balachandran, J. . Hodges, J. . Jorgensen, D. . Miller, and J. W. Richardson Jr., “Synthesis, conductivity and oxygen diffusivity of Sr2Fe3Ox,” *Mater. Lett.*, vol. 35, pp. 303–308, 1998.

[53] Y. Teraoka, H. M. Zhang, K. Okamoto, and N. Yamazoe, “Mixed ionic-electronic conductivity of La1-xSrxCo1-yFeyO3-?? perovskite-type oxides,” *Mater. Res. Bull.*, vol. 23, no. 1, pp. 51–58, 1988.

[54] B. Steele, “Ceramic ion conducting membranes and their technological applications,” *Comptes Rendus l’Académie des Sci. - Ser. IIC - Chem.*, vol. 1, no.

9, pp. 533–543, 1998.

[55] B. Ma and U. Balachandran, “Phase Stability of SrFeCo0.5Ox in Reducing Environments,” *Mater. Res. Bull.*, vol. 33, no. 2, pp. 223–236, 1998.

[56] B. J. Mitchell, R. C. Rogan, J. W. Richardson, B. Ma, and U. Balachandran, “Stability of the cubic perovskite SrFe0.8Co0.2O3-??,” *Solid State Ionics*, vol. 146, no. 3–4, pp. 313–321, 2002.

[57] E. D. Wachsman and T. L. Clites, “Stable Mixed-Conducting Bilayer Membranes for Direct Conversion of Methane to Syngas,” *J. Electrochem. Soc.*, vol. 149, no. 3, p. A242, Mar. 2002.

[58] A. V. Kovalevsky, V. V. Kharton, V. N. Tikhonovich, E. N. Naumovich, A. A. Tonoyan, O. P. Reut, and L. S. Boginsky, “Oxygen permeation through Sr(Ln)CoO3-δ (Ln = La, Nd, Sm, Gd) ceramic membranes,” *Mater. Sci. Eng. B*, vol. B52, no. 2–3, pp. 105–116, 1998.

[59] L. Siwen, C. You, F. Lianqing, Y. Weishen, L. Liwu, M. Jian, and R. Yufang, “Oxygen Permeating Properties of the Mixed Conducting Membranes without Cobalt,” *Mater. Res. Bull.*, vol. 33, no. 2, pp. 183–188, Feb. 1998.

[60] T. H. Lee, Y. L. Yang, a J. Jacobson, B. Abeles, and M. Zhou, “Oxygen permeation in dense SrCoFeO membranes : Surface exchange kinetics versus bulk diffusion,” *Solid State Ionics*, vol. 100, pp. 77–85, 1997.

[61] T. Lee, “Oxygen permeation in SrCo0.8Fe0.2O3 − δ membranes with porous

electrodes," *Solid State Ionics*, vol. 100, no. 1–2, pp. 87–94, Sep. 1997.

[62] W. Liu, G. G. Zhang, S. Xie, C. S. Chen, G. Y. Meng, and D. K. Peng, "Electrical conduction and oxygen transport in SrFeCo0.5Ox oxide membranes," *Solid State Ionics*, vol. 135, no. 1–4, pp. 727–730, 2000.

[63] V. V. Kharton, A. P. Viskup, A. A. Yaremchenko, P. F. Kerko, E. N. Naumovich, and A. V. Kovalevsky, "Ionic transport in SrCo0.85Ti0.15O3-δ ceramics at high oxygen pressures," *Mater. Res. Bull.*, vol. 34, no. 12, pp. 1921–1928, 1999.

[64] V. V. Kharton, A. V. Kovalevsky, A. P. Viskup, F. M. Figueiredo, J. R. Frade, A. A. Yaremchenko, and E. N. Naumovich, "Faradaic efficiency and oxygen permeability of Sr0.97Ti0.60Fe0.40O3âˆ’Î´ perovskite," *Solid State Ionics*, vol. 128, no. 1–4, pp. 117–130, 2000.

[65] V. V Kharton, A. P. Viskup, A. V Kovalevsky, J. R. Jurado, E. N. Naumovich, A. A. Vecher, and J. R. Frade, "Oxygen ionic conductivity of Ti-containing strontium ferrite," *Solid State Ionics*, vol. 133, pp. 57–65, 2000.

[66] V. Kharton, "Oxygen permeability of perovskites in the system SrCoO3 − δ_SrTiO3," *Solid State Ionics*, vol. 96, pp. 141–151, 1997.

[67] V. V. Kharton, E. N. Naumovich, and A. V. Nikolaev, "Materials of high-temperature electrochemical oxygen membranes," *J. Memb. Sci.*, vol. 111, no. 2, pp. 149–157, 1996.

[68] J. R. Jurado, F. M. Figueiredo, and J. R. Frade, "Overpotential terms on the

electrochemical permeability of Sr0.97(Ti,Fe)O3-y materials," *Solid State Ionics*, vol. 122, no. 1–4, pp. 197–204, 1999.

[69] Z. P. Shao, G. X. Xiong, H. Dong, W. H. Yang, and L. W. Lin, "Synthesis, oxygen permeation study and membrane performance of a Ba0.5Sr0.5Co0.8Fe0.2O3-delta oxygen-permeable dense ceramic reactor for partial oxidation of methane to syngas," *Sep. Purif. Technol.*, vol. 25, no. 1–3, pp. 97–116, 2001.

[70] V. . Kharton, E. . Naumovich, a. . Kovalevsky, a. . Viskup, F. . Figueiredo, I. . Bashmakov, and F. M. . Marques, "Mixed electronic and ionic conductivity of LaCo(M)O3 (M=Ga, Cr, Fe or Ni): IV. Effect of preparation method on oxygen transport in LaCoO3-[delta]," *Solid State Ionics*, vol. 138, no. 1–2, pp. 135–148, 2000.

[71] V. V. Kharton, E. N. Naumovich, A. A. Vecher, and A. V. Nikolaev, "Oxide Ion Conduction in Solid Solutions Ln1-xSrxCoO3-δ(Ln = La, Pr, Nd)," *J. Solid State Chem.*, vol. 120, no. 1, pp. 128–136, 1995.

[72] C. H. Chen, H. J. M. Bouwmeester, R. H. E. van Doorn, H. Kruidhof, and A. J. Burggraaf, "Oxygen permeation of La0.3Sr0.7CoO3-d," *Solid State Ionics*, vol. 98, pp. 7–13, 1997.

[73] J. W. Stevenson, T. R. Armstrong, R. D. Carneim, L. R. Pederson, and W. J. Weber, "Electrochemical properties of mixed conducting perovskites La(1-x)M(x)Co(1-y)Fe(y)O(3-delta) (M=Sr,Ba,Ca)," *J. Electrochem. Soc.*, vol. 143, no. 9, pp. 2722–2729, 1996.

[74] V. V Kharton, A. V Kovalevsky, V. N. Tikhonovich, E. N. Naumovich, and A. P. Viskup, “Mixed electronic and ionic conductivity of LaCo(M)O-3 (M = Ga, Cr, Fe or Ni) - II. Oxygen permeation through Cr- and Ni-substituted LaCoO3,” *Solid State Ionics*, vol. 110, no. 1–2, pp. 53–60, 1998.

[75] V. V. Kharton, A. P. Viskup, E. N. Naumovich, and V. N. Tikhonovich, “Oxygen permeability of LaFe1-xNixO3-?? solid solutions,” *Mater. Res. Bull.*, vol. 34, no. 8, pp. 1311–1317, 1999.

[76] V. V Kharton, A. P. Viskup, D. M. Bochkov, E. N. Naumovich, O. P. Reut, I. I. Oxygen, N. Lacoo, V. V Kharton, a V Kovalevsky, V. N. Tikhonovich, E. N. Naumovich, and A. P. Viskup, “Mixed electronic and ionic conductivity of LaCo(M)O3 (M=Ga, Cr, Fe or Ni): III. Diffusion of oxygen through LaCo1−x−yFexNiyO3±δ ceramics,” *Solid State Ionics*, vol. 110, no. 1–2, pp. 61–68, 1998.

[77] V. Kharton, “Ionic conductivity of La(Sr)Ga(Mg,M)O3−δ (M=Ti, Cr, Fe, Co, Ni): effects of transition metal dopants,” *Solid State Ionics*, vol. 132, no. 1–2, pp. 119–130, 2000.

[78] V. V. Kharton, A. P. Viskup, E. N. Naumovich, A. A. Tonoyan, and O. P. Reut, “Oxygen ionic transport in A-site-deficient perovskites La(Pb)FeO3,” *Mater. Res. Bull.*, vol. 33, no. 7, pp. 1087–1093, Jul. 1998.

[79] N. Y. Y. Teraoka, H.M. Zhang, S. Furukawa, “Oxygen permeation through pervoskite-type oxides,” *Chem. Lett.*, no. C, pp. 1743–1746, 1985.

[80] J. E. ten Elshof, H. J. M. Bouwmeester, and H. Verweij, “Oxidative coupling of methane in a mixed-conducting perovskite membrane reactor,” *Appl. Catal. A, Gen.*, vol. 130, no. 2, pp. 195–212, 1995.

[81] S. J. Xu and W. J. Thomson, “Stability of La0.6Sr0.4Co0.2Fe0.8O3-delta perovskite membranes in reducing and nonreducing environments,” *Ind. Eng. Chem. Res.*, vol. 37, no. 4, pp. 1290–1299, 1998.

[82] T. Armstrong, F. Prado, and A. Manthiram, “Synthesis, crystal chemistry, and oxygen permeation properties of LaSr3Fe3-xCoxO10 (0???x???1.5),” *Solid State Ionics*, vol. 140, no. 1–2, pp. 89–96, 2001.

[83] S. G. Li, W. Q. Jin, N. P. Xu, and J. Shi, “Synthesis and oxygen permeation properties of La0.2Sr0.8Co0.2Fe0.8O3-delta membranes,” *Solid State Ionics*, vol. 124, pp. 161–170, 1999.

[84] S. Li, W. Jin, P. Huang, N. Xu, J. Shi, and Y. S. Lin, “Tubular lanthanum cobaltite perovskite type membrane for oxygen permeation,” *J. Memb. Sci.*, vol. 166, no. 1, pp. 51–61, 2000.

[85] V. . V Kharton, A. . P. Viskup, E. . N. Naumovich, N. . M. Lapchuk, I. Oxygen, and L. Lagao, “Mixed electronic and ionic conductivity of LaCo(M)O3 (M=Ga, Cr, Fe or Ni)I. Oxygen transport in perovskites LaCoO3–LaGaO3,” *Solid State Ionics*, vol. 104, no. 1–2, pp. 67–78, 1997.

[86] T. Ishihara, T. Yamada, H. Arikawa, H. Nishiguchi, and Y. Takita, “Mixed

electronic-oxide ionic conductivity and oxygen permeating property of Fe-, Co- or Ni-doped LaGaO3 perovskite oxide," *Solid State Ionics*, vol. 135, no. 1–4, pp. 631–636, 2000.

[87] V. V. Kharton, a. a. Yaremchenko, a. V. Kovalevsky, a. P. Viskup, E. N. Naumovich, and P. F. Kerko, "Perovskite-type oxides for high-temperature oxygen separation membranes," *J. Memb. Sci.*, vol. 163, no. 2, pp. 307–317, 1999.

[88] K. Huang, R. Tichy, and J. Goodenough, "Superior Perovskite Oxide- Ion Conductor; Strontium- and Magnesium- Doped LaGaO3: I, Phase Relationships and Electrical Properties," *J. Am.*, vol. 75, no. 190693, pp. 2565–2575, 1998.

[89] H. Ullmann and N. Trofimenko, "Composition, structure and transport properties of perovskite-type oxides," *Solid State Ionics*, vol. 119, no. 1, pp. 1–8, 1999.

[90] V. Kharton, "Faradaic efficiency and oxygen permeability of Sr0.97Ti0.60Fe0.40O3âˆ'Î´ perovskite," *Solid State Ionics*, vol. 128, no. 1–4, pp. 117–130, 2000.

[91] S. Xie, W. Liu, K. Wu, P. H. Yang, G. Y. Meng, and C. S. Chen, "Mixed oxygen ionic and electronic conduction in CaFe0.2Ti0.8O3-[delta]: a combined oxygen permeation and electrical conductivity study," *Solid State Ionics*, vol. 118, no. 1–2, pp. 23–28, 1999.

[92] Z. Shao, G. Xiong, Y. Cong, and W. Yang, "Synthesis and oxygen permeation study of novel perovskite-type BaBi(x)Co0.2Fe(0.8-x)O(3-δ) ceramic

membranes," *J. Memb. Sci.*, vol. 164, no. 1–2, pp. 167–176, 2000.

[93] Y. Zeng, Y. S. Lin, and S. L. Swartz, "Perovskite-type ceramic membrane : synthesis , oxygen permeation and membrane reactor performance for oxidative coupling of methane," vol. 150, 1998.

[94] S. J. Xu and W. J. Thomson, "Oxygen permeation rates through ion-conducting perovskite membranes," *Chem. Eng. Sci.*, vol. 54, no. 17, pp. 3839–3850, 1999.

[95] S. Kim, Y. L. Yang, R. Christoffersen, and A. J. Jacobson, "Oxygen permeation, electrical conductivity and stability of the perovskite oxide La0.2Sr0.8Cu0.4Co0.6O3-x," *Solid State Ionics*, vol. 104, no. 1–2, pp. 57–65, 1997.

[96] A. A. Yaremchenko, V. V. Kharton, A. P. Viskup, E. N. Naumovich, V. N. Tikhonovich, and N. M. Lapchuk, "Mixed electronic and ionic conductivity of LaCo(M)O3 (M = Ga, Cr, Fe or Ni) V. Oxygen permeability of Mg-doped La(Ga, Co)O3-δ perovskites," *Solid State Ionics*, vol. 120, no. 1, pp. 65–74, 1999.

[97] U. Balachandran, J. T. Dusek, R. L. Mieville, R. B. Poeppel, M. S. Kleefisch, S. Pei, T. P. Kobylinski, C. a. Udovich, and a. C. Bose, "Dense ceramic membranes for partial oxidation of methane to syngas," *Appl. Catal. A Gen.*, vol. 133, no. 1, pp. 19–29, 1995.

[98] U. Balachandran, J. T. Dusek, P. S. Maiya, B. Ma, R. L. Mieville, M. S. Kleefisch, and C. A. Udovich, "Ceramic Membrane Reactor for Converting Methane to

Syngas," *Catal. Today*, vol. 36, no. 3, pp. 265–272, 1997.

[99] B. Ma, J. P. Hodges, J. D. Jorgensen, D. J. Miller, J. W. Richardson Jr., and U. Balachandran, "No TitleStructure and Property Relationships in Mixed-Conducting Sr4(Fe12xCox)6O136d Materials," *J. Solid State Chem.*, vol. 141, pp. 576–586, 1998.

[100] S. Kim, Y. L. Yang, A. J. Jacobson, and B. Abeles, "Diffusion and surface exchange coefficients in mixed ionic electronic conducting oxides from the pressure dependence of oxygen permeation," *Solid State Ionics*, vol. 106, no. 3–4, pp. 189–195, 1998.

[101] D. M. Bochkov, V. V. Kharton, A. V. Kovalevsky, A. P. Viskup, and E. N. Naumovich, "Oxygen permeability of La2Cu(Co)O4+δ solid solutions," *Solid State Ionics*, vol. 120, no. 1, pp. 281–288, 1999.

[102] T. J. Mazanec, T. L. Cable, and J. G. Frye, "Electrocatalytic cells for chemical reaction," *Solid State Ionics*, vol. 53–56, no. PART 1, pp. 111–118, 1992.

[103] C. S. Chen, H. Kruidhof, H. J. M. Bouwmeester, H. Verweij, and A. J. Burggraaf, "Oxygen permeation through oxygen ion oxide-noble metal dual phase composites," *Solid State Ionics*, vol. 86–88, pp. 569–572, 1996.

[104] C. S. Chen, B. A. Boukamp, H. J. M. Bouwmeester, G. Z. Cao, H. Kruidhof, A. J. A. Winnubst, and A. J. Burggraaf, "Microstructural development, electrical properties and oxygen permeation of zirconia-palladium composites," *Solid State*

Ionics, vol. 76, no. 1–2, pp. 23–28, 1995.

[105] C. S. Chen, H. Kruidhof, H. J. M. Bouwmeester, H. Verweij, and A. J. Burggraaf, "Thickness dependence of oxygen permeation through erbiastabilized bismuth oxide-silver composites," *Solid State Ionics*, vol. 99, no. 3–4, pp. 215–219, 1997.

[106] H. Wang, "Investigation on the partial oxidation of methane to syngas in a tubular Ba0.5Sr0.5Co0.8Fe0.2O3$minus;$delta; membrane reactor," *Catal. Today*, vol. 82, no. 1–4, pp. 157–166, 2003.

[107] V. V Kharton, A. V Kovalevsky, A. P. Viskup, A. L. Shaula, F. M. Figueiredo, E. N. Naumovich, and F. M. B. Marques, "Oxygen transport in Ce0.8Gd0.2O2-d-based composite membranes," *Solid State Ionics*, vol. 160. pp. 247–258, 2003.

[108] S. Engels, F. Beggel, M. Modigell, and H. Stadler, "Simulation of a membrane unit for oxyfuel power plants under consideration of realistic BSCF membrane properties," *J. Memb. Sci.*, vol. 359, no. 1–2, pp. 93–101, 2010.

[109] R. Y. Muydinov, M. N. Popova, and A. R. Kaul, "Development and Characterization of Thin-Film Oxygen Membranes Based on Ba0.5Sr0.5Co0.8Fe0.2O3 − δ," *Dokl. Chem.*, vol. 402, no. 1–3, pp. 88–90, May 2005.

[110] Z. Chen, Z. Shao, R. Ran, W. Zhou, P. Zeng, and S. Liu, "A dense oxygen separation membrane with a layered morphologic structure," *J. Memb. Sci.*, vol. 300, no. 1–2, pp. 182–190, 2007.

[111] O. BUCHLER, J. SERRA, W. MEULENBERG, D. SEBOLD, and H. BUCHKREMER, “Preparation and properties of thin La1−xSrxCo1−yFeyO3−δ perovskitic membranes supported on tailored ceramic substrates,” *Solid State Ionics*, vol. 178, no. 1–2, pp. 91–99, Jan. 2007.

[112] M. L. Fontaine, J. B. Smith, Y. Larring, and R. Bredesen, “On the preparation of asymmetric CaTi0.9Fe0.1O3-δ membranes by tape-casting and co-sintering process,” *J. Memb. Sci.*, vol. 326, no. 2, pp. 310–315, 2009.

[113] X. Li, T. Kerstiens, and T. Markus, “Oxygen permeability and phase stability of Ba0.5Sr0.5Co0.8Fe0.2O3−δ perovskite at intermediate temperatures,” *J. Memb. Sci.*, vol. 438, pp. 83–89, Jul. 2013.

[114] N. H. Menzler, F. Han, T. van Gestel, W. Schafbauer, F. Schulze-Küppers, S. Baumann, S. Uhlenbruck, W. a. Meulenberg, L. Blum, and H. P. Buchkremer, “Application of Thin-Film Manufacturing Technologies to Solid Oxide Fuel Cells and Gas Separation Membranes,” *Int. J. Appl. Ceram. Technol.*, vol. 10, no. 3, pp. 421–427, May 2013.

[115] A. V. Kovalevsky, A. A. Yaremchenko, V. A. Kolotygin, F. M. M. Snijkers, V. V. Kharton, A. Buekenhoudt, and J. J. Luyten, “Oxygen permeability and stability of asymmetric multilayer Ba0.5Sr0.5Co0.8Fe0.2O3−δ ceramic membranes,” *Solid State Ionics*, vol. 192, no. 1, pp. 677–681, Jun. 2011.

[116] P. F. Haworth, S. Smart, J. M. Serra, and J. C. Diniz da Costa, “Combined investigation of bulk diffusion and surface exchange parameters of silver catalyst

coated yttrium-doped BSCF membranes.," *Phys. Chem. Chem. Phys.*, vol. 14, no. 25, pp. 9104–11, Jul. 2012.

[117] Z. Shen, P. Lu, G. Yan, and X. Hu, "Enhancing the oxygen permeability of Ba0.5Sr0.5Co0.8Fe0.2O5+δ membranes by coating RBaCo2O5+δ(R= Pr, Nd, Sm, Gd) layers," *Mater. Lett.*, vol. 64, no. 8, pp. 980–982, Apr. 2010.

[118] W. K. Hong and G. M. Choi, "Oxygen permeation of BSCF membrane with varying thickness and surface coating," *J. Memb. Sci.*, vol. 346, no. 2, pp. 353–360, Jan. 2010.

[119] J. P. Kim, J. H. Park, E. Magnone, and Y. Lee, "Significant improvement of the oxygen permeation flux of tubular Ba0.5Sr0.5Co0.8Fe0.2O3−δ membranes covered by a thin La0.6Sr0.4Ti0.3Fe0.7O3−δ layer," *Mater. Lett.*, vol. 65, no. 14, pp. 2168–2170, Jul. 2011.

[120] M. P. Lobera, J. M. Serra, S. P. Foghmoes, M. Søgaard, and A. Kaiser, "On the use of supported ceria membranes for oxyfuel process/syngas production," *J. Memb. Sci.*, vol. 385–386, pp. 154–161, Dec. 2011.

[121] X. Zhu, Y. Cong, and W. Yang, "Oxygen permeability and structural stability of BaCe0.15Fe0.85O3−δ membranes," *J. Memb. Sci.*, vol. 283, no. 1–2, pp. 38–44, Oct. 2006.

[122] S. Baumann, W. a. Meulenberg, and H. P. Buchkremer, "Manufacturing strategies for asymmetric ceramic membranes for efficient separation of oxygen from air," *J.*

Eur. Ceram. Soc., vol. 33, no. 7, pp. 1251–1261, Jul. 2013.

[123] L. Hong, X. Chen, and Z. Cao, "Preparation of a perovskite La0.2Sr0.8CoO3-x membrane on a porous MgO substrate," *J. Eur. Ceram. Soc.*, vol. 21, pp. 2207–2215, 2001.

[124] J. Donald Bright, M. F. Carolan, R. A. Cutler, P. N. Dyer, E. Minford, D. W. Prouse, R. E. Richards, S. L. Russek, D. M. Taylor, and M. A. Wilson, "Planar solid-state membrane module," EP 0732138 B1, 2001.

[125] C. Zhang, Z. Xu, X. Chang, Z. Zhang, and W. Jin, "Preparation and characterization of mixed-conducting thin tubular membrane," *J. Memb. Sci.*, vol. 299, no. 1–2, pp. 261–267, 2007.

[126] H. Wang, C. Tablet, and J. Caro, "Oxygen production at low temperature using dense perovskite hollow fiber membranes," *J. Memb. Sci.*, vol. 322, no. 1, pp. 214–217, 2008.

[127] A. Leo, S. Liu, J. C. Diniz da Costa, and Z. Shao, "Oxygen permeation through perovskite membranes and the improvement of oxygen flux by surface modification," *Sci. Technol. Adv. Mater.*, vol. 7, pp. 819–825, 2006.

[128] X. Tan, Z. Wang, B. Meng, X. Meng, and K. Li, "Pilot-scale production of oxygen from air using perovskite hollow fibre membranes," *J. Memb. Sci.*, vol. 352, no. 1–2, pp. 189–196, 2010.

[129] J. Da Costa, S. Smart, J. Motuzas, L. Shaomin, and D. Zhang, "State of Art (

SOTA) Report on Dense Ceramic Membranes for Oxygen Separation from Air," 2013.

[130] W. B. Hanson, K. I. Ironside, and J. A. Fernie, "Active metal brazing of zirconia," *Acta Mater.*, vol. 48, no. 18–19, pp. 4673–4676, 2000.

[131] A. Kaletsch, A. Bezold, E. M. Pfaff, and C. Broeckmann, "Effects of Copper Oxide Content in AgCuO Braze Alloy on Microstructure and Mechanical Properties of Reactive-Air-Brazed Ba0.5Sr0.5Co0.8Fe0.2O3-δ (BSCF)," *J. Ceram. Sci. Technol.*, vol. 3, no. 2, pp. 95–104, 2012.

[132] H. Cheng, J. Liu, X. Lu, and W. Ding, "Enhancing the Oxygen Permeability of BaCo0. 7Fe0. 2Nb0. 1O3− δ Membranes by Coating GdBaCo2-x Fe x O5+ δ for Partial Oxidation of Coke Oven Gas to Syngas.," *ACS Appl. Mater. Interfaces*, vol. 3, no. 10, pp. 4032–4039, 2011.

[133] P. Zeng, R. Ran, Z. Chen, H. Gu, Z. Shao, J. Dacosta, and S. Liu, "Significant effects of sintering temperature on the performance of La0.6Sr0.4Co0.2Fe0.8O3−δ oxygen selective membranes," *J. Memb. Sci.*, vol. 302, no. 1–2, pp. 171–179, Sep. 2007.

[134] A. Leo, S. Smart, S. Liu, and J. C. Diniz da Costa, "High performance perovskite hollow fibres for oxygen separation," *J. Memb. Sci.*, vol. 368, no. 1–2, pp. 64–68, Feb. 2011.

[135] P. Haworth, S. Smart, J. Glasscock, and J. C. Diniz da Costa, "Yttrium doped

BSCF membranes for oxygen separation," *Sep. Purif. Technol.*, vol. 81, no. 1, pp. 88–93, Sep. 2011.

[136] Z. Wu, W. Zhou, W. Jin, and N. Xu, "Effect of pH on synthesis and properties of perovskite oxide via a citrate process," *AIChE J.*, vol. 52, no. 2, pp. 769–776, Feb. 2006.

[137] J. Hoon Park, J. Pyo Kim, and S. Hwan Son, "Oxygen permeation and stability of Ba0.5Sr0.5Co0.8Fe0.2O3−δ membrane according to trace elements and oxygen partial pressure in synthetic air," *Energy Procedia*, vol. 1, no. 1, pp. 369–374, Feb. 2009.

[138] S.-Y. Jeon, M.-B. Choi, H.-N. Im, J.-H. Hwang, and S.-J. Song, "Oxygen ionic conductivity of La2NiO4+δ via interstitial oxygen defect," *J. Phys. Chem. Solids*, vol. 73, no. 5, pp. 656–660, May 2012.

[139] F. SCHULZE-KÜPPERS, S. BAUMANN, W. A. MEULENBERG, D. STÖVER, and H.-P. BUCHKREMER, "Manufacturing and performance of advanced supported Ba0.5Sr0.5Co0.8Fe0.2O3—δ (BSCF) oxygen transport membranes," *J. Memb. Sci.*, vol. 433, pp. 121–125.

[140] M. Arnold, H. Wang, and a Feldhoff, "Influence of CO2 on the oxygen permeation performance and the microstructure of perovskite-type (Ba0.5Sr0.5)(Co0.8Fe0.2)O3−δ membranes," *J. Memb. Sci.*, vol. 293, no. 1–2, pp. 44–52, Apr. 2007.

[141] M. Arnold, J. Martynczuk, K. Efimov, H. Wang, and A. Feldhoff, “Grain boundaries as barrier for oxygen transport in perovskite-type membranes,” *J. Memb. Sci.*, vol. 316, no. 1–2, pp. 137–144, May 2008.

[142] T. Klande, K. Efimov, S. Cusenza, K.-D. Becker, and A. Feldhoff, “Effect of doping, microstructure, and CO2 on La2NiO4+δ-based oxygen-transporting materials,” *J. Solid State Chem.*, vol. 184, no. 12, pp. 3310–3318, Dec. 2011.

[143] J. Caro, H. H. Wang, C. Tablet, a. Kleinert, a. Feldhoff, T. Schiestel, M. Kilgus, P. Kölsch, and S. Werth, “Evaluation of perovskites in hollow fibre and disk geometry in catalytic membrane reactors and in oxygen separators,” *Catal. Today*, vol. 118, no. 1–2, pp. 128–135, Oct. 2006.

[144] T. Klande, O. Ravkina, and A. Feldhoff, “Effect of microstructure on oxygen permeation of Ba0.5Sr0.5Co0.8Fe0.2O3−δ and SrCo0.8Fe0.2O3−δ membranes,” *J. Eur. Ceram. Soc.*, vol. 33, no. 6, pp. 1129–1136, Jun. 2013.

[145] X. Qi, F. . Akin, and Y. . Lin, “Ceramic–glass composite high temperature seals for dense ionic-conducting ceramic membranes,” *J. Memb. Sci.*, vol. 193, no. 2, pp. 185–193, Nov. 2001.

[146] P. Zeng, Z. Chen, W. Zhou, H. Gu, Z. Shao, and S. Liu, “Re-evaluation of Ba0.5Sr0.5Co0.8Fe0.2O3−δ perovskite as oxygen semi-permeable membrane,” *J. Memb. Sci.*, vol. 291, no. 1–2, pp. 148–156, Mar. 2007.

[147] A. Kather and G. Scheffknecht, “The oxycoal process with cryogenic oxygen

supply.,” *Naturwissenschaften*, vol. 96, no. 9, pp. 993–1010, 2009.

[148] H. Stadler, F. Beggel, M. Habermehl, B. Persigehl, R. Kneer, M. Modigell, and P. Jeschke, “Oxyfuel coal combustion by efficient integration of oxygen transport membranes,” *Int. J. Greenh. Gas Control*, vol. 5, no. 1, pp. 7–15, 2011.

[149] M. J. den Exter, W. G. Haije, and J. F. Vente, “Validity of ITM Technology for Oxygen Production and Oxidation Processes; Material, System, and Process Aspects,” in *Inorganic Membranes for Energy and Environmental Applications*, A. C. Bose, Ed. Berlin: Springer, 2009, pp. 27–51.

[150] W. A. Meulenberg, I. Voight, R. Kriegel, S. Baumann, M. Ivanova, and T. van Gestel, “Inorganic Membranes for CO2 Separation,” in *Efficient Carbon Capture for Coal Power Plants*, D. Stolten and V. Scherer, Eds. Weinheim: Wiley-VCH, 2011, pp. 319–350.

[151] H. Yang, Z. Xu, M. Fan, R. B. Slimane, A. E. Bland, and I. Wright, “Progress in carbon dioxide seperation and capture: A review,” *J. Environ. Sci.*, vol. 20, pp. 14–27, 2008.

[152] H. Herzog and D. a N. Golomb, “Carbon Capture and Storage From Fossil Fuels and Biomass,” *Clim. Change*, vol. 379, no. 6562, pp. 240–79, 2006.

[153] M. A. Habib, H. M. Badr, S. F. Ahmed, R. Ben-Mansour, K. Mezghani, S. Imashuku, G. J. la O’, Y. Shao-Horn, N. D. Mancini, A. Mitsos, P. Kirchen, and A. F. Ghoneim, “A review of recent developments in carbon capture utilizing oxy-

fuel combustion in conventional and ion transport membrane systems," *Int. J. Energy Res.*, vol. 35, no. 9, pp. 741–764, 2011.

[154] M. den Exter, J. F. Vente, D. Jansen, and W. G. Haije, "Viability of mixed conducting membranes for oxygen production and oxyfuel processes in power production," *Energy Procedia*, vol. 1, no. 1, pp. 455–459, 2009.

[155] K. Foy, "Investigation into the possible use of an oxygen ion transport membrane combustion unit in an oxyfired power plant," Dublin Institute of Technology, 2007.

[156] H. Stadler, F. Beggel, M. Habermehl, B. Persigehl, R. Kneer, M. Modigell, and P. Jeschke, "Oxyfuel coal combustion by efficient integration of oxygen transport membranes," *Int. J. Greenh. Gas Control*, vol. 5, no. 1, pp. 7–15, 2011.

[157] C. Kunze and H. Spliethoff, "Assessment of oxy-fuel, pre- and post-combustion-based carbon capture for future IGCC plants," *Appl. Energy*, vol. 94, pp. 109–116, 2012.

[158] C. Tsai, A. G. Dixon, W. R. Moser, and Y. H. Ma, "Dense Perovskite Membrane Reactors for Partial Oxidation of Methane to Syngas," *AIChE J.*, vol. 43, no. 11, pp. 2741–2750, 1997.

[159] X. Zhu, H. Wang, and W. Yang, "Novel cobalt-free oxygen permeable membrane.," *Chem. Commun. (Camb).*, no. 9, pp. 1130–1131, 2004.

[160] H. Wang, C. Tablet, A. Feldhoff, and J. Caro, "A cobalt-free oxygen-permeable

membrane based on the perovskite-type oxide Ba0.5Sr0.5Zn0.2Fe0.8O 3-δ," *Adv. Mater.*, vol. 17, no. 14, pp. 1785–1788, 2005.

[161] A. Yan, B. Liu, Y. Dong, Z. Tian, D. Wang, and M. Cheng, "A temperature programmed desorption investigation on the interaction of Ba0.5Sr0.5Co0.8Fe0.2O3-δ perovskite oxides with CO2 in the absence and presence of H2O and O2," *Appl. Catal. B Environ.*, vol. 80, no. 1–2, pp. 24–31, 2008.

[162] S. Mcintosh, J. Vente, W. Haije, D. Blank, and H. Bouwmeester, "Structure and oxygen stoichiometry of SrCo0.8Fe0.2O3−δ and Ba0.5Sr0.5Co0.8Fe0.2O3−δ," *Solid State Ionics*, vol. 177, no. 19–25, pp. 1737–1742, Oct. 2006.

[163] A. J. Ellett, *Oxygen Permeation and Thermo-Chemical Stability of Oxygen Separation Membrane Materials for the Oxyfuel Process*. Forschungszentrum Jülich, 2010.

[164] J. Kim, S. Choi, A. Jun, H. Y. Jeong, J. Shin, and G. Kim, "Chemically Stable Perovskites as Cathode Materials for Solid Oxide Fuel Cells: La-Doped Ba0.5 Sr0.5 Co0.8 Fe0.2 O3-δ.," *ChemSusChem*, vol. 7, no. 6, pp. 1669–75, 2014.

[165] F. Wang, T. Nakamura, K. Yashiro, J. Mizusaki, and K. Amezawa, "Effect of Nb doping on the chemical stability of BSCF-based solid solutions," *Solid State Ionics*, vol. 262, no. 3, pp. 719–723, 2014.

[166] K. Efimov, T. Klande, N. Juditzki, and A. Feldhoff, "Ca-containing CO2-tolerant

perovskite materials for oxygen separation," *J. Memb. Sci.*, vol. 389, pp. 205–215, Feb. 2012.

[167] J. H. Park, K. Y. Kim, and S. Do Park, "Oxygen permeation and stability of La0.6Sr0.4TixFe1-xO3-δ (x = 0.2 and 0.3) membrane," *Desalination*, vol. 245, no. 1–3, pp. 559–569, 2009.

[168] J. Yi, T. E. Weirich, and M. Schroeder, "CO2 corrosion and recovery of perovskite-type BaCo1-x-y Fex Nby O3-δ membranes," vol. 437, pp. 49–56, 2013.

[169] W. Chen, C. Chen, H. J. M. Bouwmeester, A. Nijmeijer, and L. Winnubst, "Oxygen-selective membranes integrated with oxy-fuel combustion," *J. Memb. Sci.*, vol. 463, pp. 166–172, 2014.

[170] R. Kneer, D. Toporov, M. Förster, D. Christ, C. Broeckmann, E. Pfaff, M. Zwick, S. Engels, and M. Modigell, "OXYCOAL-AC: Towards an integrated coal-fired power plant process with ion transport membrane-based oxygen supply," *Energy Environ. Sci.*, vol. 3, p. 198, 2010.

[171] R. Castillo, "Thermodynamic analysis of a hard coal oxyfuel power plant with high temperature three-end membrane for air separation," *Appl. Energy*, vol. 88, no. 5, pp. 1480–1493, 2011.

[172] S. Gupta, J. J. Adams, J. R. Wilson, E. G. Eddings, M. K. Mahapatra, and P. Singh, "Performance and post-test characterization of an OTM system in an experimental coal gasifier," *Appl. Energy*, vol. 165, pp. 72–80, 2016.

[173] Y. Wei, Y. Wang, J. Tang, Z. Li, and H. Wang, "Oxy-Fuel Combustion for CO2 Capture using a CO2-Tolerant Oxygen Transporting Membrane," *AIChE J.*, vol. 59, no. 10, pp. 3856–3862, 2013.

[174] "Air Products and EPRI further develop ion transport membranes," *Membr. Technol.*, vol. 2009, no. 7, pp. 2–3, Jul. 2009.

[175] J. M. Repasky, L. L. Anderson, V. E. Stein, P. a Armstrong, and E. P. Foster, "ITM Oxygen technology : scale-up toward clean energy applications," *Int. Pittsburgh Coal Conf. 2012 Pittsburgh, Pa., U.S.A. Oct. 15–18, 2012*, 2012.

[176] M. Shah, "Oxy-Fuel Combustion Using OTM For CO2 Capture from Coal Power Plants," in *2nd Workshop on International Oxy-Combustion Research Network*, 2007.

[177] A. Kaletsch, E. M. Pfaff, C. Broeckmann, M. Modigell, and N. Nauels, "Pilot Module for oxygen separation with BSCF membranes OXYCOAL-AC," in *2nd International Conference on Energy and Power Engineering*, 2011.

[178] M. P. Pechini, "Method of preparing lead and alkaline earth titanates and niobates and coating method using the same to form a capacitor," US3330697 A, 11-Jul-1967.

[179] J. Park, "Oxygen permeability and structural stability of La 0.6 Sr 0.4 Co 0.2 Fe 0.8 O 3− δ membrane," *Korean J. Chem. Eng.*, 2007.

[180] A. L. Shaula, R. O. Fuentes, F. M. Figueiredo, V. V. Kharton, F. M. B. Marques,

and J. R. Frade, “Grain size effects on oxygen permeation in submicrometric CaTi0.8Fe0.2O3-?? ceramics obtained by mechanical activation,” *J. Eur. Ceram. Soc.*, vol. 25, no. 12 SPEC. ISS., pp. 2613–2616, 2005.

[181] H. J. M. Bouwmeester, H. Kruidhof, and A. J. Burggraaf, “Importance of the surface exchange kinetics as rate limiting step in oxygen permeation through mixed-conducting oxides,” *Solid State Ionics*, vol. 72, no. PART 2, pp. 185–194, 1994.

[182] J. A. Lane, S. J. Benson, D. Waller, and J. A. Kilner, “Oxygen transport in La0.6Sr0.4Co0.2Fe0.8O3-δ,” *Solid State Ionics*, vol. 121, no. 1, pp. 201–208, 1999.

[183] K. Wiik, S. Aasland, H. L. Hansen, I. L. Tangen, and R. Ødegård, “Oxygen permeation in the system SrFeO3-x-SrCoO3-y,” in *Solid State Ionics*, 2002, vol. 152–153, pp. 675–680.

VITAE

Name: Amir Hamza

Date of Birth: August 8, 1983

Present Address: KFUPM P. O. Box 8642, King Fahd University of Petroleum and Mineral, Dhahran-31261, Saudi Arabia

Permanent Address: H. No. F-18, Street 7, Phase IV, Officers Colony, Wah Cantt., Rawalpindi, Pakistan

Email Address: amirh@kfupm.edu.sa, hamza743@gmail.com

Educational Qualification:

Ph.D.
May, 2016
King Fahd University of Petroleum and Minerals, Dhahran, Saudi Arabia
M.S (Mechanical Engineering)
August, 2008
Seoul National University, Seoul, South Korea
B.E. (Mechatronics Engineering)
May, 2005
National University of Sciences & Technology, Rawalpindi, Pakistan.

Publications

1. K. Mezghani, A. Hamza, "Application of Ba0.5Sr0.5Co0.8Fe0.2O3-δ membranes in an oxy-fuel combustion reactor," *Journal of Membrane Science*, vol. 518, pp. 254-262, Nov. 2016.
2. K. Mezghani, A. Hamza, M. A. Habib, D. Lee, and Y. Shao-Horn, "Effect of microstructure and thickness on oxygen permeation of $La_2NiO_{4+\delta}$ membranes," *Ceram. Int.*, vol. 42, no. 1, pp. 666–672, Jan. 2016.
3. Hamza and Y. J. Kang, "Hybrid experimental/numerical technique for determination of the complex dynamic moduli of elastic porous materials," *J. Mech. Sci. Technol.*, vol. 23, no. 2, pp. 283–290, 2009.